2011

Analysis of high performance polypyrrole actuators

Wen Zheng
University of Wollongong

Analysis of High Performance Polypyrrole Actuators

A thesis submitted in fulfilment of the requirements

for the award of the degree

of

Doctor of Philosophy

from

UNIVERSITY OF WOLLONGONG

by

WEN ZHENG, B.E.

Department of Chemistry

February. 2011.

To my dearest parents

Acknowledgment

Pursuing a Ph.D is regarded as a great decision in one's life. However, achieving it is another story. It is not only an individual effort, but also contains many people's help and support.

I would like to express my sincere gratitude to my advisors Prof. Geoff Spinks and Prof. Gordon Wallace for their continuous support of my Ph.D. Their friendly nature, immense knowledge, optimistic attitude, hard working effort and firm belief of science not only make them perfect supervisors, but also great scientists and spirit guiders. Being their student is one of the luckiest things in my life. Their generously granted time and effort to help me in the research and writing up of this thesis is greatly appreciated.

I would like to thank Dr. Philip Whitten, Dr. Van Tan Turong and Dr Joselito Razal, for their great collaboration and discussion in this study. Our actuator team members: Mr. Adrian Gestos and Mr. Sina Naficy are also specially thanked for great friendships.

I would also like to acknowledge the genius staff and students at the Intelligent Polymer Research Institute. Their generous sharing of knowledge and experience let me learn a lot and avoid lots of mistakes.

My special thanks go to my fiancée, Miss Ning Chen, for her faith and caring on me.

Abstract

Electrochemical actuators based on polypyrrole (PPy) have been constructed and characterized. The actuation performance was analyzed in terms of several main parameters: thickness, scan rate, applied stress, cycle life and creep. Two different dopants and two different forms (tubes and free standing films) were produced to investigate their effects on the actuation performance and the underlying mechanisms of actuation.

The actuation strain generated by the PPy materials when an external load was applied was found to be the sum of three individual time-dependent processes: strain generated directly from charge and solvent injection; strain generated from elastic modulus changes; and strain caused by creep. It was found that the strain generated from charge and solvent injection behaved like a diffusion-controlled process and the process were found to be relatively slow, whether during ramp or step voltage scanning. A semi-empirical model based on Fickian diffusion was built to predict the actuation strain under different loads at different scan rate in ramp voltage scanning and for different actuator thicknesses. By using the model, work and power of PPy actuators were analyzed. A consequence of the slow charging process is that the thicker PPy materials produce a larger work output but a lower power output.

The effect of dopant used for the PPy was quite significant with bis-(trifluoromethane-sulfonimide) (TFSI) producing higher strains for equivalent conditions than hexafluorophosphate (PF_6) doped PPy. PPy/TFSI films were found to respond slowly to a step voltage change with a significant amount of strain occurring after the applied current had decayed to zero. This contribution to strain was assumed to be due to solvent ingress

associated with osmotic pressure. It was also found that the large strains produced in PPy/TFSI degraded rapidly cycle by cycle. Several approaches were investigated to improve stability. Current stimulation rather than voltage stimulation ensures equal oxidation and reduction per cycle and resulted in a constant 4% strain for at least 100 cycles.

Creep of PPy at different redox state was investigated and modeled for the first time using classical spring-dashpot models. The model could successfully fit and predicting the creep behavior of PPy at different redox states. The viscoelastic parameters are found to be voltage-dependent with the modulus (instantaneous and delayed) and viscosity decreasing when the PPy/TFSI was reduced. By using Boltzmann superposition principle, an attempt to combine all strains was conducted.

ABBRAVATIONS

α	volume fraction
A	area
β	modulus shift factor
C	concentration
CV	cyclic voltammograms
CPs	conducting polymers
d_c	oxidized layer thickness
D	diffusion coefficient
E	potential
F	force
i	current
L	length
Li.TFSI	bis-trifluoromethanesulfonimide lithium
MB	methyl benzoate
PPy	polypyrrole
PANi	polyaniline
PTh	polythiophene
γ	strain to charge ratio
ε	strain
Y	elastic modulus
σ	stress
PF_6^-	hexafluorophosphate
Q	charge
t	time
r	scan rate
ρ	resistance
$Ag\|Ag^+$	silver|silver ion reference electrode

PC	propylene carbonate
τ	relaxation time
η	viscosity term
p	power density
w	work density

LIST OF FFIGURES AND TABLES

1. FIGURES

2. TABLES

CONTENTS

CHAPTER 1 LITERATURE REVIEW

1.1 Thesis motivations

It is always interesting and challenging to build actuators that can mimic natural muscles. Since conducting polymers (CPs) were discovered by Hideki Shirakawa, Alan Heeger and Alan G MacDiarmid [1], using those new types of materials offers a new approach to fabricate actuators [2, 3]. During the last decades, conducting polymer actuators have made great progress in actuator performance by material selections, actuator designs and polymerization optimization. All those achievements greatly extend the application of actuators.

For macro scale linear actuations, a simple way to predict its position (actuation) is necessary for engineering applications. It is widely proposed that the total actuation strain is a combination of the free actuation strain (strain occurring at zero external load), strain caused be a shift in the elastic modulus and creep induced strain. The aim of this thesis is to evaluate those strains under different conditions and attempt to mathematically prediction the total strain by combining them. Free strain, elastic strain and creep strain will be discussed separately.

1.2 History of conducting polymers

Back to the mid of 1800s, perhaps the first conductive polymer was synthesized as the discovery of aniline. But the ability to conduct charge was not noticed at that time. After a century, as early as 1963, three Australia researchers produced conductive PPy which reached the conductivity of 1S/cm [4]. Theoretically, those PPy belongs to the semiconductors. After 14 years, in 1977, Hideki Shirakawa, Alan Heeger and Alan G MacDiarmid synthesized the halogen doped $(CH)_x$ and $(SN)_x$ with 10^3 S/cm

conductivity which is 10^9 times more conductive than its undoped state. These materials were called 'organic metals'. Their work was soon widely recognized and initiated a great deal of research into the synthesis, characterization and application of similar organic conducting polymers.

Generally, the conductivity in CPs was from polarons and bipolarons[5]. Under an electrical field, the movement of bipolarons conducts the charge. The formation of polarons and bipolarons is due to the electron structure in CPs. In CPs, the π molecular orbit is overlapping because of the high degree of π bond conjugation. The delocalization of π electrons generates the polarons and bipolarons. The bipolarons widely exist in the conducting polymer as it has a lower energy than polarons.

However, the stability of $(CH)_x$ and $(SN)_x$ is very poor, limiting their application. Most of applications are using more stable CPs such as polypyrrole (PPy), polyaniline (PANi) and polythiophene (Pth).

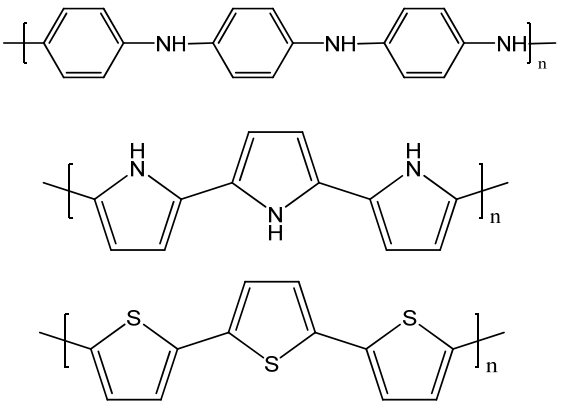

Figure 1. 1 Three typical conducing polymers. Top to down: Polyaniline (PANi); Polypyrrole (PPy); Polythiophene (PTh)

As listed in Figure 1. 1, PANi, PPy & Pth are three main CPs actuator material widely reported in the literature. Diaz et al synthesized PPy, PANi and Pth successfully through electrochemical methods [6-8]. When oxidizing CPs, electrons are removed from polymer bulk and counter ions will transfer into polymer bulk to balance charge.

And when reducing them, electrons flux in and counterions will move out. Such irreversible process generates a pair of redox peaks in cyclic voltammograms.

1.3 Conducting polymer actuators:

Nowadays, there are so many applications for conducting polymers in electronics, batteries, electro chromic devices, bionics, solar cells, drug delivery systems, corrosion protection, electrochemical sensors and actuators [9-17]. Among those tremendous applications, actuators attract a lot of scientists because of its similarity to natural muscles and potentially wide application.

1.3.1 Natural muscles

The typical natural mammal skeletal muscles can generate around 30% of deformation and stress to 0.35MPa. A summary of the performance of skeletal muscles is listed in Table 1. 1

Table 1. 1 The properties of skeletal muscles [18].

Property	Typical value	Maximum value
Strain (%)	20	>40
Stress (MPa)	0.1 (sustainable)	0.35
Work density(kJ/m^3)	8	
Density (kg/m^3)	1037	
Strain rate %/s		500
Power to mass (W/kg)	50	200
Efficiency %		40

Cycle life	10^9
Modulus (MPa)	10-60

1.3.2 Actuators based on CPs:

The early use of conducting polymers as artificial muscles to emulate natural muscles has been reviewed by Baughman[3]. As seen in Figure 1. 2, because of their similarity to natural muscle, conducting polymer actuators is also sometimes called 'artificial muscles'. Conducting polymer actuators and natural muscles have many features in common: both of them are driven by electro stimulation and flux of ions; they are both soft and flexible; only operate in a wet state (in contact with an ion reservoir); both transfer chemical energy to mechanical energy; and are easily controllable [19].

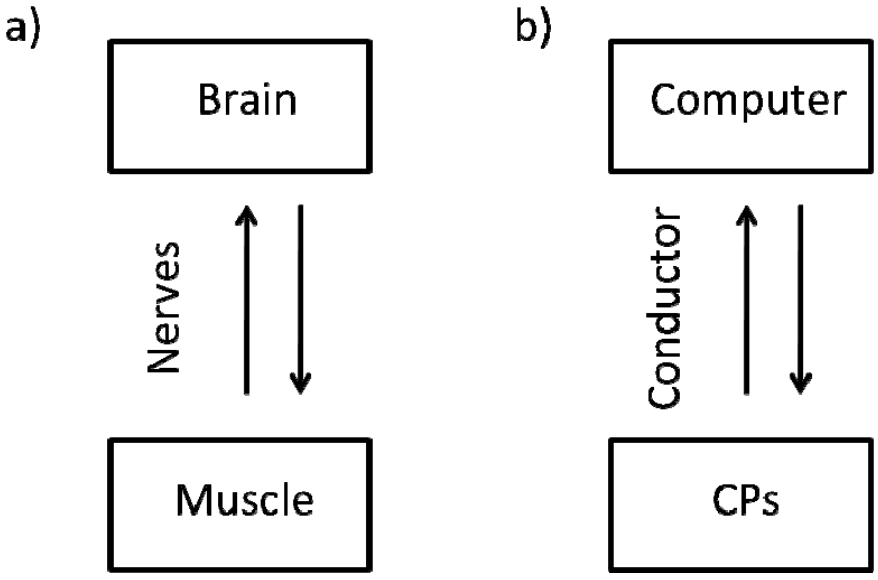

Figure 1. 2 Schematics of actuation: muscles (a) and conducting polymer actuators (b)

Generally, the dimensional changes in CPs are the result of ions and solvent

molecular influx and efflux. Such volume changes are required to accommodate the anions and cations, and sometimes also solvent molecules which accompany redox reactions in CPs. This general process is illustrated in Figure 1.3. Reversible redox reactions in CPs lead to electrochemical charging and discharging. These processes generate charged sites on the polymer backbone and each site is accompanied by an oppositely charged "counter-ion". Counterions enter and leave the polymer from and to an external electrolyte. The electrolyte commonly consists of ions dissolved in a solvent and it is known that solvent molecules can also enter the CP. The solvent content varies with the extent of charging, so solvent ingress/egress can contribute to the volume changes that drive actuation.

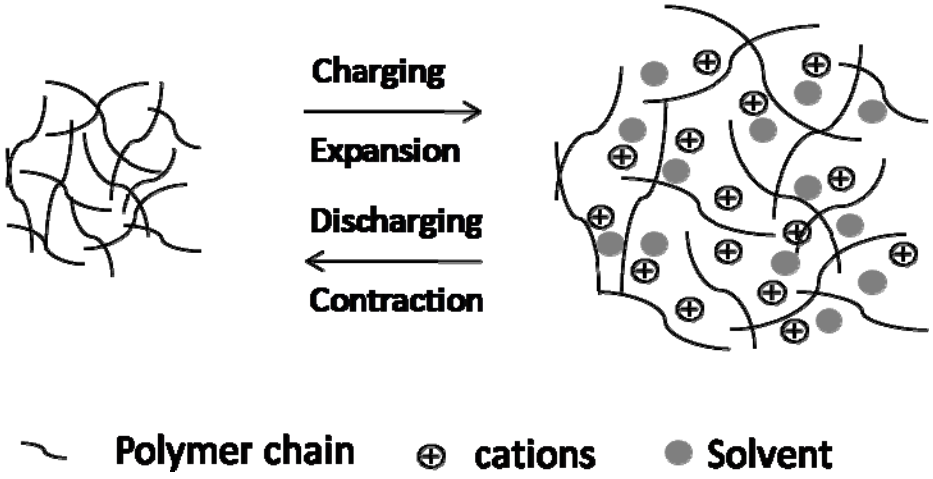

Figure 1. 3 Proposed mechanisms of actuation via ions insertion accompanied by solvent.

Through a continuing effort on selecting dopant counterions and solvents, CP actuators are now much improved compared to the early versions. As compared in Table 1. 2, PPy actuators generate much higher work density and can work under 100 times more stress than mammalian skeletal muscles. But CPs actuators can't last as long as muscle does.

Table 1. 2 Comparison of biological muscles & PPy actuators[18].

	Skeletal muscles	PPy actuators
Operating stress (MPa)	0.1 MPa	Typically under 10 MPa
Strain (%)	20	Up to 40
Durability	Typically 10^9	Up to 10^6
Work density (kJ/m^3)	8	Up to 140

Using conducting polymer to build actuators has significant advantages compared with other actuator materials like shape memory alloys and piezoelectric materials. These advantages include operation at low voltage (typically 1V or less); light weight (density is roughly 0.5~2 g/cm^3); relative large dimensional changes (as large as 40% in some special cases); and high power density (up to 300 kJ/m^3). A summarization of CP actuators' performance is listed in Table 1. 3, Section 1.6.1.

1.4 Materials used to build CP actuators.

As mentioned before, among so many types of CPs, three of them are widely and intensely used for studying CPs actuators. They are PANi, Pth and PPy actuators. The methods for preparing and operating these materials as actuators, as well as their actuation performance are reviewed in the following sections.

1.4.1 Polyaniline actuators

PANi can be produced by chemical and electrochemical oxidization from its monomer (Figure 1. 4).

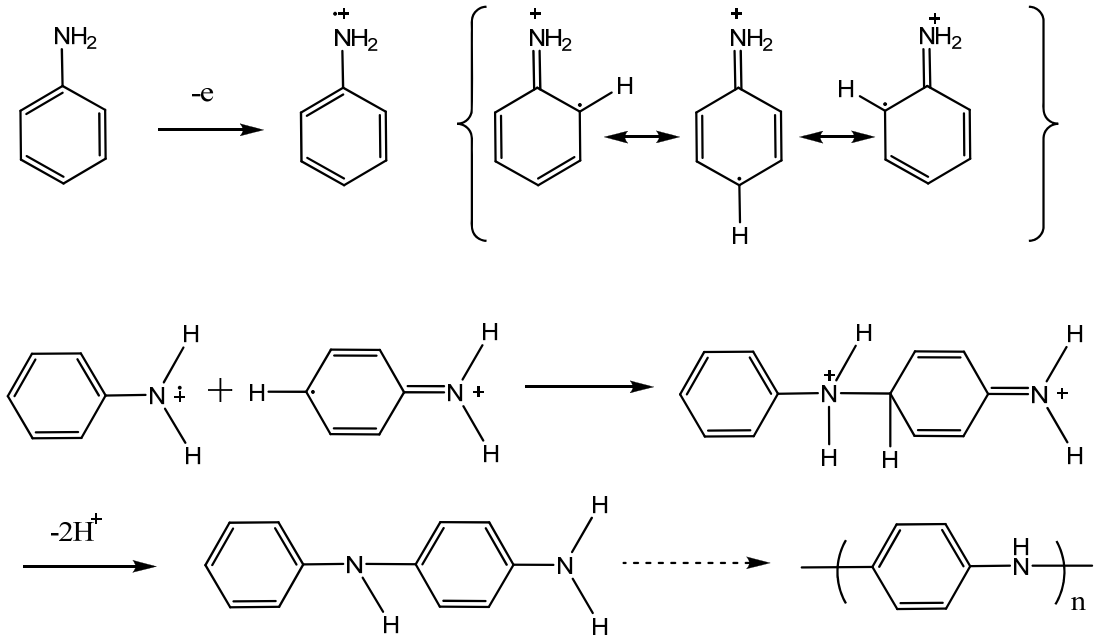

Figure 1. 4 Polymerization pathways of PANi [20].

PANi films have been found to expand and contract by oxidation and reduction [21]. The actuation process of PANi is complicated as protons affect the actuation behavior. A current accepted model for the molecular structure and oxidation levels of PANi including all the pathways between them was summarized by Smela et.al [22, 23]. The important states are illustrated in Figure 1.5. Polyaniline actuators are operated in an acid environment as polyaniline is electroactive below pH4. In aqueous solution, the electrochemical reaction changes the PANi between three states: leucoemeraldine, emeraldine salt and pernigraniline, in which only emeraldine salt is a conductor (Figure 1. 5). When the pH is between 0 and 2, the oxidation of PANi produces an expansion due to anion insertion as PANi changes from leucoemeraldine to emeraldine salt. If further oxidation continues, the transition from emeraldine salt to pernigraniline leads to a contraction as the lost of protons will trigger decomposition happens [24, 25]. The reaction process is shown in Figure 1. 5.

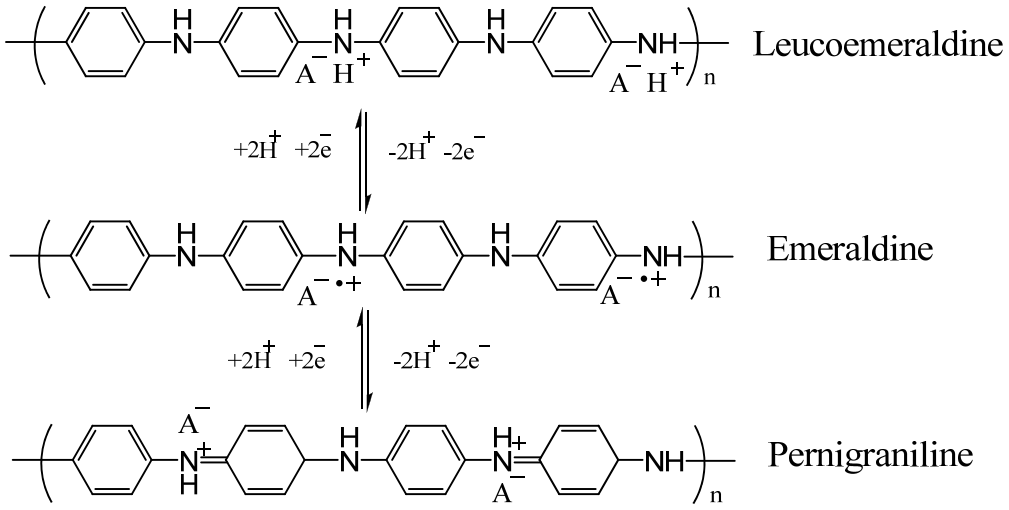

Figure 1. 5 Redox states of PANi (switching property): leucoemeraldine, emeraldine salt and pernigraniline.

PANi can also actuate when operated in organic electrolytes will also expand while turning leucoemeraldine to emeraldine even there are no protons incorporate during redox in organic electrolytes. Continuing oxidizing will bring more anions in, further expansion can be observed [26].

Strain generated by PANi actuators is usually below 2% at free load, which is small compared to some recently-developed PPy actuators. The interesting part of PANi is perhaps its high mechanical strength. Actuation strains from 1% to 3% have been obtained at stresses of 5MPa, which is attractive to engineers [3, 24, 27]. Spinks et al have produced actuating fibers of PANi and PANi with carbon nanotubes to reinforce the material. PANi fibers showed actuation strains of 1.2% and could operate at stresses to 90 MPa (with diminished strain). The addition of carbon nanotubes reduced the actuation strain to 0.8% but greatly enhance the strength so that actuation could be achieved at 125 MPa. These materials showed a large work output (320 kJ/m^{-3}) [28].

Another advantage of using PANi is its capability of processing suitable for mass-production, which makes the material attractive for commercialization. PANi can be synthesized chemically and dissolved into some certain organic solvents. The solution

can be wet spun into fibers or cast to films to achieve different requirement [29-31]. As mentioned above, the PANi fibres could be used to generate high strength actuators.

There are also some limitations in using PANi as an actuator material. The acidic aqueous environment perhaps limits the further application of the PANi actuators. PANi is also not biocompatible, which limits some applications. What's more, the pernigraniline is not stable and rapidly degrades in many commonly used acids [32]. Perhaps the main limitation at this stage, however, is the small strains that have been produced using PANi. Most applications benefit from a higher strain output, which is possible with other CP materials.

1.4.2 Polythiophene actuators

Pth and its derivatives can be prepared chemically or electrochemically through oxidation of its monomer (Figure 1. 6). The advantages of using Pth in electrochemical applications include its high conductivity, relative wide potential window and structure stability.

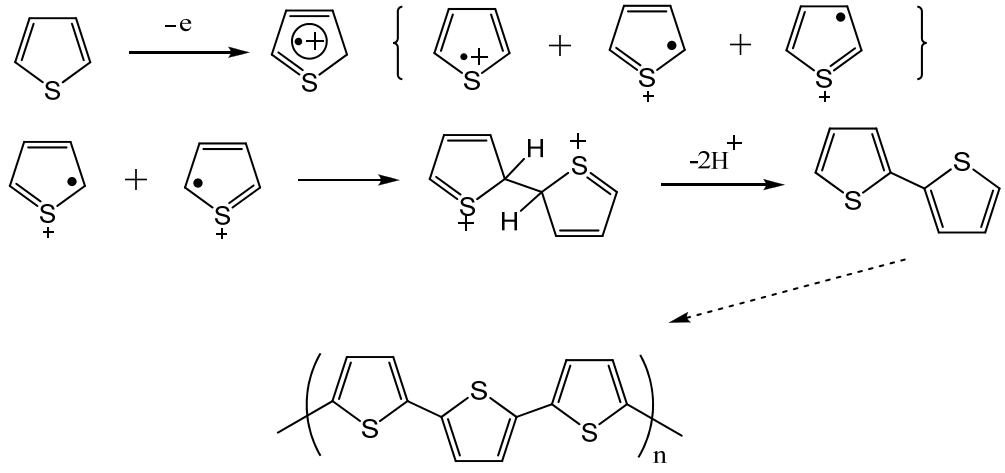

Figure 1. 6 Polymerization pathways of Pth[8]

Pth actuators have been demonstrated [33-36]. Kaneto et al realized 2% electrochemical strain using poly (3-hexylthiophene) and poly (3-dodecyithiophene) [37].Poly (3-methylthiophene) was utilized for fabricating actuators [38] that showed ~2% strain when used in an organic electrolyte and ~0.5% strain when an ionic liquid was used as the electrolyte. The interesting part was that the elastic modulus of poly (3-methylthiophene) in the expanded state was significant higher than that in the contract state. This change in modulus leads to a higher electrochemical strain when higher (isotonic) loads were used. This situation is most unusual, as it has been found that elastic modulus is usually lower in the expanded state that the actuation strain diminishes with an increasing applied load. Higher strains have been generated from a solution-processable poly((E)-4,4''-didecoxy-3'-styryl[2,2':5',2'']terthiophene). Strains as high as 11.5% were recorded, although the strain diminished rapidly with increasing voltage scan rate and higher isotonic loads [39]. The solution processability allows further developments in terms of PTh fibers, however these have not yet been reported for actuators.

1.4.3 polypyrrole actuators

Perhaps PPy is the most attractive conducting polymers due to its high conductivity, stability in both of the aqueous and organic solvent, high mechanical strength, biocompatibility and large actuation strain. The strain of polypyrrole actuators is typically 2%-10%. Bay et al [40] using PPy/DBS film achieved 12% strain at a stress of 0.5MPa. The free-standing PPy/TFSI films, without load, can show extremely high strain as much as 40% by carefully selecting dopants and solvents [41-44].

1.4.3.1 Synthesis of Polypyrrole

As with PANi and Pth, PPy can be polymerized both chemically and electrochemically.

Chemical polymerization:

Chemical polymerization of pyrrole requires an oxidant, which is typically Fe^{3+} [45]. Other oxidizing agents can be used as well [46, 47]. The reaction scheme is shown in Figure 1.7. Different substrates and copolymers are also studied when chemical deposition happens.

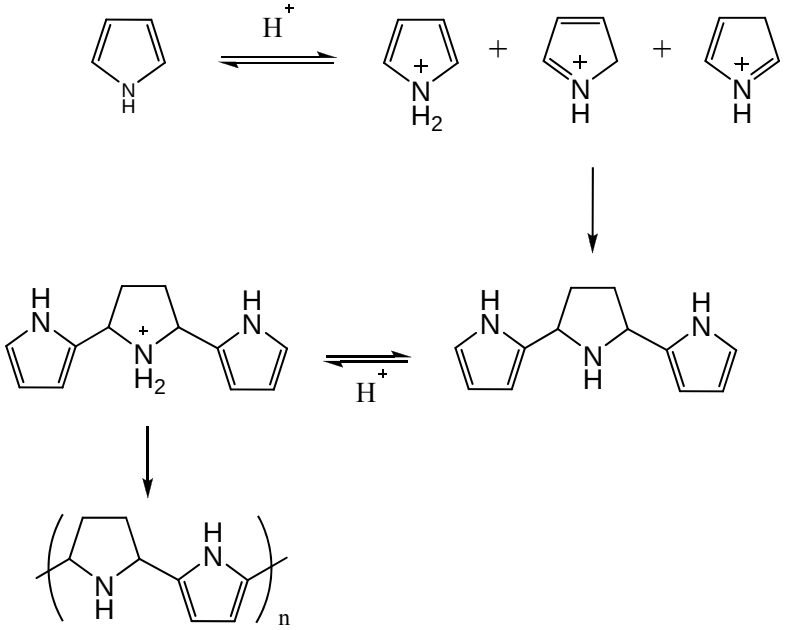

Figure 1. 7 Reaction pathway of PPy chemical polymerization

The main limitation of chemical polymerization of pyrrole for producing actuators is that the polymer is formed as particles or porous coatings of poor mechanical properties. In addition, the conductivity is often low. The reasons could be that the polypyrrole made from chemical ways forms particles instead of continuous phase and

it is more likely to form a partially conjugated structure (Figure 1. 7). The conductivity of chemical deposition polypyrrole is roughly at 10^{-4} S/cm and reaches 100 S/cm by using careful polymerization methods [46, 48]. The typical conductivity of PPy formed by chemical ways is less than that from electrochemically-produced polypyrrole by several orders of magnitude. Nanofibers (~50S/cm) have better conductivity than nanoparticles [49]. However, the chemically synthesized PPy still couldn't be used as actuator materials as the poor mechanical property limits its further application. Chemical deposited polypyrrole has chemical activities so, chemical deposition of polypyrrole is mainly used to develop sensors. [50].

Electropolymerization:

Electrodeposition is generally preferred by researchers to prepare PPy materials as it provides a good control of film thickness, morphology, improved mechanical properties and higher conductivity. Normally, the film was deposited on conductive substrates, such as gold, platinum, glassy carbon, tin or indium-tin oxide (ITO) coated glass. Further study shows that there are differences among the films from those substrates[41]. Polymerization onto platinum or glassy carbon electrodes has been found to result in smoother, better adhering films than others.

Electrodeposition can be achieved using a range of different potential or current control methods. Typical chronoamperogram and chronopotentiogram for the electrochemical depositions of PPy can identify several reaction / deposition steps (Figure 1. 8). Take the chronopotentiogram for instance, when the potential is firstly applied, a large current spike will be observed resulting from the charging of the electrochemical double layer. After this process which will reach the lowest current in

the whole growth, the real polymerization now begins starting with nucleation. Next, the current reaches a plateau while PPy is continuously being formed, doped and depositing on the electrode surface. It has been concluded that the deposition rate is almost constant which means the films thickness increases linearly with time [51].

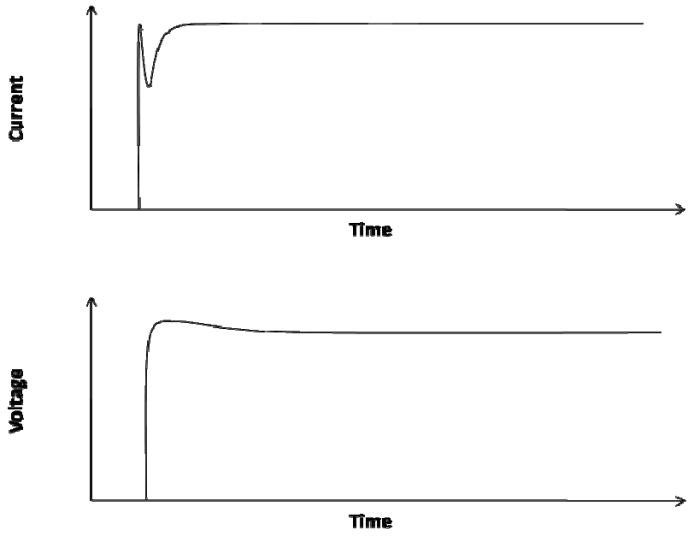

Figure 1. 8 Typical constant potential (up) and current (down) deposition of PPy.

The exact processes by which polypyrrole forms from its monomer during electropolymerization are not fully understood. Several steps in polymerization occur rapidly and are difficult to separate. In addition, the insolubility of the polypyrrole and its non-crystalline nature make the characterization and analysis of the structure difficult. As a result, there is no agreement on the mechanism. The most accepted mechanism was explained by Diaz et al[51-53], which have been supported by Electron Paramagnetic Resonance (EPR) studies [54] and is summarized in Figure 1.9.

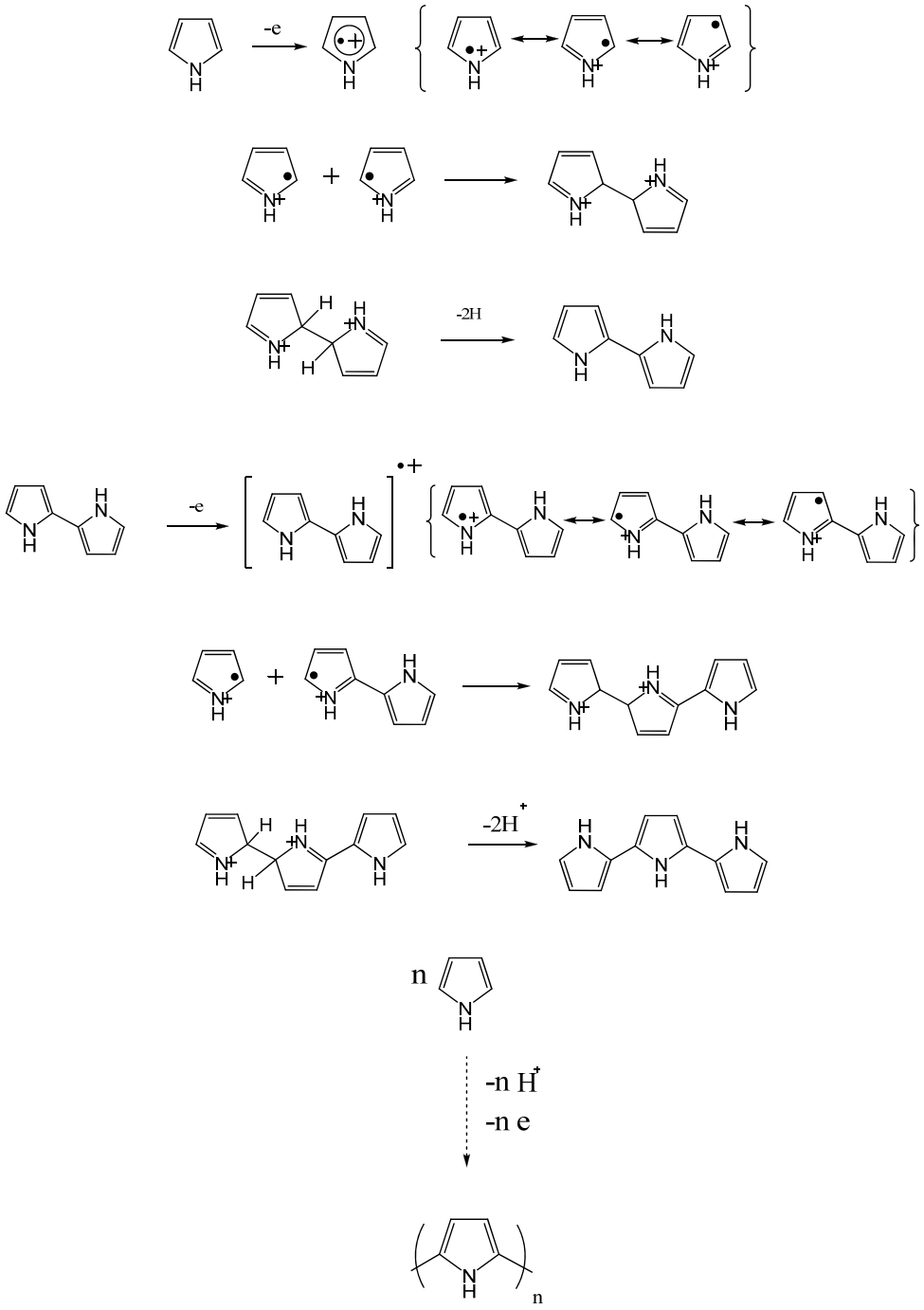

Figure 1. 9 Reaction pathways of PPy electropolymerization.

Protons released from the coupling reaction in Figure 1. 9 could prevent electrochemical polymerization of pyrrole [55]. Otero et al proposed that acid-catalyzed chemical polymerization leads to generation of non conjugated polymer and thus dramatically reduce the conductivity [56, 57]. Thus in order to receive high quality of PPy, protons release from coupling reaction must be removed. To remove protons,

adding a proton acceptor is a simple and effective method. It is common to see that 1% (w/w) of water is added to the electrolyte before polymerization. The small amount of water will help to capture the reaction-released protons and prevents pyrrole from being protonated. Hence, the partially conjugated (Figure 1. 10 right) will be less favored. Further experiments indicate that not only water, but also other basic solvents, like methanol, ethanol and tetrahydrofuran have similar action [58]. That critical role of water as a proton-acceptor has long been known during polymerization, and is especially important in the polymerization of pyrrole in non-aqueous solvents, such as acetonitrile [6, 59-61].

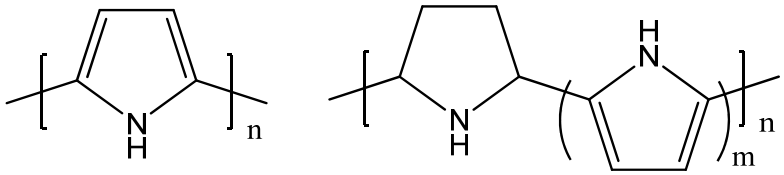

Figure 1. 10 Conjugated and partially conjugated PPy.

Other polymerization parameters such as growth temperature and current density also could greatly influence final properties of PPy.

Growth temperature has a substantial influence on kinetics of polymerization as well as conductivity. Generally, low polymerization temperature is helpful to obtain high conductivity of PPy [62, 63]. It is believed that low temperature will slow down side reaction and generate a more regular structure of PPy, thus improving conductivity. Different current density will lead to different porosity, conductivity and mechanical property [64-66]. Low polymerization current density allows for better alignment of polymer chains [67]. However, low current will also lead to high compactness of PPy, which might slow down transfer of ions and strain rate.

In this thesis, polymerization of PPy happens at a current density of 0.1 mA/cm^2 in

a mixture solvent of water (1% w/w)/PC at -30˚C. That polymerization conduction could generate high quality of PPy.

1.4.3.2 The switching principles of PPy actuators

The reversible oxidation and reduction of PPy are referred to its 'switching' property. While reducing/oxidizing PPy electrons flow in/out of the polymer to form charged or uncharged sites on the polymer chains. Ions also have to move in/out of the polymer to balance the extra charge. As a result of the ion movements (and other processes) the volume of PPy will change during redox cycling (Figure 1. 11). It has been estimated that roughly three pyrrole monomers are associated with each positive charge in the fully oxidized state.

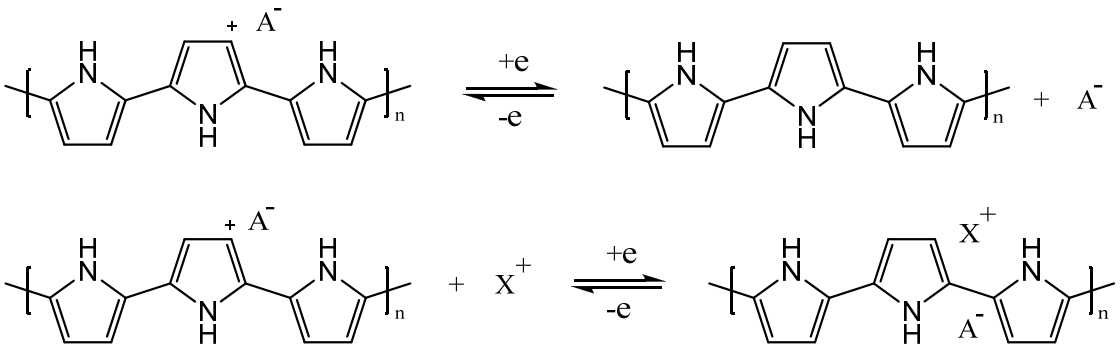

Figure 1. 11 The switching property of PPy where A^- represents anion incorporated into the polypyrrole, X^+ represents the cation from the electrolyte.

The changing of PPy redox state is always accompanied by ion exchange between the polymer and the surrounding electrolyte. Gandhi et al [68] summarized that in general cases, there are four-stages of oxidation/reduction process that may occur during actuation:

1) oxidation by cation ejection;

2) oxidation by anion incorporation;

3) reduction by anion ejection; and

4) reduction by cation incorporation.

These 4 processes are illustrated in Figure 1.11. While shown as two separate, reversible reactions, it is possible (perhaps likely) that both reactions occur simultaneously during oxidation and reduction of PPy.

It is commonly suggested that the size of ions being exchanged between the polymer and electrolyte will affect the magnitude of the actuation strain. It has been observed by Kaneto and co-workers that the strain was linearly proportional to the size of anion in poly(styrene sulfonate)-doped PPy [69]. Further investigations on TFSI derivatives ($(C_nF_{2n-1}SO_2)_2N^-$) as dopant reveal that the strain increased in the order of bis-nanofluorobutanessulfonyl-imide (NFSI)> bis-heptafluo-robutanessulfonyl-imide(HFSI)>bis-pentafluorobutanessulfonyl-imide PSFI> bis-trifluorobutanessulfonyl-imide (TFSI) [43]. These anions are of increasing size, supporting the idea that larger anions incorporated during oxidation of PPy cause a larger volume increase for a given amount of charge passed.

However, it is likely that there is a critical size beyond which increasing ion size will not bring more strain. Qi et al [70] used polyaniline films and found that anions smaller than Br^-, a larger strain was obtained for a larger anion. In their study, for anions' size of $Br^- > Cl^- > F^-$, the strain obtained followed this trend. Once the anions were larger than Br^-, $CF_3SO_3^- > ClO_4^- > BF_4^-$, the largest anion $CF_3SO_3^-$ produced the smallest strain. They concluded that when anions become larger, they will be more difficult to insert into the polymer chain. In such cases, the reduction of the polymer is favored by the incorporation of cations and subsequent oxidation involves ejection of cations and a volume decrease. It seems the size of Br^- is the critical value for the PANi

systems studied.

Experimental evidence supports the "cation-dominated" actuation in PPy prepared with large dopant anions. Those large ions are immobile and trapped within the polymer during polymerization and can't be easily released during subsequent reduction. Similarly, if large anions are found with the electrolyte they may be too large to penetrate inside the polymer. In such cases, the PPy redox occurs by cation exchange, leading to swelling on reduction and contraction on oxidation. So CPs actuators can be categorized as either cation driven or anion driven actuators. Mixed ion actuation has also been observed [65]. Polypyrrole doped with dodecylbenzenesulfonate (PPy/DBS) and polypyrrole doped with *p*-toluene sulfonic acid sodium salt (PPy/*p*TS) are two typical cation driven actuators, as only the small mobile cation like Na^+ can move in and out of polymer as pTS and DBS were trapped in the polymer bulk [71-73]. While in tetrabutylammonium hexafluorophosphate ($TBAPF_6$) system, because of the large size of TBA^+, the PF_6^- dominates actuation strain. In this case the actuation of PPy/PF_6 is mainly driven by anion movement.

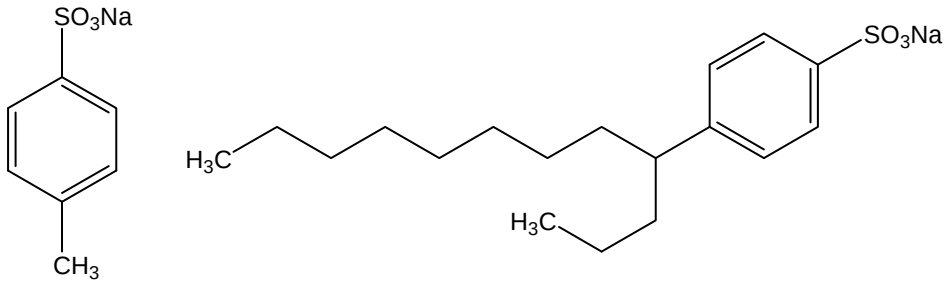

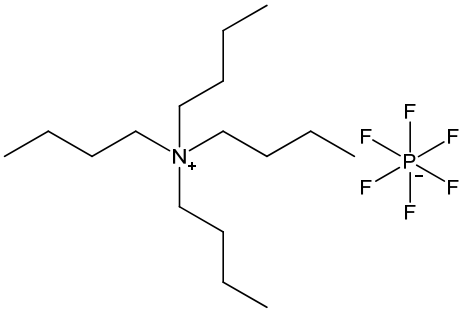

Figure 1. 12 The chemical formulas of Na*p*TS (top left), NaDBS (top right), $TBAPF_6$ (down).

Experimental studies show that there is no clear advantage offered by either cation-driven or anion-driven PPy actuators. . With 100kJ/m^3 work output, 2~3% of strain under 5 MPa and 0.06% efficiency was achieved using PPy/DBS system[74], which is comparable to most anion driven PPy actuators.

Besides ion movements, the solvent also plays a major role in the actuation process. It is realized that the solvent and solvated ions could accompany the doping/dedoping process [36, 75, 76]. In an aqueous electrolyte system, up to ten water molecules per one anion has been determined to enter the polymer during oxidation [77]. The size of solvated ions is significantly larger than naked ions; hence the actuation is strongly affected. The solvent transportation into and out of the polymer not only depends on the solvent bound to solvated ions, but an osmotic pressure can also drives a certain amount of solvent and creates actuation [78-80]. The osmotic pressure is derived from the difference in ion concentration within the polymer and compared to the ion concentration in the external electrolyte. In highly charged PPy, the ion concentration inside the polymer is higher that the surrounding electrolyte, this situation develops an osmotic pressure that drives solvent molecules into the polymer.

In conclusion, the actuation strain in PPy is influenced by many parameters. Dopant species, polymerization conditions, actuation test environment and actuator design will all strongly affect the performance.

1.4.3.3 Rate limits of actuation

One of the major limitations of CP actuators is their slow response compared with natural muscle. Understanding the rate limits of conducting polymers actuation enable actuator designers to evaluate and optimize performance. There are several aspects involved in determining the actuation rate of CP actuators, which are summarized below.

Now it is widely accepted that the charge exchange occurs first, which is between the interface of conducting polymer and electrode, following by transferring of the ions and solvent through the polymer/solution interface to balance the charge. The completeness of redox at a particular time depends on the arrival of ions and the conduction of electrons.

While applying anionic potential, the Fermi level of electrodes drops due to the applying of positive potential, the electrons will immediately left polymer to electrode and create positive charge center there. The anion will immigrate to balance the positive charge then the Fermi level of PPy raise up again. Thus the electrons could transfer into the electrode again. That process will repeat until the polymer is fully oxidized [81]. The process could be reversed when reducing the polymer. Since color change accompanies the change in redox state of PPy, the diffusion of ions can be observed in thin films and the diffusion coefficient of ion species could be estimated [82, 83].

Ions transfer in PPy is believed to be a diffusion process and can be illustrated by Fick's law. In semi-infinite system (diffusion in plate sheet e.g.),

$$\frac{\partial C}{\partial t} = D\frac{\partial^2 C}{\partial x^2}$$

where C is the concentration of ions at position x and time t. The boundary conditions

are:

$$C = C_0,\ x = 0,\ t > 0$$

and

$$C = 0,\ x > 0,\ t = 0$$

The solution is:

$$C = \frac{C_0 erfcx}{2\sqrt{Dt}}$$

As seen from the expression, the distance of penetration of any given concentration of ions is proportional to square root of time:

$$d_c = 2\sqrt{Dt}$$

in which D is diffusion coefficient; t refers to time and d_c represents charged layer thickness.

Diffusion coefficients measured by various experiments for ions diffusing through PPy is in the range of ~10^{-13} and ~10^{-11} m^2/s [84-86]. The value of the diffusion coefficient depends on the type of dopant ion involved, the solvent and the redox state of PPy. It has been concluded that diffusion in oxidized films is significantly quicker than in reduced films [87].

1.5 Strain calculation of conducting polymers actuators.

The ability to quantitatively predict the actuation response is most useful in desiging actuation systems. Conducting polymer actuators have been studied by various theoretical models based on experiment results. Different mechanisms have been proposed to calculate volume changes occurring during the redox cycling of CPs.

1.5.1 Strain to volumetric charge ratio

A simple way to connect charge and strain is using the strain to charge ratio (γ). As free strain (ε) is believed to be only function of charge. Thus:

$$\varepsilon = \gamma\rho$$

where ρ is the charge density (charge per unit volume of actuator material) passed through the polymer [88, 89]. The absolute value of γ is estimated approximately as $1 \sim 5*10^{-10} m^3/C$, depending on dopants and solvent [90, 91].

The strain to charge ratio predicts free strain quite well. But the model only focus on the charge passed. Later experiments shows that solvent driven by osmotic pressure can also contribute to the strain achieved [79]. However, the osmotic process is significant slower than charge-induced ion diffusion [92]. In short periods of time, the solvent induced strain is limited and can be neglected.

1.5.2 Solvent induced strain by osmotic pressure

Bay et al found that PPy is soft enough to be expanded by osmotic pressure [79]. Osmotic pressure could drive significant amount of solvent in thus causes strain. The osmotic pressure differences can be given by:

$$\pi = RT(\phi_p c_p - \phi_l \nu c_l)$$

where ϕ_p and ϕ_l is the osmotic coefficient in the polymer and electrolyte; c_p is the total concentration of free particles in polymer; c_l is the molar concentration; ν is the number of ions formed from one unit of electrolyte salt. Combining osmotic pressure (π), mechanic pressure (P) and the redox state depending on potential (E_p), the

changing in dimensions can be written as

$$l = f(\pi, P, E_p)$$

As mentioned before, it takes time to observe solvent induced strain during actuation [92]. Take PPy/DBS in 0.1M NaCl aqueous system for instance, a 1.9% of osmotic strain happens in time scale of 500s [92].

The effect must be considered for long time experiment, such as creeping test.

1.5.3 Strain caused by elastic modulus shifting

Actuators usually work against an external stress. To develop actuators for practical applications it is not sufficient to only discuss free strain. It is essential to consider how an external stress affects the strain generated by CP actuators[93].

Mechanical properties shift while switching the redox state of CPs [94, 95]. In some cases, the elastic modulus can increase 300% from the reduced state to the oxidized state[96]. Since the elastic modulus determines the strain response of a material that is subjected to a stress, then any changes in the elastic modulus will be very critical to the actuation response [93].

Through focusing on elastic modulus shift, Spinks et al [97] thoroughly discussed the influence of a changing modulus on the actuation. While under isotonic test, part of the actuation strain is caused by a change in modulus and it is estimated as:

$$\varepsilon_{elastic} = \sigma(\frac{1}{Y'} - \frac{1}{Y})$$

where σ refers to isotonic stress; Y is initial Young's modulus and Y' is the Young's modulus after the electrochemical potential has been applied. The simple linear-elastic model is quite successful in predicting the trend of actuation while under stress. If the

modulus in the expanded state is greater than the modulus in the contracted state, then changes in modulus will counteract against the "natural" actuation. If the actuation causes a contraction at zero load, then an additional expansion will occur when a load is applied due to the decrease in elastic modulus. The overall actuation can be taken as the sum of the two processes and an increasing load will lead to decreasing overall net strain. This situation has been observed widely in experiment [23, 69, 93, 98]. If the modulus is lower in the expanded state then an increasing load will lead to increasing net actuation strain [38]. If the modulus does not change during swelling/contraction of the actuator material then the actuation strain will be independent of the applied load.

As analyzed by Spinks et al[97], differences between Y' and Y also shift the work output of CPs actuators. Volumetric work per cycle is calculated from:

$$W_v = W/V = \frac{f * |\Delta l_f|}{S * l} = \sigma * |\varepsilon| = \sigma * (\varepsilon + \sigma * (\frac{1}{Y'} - \frac{1}{Y}))$$

where S and l are the cross-sectional area and the length of the sample; σ presents the isotonic stress applied; If $Y' \leq Y$ for an expanding actuation, the net strain increases with increasing stress, and high stress leads to high work output. If $Y' > Y$ for expanding actuation, an increasing stress will reduce the net strain, hence there will be a maximum value of work output and a particular stress.

1.5.4. Creep strain

Previous studies have noted that PPy suffers from creep, or irreversible, time-dependent strain when subject to an external stress [99]. As commonly occurs in other polymers, creep happens under load and over long time scales. Creep effects mean that the strain in polymers is a history dependant process. Higher loads and longer times

generate larger creep strains.

Creep and its recovery will shift final strain during actuation [100, 101]. Mechanical properties of PPy are known to change while changing the polymer's redox state [96].Secondly, it is known that solvent-saturated CPs are softer than in their dry state [102]. Due to those reasons, creep of CPs is complex. However, there is lacking a method of predicting the creep behavior of CPs. Such prediction is essential as for the purpose of accurate position control.

1.6 Performance of PPy actuators and their improvement.

1.6.1 The performance of PPy actuators

The performance of PPy actuators with common dopants is summarized in Table 1. 3. It is clearly seen that dopants and solvents play critically roles in determining the actuation performance. Despite the large differences in actuation strain, stress and work density, there is no clear and obvious explanation. As described above, the actuation strain is partly related to the size of the ions and the amount of solvent that enters or exits the polymer. It is also apparent that the effect of the voltage (or current) control can affect the measured performance, especially since the actuation response is rather slow. Finally, the actuation behavior is affected by the external loading conditions and changing mechanical properties of the polymer. Different studies reported in Table 1.3 have used different testing conditions. It is not known whether the differences in actuation performance relate to these testing differences or to more fundamental differences in the polymer composition or structure.

Table 1. 3 Summarizing the performance of PPy actuators.

Materials*	Testing media	Work density (kJ/m^3)	Typical strain (%)	Strain rate (%/s)	Operating stress (MPa)	References
PPy/PF_6 PPy/TFSI PPy/BF_4 PPy/ClO_4	$NaPF_6$ aqueous solution		11.2~12.4	0.7~0.8	10.6~22	[103]
PPy/PF_6	$TBAPF_6$-agar gel	40	2		0.5	[104]
PPy/PF_6	$TBAPF_6$ Propylene carbonate solution	2.8~35	0.2~1	0.01	1.4~3.5	[105]
PPy/TFSI	LiTFSI water & PC mixture	15	1.5	10.8		[106]
PPy/TFSI	NH_4PF_6 aqueous solution	140	6		3	[100]
PPy/DBS	NaCl aqueous solution	100	1.4		5	[74]
PPy/BF_4	$NaBF_4/NaCF_3SO_3$ aqueous solution		9.5		1.3	[107]
PPy/PF_6	BMIM BF_4		14		2.5	[108]
$PPy/Fe(CN)_6^{3-}$	LiCl/NaCl/KCl aqueous solution		1.2~2.3		Free load	[109]
PPy/DBS **	NaCl aqueous solution		5.6		0.6	[110]
PPy/BS	NaBS acetonitrile and aqueous mixture	73	1		3	[90]
PPy/PPs	$NaCl/RbCl/NaClO_4$ aqueous solution		1.2		5	[69]

*** Chemicals in the table: PF_6 hexafluorophosphate; BF_4 tetrafluoroborate; ClO_4 perchlorate; PPs phenolsulfonate; DBS dodecylbenzenesulfonate.**
****co-surfactant was added when polymerization happens**

1.6.2 Ways to improve PPy actuators.

There are already some devices based on PPy have been designed and developed. However, materials used in those devices can still be improved to better meet real application requirements.

Reduce the resistance

In macroscopic actuators, there are significant IR (current times resistance) drop along CP's length. Thus, the region close to electrode is fully oxidized and reduced. Regions far away electrode might not experience the same extent of redox process as IR drop reduces the effective voltage. Those regions will not actuate as much during potential scanning. Another issue is that CPs turns to insulators in the reduced state and hinders charge flows. Those issues relating to the electronic conductivity will limit the performance of CPs actuators.

A simple way to overcome such issues is to incorporate metal as a substrate to conduct charge. Hutchison et al [111] coated platinum onto electrochemically polymerized PPy film and achieved force density six times higher than unplatinised samples. Ding et al [112] utilized a tubular geometry and helical wire interconnects. A high work density of 83 kJ/m^3, fast contract rate 13%/s and >1% strain with 8 MPa stress was achieved. Later, those helix tubes were bundled to produce high force [113]. Similar work was performed by Hara et al [114]. PPy was electrochemically deposited on metal micro-coils and assembled in a multi-coil bundle. A huge force lifting 22 kg loads was obtained with a bundle that contained 1600 pieces of PPy coated metal coils.

Increase strain rate

Typical linear actuation strain rates in CPs are quite low. By embedding supporting electrode or carefully selecting dopants and solvents, strain rates can reach to ~10%/s [106, 112], which still 10 times lower than mammalian skeletal muscles. As described previously, the speed limiting step of actuation is believed to be the diffusion of ions. Reducing film thickness will be helpful to achieve high strain rates by reducing diffusion times. Smela et al achieved strain rate of 3%/s though testing a ultra thin PPy film (<3μm) [115]. Increasing applied voltage will also increase strain rate but can lead to degradation [116]. Short period of high potential is helpful to avoid rapid degradation. Electrolyte has resistance and cause ohmic (*IR*) drop across electrolyte. Such drop could consume some charge which doesn't contribute to actuation strain. Therefore, electrochemical potential at electrode/electrolyte surface is lower and actuation strain is slower. By using resistance compensation method, actuation strain could be increased [117]. Such method eliminates rate limiting effects and shifts the rate limit step to actuator itself.

Enhanced cycle life

Like natural muscle, some applications for artificial muscles will require a long working life yet many CP actuators degrade rapidly. The biological muscle is usually able to work for decades of years without replacing. An artificial urinary sphincter needs 16,000 working cycles for over 10 years (working 3~4times per day). A long working cycle life is also needed for actuators acting as a pump to help contract the heart: one

every second for at least 5 years—about 200 million cycles [99]. Unfortunately, there is no conducting polymer actuators that can last such a long time. Conformational change, degradation of electrolyte and overoxidation are three main reasons for instability. Degradation in the electroactivity of CPs has been reported when the cyclic voltammogram showed an obvious reduction in currents while cycling [118, 119]. Overoxidation of PPy results in dedoping of CPs and formation of carboxyl group and loss of conjugation [120]. Degradation of the electrolyte will also lead to failure of the PPy. Anodic oxidation of PC with water present will produce H_2CO_3. Nucleophilic HCO_3^- and OH^- then attack PPy chains, interrupting conjugation and diminishing conjugation length [121]. Obviously carefully selecting the electrolyte is helpful for improving the stability of PPy. Ionic liquids (ILs) are good choices as they are environmentally stable, have high ionic conductivity, high evaporating point and, most importantly, a wide potential window. Lu et al [122] described adopting ionic liquid as electrolyte for conducting polymer devices that lead to long periods of stable device performance. It has also been found that CPs have a stable CV in ionic liquid, indicating the electroactivity is maintained in ILs[118].

Conformational change in PPy can sometimes result in irreversible structural change, especially during reduction [123]. Otero et al [124] pointed out that during cathodic potential step, accompanied by positive charges on the polymer are neutralized and counter ions being expelled, polymeric chains will diffuse into the free volume left by counter ions. The ‘channel’ for ions in/out will be closed. To re-open those structures requires more energy and time. In normal electrochemistry tests, PPy becomes compacted during reduction and hinders the transfer of ions. Continued reduction from cycle to cycle can lead to a gradual compaction that diminishes the ability of the polymer to be oxidized. Later studies by same author found that such conformational

change is irreversible and responsible of degradation of PPy [86].

Spinks et al pointed out another possible source of instability of PPy [125]. During symmetrical cyclic voltammetry, instead of returning to its original redox state, PPy shifts towards a higher oxidized state from one cycle to another. Thus, a slow net oxidation of PPy causes a loss of redox capactity after several tens of cycles. In that study, current control provided a more stable electroactivity than voltage control. With current control, the amount of charge injected during oxidation could be matched to that occurring during reduction. After each cycle, the polymer was returned to the same redox state.

Reinforce of mechanical properties.

The mechanical properties of CPs measured in the dry and wet states are quite different. The elastic modulus and the tensile strength are much lower in wet state [102]. Hence, reinforcement of CPs becomes necessary in order to achieve higher working capacity. Building co-polymers or composites by introducing another strong material is an effective way for improving strength. Generally, mechanical properties of composite could be estimated through the 'rule if mixtures' approach. If using fibers to reinforce CPs, elastic modulus of composites is located between:

$$\frac{E_1 E_2}{(1-\alpha)E_2 + \alpha E_2} \le E_m \le (1-\alpha)E_1 + \alpha E_2$$

where E_1 and E_2 are the moduli of the CP and the reinforcement; E_m is the modulus of the composite; and α is the volume fraction of reinforcement. The left equation represents the case where the reinforcement is transverse to the fiber direction. The right side equation represents reinforcement along the fiber direction. If fibers are random

dispersed in CPs, then the modulus value should between those two extremes.

Carbon nanotube is an ideal material to be used as reinforcement. Individual CNT ropes have been shown to have an axial modulus of 640 GPa [126]. The carbon nanotubes fibers generated from fiber spinning process have modulus of 40 GPa [127]. Such high modulus indicates that theoretically, only a small amount of CNT will lead to substantial increasing on the modulus of CPs. The improvement on modulus and strength be adding carbon nanotubes to other polymers is significant [28, 128].

Also, carbon nanotubes have been shown to actuate and capable of producing 2500kJ/m^3 work density while electrical charged [129-132]. When CNTs are combined with CPs, the actuation of the new composites could be estimated as:

$$\varepsilon_c = \frac{\alpha_m \varepsilon_m E_m + \alpha_f \varepsilon_f E_f}{E_c}$$

where subscript c, m and f represent to composite, CPs matrix and carbon nanotube fibers respectively. E and V are the elastic moduli and volume fraction for each phase; ε refers to the actuation strain [28].

Another merit of adding CNTs is the improvement in the conductivity and efficieny of conducting charge. CNTs are claimed to have low resistance. The resistance of individual single carbon nanotube is less than 0.41 Ohm/m [133]. The addition of CNTs to CPs allows composites to conduct charge even when CPs have been reduced and become insulators.

1.6.3 PPy actuators examples

Bending type actuators

Through a sandwich structure design, linear actuation can be converted to bending actuation. A typical structure contains 2 PPy layers that forms the outside layers on either side of a polymer electrolyte layer in the middle. The polymer electrolyte layer could be solid state electrolyte or electrolyte saturated media (e.g. porous PVDF film).

Because the electrolyte layer and CP layers have already been integrated, benders are able to work in air. Once a voltage is applied, one PPy layer performs as cathode and the other performs as the anode. Since oxidation and reduction occur separately at both sides, expansion and contraction on each side will cause bending actuation (Figure 1. 13).

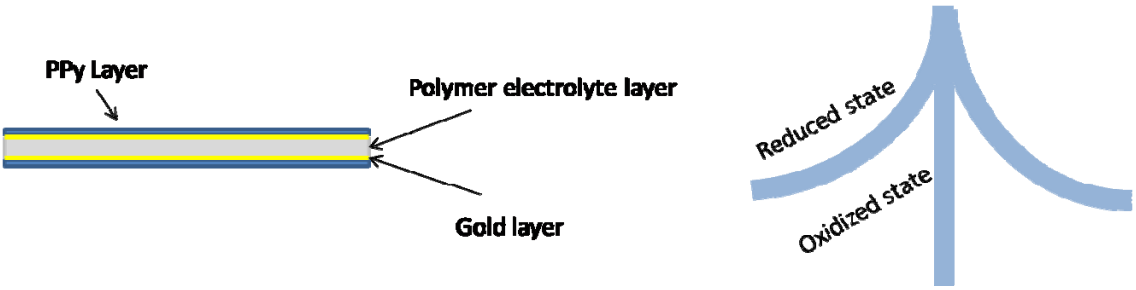

Figure 1. 13 Schematic structure of PPy bender and its working state.

One main issue with bending type actuators operating in air is a degradation process in performance over time. The reasons are mainly focused on two aspects: the evaporation of electrolyte and the delaminating of the tri-layer structure. By utilizing a high boiling point electrolyte, bender lifetime has been improved and some could keep working for weeks. Solid state electrolytes have also been used in bender technology. Otero et al [134] developed a solid state actuators based on PPy and poly(epichlorohydrin-co-ethylene oxide) (P(ECH-co-EO))/$LiCLO_4$ and observed an angular movement in the air. Polymer-in-Ionic-Liquid Electrolytes (PILE) combined good rubbery compliance and high conductivity and was first used in actuators as electrolytes. PPy trilayer bending actuators using PILE have been working in air for 2

months without any degradation [135]. Bucky gels, which are made from carbon nanotube and ionic liquid, also can make actuators working lasts for a long time without notable degradation [136].

The delaminating of layers in the sandwich structure can cause deterioration in performance. Delaminating can be restricted by increasing the roughness of metal layers. The adhesion between roughened gold and PPy is significant stronger than smooth on smooth gold layers [137].

The evaluation of bender movement has been carried out through building models. Philippe et al [138] established a lumped-parameter model for PPy actuators. Smela et al [139]also modeled and characterized PPy (DBS) bilayer microactuators. Alici et al [140] built up scalable models for tri-layer conjugated polymers.

Benders are semi-finished products that have been utilized in some prototype devices. One direct use it in building a robotic fish fins [141]. Another application is used in the cochlear implant [142].

Microfluidic pump

The design of the microfluidic pump shown in Figure 1.14 is based on the expansion/contraction of concentric PPy tubes [143]. Application of a reducing voltage (e.g. -1 V) at one end of the pump assembly will cause contraction to start at this inlet end. With time the contraction progresses along the whole pump length until reaching full contraction. Upon switching to an oxidizing voltage, the expansion will follow the same path until whole pump becomes fully expanded. Such expansion and contraction could transfer several μL of liquids.

Other pumps based on expansion and contraction of PPy actuators have also been

developed [144-146].

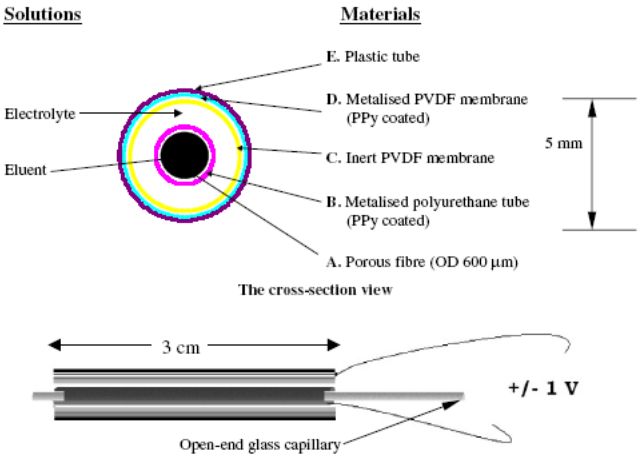

Figure 1. 14 The structure of microfluidic pump [143].

Braille cell

A multi-dot Braille cell has been proposed that utilizes CP actuators [147]. By using this technology, a 2-D Braille screen could be developed to help visually disabled people. The Braille cell consists of an array of pins which each end connected to a PPy hollow actuator tube (Figure 1. 15). The pins can be lowered or raised up by contraction or expansion of the PPy. The individual pin are well controlled hence the different pattern of raised dots will form. Thus, the visually disabled people could learn information on the screen through the changing of dot patterns.

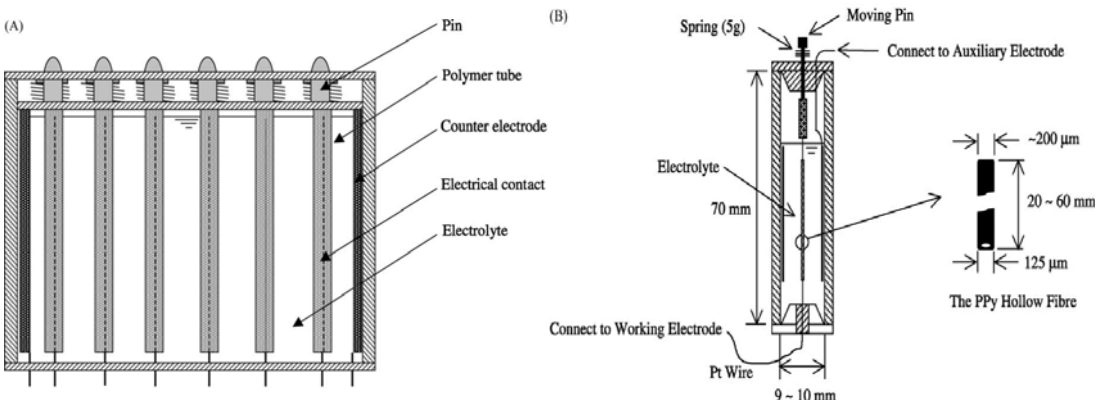

Figure 1. 15 Schematic diagrams of Braille cell (left) and single pin (right) [112].

1.7 Research Questions

As described in Section 1.6.3, actuating devices require accurate position control in most applications. Robotic fish need to control the moving speed and direction which is determined by the amplitude, speed and average position of PPy benders. Similarly, the failure of position control of the cochlear implant during assisted surgical insertion using a CP actuator will cause major problems. Pumps for microfluidics only transfer several μl of liquid, thus a high level of position control is required. In Braille cells the loss of position control will deliver the wrong information.

Can PPy actuators meet these demands? This is the central question of this thesis. Obviously, position control is a result of strain control. Hence, all factors contributing to the total strain must be evaluated. As pointed out at the beginning, actuation strain is believed to be a combination of free strain, elastic strain and creep strain.

$$\varepsilon = \varepsilon_{actuation} + \varepsilon_{elastic} + \varepsilon_{creep}$$

However, there are still not enough known about the total strain of CPs during actuation. Nor is it known whether it is appropriate to separate the three contributions as suggested by the above equation. In this thesis, the most important factors that affect strain are discussed. Each is summarized below.

Free strain

Free strain is induced by charge. An important parameter connecting strain and charge is called the strain:charge ratio (γ). It allows us to judge the capacity of strain generation efficiency of CPs. Samples having different compositions can be compared

in terms of their strain:charge ratios. As widely seen in the literature, increasing scan rate will reduce strain in CP actuators. Most researchers relate the decline in strain at higher scan rates to be due to incomplete charging. The strain:charge ratio may, therefore, be constant with scan rate. There is little information in the literature regarding how scan rate affects this ratio.

One aim of this thesis is to measure the strain:charge ratio of different PPy materials and under different actuation conditions. The objective is to determine how useful the strain:charge ratio is in predicting strain output and discriminating between different PPy compositions.

Effect of redox state on PPy mechanical properties

Elastic strain contribution to actuation is caused by a changing elastic modulus upon the application of a voltage to CPs. This effect has been thoroughly studied. However, viscoelastic parameters under different redox state have not been investigated yet. PPy is known to be viscoelastic and suffer from creep. The importance of these processes to position control and the speed of actuation in CPs have not been examined in the literature.

A second aim of this thesis is to characterize the viscoelasticity of PPy actuator materials and determine how the redox properties are affected by the polymer's redox state.

Modeling

The position control of PPy actuators needs useable and accurate models to predict

the strain response from an input. New models which combine the electrochemical actuation and viscoelastic actuation are required. This thesis attempts to develop such models.

1.8 Structure of thesis

The following chapter describes the general experimental details.

Chapter three will focus on evaluating the strain:charge characteristics of well-studied PPy helix tube actuators. Tube thicknesses were varied as was the scan rate so as to cause only partially completed redox reactions during a voltage cycle. In addition, the strain generated against different operating stresses is analyzed. At the end, work-stress and power-stress relationships will be explored.

Chapter four will considers the performance of high strain PPy/TFSI actuators. The cycle-to-cycle degradation of PPy/TFSI was investigated and at last, operation conditions were optimized.

In chapter five, the viscoelastic behavior of PPy/TFSI films under different redox states was discussed. An empirical model which combines creep actuation will be built to predict the deformation of PPy actuators.

Finally, a general conclusion and future work is given in chapter six.

1.9 References:

1. Shirakawa, H., Louis, E.J., Macdiarmid, A.G., Chiang, C.K. and Heeger, A.J., *Synthesis of Electrically Conducting Organic Polymers - Halogen Derivatives of Polyacetylene, (Ch)X.* Journal of the Chemical Society-Chemical Communications, 1977(16): p. 578-580.
2. Baughman, R.H., *Conducting Polymer Actuators and Related Devices.* Abstracts of Papers of the American Chemical Society, 1994. **208**: p. 385-PMSE.
3. Baughman, R.H., *Conducting Polymer Artificial Muscles.* Synthetic Metals, 1996. **78**(3): p. 339-353.
4. BA Bolto, R.M., DE Weiss, *Electronic Conduction in Polymers. Part3. Electronic Properties of Polypyrrole.* Australian Journal of Chemistry, 1963. **16**(6): p. 13.
5. Bredas, J.L. and Street, G.B., *Polarons, Bipolarons, and Solitons in Conducting Polymers.* Accounts of Chemical Research, 1985. **18**(10): p. 309-315.
6. Diaz, A.F., Kanazawa, K.K. and Gardini, G.P., *Electrochemical Polymerization of Pyrrole.* Journal of the Chemical Society-Chemical Communications, 1979(14): p. 635-636.
7. Diaz, A.F. and Logan, J.A., *Electroactive Polyaniline Films.* Journal of Electroanalytical Chemistry, 1980. **111**(1): p. 111-114.
8. Waltman, R.J., Bargon, J. and Diaz, A.F., *Electrochemical Studies of Some Conducting Polythiophene Films.* Journal of Physical Chemistry, 1983. **87**(8): p. 1459-1463.
9. Gurunathan, K., Murugan, A.V., Marimuthu, R., Mulik, U.P. and Amalnerkar, D.P., *Electrochemically Synthesised Conducting Polymeric Materials for Applications Towards Technology in Electronics, Optoelectronics and Energy Storage Devices.* Materials Chemistry and Physics, 1999. **61**(3): p. 173-191.
10. Roncali, J., *Conjugated Poly(Thiophenes) - Synthesis, Functionalization, and Applications.* Chemical Reviews, 1992. **92**(4): p. 711-738.
11. Beaujuge, P.M. and Reynolds, J.R., *Color Control in Pi-Conjugated Organic Polymers for Use in Electrochromic Devices.* Chemical Reviews. **110**(1): p. 268-320.
12. Gerard, M., Chaubey, A. and Malhotra, B.D., *Application of Conducting Polymers to Biosensors.* Biosensors & Bioelectronics, 2002. **17**(5): p. 345-359.
13. Killian, J.G., Coffey, B.M., Gao, F., Poehler, T.O. and Searson, P.C., *Polypyrrole Composite Electrodes in an All-Polymer Battery System.* Journal of the Electrochemical Society, 1996. **143**(3): p. 936-942.
14. Mirfakhrai, T., Madden, J.D.W. and Baughman, R.H., *Polymer Artificial Muscles.* Materials Today, 2007. **10**(4): p. 30-38.
15. Spinks, G.M., Dominis, A.J., Wallace, G.G. and Tallman, D.E., *Electroactive Conducting Polymers for Corrosion Control - Part 2. Ferrous Metals.* Journal of Solid State Electrochemistry, 2002. **6**(2): p. 85-100.
16. Abidian, M.R., Kim, D.H. and Martin, D.C., *Conducting-Polymer Nanotubes for Controlled Drug Release.* Advanced materials, 2006. **18**(4): p. 405-+.
17. Williams, E.L., et al., *Conducting Polymer and Hydrogenated Amorphous Silicon Hybrid Solar Cells.* Applied Physics Letters, 2005. **87**(22): p. 3.
18. Madden, J.D.W., et al., *Artificial Muscle Technology: Physical Principles and Naval Prospects.* Ieee Journal of Oceanic Engineering, 2004. **29**(3): p. 706-728.
19. Otero, T.F. *Reactive Conducting Polymers as Actuating Sensors and Tactile Muscles*. in *Conference on Toward Autonomous Robotic Systems 2007*. 2007.

Aberystwyth, WALES: Iop Publishing Ltd.
20. Genies, E.M., Boyle, A., Lapkowski, M. and Tsintavis, C., *Polyaniline - a Historical Survey.* synthetic metals, 1990. **36**(2): p. 139-182.
21. Kaneto, K., Kaneko, M., Min, Y. and Macdiarmid, A.G., *Artificial Muscle - Electromechanical Actuators Using Polyaniline Films.* synthetic metals, 1995. **71**(1-3): p. 2211-2212.
22. Smela, E. and Mattes, B.R., *Polyaniline Actuators - Part 2. Pani(Amps) in Methanesulfonic Acid.* Synthetic Metals, 2005. **151**(1): p. 43-48.
23. Smela, E., Lu, W. and Mattes, B.R., *Polyaniline Actuators: Part 1. Pani(Amps) in Hcl.* Synthetic Metals, 2005. **151**(1): p. 25-42.
24. Kaneko, M., Fukui, M., Takashima, W. and Kaneto, K., *Electrolyte and Strain Dependences of Chemomechanical Deformation of Polyaniline Film.* synthetic metals, 1997. **84**(1-3): p. 795-796.
25. Kaneko, M. and Kaneto, K., *Electrochemomechanical Deformation of Polyaniline Films Doped with Self-Existent and Giant Anions.* Reactive and Functional Polymers, 1998. **37**(1-3): p. 155-161.
26. Desilvestro, J., Scheifele, W. and Haas, O., *Insitu Determination of Gravimetric and Volumetric Charge-Densities of Battery Electrodes - Polyaniline in Aqueous and Nonaqueous Electrolytes.* Journal of the Electrochemical Society, 1992. **139**(10): p. 2727-2736.
27. Mazzoldi, A., DeglInnocenti, C., De Rossi, M. D., *Actuative Properties of Polyaniline Fibers under Electrochemical Stimulation* Mater. Sci. Eng. C, 1998. **6**: p. 65-72.
28. Spinks, G.M., Mottaghitalab, V., Bahrami-Saniani, M., Whitten, P.G. and Wallace, G.G., *Carbon-Nanotube-Reinforced Polyaniline Fibers for High-Strength Artificial Muscles.* Advanced Materials, 2006. **18**(5): p. 637.
29. Mattes, B.R., et al., *Formation of Conductive Polyaniline Fibers Derived from Highly Concentrated Emeraldine Base Solutions.* synthetic metals, 1997. **84**(1-3): p. 45-49.
30. Wang, H.L., Romero, R.J., Mattes, B.R., Zhu, Y.T. and Winokur, M.J., *Effect of Processing Conditions on the Properties of High Molecular Weight Conductive Polyaniline Fiber.* Journal of Polymer Science Part B-Polymer Physics, 2000. **38**(1): p. 194-204.
31. Adams, P.N., Bowman, D., Brown, L., Yang, D. and Mattes, B.R., *Molecular Weight Dependence of the Physical Properties of Protonated Polyaniline Films and Fibers*, in *Smart Structures and Materials 2001: Electroactive Polymer Actuators and Devices*, Y. BarCohen, Editor. 2001, Spie-Int Soc Optical Engineering: Bellingham. p. 475-481.
32. Huang, W.S., Humphrey, B.D. and Macdiarmid, A.G., *Polyaniline, a Novel Conducting Polymer - Morphology and Chemistry of Its Oxidation and Reduction in Aqueous-Electrolytes.* Journal of the Chemical Society-Faraday Transactions I, 1986. **82**: p. 2385-&.
33. Pei, Q.B. and Inganas, O., *Electroelastomers - Conjugated Poly(3-Octylthiophene) Gels with Controlled Cross-Linking.* synthetic metals, 1993. **57**(1): p. 3724-3729.
34. Irvin, D.J., Goods, S.H. and Whinnery, L.L., *Direct Measurement of Extension and Force in Conductive Polymer Gel Actuators.* Chemistry of Materials, 2001. **13**(4): p. 1143-1145.
35. Marsella, M.J., Reid, R.J. and McCormick, M.T., *A New Technique for Monitoring Real-Time Dimensional Changes in Polymeric Electromechanical*

Actuators and Vaporesistive Sensors. synthetic metals, 2001. **118**(1-3): p. 171-174.

36. Chen, X.W. and Inganas, O., *Doping-Induced Volume Changes in Poly(3-Octylthiophene) Solids and Gels.* synthetic metals, 1995. **74**(2): p. 159-164.
37. Fuchiwaki, M., Takashima, W. and Kaneto, K., *Soft Actuators Based on Poly(3-Alkyl Thiophene) Films Upon Electrochemical Oxidation and Reduction.* Molecular Crystals and Liquid Crystals, 2002. **374**: p. 513-520.
38. Xi, B., et al., *Poly(3-Methylthiophene) Electrochemical Actuators Showing Increased Strain and Work Per Cycle at Higher Operating Stresses.* Polymer, 2006. **47**(22): p. 7720-7725.
39. Wu, Y., et al., *Electrochemical Actuation Properties of a Novel Solution-Processable Polythiophene.* Electrochimica Acta, 2007. **53**(4): p. 1830-1836.
40. Bay, L., West, K., Sommer-Larsen, P., Skaarup, S. and Benslimane, M., *A Conducting Polymer Artificial Muscle with 12% Linear Strain.* Advanced Materials, 2003. **15**(4): p. 310-313.
41. Susumu Hara, Tetsuji Zama, Wataru Takashima and Kaneto, K., *Free-Standing Gel-Like Polypyrrole Actuators Doped with Bis(Perfluroroalkylsulfonyl)Imide Exhibiting Extremely Large Strain* smart materials and structures, 2005. **15**: p. 1501-1510.
42. Hara, S., Zama, T., Takashima, W. and Kaneto, K., *Tfsi-Doped Polypyrrole Actuator with 26% Strain.* Journal of Materials Chemistry, 2004. **14**(10): p. 1516-1517.
43. Hara, S., Zama, T., Takashima, W. and Kaneto, K., *Gel-Like Polypyrrole Based Artificial Muscles with Extremely Large Strain.* Polymer Journal, 2004. **36**(11): p. 933-936.
44. Hara, S., Zama, T., Takashima, W. and Kaneto, K., *Tris(Trifluoromethylsulfonyl)Methide-Doped Polypyrrole as a Conducting Polymer Actuator with Large Electrochemical Strain.* synthetic metals, 2006. **156**(2-4): p. 351-355.
45. Kanazawa, K.K., et al., *Organic Metals - Polypyrrole, a Stable Synthetic Metallic Polymer.* Journal of the Chemical Society-Chemical Communications, 1979(19): p. 854-855.
46. Castillo-Ortega, M.M., Inoue, M.B. and Inoue, M., *Chemical Synthesis of Highly Conducting Polypyrrole by the Use of Copper(Ii) Perchlorate as an Oxidant.* synthetic metals, 1989. **28**(1-2): p. 65-70.
47. Mohammadi, A., Lundstrom, I., Salaneck, W.R. and Inganas, O., *Polypyrrole Prepared by Chemical Vapor-Deposition Using Hydrogen-Peroxide and Hydrochloric Acid.* synthetic metals, 1987. **21**(2): p. 169-173.
48. Ng, S.C., Chan, H.S.O., Xia, J.F. and Yu, W.L., *Electrically Conductive Graft Copolymers of Poly(Methyl Methacrylate) with Varying Polypyrrole and Poly(3-Alkylpyrroles) Contents.* Journal of Materials Chemistry, 1998. **8**(11): p. 2347-2352.
49. Wu, A.M., Kolla, H. and Manohar, S.K., *Chemical Synthesis of Highly Conducting Polypyrrole Nanofiber Film.* macromolecules, 2005. **38**(19): p. 7873-7875.
50. Bai, H. and Shi, G.Q., *Gas Sensors Based on Conducting Polymers.* Sensors, 2007. **7**(3): p. 267-307.
51. E.M. Geniesa, G.B.a.A.F.D., *Spectroelectrochemical Study of Polypyrrole Films* Journal of Electroanalytical Chemistry, 1983. **149**(1-2): p. 13.
52. Robert J. Waltman and Bargon, J., *Reactivity/Structure Correlations for the*

Electropolymerization of Pyrrole: An Indo/Cndo Study of the Reactive Sites of Oligomeric Radical Cations Tetrahedron, 1984. **40**(20): p. 8.

53. Robert J. Waltman and Bargon, J., *The Electropolymerization of Polycyclic Hydrocarbons: Substituent Effects and Reactivity/Structure Correlations* Journal of Electroanalytical Chemistry, 1985. **194**(1): p. 14.
54. Street, G.B., *Handbook of Conducting Polymers*. 1986, Marcel Deckker: New York. p. 188.
55. Zotti, G., Schiavon, G., Berlin, A. and Pagani, G., *The Role of Water in the Electrochemical Polymerization of Pyrroles.* Electrochimica Acta, 1989. **34**(6): p. 881-884.
56. Otero, T.F. and Rodriguez, J., *Role of Protons on the Electrochemical Polymerization of Pyrrole from Acetonitrile Solutions.* Journal Of Electroanalytical Chemistry, 1994. **379**(1-2): p. 513-516.
57. Otero, T.F. and Rodriguez, J., *Parallel Kinetic-Studies of the Electrogeneration of Conducting Polymers - Mixed Materials, Composition and Properties Control.* Electrochimica Acta, 1994. **39**(2): p. 245-253.
58. Zhou, M. and Heinze, J., *Electropolymerization of Pyrrole and Electrochemical Study of Polypyrrole. 3. Nature Of "Water Effect" In Acetonitrile.* Journal of Physical Chemistry B, 1999. **103**(40): p. 8451-8457.
59. Kanazawa, K.K., et al., *Polypyrrole - an Electrochemically Synthesized Conducting Organic Polymer.* synthetic metals, 1980. **1**(3): p. 329-336.
60. Downard, A.J. and Pletcher, D., *The Influence of Water on the Electrodeposition of Polypyrrole in Acetonitrile.* Journal of Electroanalytical Chemistry, 1986. **206**(1-2): p. 139-145.
61. Street, G.B., Lindsey, S.E., Nazzal, A.I. and Wynne, K.J., *The Structure and Mechanical-Properties of Polypyrrole.* Molecular Crystals and Liquid Crystals, 1985. **118**(1-4): p. 137-148.
62. Satoh, M., Kaneto, K. and Yoshino, K., *Dependences of Electrical and Mechanical-Properties of Conducting Polypyrrole Films on Conditions of Electrochemical Polymerization in an Aqueous-Medium.* synthetic metals, 1986. **14**(4): p. 289-296.
63. Ogasawara, M., Funahashi, K., Demura, T., Hagiwara, T. and Iwata, K., *Enhancement of Electrical-Conductivity of Polypyrrole by Streching.* synthetic metals, 1986. **14**(1-2): p. 61-69.
64. Shu Yi Chu and al, e., *Effect of Deposition Current Density on the Linear Actuation Behavior of Ppy (Cf3so3) Films.* Current Applied Physics, 2008. **8**: p. 4.
65. Sui, J., Travas-Sejdic, J., Chu, S.Y., Li, K.C. and Kilmartin, P.A., *The Actuation Behavior and Stability of P-Toluene Sulfonate Doped Polypyrrole Films Formed at Different Deposition Current Densities.* Journal of Applied Polymer Science, 2009. **111**(2): p. 876-882.
66. Ashrafi, A., Golozar, M.A. and Mallakpour, S., *Morphological Investigations of Polypyrrole Coatings on Stainless Steel.* synthetic metals, 2006. **156**(18-20): p. 1280-1285.
67. Bufon, C.C.B., et al., *Relationship between Chain Length, Disorder, and Resistivity in Polypyrrole Films.* Journal of Physical Chemistry B, 2005. **109**(41): p. 19191-19199.
68. Gandhi, M.R., Murray, P., Spinks, G.M. and Wallace, G.G., *Mechanism of Electromechanical Actuation in Polypyrrole.* Synth. Met., 1995. **73**(3): p. 247-256.

69. Sonoda, Y., Takashima, W. and Kaneto, K., *Characteristics of Soft Actuators Based on Polypyrrole Films.* synthetic metals, 2001. **119**(1-3): p. 267-268.
70. Qi, B., Lu, W., Mattes, B. R.,, *Strain and Energy Efficiency of Polyaniline Fibre Electrochemical Actuators in Aqueous Electrolytes.* J. Phys.Chem.B, 2004. **108**: p. 6222-6227.
71. Pei, Q. and Inganaes, O., *Electrochemical Applications of the Bending Beam Method. 2. Electroshrinking and Slow Relaxation in Polypyrrole.* The Journal of Physical Chemistry, 1993. **97**(22): p. 6034-6041.
72. Pei, Q.B. and Inganas, O., *Electrochemical Applications of the Bending Beam Method, a Novel Way to Study Ion-Transport in Electroactive Polymers.* Solid State Ionics, 1993. **60**(1-3): p. 161-166.
73. Matencio, T., Depaoli, M.A., Peres, R.C.D., Torresi, R.M. and Detorresi, S.I.C., *Ionic Exchanges in Dodecylbenezesulfonate Doped Polypyrrole.1. Optical Beam Deflection Studies.* synthetic metals, 1995. **72**(1): p. 59-64.
74. Fujisue, H., Sendai, T., Yamato, K., Takashima, W. and Kaneto, K., *Work Behaviors of Artificial Muscle Based on Cation Driven Polypyrrole.* Bioinspiration & Biomimetics, 2007. **2**(2): p. S1-S5.
75. Otero, T.F., *Soft, Wet, and Reactive Polymers. Sensing Artificial Muscles and Conformational Energy.* Journal of Materials Chemistry, 2009. **19**(6): p. 681-689.
76. Maia, G., Torresi, R.M., Ticianelli, E.A. and Nart, F.C., *Charge Compensation Dynamics in the Redox Processes of Polypyrrole-Modified Electrodes.* Journal of Physical Chemistry, 1996. **100**(39): p. 15910-15916.
77. Pruneanu, S., Csahok, E., Kertesz, V. and Inzelt, G., *Electrochemical Quartz Crystal Microbalance Study of the Influence of the Solution Composition on the Behaviour of Poly(Aniline) Electrodes.* Electrochimica Acta, 1998. **43**(16-17): p. 2305-2323.
78. Bruckenstein, S., Chen, J.H., Jureviciute, I. and Hillman, A.R., *Ion and Solvent Transfers Accompanying Redox Switching of Polypyrrole Films Immersed in Divalent Anion Solutions.* Electrochimica Acta, 2009. **54**(13): p. 3516-3525.
79. Bay, L., Jacobsen, T., Skaarup, S. and West, K., *Mechanism of Actuation in Conducting Polymers: Osmotic Expansion.* J. Phys. Chem. B, 2001. **105**: p. 8492-8497.
80. Okuzaki, H., Kondo, T. and Kunugi, T., *Characteristics of Water in Polypyrrole Films.* Polymer, 1999. **40**(4): p. 995-1000.
81. Wang, X.Z. and Smela, E., *Experimental Studies of Ion Transport in Ppy(Dbs).* Journal of Physical Chemistry C, 2009. **113**(1): p. 369-381.
82. Xuezheng Wang, B.S., Elisabeth Smela, *Visualizing Ion Currents in Conjugated Polymers.* Advanced materials, 2004. **16**: p. 1605-1609.
83. Wang, X.Z. and Smela, E., *Color and Volume Change in Ppy(Dbs).* Journal of Physical Chemistry C, 2009. **113**(1): p. 359-368.
84. Tso, C.H., Madden, J.D. and Michal, C.A., *An Nmr Study of Pf6- Ions in Polypyrrole.* synthetic metals, 2007. **157**(10-12): p. 460-466.
85. West, K., Careem, M.A. and Skaarup, S., *An Impedance Study of the Doping of Polypyrrole in Liclo4/Pc.* Solid State Ionics, 1993. **60**(1-3): p. 153-159.
86. Otero, T.F., Marquez, M. and Suarez, I.J., *Polypyrrole: Diffusion Coefficients and Degradation by Overoxidation.* Journal Of Physical Chemistry B, 2004. **108**(39): p. 15429-15433.
87. Mostany, J. and Scharifker, B.R., *Impedance Spectroscopy of Undoped, Doped and Overoxidized Polypyrrole Films.* synthetic metals, 1997. **87**(3): p. 179-185.
88. Madden, J., et al., *Artificial Muscle Technology: Physical Principles and Naval*

Prospects. IEEE J. of Oceanic Engineering, 2004. **29**: p. 706-729.
89. Madden, J.D., Madden, P.G. and Hunter, I.W., *Characterization of Polypyrrole Actuators: Modeling and Performance*, in *Proceedings of Spie 8th Annual Symposium on Smart Structures and Materials: Electroactive Polymer Actuators and Devices*, Y. Bar-Cohen, Editor. 2001, SPIE: Bellingham WA. p. 72-83.
90. DellaSanta, A., DeRossi, D. and Mazzoldi, A., *Performance and Work Capacity of a Polypyrrole Conducting Polymer Linear Actuator.* synthetic metals, 1997. **90**(2): p. 93-100.
91. Pei, Q.B.a.I., O., , *Electrochemical Application of the Bending Beam Method. 1. Mass Transport and Volume Changes in Polypyrrole During Redox.* J. Phys.Chem., 1992. **96**: p. 10507-10514.
92. Jafeen, M.J.M., Careem, M.A. and Skaarup, S., *Speed and Strain of Polypyrrole Actuators: Dependence on Cation Hydration Number.* Ionics, 2010. **16**(1): p. 1-6.
93. Spinks, G.M., Liu, L., Zhou, D. and Wallace, G.G., *Strain Response from Polypyrrole Actuators under Load.* Advanced Functional Materials, 2002. **12**(6-7): p. 437-440.
94. Murray, P., Spinks, G.M., Wallace, G.G. and Burford, R.P. *In-Situ Mechanical Properties of Tosylate Doped (Pts) Polypyrrole*. in *International Conference on the Science and Technology of Synthetic Metals*. 1996. Snowbird, Ut: Elsevier Science Sa Lausanne.
95. Murray, P., Spinks, G.M., Wallace, G.G. and Burford, R.P., *Electrochemical Induced Ductile-Brittle Transition in Tosylate-Doped (Pts) Polypyrrole.* synthetic metals, 1998. **97**(2): p. 117-121.
96. Pytel, R.Z., Thomas, E.L. and Hunter, I.W., *In Situ Observation of Dynamic Elastic Modulus in Polypyrrole Actuators.* Polymer, 2008. **49**(8): p. 2008-2013.
97. Spinks, G.M. and Truong, V.-T., *Work-Per-Cycle Analysis for Electromechanical Actuators.* Sensors and Actuators A: Physical, 2005. **119**(2): p. 455-461.
98. Kaneto, K., Fujisue, H., Yamato, K. and Takashima, W., *Load Dependence of Soft Actuators Based on Polypyrrole Tubes.* Thin Solid Films, 2008. **516**(9): p. 2808-2812.
99. Madden J.D, Rinderknecht D., Anquetil P.A and I.W, H., *Creep and Cycle Life in Polypyrrole Actuators.* Sensors and Actuators A: Physical, 2007. **133**: p. 210-217.
100. Kaneto, K., Fujisue, H., Kunifusa, M. and Takashima, W., *Conducting Polymer Soft Actuators Based on Polypyrrole Films - Energy Conversion Efficiency.* Smart Materials & Structures, 2007. **16**(2): p. S250-S255.
101. Kaneto, K., Suematsu, H. and Yamato, K., *Training Effect and Fatigue in Polypyrrole-Based Artificial Muscles.* Bioinspiration & Biomimetics, 2008. **3**(3): p. 6.
102. Otero, T.F., Cascales, J.J.L. and Arenas, G.V., *Mechanical Characterization of Free-Standing Polypyrrole Film.* Materials Science & Engineering C-Biomimetic and Supramolecular Systems, 2007. **27**(1): p. 18-22.
103. Zama, T., Hara, S., Takashima, W. and Kaneto, K., *Comparison of Conducting Polymer Actuators Based on Polypyrrole Doped with Bf4(-), Pf6(-), Cf3so3-, and Clo4.* Bulletin of the Chemical Society of Japan, 2005. **78**(3): p. 506-511.
104. Madden, J.D., Cush, R.A., Kanigan, T.S., Brenan, C.J. and Hunter, I.W., *Encapsulated Polypyrrole Actuators.* Synth. Met., 1999. **105**(1): p. 61-64.
105. Spinks, G.M., Wallace, G.G., Liu, L. and Zhou, D., *Conducting Polymers Electromechanical Actuators and Strain Sensors.* Macromolecular Symposia, 2003. **192**(1): p. 161-170.

106. Hara, S., Zama, T., Takashima, W. and Kaneto, K., *Free-Standing Polypyrrole Actuators with Response Rate of 10.8% S(-1).* Synthetic Metals, 2005. **149**(2-3): p. 199-201.
107. Skaarup, S., Bay, L. and West, K., *Polypyrrole Actuators Working at 2-30 Hz.* synthetic metals, 2007. **157**(6-7): p. 323-326.
108. Anquetil, P.A., Rinderknecht, D., Vandesteeg, N.A., Madden, J.D. and Hunter, I.W., *Large Strain Actuation in Polypyrrole Actuators*, in *Smart Structures and Materials 2004: Electroactive Polymer Actuators and Devices*, Y. BarCohen, Editor. 2004, Spie-Int Soc Optical Engineering: Bellingham. p. 380-387.
109. Rajesh, Pandey, S.S., Kumar, D., Takashima, W. and Kaneto, K., *Electrochemomechanical Deformation Studies of [Fe(Cn)(6)](3-) Ion Doped Conducting Polypyrrole Film.* Thin Solid Films, 2004. **467**(1-2): p. 227-230.
110. Bay, L., West, K. and Skaarup, S., *Pentanol as Co-Surfactant in Polypyrrole Actuators.* Polymer, 2002. **43**(12): p. 3527-3532.
111. Hutchison, A.S., Lewis, T.W., Moulton, S.E., Spinks, G.M. and Wallace, G.G., *Development of Polypyrrole Based Electromechanical Actuators.* Synthetic Metals, 2000. **113**: p. 121-127.
112. Ding, J., et al., *High Performance Conducting Polymer Actuators Utilising a Tubular Geometry and Helical Wire Interconnects.* Synthetic Metals, 2003. **138**: p. 391-398.
113. Spinks, G.M., Campbell, T.E. and Wallace, G.G., *Force Generation from Polypyrrole Actuators.* Smart Materials & Structures, 2005. **14**(2): p. 406-412.
114. Susumu Hara, T.Z., Wataru Takashimab, Keiichi Kanetob, *Polypyrrole–Metal Coil Composite Actuators as Artificial Muscle Fibres.* synthetic metals, 2004. **146**: p. 47-55.
115. Smela, E. and Gadegaard, N., *Surprising Volume Change in Ppy(Dbs): An Atomic Force Microscopy Study.* Advanced Materials, 1999. **11**(11): p. 953-+.
116. Otero, T.F., *Handbook of Organic and Conductive Molecules and Polymers*. Vol. 4. 1997, Chichester: Wiley.
117. Barisci, J.N., Spinks, G.M., Wallace, G.G., Madden, J.D. and Baughman, R.H., *Increased Actuation Rate of Electromechanical Carbon Nanotube Actuators Using Potential Pulses with Resistance Compensation.* Smart Materials & Structures, 2003. **12**(4): p. 549-555.
118. Ding, J., et al., *Use of Ionic Liquids as Electrolytes in Electromechanical Actuator Systems Based on Inherently Conducting Polymers.* Chemistry of Materials, 2003. **15**(12): p. 2392-2398.
119. Yamato, K., Tominaga, K., Takashima, W. and Kaneto, K., *Stability of Electrochemomechanical Strains in Polypyrrole Films Using Ionic Liquids.* synthetic metals, 2009. **159**(9-10): p. 839-842.
120. Li, Y.F. and Qian, R.Y., *Electrochemical Overoxidation of Conducting Polypyrrole Nitrate Film in Aqueous Solutions.* Electrochimica Acta, 2000. **45**(11): p. 1727-1731.
121. Novak, P., Rasch, B. and Vielstich, W., *Overoxidation of Polypyrrole in Propylene Carbonate - an Insitu Ftir Study.* Journal of the Electrochemical Society, 1991. **138**(11): p. 3300-3304.
122. Lu, W., et al., *Use of Ionic Liquids For .Pi.-Conjugated Polymer Electrochemical Devices.* Science, 2002. **297**(5583): p. 983-987.
123. Otero, T.F. and Boyano, I., *Characterization of Polypyrrole Degradation by the Conformational Relaxation Model.* Electrochimica Acta, 2006. **51**(28): p. 6238-6242.

124. Otero, T.F., Grande, H. and Rodriguez, J., *Conformational Relaxation During Polypyrrole Oxidation: From Experiment to Theory.* Electrochimica Acta, 1996. **41**(11-12): p. 1863-1869.
125. Spinks, G.M., Xi, B., Zhou, D., Truong, V.T. and Wallace, G.G., *Enhanced Stability and Control of Polypyrrole Electromechancial Actuators.* Synthetic Metals, 2004. **140**: p. 273-280.
126. Salvetat, J.P., et al., *Elastic and Shear Moduli of Single-Walled Carbon Nanotube Ropes.* Physical Review Letters, 1999. **82**(5): p. 944-947.
127. Vigolo, B., Poulin, P., Lucas, M., Launois, P. and Bernier, P., *Improved Structure and Properties of Single-Wall Carbon Nanotube Spun Fibers.* Applied Physics Letters, 2002. **81**(7): p. 1210-1212.
128. Laborde-Lahoz, P., et al., *Mechanical Characterization of Carbon Nanotube Composite Materials.* Mechanics Of Advanced Materials And Structures, 2005. **12**(1): p. 13-19.
129. Baughman, R.H., et al., *Carbon Nanotube Actuators.* Science, 1999. **284**(5418): p. 1340-1344.
130. Hughes, M. and Spinks, G.M., *Multiwalled Carbon-Nanotube Actuators.* Advanced Materials, 2005. **17**(4): p. 443-+.
131. Madden, J.D.W., et al., *Fast Carbon Nanotube Charging and Actuation.* Advanced Materials, 2006. **18**(7): p. 870-+.
132. Spinks, G.M., Wallace, G.G., Baughman, R.H. and Dai, L., *Carbon Nanotube Actuators*, in *Electroactive Polymer (Eap) Actuators as Artificial Muscles-Reality, Potential and Challenges*, Y. Bar-Cohen, Editor. 2001, SPIE - The International Society for Optical Engineering: Bellingham, Washington, USA. p. 223-246.
133. Dai, H.J., Wong, E.W. and Lieber, C.M., *Probing Electrical Transport in Nanomaterials: Conductivity of Individual Carbon Nanotubes.* Science, 1996. **272**(5261): p. 523-526.
134. Sansinena, J.M., Olazabal, V., Otero, T.F., daFonseca, C.N.P. and DePaoli, M.A., *A Solid State Artificial Muscle Based on Polypyrrole and a Solid Polymeric Electrolyte Working in Air.* Chemical Communications, 1997(22): p. 2217-2218.
135. Zhou, D., et al., *Solid State Actuators Based on Polypyrrole and Polymer in Ionic Liquid Electrolytes.* Electrochemica Acta, 2003. **48**(14-16): p. 2355-2359.
136. Fukushima, T. and Aida, T., *Ionic Liquids for Soft Functional Materials with Carbon Nanotubes.* Chemistry-a European Journal, 2007. **13**(18): p. 5048-5058.
137. Myoungho Pyo, C.C.B., Elisabeth Smela,John R.Reynolds & Anthony B.Brennan, *Direct Strain Measurement of Polypyrrole Actuators Controlled by the Polymer/Gold Interface.* Chem.Mater, 2003. **15**: p. 7.
138. Philippe Metza, G.u.A., Geoffrey M. Spinks, *A Finite Element Model for Bending Behaviour of Conducting Polymer Electromechanical Actuators.* Sensors and Actuators A: Physical, 2006. **130**: p. 11.
139. E.Smela, *Characterization and Modeling of Ppy Bilayer Microactuators* Sensors and Actuators B: Chemical, 2006. **115**: p. 15.
140. Fang, Y., Tan, X.O., Shen, Y.T., Xi, N. and Alici, G., *A Scalable Model for Trilayer Conjugated Polymer Actuators and Its Experimental Validation.* Materials Science & Engineering C-Biomimetic and Supramolecular Systems, 2008. **28**(3): p. 421-428.
141. McGovern, S.T., et al. *Fast Bender Actuators for Fish-Like Aquatic Robots - Art. No. 69271l.* in *Conference on Electroactive Polymer Actuators and Devices (EAPAD 2008)*. 2008. San Diego, CA: Spie-Int Soc Optical Engineering.

142. Zhou, D., et al., *Actuators for the Cochlear Implant.* synthetic metals, 2003. **135**(1-3): p. 39-40.
143. Wu, Y., et al., *Titan: A Conducting Polymer Based Microfluidic Pump.* Smart Materials & Structures, 2005. **14**(6): p. 1511-1516.
144. Fuchiwaki, M., Tanaka, K. and Kaneto, K., *Planate Conducting Polymer Actuator Based on Polypyrrole and Its Application.* Sensors and Actuators A: Physical, 2009. **150**(2): p. 272-276.
145. Ramirez-Garcia, S. and Diamond, D., *Biomimetic, Low Power Pumps Based on Soft Actuators.* Sensors and Actuators a-Physical, 2007. **135**(1): p. 229-235.
146. Naka, Y., Fuchiwaki, M. and Tanaka, K., *A Micropump Driven by a Polypyrrole-Based Conducting Polymer Soft Actuator.* Polymer International. **59**(3): p. 352-356.
147. Spinks, G.M., et al., *Ionic Liquids and Polypyrrole Helix Tubes: Bringing the Electronic Braille Screen Closer to Reality*, in *Smart Structures and Materials 2003: Electroactive Polymer Actuators and Devices*, Y. BarCohen, Editor. 2003, Spie-Int Soc Optical Engineering: Bellingham. p. 372-380.

CHAPTER 2 EXPERIMENTAL

2.1 Introduction

The experimental method, technical and set up are briefly explained in this chapter, including polymer preparation, electrochemistry characterization, actuation test et al. The general procedures will be given below. The detailed process will be presented in each chapter.

2.2 Methods used for Polymer preparation.

In this thesis, the electrochemical deposition is the main way to obtain CPs. The reason has been explained in chapter 1.

2.2.1 Electrochemical polymerization.

Polypyrrole was obtained from electrochemical polymerization. Depending on the geometry of samples, different designs of cells were developed. Generally, a two electrode system was used for the deposition of PPy. The electrochemical deposition cells are illustrated in Figure 2. 1. Different cells were used to fit to different geometries of PPy.

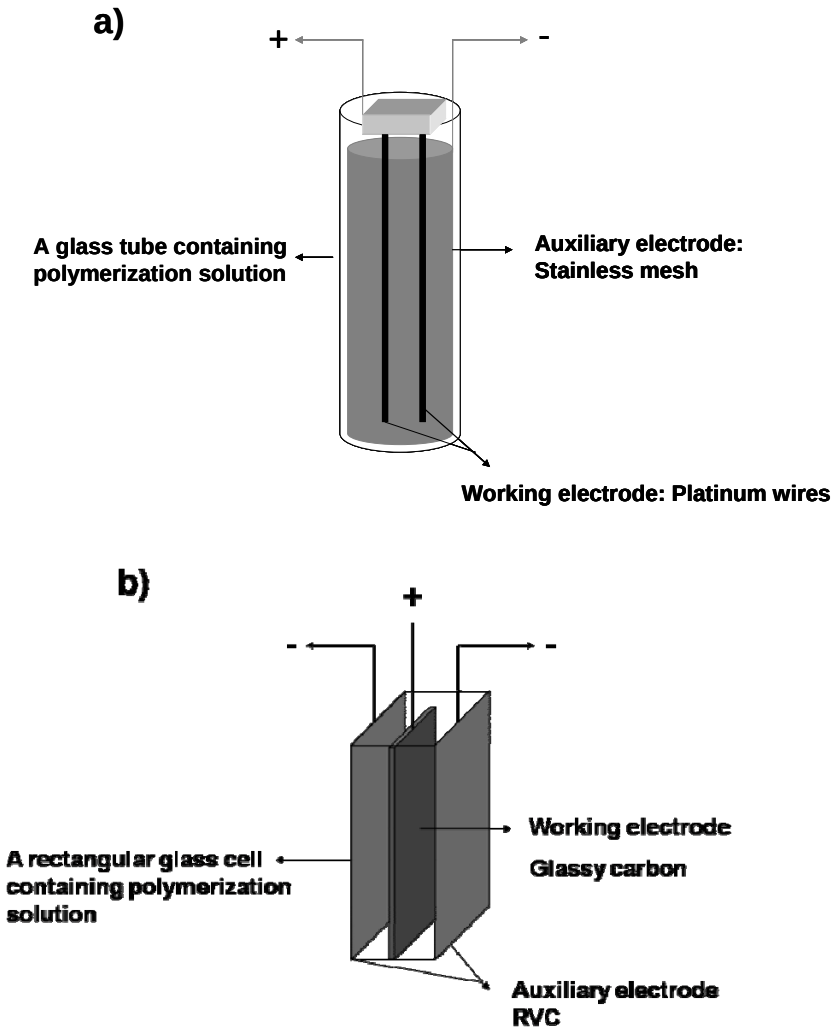

Figure 2. 1 The electrochemical polymerization cells for actuator preparation. a) for helix tubes; b) for free standing films;

The substrate used for CP deposition plays a critical role as it can markedly affect the structure of CPs which in turn influences there mechanical properties and actuation performance [1, 2]. But all materials used as a working electrode for polymerizing CPs must meet the criteria of being stable under polymerization conditions to avoid the oxidation of the electrode itself. In this thesis, electrode materials used were platinum (Pt) and glassy carbon (GC). A Pt helix was formed by a 250μm Pt wire with a 50μm Pt wire wound around it, while a glassy carbon plate, 2cm wide, 4 cm long and 0.2 cm thick was used. These materials were chosen as it has been proven that CPs grown from

Pt and GC are usually dense, strong and flexible. The selecting of the auxiliary or counter electrode also should meet the stability requirements under experimental conditions. In this thesis, stainless mesh (model 363) and reticulated vitreous carbon (RVC) with 100 ppi were used as counter electrodes. Details of them were described in chapter 3, chapter 4 and chapter 5 respectively.

There are typically three different kinds of electrochemical deposition approaches according to the electrical signals provided: galvanostatic, potentiostatic and potentiodynamic polymerization. The electro polymerization of CPs in this thesis is under constant current, as it is easier to control the charge flow and the polymer properties thus producing repeatable results.

During the constant current deposition process, a two electrode system was used. A constant current signal was applied between the working electrode and the auxiliary electrode. Monomers will gradually be oxidized and form a polymer coating on the working electrode with dopants being incorporated also. As mentioned above, the amount of polymer deposited can be monitored by varying the charge which depends on current density and polymerization time. Simply, the total charge Q passed through could be calculated as

$$Q = \int i \cdot dt \tag{2.1}$$

Where i and t is the current and the deposition time respectively. It must be pointed out that the magnitude of current density is known as another critical parameter to affect the surface morphology, conductivity, and mechanical properties of the polymer [3].

Usually, as explained in chapter 1, a low temperature is helpful to form high quality CPs as uniform conjugated chains. Thus polypyrrole grown from propylene carbonate (PC) and methyl benzoate (MB) was carried out at -28ºCand -10 ºC respectively. Too

low a temperature will freeze electrolyte and more over, no coherent polymer could be obtained [4].

2.2.2 Techniques used for polymer characterization

2.2.2.1 Cyclic Voltammetry (CV)

Cyclic voltammetry is a simple but powerful technique for initial electrochemical studies and has proven very useful in obtaining information for even fairly complicated electrode reactions. During the CV, the potential will linearly scan over a certain range of voltage (Figure 2. 2 a). Potential will start from an initial value and continuously sweep between an upper and lower limit for a number of cycles at a set linear scan rate then return to the final potential at the end of the experiment.

The current is collected during the potential scan and a graph containing current as Y-axis and potential as X-axis will be drawn for further analysis (Figure 2. 2 b).

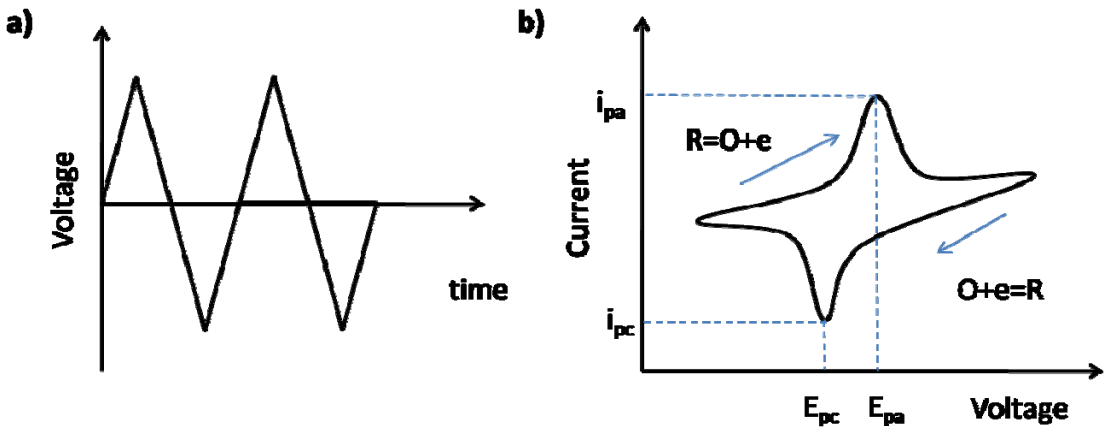

Figure 2. 2 Cyclic voltammogram. a) a ramp voltage signal versus time; b) a typical CV of redox process.

There are several important parameters in CV: peak anodic current i_{pa} , peak cathodic current i_{pc}, peak anodic potential E_{pa} and peak cathodic potential E_{pc}. In a stable reversible system, the following conditions should be satisfied (at 21ºC):

$$\Delta E = E_{pa} - E_{pc} = 59/n \text{ (mV)} \quad (2.2)$$

$$i_{pa}/i_{pc} = 1 \quad (2.3)$$

$$i_p \propto r^{1/2} \quad (2.4)$$

where n is the number of electrons transferred in the redox process, i_p is absolute value of peak current and r is the scan rate. It must be pointed out that those conditions hold for ideal systems and may not be observed in real system partially because of uncompensated solution resistance.

2.2.2.2 Chronoamperometry

Chronoamperometry involves instantaneous switching from one potential (V_1) to another (V_2) and recording the current response over time. A typical chronoamperometric response of a CP system is shown in Figure 2. 3.

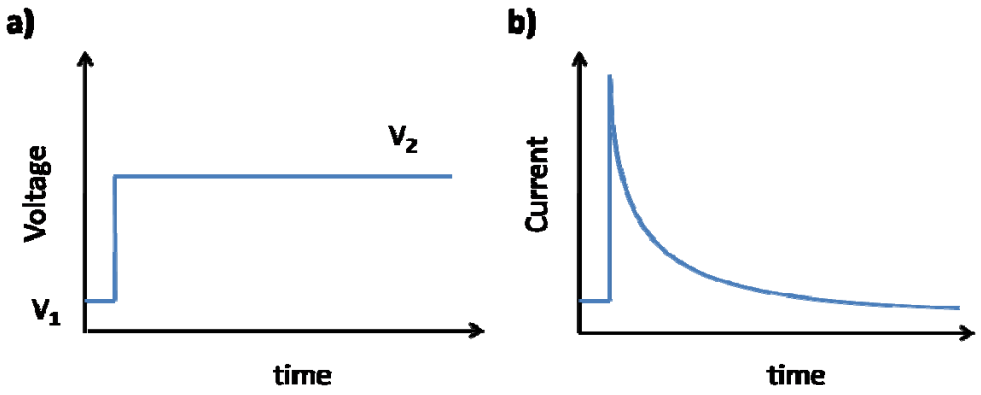

Figure 2. 3 A typical chronoamperometry experiment for oxidizing PPy. (a) voltage is switched from V_1 (usually V_1=0) to V_2 and (b) recorded current signal.

Usually in chronoamperometry, a decaying current can be observed. For a system using plate in electrochemical process is under diffusion control, current could be estimated from the Cottrell equation:

$$\boldsymbol{i = \frac{nFCD^{1/2}}{\pi^{1/2}t^{1/2}}} \qquad (\mathbf{2.5})$$

where *n* is the stoichiometric number of electrons, *F* is Faraday constant, *C* is the bulk concentration of electroactive species and *D* is the diffusion coefficient of electroactive species. In this thesis, the actuation of CPs under chronoamperometric stimulation will be studied in chapter 5.

2.2.2.3 The electrical conductivity

Many of the applications of conducting polymers are based on the ability to conduct electricity. In this thesis, the electrical conductivity is obtained by using ASTM (American society for testing and material) 4 point probe instrument, a schematic of theinstrument is illustrated in Figure 2. 4.

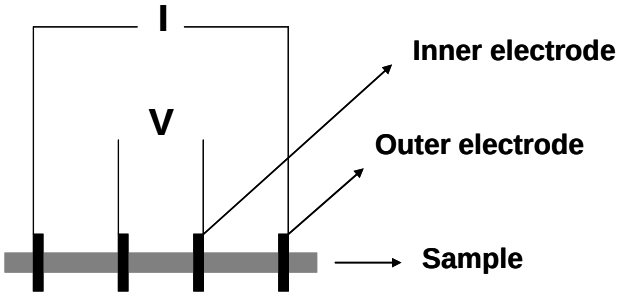

Figure 2. 4 The four point probe used for measuring the conductivity.

The current is applied between outer electrode and the potential is measured between the inner electrodes. According to ohm's law, resistivity can be calculated as:

$$\rho_s = \frac{whv}{il} \qquad (2.6)$$

where *w* represents sample witdth, *h* is thickness of sample, *v* is potential drop, *i* is the applied current, *l* is the distance between inner electrodes and ρ_s is surface resistivity or sheet resistivity.

The calculation of resistance based on ohms' law usually varies for different instruments. In our lab, the sheet resistance can be calculated as:

$$R_s = 4.532 * V / I \quad \text{(Ohms per square)} \tag{2.7}$$

The resistivity for films and wafers

$$\rho = 4.532 * V * h / I \tag{2.8}$$

where h is the thickness in cm. The conductivity is reciprocal of resistivity.

2.2.2.4 Scanning electro microscope (SEM)

The scanning electro microscope is a powerful and widely used tool in material studies. While the SEM is working, a beam of high energy electrons is thermionically emitted from an electron gun fitted with a tungsten filament cathode. When the electrons hit the surface of the target, the electrons from κ-orbit of sample's atom will form the secondary electrons. The images are usually captured by collecting secondary electrons. The detailed morphology such as surface microstructure or inner structure of fracture cross-sections was investigated by scanning electro microscope. A schematic of a typical SEM setup is shown in figure 2.5.

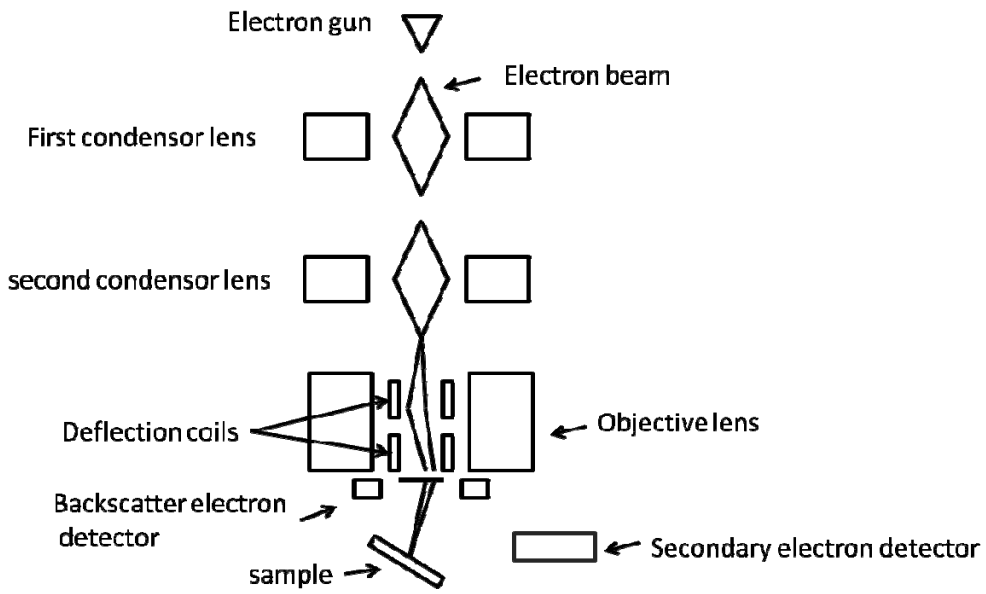

Figure 2. 5 Schematic diagram of a SEM.

2.2.2.5 Mechanical properties.

The major mechanical property tested is elastic modulus. Elastic modulus of CPs is obtained by fitting the linear area of a strain-stress curve (Figure 2. 4). In the linear region, the strain-stress relationship of CPs obeys Hook's law:

$$Y = \frac{\sigma}{\varepsilon} \tag{2.9}$$

where Y refers elastic modulus (or Young's modulus), σ is stress applied and ε is strain caused by load. Different polymer properties have varying effects on stress-strain curves.

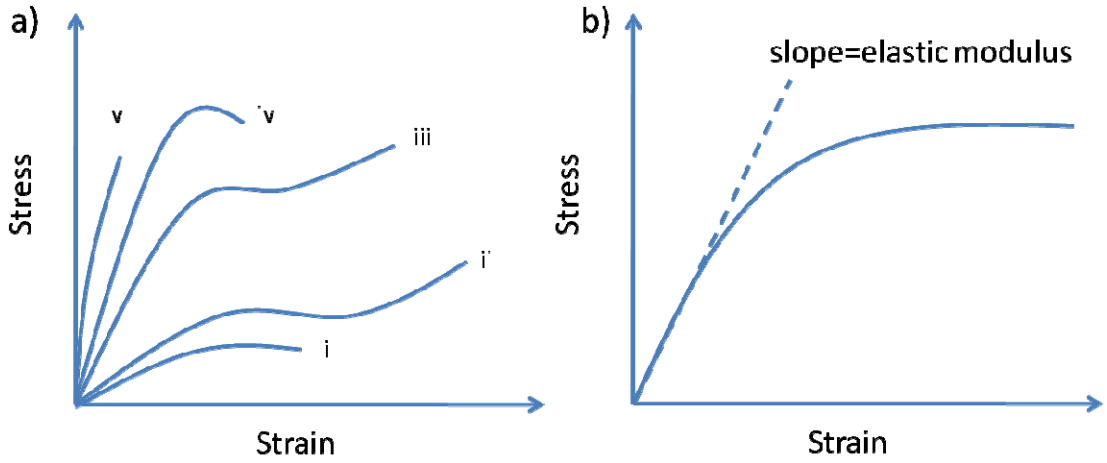

Figure 2. 6 Tensile stress-strain curves for (a) five types of polymeric material including i) soft & weak; ii) soft & tough; iii) hard & tough; iv) hard & strong; v) hard & brittle and (b) typical stress-strain curve for CPs. .

CPs usually have stress-strain curves like Figure 2. 6a), a soft and weak material [5, 6]. In our lab, Young's modulus was tested using Shimadzu EZ Tensile test machine. According to the instrument manual, it has 0.001mm resolution in length measurement and 1/50000*load cell capacity resolution in force measurement (2N cell will give 2N/50000=0.04mN resolution).

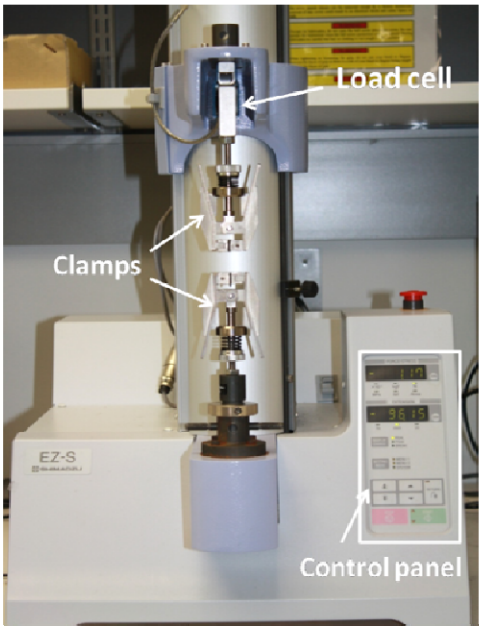

Figure 2. 7 Shimadzu EZ Tensile test machine.

2.3 Techniques for CP actuation tests

2.3.1 The design of the electrochemical cell.

Electrochemical actuation test was conducted in a conventional three electrodes system and deformation changes were recorded by Aurora Scientific Inc. Dual Lever Arm system. A convenient electrochemical cell was widely used in this thesis. Due to the different geometry and design of the sample, two kinds of the cells were designed and illustrated in Figure 2. 8:

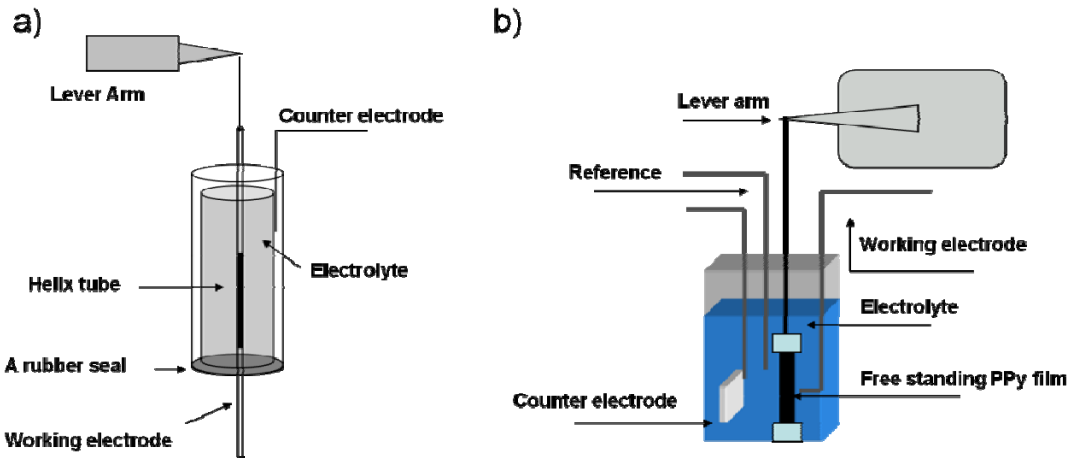

Figure 2. 8 The experiment set up for actuation test. a) for tubes; b): for films.

The reference electrode used in this thesis is $Ag|Ag^{+}$, which is suitable for organic electrolyte. Whilst in aqueous systems, Ag|AgCl was employed.

2.3.2 Mechanical properties test and actuation test.

A Dual Mode Lever System was used for most actuation test (Figure 2. 9). Two models 300B and 305B have been purchased in our lab. According to the instrument

menu, 300B would give a force range from 0 to 500 mN with a signal resolution of 0.2 mN and length excursion of 10 mm. The 305B gives a force range from 0 to 5.0 N with a signal resolution of 1 mN and length excursion of 20 mm. The contraction/expansion was measured by the arm and then recorded by computer for further analysing.

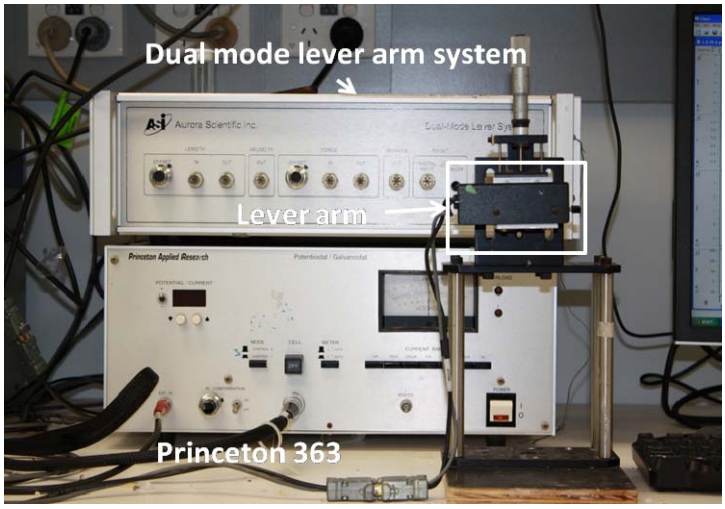

Figure 2. 9 Dual mode lever system for actuation test.

2.4 References:

1. Witkowski, A., M.S. Freund, and A. Brajtertoth, *Effect of Electrode Substrate on the Morphology and Selectivity of Overoxidized Polypyrrole Films.* Analytical Chemistry, 1991. **63**(6): p. 622-626.
2. Hara, S., et al., *Tris(Trifluoromethylsulfonyl)Methide-Doped Polypyrrole as a Conducting Polymer Actuator with Large Electrochemical Strain.* Synthetic Metals, 2006. **156**(2-4): p. 351-355.
3. Shu Yi Chu and e. al, *Effect of Deposition Current Density on the Linear Actuation Behavior of Ppy (Cf3so3) Films.* Current Applied Physics, 2008. **8**: p. 4.
4. Sato, M., Tanaka, S., Kaeriyama, K., *Electrochemical Preparation of Highly Conducting Polythiophene Films.* J. Chem. Soc. Chem. Comm., 1985: p. 713-714.
5. Madden J.D, et al., *Creep and Cycle Life in Polypyrrole Actuators.* Sensors and Actuators A: Physical, 2007. **133**: p. 210-217.
6. Kaneto, K., H. Suematsu, and K. Yamato, *Training Effect and Fatigue in Polypyrrole-Based Artificial Muscles.* Bioinspiration & Biomimetics, 2008. **3**(3): p. 6.

CHAPTER 3 THE EFFECT OF THICKNESS AND CHARGE TRAPPING

3.1 Introduction

Polypyrrole (PPy) undergoes volume changes and hence actuates by the migration of ions and solvent in response to the electrochemical oxidation and reduction of the polymer. The oxidation and reduction reactions for polypyrrole, the best known conducting polymer actuator material are presented in Figure 1.10 (Chapter 1). In response to the oxidation and reduction, solvated ions from the electrolyte form a complex with polymer chains or are released to the solvent thereby restoring a balanced charge [1]. This migration of ions and associated solvent is physically apparent by the expansion or contraction of the polymer [2]. The actuation strain rate is more likely to be diffusion limited, with the diffusion of ions through the polymer believed to be the slowest process. Some early studies found that the mobility of the oxidized sites on the polymer backbone was estimated to be 10^7 to 10^{10} higher than that of the mobile counter ions [3, 4].

Several previous studies have considered the processes involved in the oxidation and reduction of conducting polymers. The Aoki model assumed that the rate determining step of the whole process is charge transfer from the neutral species to the oxidized species at a moving boundary from the metal connector through the polymer [5, 6]. However, fast scan rate voltammetry experiments indicated that the switching response is also sensitive to the anion size, which is believed as a consequence of diffusion[7]. Work by Lacroix *et al.* [11] suggested that the speed of boundary movement could be determined by either electron movement or counter-ion movement and the two processes could be explained by diffusion in a semi infinite medium using different diffusion coefficients for electrons and counter-ions. A consequence of the diffusion controlled process is that when the scan rate is significant high, the counter

ions have not reached the metal electrode the polymer is only partly oxidized (or reduced) hence the performance is limited.

For practical realization PPy actuators need to be able to produce maximum length changes and support large loads. For example, the ability to open and close the fingers on an adult hand requires 16 mm change and 1250 mN force [8]. Forces in the range from 100-300 mN for individual free standing PPy films under isometric conditions were previously been obtained [9]. Achieving a large force for PPy actuators still remains a challenge. Through bundling PPy helix fibers, a force as large as 2 N with 0.5% strain was obtained [10]. Kaneto's group went further as they combined 1600 pieces of PPy-Ni-stainless steel coil composite actuator to lift up to 22 kg of weight (216N). However, the lifting capacity was far below the predict value 600 kg. In those cases, relatively thick conducting polymers (more than 30 μm) were used to make it easier to bundle the fibers.

There is no conclusion yet as to the optimal thickness of PPy that should be produced to achieve the best actuation performance. It is clear that the dimension of PPy plays an important role in the electrochemistry of conducting polymers [11]. Relatively thin actuators are expected to exhibit much higher strain rates at the same applied voltage compared to relatively thick actuators as the diffusion distance is much smaller. Understanding the effects of polymer film thickness on the observed actuation performance are important, as the most common approach to increasing the force output is to make an actuator of larger cross-sectional area. The purpose of this chapter is to determine the actuation strain / stress relationships of PPy actuators of different thicknesses and investigate the mechanisms of actuation as a function of thickness.

3.2 Experimental

3.2.1 Reagents and materials

Tetrabutylammonium hexafluorophosphate ($TBA.PF_6$) and propylene carbonate (PC) were obtained from Sigma. Pyrrole was obtained from Fluka and was distilled before use. Platinum (Pt) wires that were used as supporting substrates for the electrochemical polymerization of pyrrole with diameters 0.25 *mm* and 0.05 *mm* respectively were bought from Goodfellow.

3.2.2 Instrumentation

A EG&G Princeton Applied Research Model 363 potentiostat/galvanostat or a BAS CV-27 was used to regulate and measure the current and/or voltage was used for constant current electropolymerization of pyrrole and for all of the electrochemical cells reported. A MacLab/4e AD analogue to digital converter was used to record electrochemical results.

3.2.3 The preparation of PPy helix tube.

The preparation of linear PPy helix tube actuators was described previously [12]. Briefly, a 0.05 *mm* Pt wire is wrapped around a 0.25 *mm* Pt wire forming a helix spiral. The polymerization solution consisted of 0.06 M pyrrole monomer, 0.05 M $TBA.PF_6$ and 0.5 %(v/v) H_2O in PC. Dissolved O_2 was removed by bubbling with $N_{2(g)}$ gas for 300 s. Electropolymerization of pyrrole was conducted at a constant current density of 0.15 mA/cm^2 for 4 hours at -31°C. Following the polymerization of pyrrole, the 0.25

mm Pt wire was removed from the PPy Pt wire helix structure. The PPy samples were then stored in 0.25M TBA.PF_6 PC solution until further testing.

3.2.4 Thickness measurements

The wet PPy helix tubes (with Pt central core) were cut to 10 *mm* lengths and mounted in room temperature curing epoxy resin. Following curing, the samples were mechanically polished and then soaked again in PC to ensure that the PPy thickness is similar to that used for actuators. Optical micrographs were taken of the wet polished samples and analyzed to measure the film thickness (Figure 3. 2).

3.2.5 Electrochemical studies

Cyclic voltammograms (CV) were conducted in a 0.25M TBA.PF_6 PC solution with an organic reference electrode ($Ag|Ag^+$ in acetonitrile) and a Pt mesh counter electrode. The scan range is from -1.0 to 0.8 V and the start point is -1.0 V at scan rates ranging from 5 and 50 mV/s.

3.2.6 Actuation tests

The PPy helix tubes used for actuation tests were between 10 and 20 *mm* in length. To achieve electrical and mechanical contact two separate pieces of 0.25 *mm* diameter Pt were inserted into each end of the PPy tubes and fixed with epoxy glue. The gauge length was the length measured between the glue at each end. The actuation testing equipment is shown schematically in Figure 3. 1. The force was applied, and the

change in length measured by a Model 305B Lever Arm Dual Mode System (Aurora Scientific). Actuations tests were performed in the 0.25M TBA.PF_6 PC electrolyte using a conventional three electrode setup. The counter electrode was stainless steel mesh and the reference electrode was $Ag \mid Ag^+$ in acetonitrile.

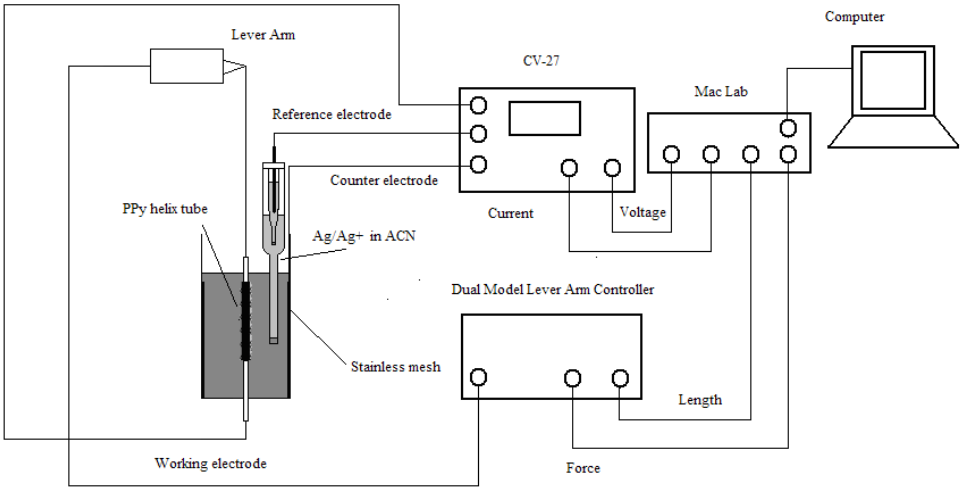

Figure 3. 1 Schematic diagram of actuation test system.

3.3 Results and Discussion

3.3.1 Tube Thickness

The wall thickness of the PPy tube mounted in epoxy resin was measured by optical microscopy. There was strong contrast when viewed by optical microscopy as the PPy appears black and absorbs light whilst the epoxy was translucent (Figure 3. 2).

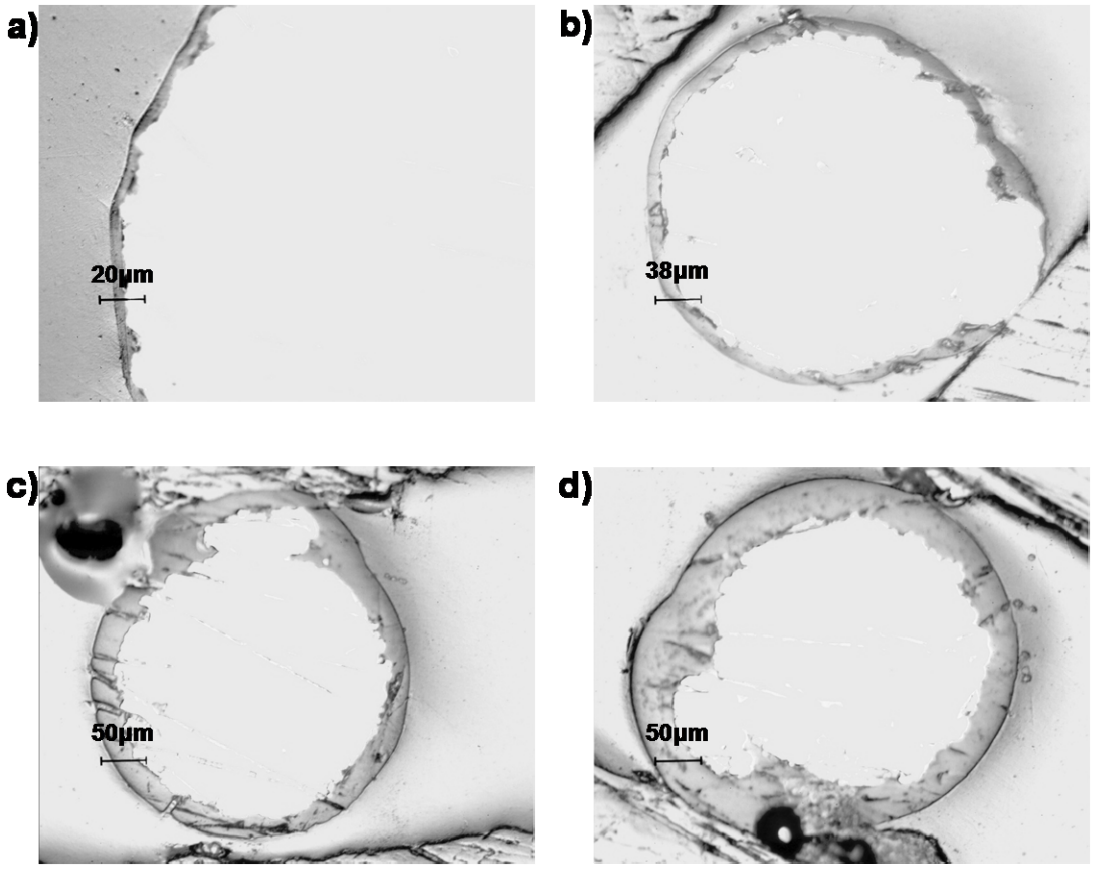

Figure 3. 2 Cross section of PPy helix tubes obtained after different polymerization times: a) 4hours; b) 8hours; c) 16 hours and d) 20 hours.

The wall thickness of the PPy helix tube increases linearly with the polymerization time and hence the charge consumed during polymerization, as expected (Figure 3. 3 b). Prior to polymerization, charge is consumed by the formation of a double layer at the electrode surface and by undesirable reactions and as such it should take a finite amount of time before a polymer film begins to form (Figure 3. 3 a).

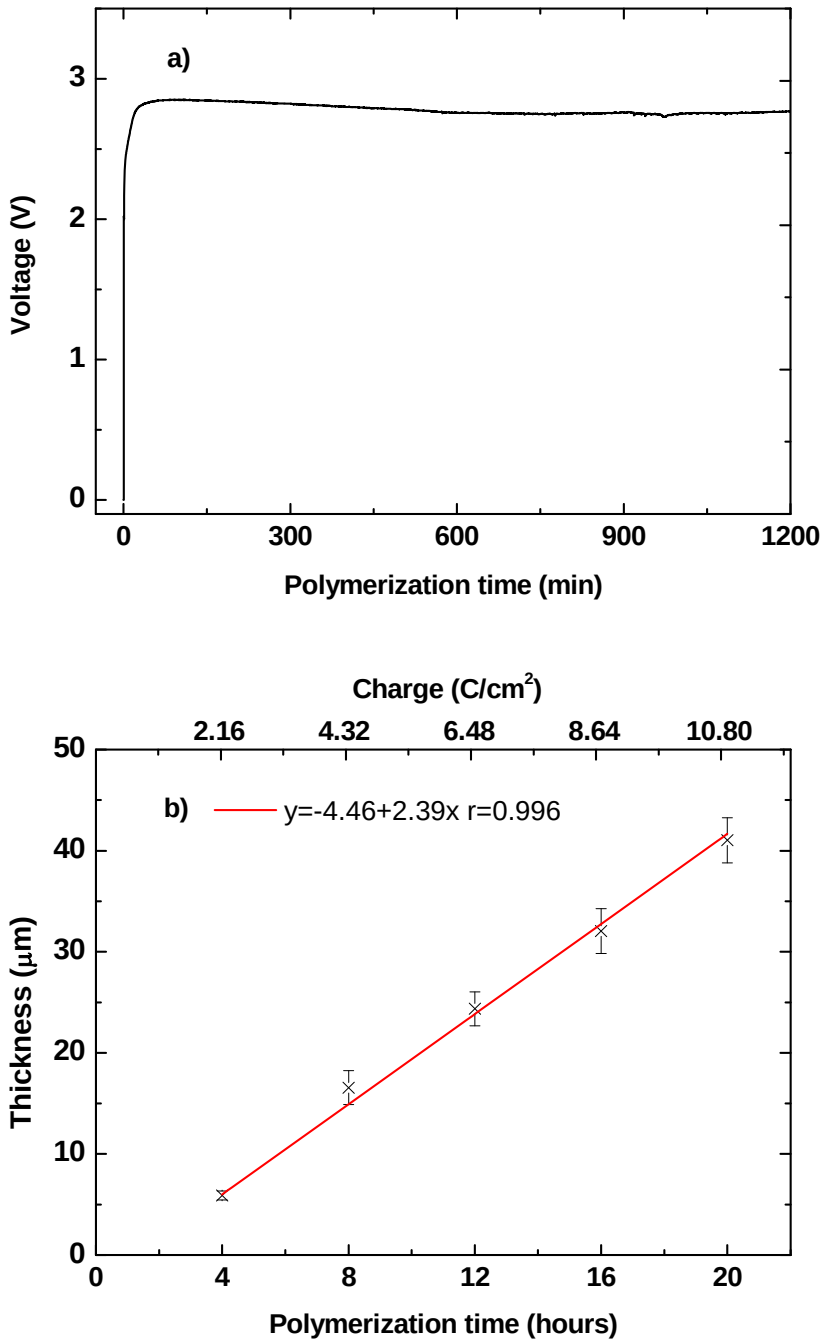

Figure 3. 3 a) a typical chronopotentiogram of PPy polymerization using two electrodes system (20hrs); b) The relationship between PPy helix tube wall thickness and polymerization time and charge passed during polymerization. The error bars represent 3 standard deviations.

3.3.2 Cyclic voltammograms of PPy helix tubes

A cyclic voltammetric sweep was used to simultaneously actuate and study the oxidation and reduction of the PPy helix tubes. At the relatively slow scan rate of 5 mV/s distinct oxidation and reduction peaks were observed for all helix tubes (Figure 3. 4). Of note, the oxidation peak potential shifted from -0.25 V to +0.08 V with increase wall thickness from 5 to 34 μm. The position of the reduction peak was similar for all tube thicknesses. At higher scan rates, the oxidation and reduction peaks became broader and less identifiable particularly in the thicker helix tubes. For thicker films at higher scan rates the oxidation peaks were not observed with the potential range used, although reduction peaks were always present. In general, the oxidation and reduction peaks were shifted to higher anodic and cathodic potentials, respectively, as the scan rate increased.

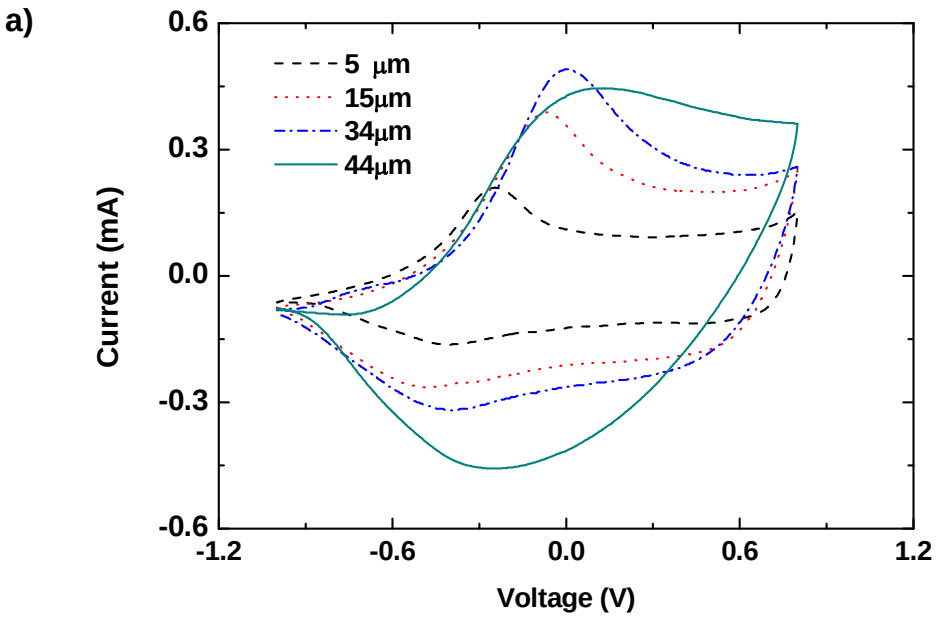

b)

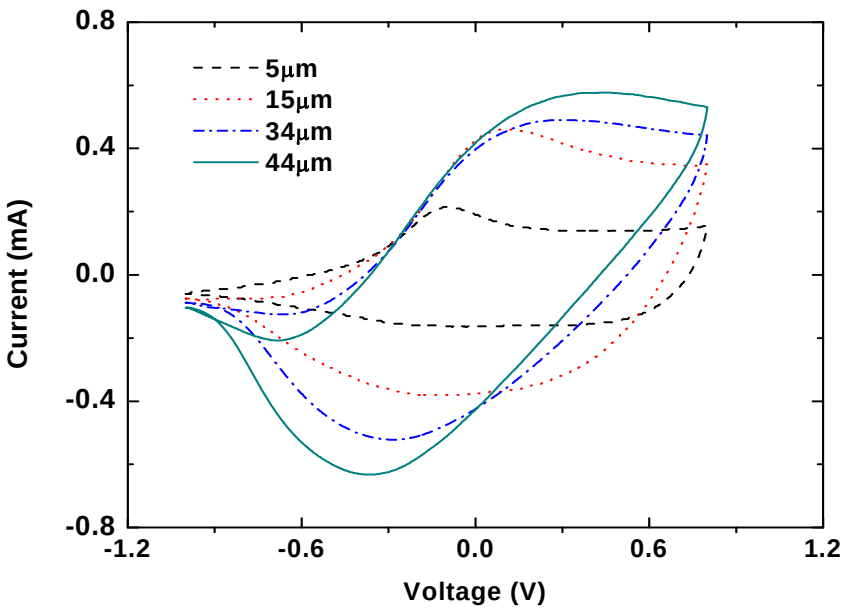
5μm
15μm
34μm
44μm
Current (mA)
Voltage (V)
0.8
0.4
0.0
-0.4
-0.8
-1.2
-0.6
0.0
0.6
1.2

c)

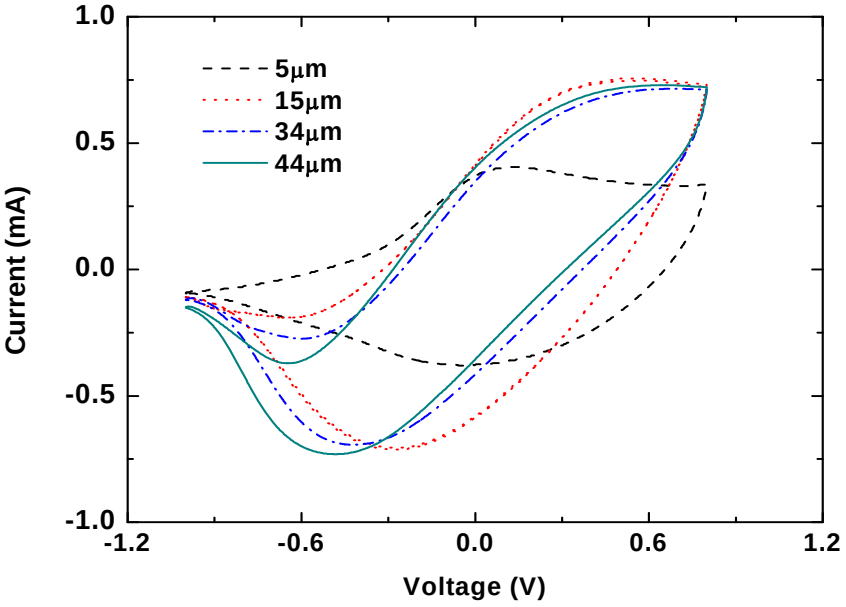
5μm
15μm
34μm
44μm
Current (mA)
Voltage (V)
1.0
0.5
0.0
-0.5
-1.0
-1.2
-0.6
0.0
0.6
1.2

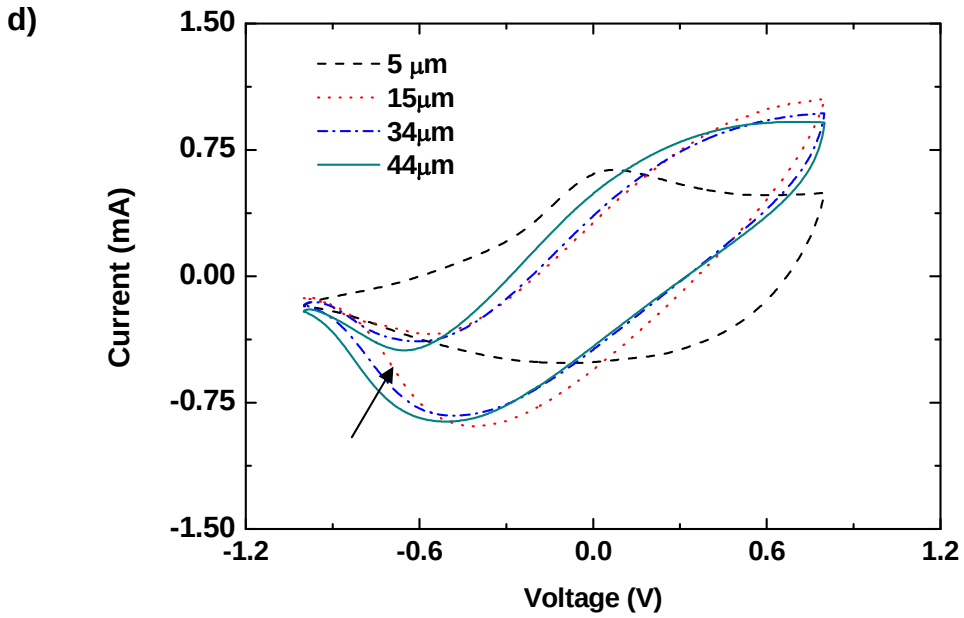

Figure 3. 4 Cyclic voltammogram of PPy helix tubes at 5, 10, 25, 50 mV/s (a-d) and for different wall thicknesses, as indicated. The arrow shows an example of a reductive current observed during the initial stages of the anodic scan.

A curious feature was noted in the anodic scan for certain PPy samples. For tubes 15 μm and thicker, a decrease in current with a minimum was observed in the initial part of the anodic scan at a scan rate of 50 mV/s. An arrow indicates the presence of this minimum in Figure 3. 4 d). A summary of the circumstance when a decreasing current with a minimum was observed in the anodic scan is presented in (Table 3. 1). It seems that the minimum first appears at slower scan rates in the thicker helix tubes. For example, in the 44 μm thick film, a minimum was observed for scan rates above 5 mV/s, while the reduction minimum was only observed above 10 mV/s in the 34 um thick tubes and above 25 mV/s in the 15 μm thick tubes. The minimum was not observed in the thinnest helix tubes at scan rates up to 50 mV/s. The reasons for the appearance of the reduction minimum during the anodic scan are considered in Section 3.4.

Table 3. 1 Reduction peak observed during anodic scan.

Tube Thickness	Scan Rate(mv/s)				
(μm)	0.2	5	10	25	50
5	**No**	**No**	**No**	**No**	**No**
15	**No**	**No**	**No**	**No**	**Yes**
34	**No**	**No**	**No**	**Yes**	**Yes**
44	**No**	**No**	**Yes**	**Yes**	**Yes**

3.3.3 A semi-empirical diffusion –based charging model

Analysis of the charge passed during the anodic voltage scan indicated that the extent of oxidation depended on both the scan rate and the film thickness. Charge was calculated by integration of current during the anodic scan of the CV measurement. Figure 3. 5 a) shows the charge passed for the different helix tube thicknesses at different scan rates. For each thickness, the charge passed drops rapidly as scan rate increases, indicating that charging is a comparatively slow process. Thickness appears to be important only for the slower scan speeds (eg. 5 mV/s) with a gradual increase in charge passed with increasing thickness was noted at slower scan rates. Since there is more material available to be oxidized it is expected that the charge passed should increase with increasing PPy volume. The observation that the charge passed does not depend on the tube thickness at faster scan rates is somewhat expected as the process is diffusion rate limited. Figure 3. 5b) shows the charge passed expressed as a fraction of the available charge. The theoretical charge capacity ($Q_{v,max}$) was

calculated from the volume of PPy and assuming that one in three pyrrole units could be oxidized (and using a PPy density of 1.5 g/cm^3) [13]. For the 5 μm thick tube, the extent of oxidation at the slowest scan rate slightly exceeded the theoretical charge capacity indicating that some additional (parasitic) redox reactions may be occurring. The fraction of anodic charging tended to decrease with increasing scan rate and for increasing tube wall thickness. Previous studies of PPy coatings had also shown that the extent of redox reaction decreased rapidly with increasing film thickness in the sub-micron range [14].

Madden has proposed a model for PPy charging that involves transport of ions through the polymer film as a rate controlling process [15]. Oxidation of the polymer occurs first at the polymer-electrolyte interface and penetrates deeper into the polymer over time. Ion transport in PPy is treated here as diffusion controlled process with ion transport assumed to follow normal Fickian diffusion. The model is semi-empirical in nature and designed to capture the main features of the relatively slow charging observed in PPy helix tubes. A more accurate model of PPy charging would require a detailed analysis of the thermodynamic driving force that causes the diffusion of ions into and out of the polymer. Here it is assumed that a single voltage scan (over a given potential range) generates an "average" free energy change that causes a Fickian-type diffusion of ions through the tube wall thickness.

To further simplify the estimation, a plate model is considered rather than the hollow tube. It is also assumed that oxidation first occurs at the polymer-electrolyte interface and then penetrates through whole film at a rate dependent upon the ion diffusion kinetics. The oxidized layer thickness (d_c) at the polymer-electrolyte interface is assumed to be proportional to the square root of the diffusion coefficient (D) and response time (t).

$$d_c = 2\sqrt{Dt} \tag{3.1}$$

The time available for oxidation is given by:

$$t = \frac{\Delta V}{r} \tag{3.2}$$

where ΔV and r represent the voltage range and scan rate, respectively, of the anodic scan.

Hence the diffusion coefficient can be written as:

$$D = \frac{1}{4}\frac{d_c^2 r}{\Delta V} \tag{3.3}$$

For the simple plate model consisting of a layer of fully oxidized polymer penetrating into the reduced polymer over time, then:

$$\frac{d_c}{d} = \frac{Q_v}{Q_{vmax}} \tag{3.4}$$

in which d is the total thickness of PPy helix tube, Q_v is the total charge passed and Q_{vmax} is the theoretical charge as defined above. The simple plate geometry used in this analysis introduces a geometric error of 2-15% depending on wall thickness.

Now the diffusion coefficient is given by:

$$D \approx \frac{1}{4}\frac{Q_v^2}{Q_{vmax}^2} \times d^2 \times \frac{r}{\Delta V}$$

$$\frac{Q_v}{Q_{vmax}} = 2\sqrt{D}\frac{\sqrt{\Delta V}}{d\sqrt{r}} \tag{3.5}$$

This expression suggests a linear relationship would exist between the charge passed and the inverse square root of the scan rate. The experimental data is shown as $1/r^{1/2}$ (Figure 3. 5c), and the values for each tube thickness appear to fall on a series of linear lines passing through the origin. The slope of these lines increases with decreasing wall thickness. When the charge passed is plotted against $1/dr^{1/2}$ the data for all thicknesses now fall on one linear line (Figure 3. 5 d), in agreement with the predicted trend. This agreement between the experimental and calculated results

suggests that the semi-empirical modeling approach taken is appropriate for describing the charging process in the helix tubes.

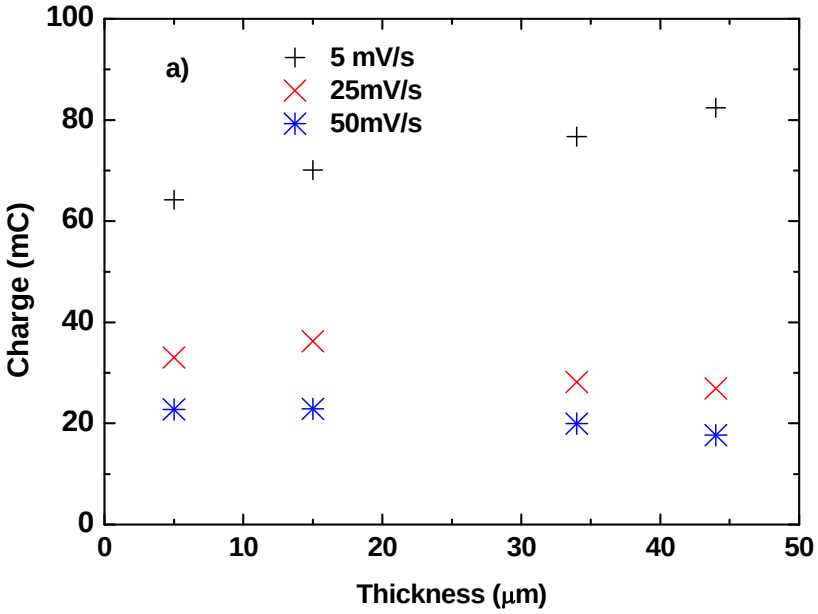

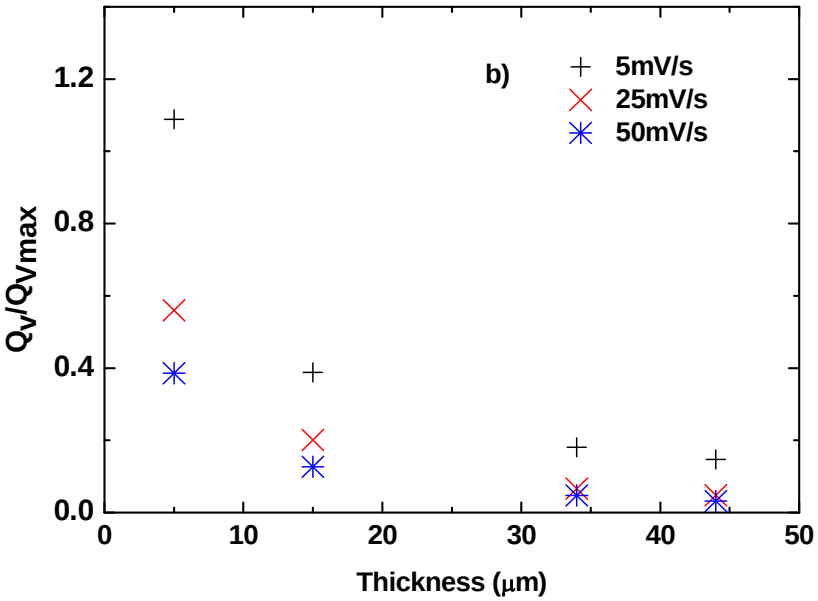

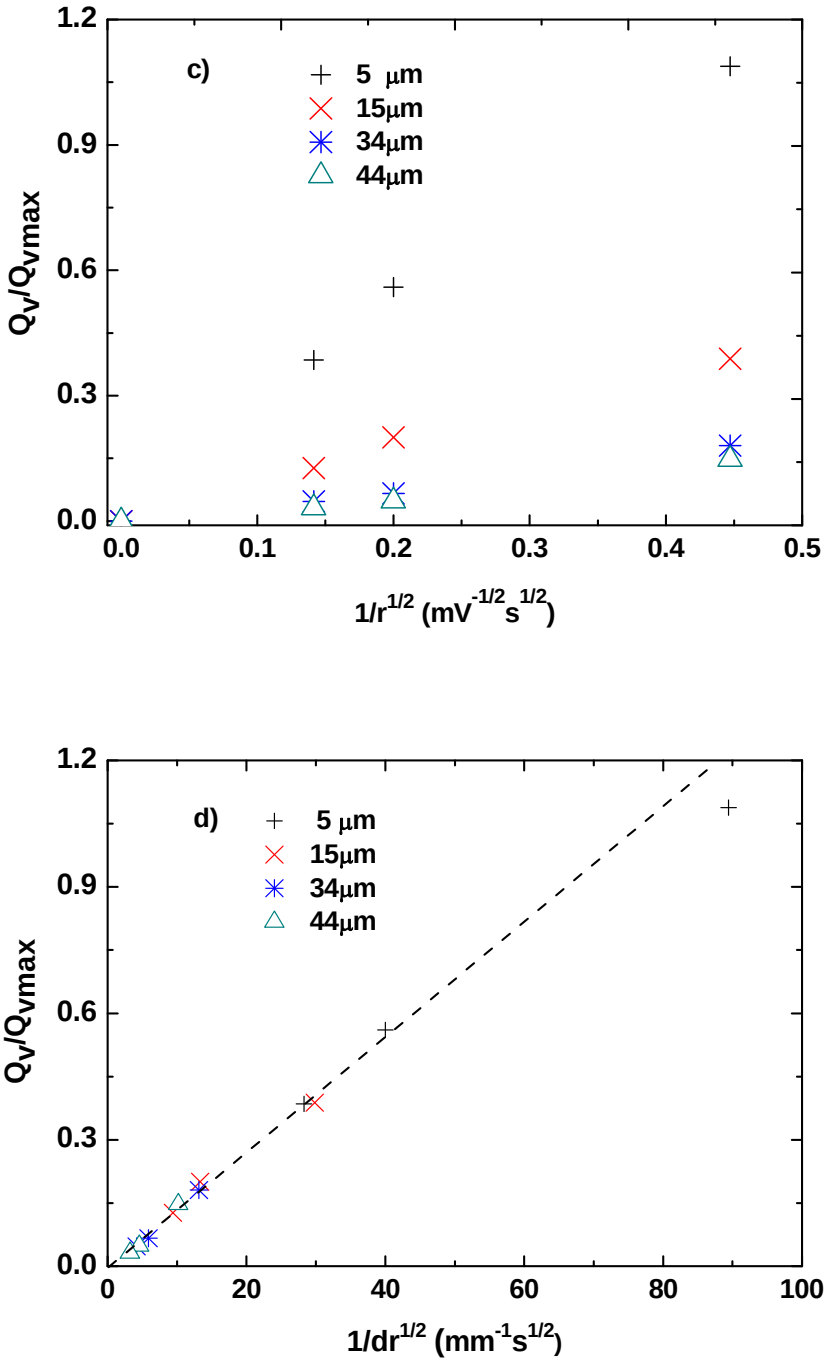

Figure 3. 5 Charge passed during the anodic scan for helix tubes of varying thicknesses (*d*) and as a function of scan rate (*r*); a) total charge integrated from anodic current; b) Charge normalized to the theoretical charge capacity and plotted against scan rate; Same data plotted against c) $1/r^{1/2}$; and d) $1/dr^{1/2}$. Symbols correspond to the wall thickness of helix tubes: 5 μm, 15 μm, 34 μm and 44 μm.

The charge data can now be used to estimate an average diffusion coefficient for the ionic species involved in the redox reactions. The slope of the line drawn through the data points in Figure 3. 5 d) enables the diffusion coefficient to be calculated as:

$$D = 3.84 * 10^{-11}\ m^2/s$$

This value is close to that obtained by impedance spectroscopy measurements. The measured diffusion coefficient of ClO_4^- in PPy is ~$10^{-11}\ m^2/s$ at the oxidized state while using PC as solvent [16]. The diffusion coefficient of NO_3^- in PPy in the oxidized state is also ~$10^{-11}\ m^2/s$ when water was used as solvent[17]. Those values are similar to the diffusion coefficient calculated in the present study, but significantly larger than the NMR measured diffusion coefficient for PF_6^- in PPy ($5 * 10^{-13}\ m^2/s$, PC as solvent) [18]. In the NMR study, the PPy was not fully oxidized. The diffusion coefficients of ions are likely to be the function of redox state of PPy [16, 17], with slower diffusion occurring in the reduced state. In the present study, the redox state of the PPy is being changed significantly, with oxidation of the fully reduced polymer occurring at the electrolyte surface and penetrating inwards. The diffusion coefficient determined here is likely to be related mainly to the diffusion of anions through the oxidized surface layer as these ions need to penetrate through this layer to reach the underlying reduced PPy to allow oxidation of the latter to occur.

The implications of this charging mechanism on the actuation behavior of PPy helix tubes are considered in the next section.

3.3.4 Mixed Mode Actuation and Charge Trapping

The actuation strain was recorded from length change measurements under isotonic conditions and as a function of scan rate. Examples of the strain response for two tube

thicknesses and two scan rates are shown in Figure 3. 6. Generally, the strain increased at anodic potentials as a result of anion ingress during oxidation of the polymer. The strain / voltage curves show a large hysteresis and some creep (higher strain at the end of the voltage scan compared with the beginning) was noted in the thinner tubes. The magnitude of the strain increased with decreasing scan rate and with thinner helix tubes.

Close inspection of the dynamic actuation response showed that the thick films at fast scan rates exhibited mixed ion actuation during reduction whilst at slow scan rates they did not. The mixed ion actuation is evident by an increase in strain during the last stages of the cathodic scan and is due to the ingress of cations that cause swelling of the polymer. Significantly, the cationic actuation only occurred in situations where a decreasing current was observed in the anodic scan (Section 3.2), so it is likely that the two processes are connected. Cation dominated and mixed mode actuation is well known for PPy actuators [12, 19, 20] and is normally restricted to situations where the cation is much smaller or more mobile than the anion. In these cases both the relative size of the ions and the solvent used for the electrolyte are critical in determining which ionic carrier is dominant [20]. The results of the present study show that scan rate can determine the actuation and hence the type of ion causing actuation.

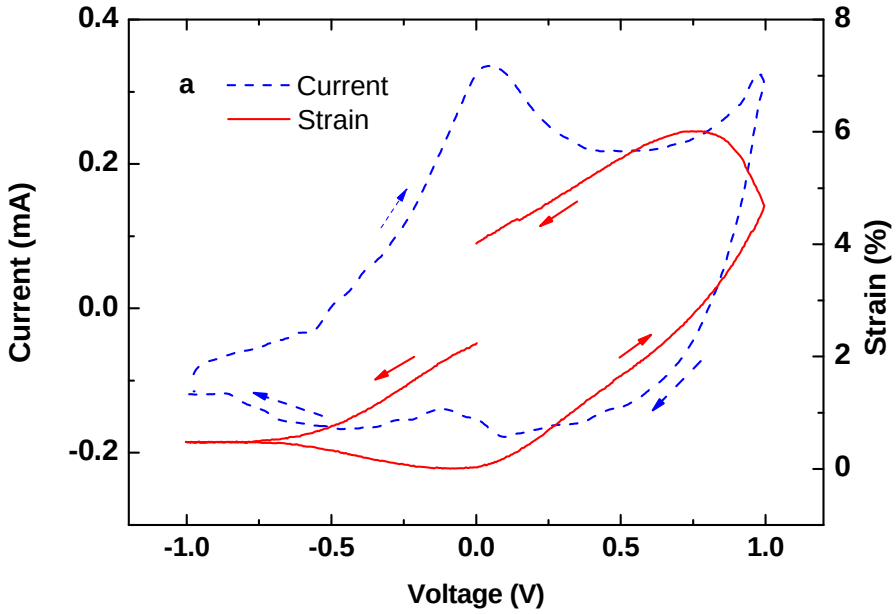
a
Current
Strain
Current (mA)
Strain (%)
Voltage (V)
0.4
0.2
0.0
-0.2
8
6
4
2
0
-1.0
-0.5
0.0
0.5
1.0

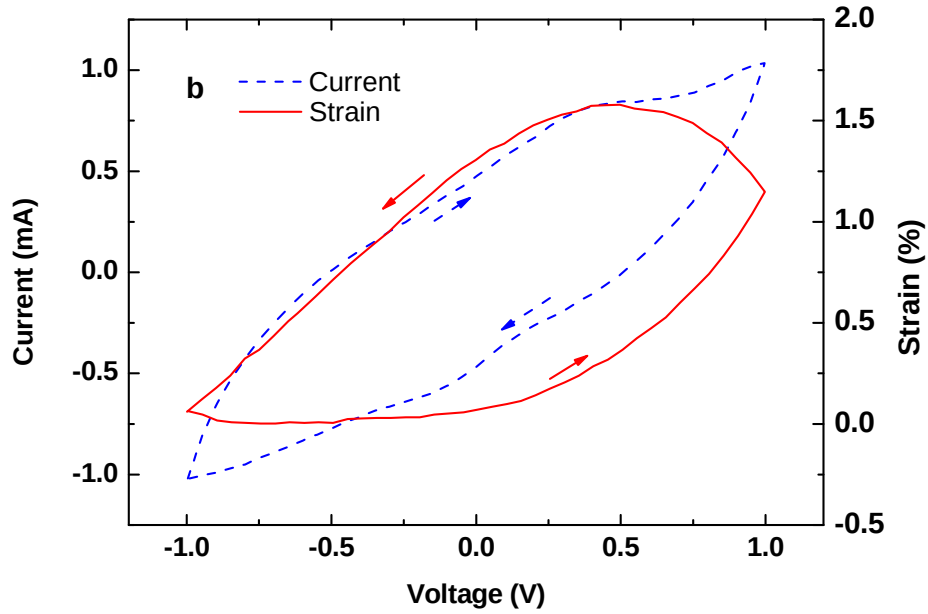
b
Current
Strain
Current (mA)
Strain (%)
Voltage (V)
1.0
0.5
0.0
-0.5
-1.0
2.0
1.5
1.0
0.5
0.0
-0.5
-1.0
-0.5
0.0
0.5
1.0

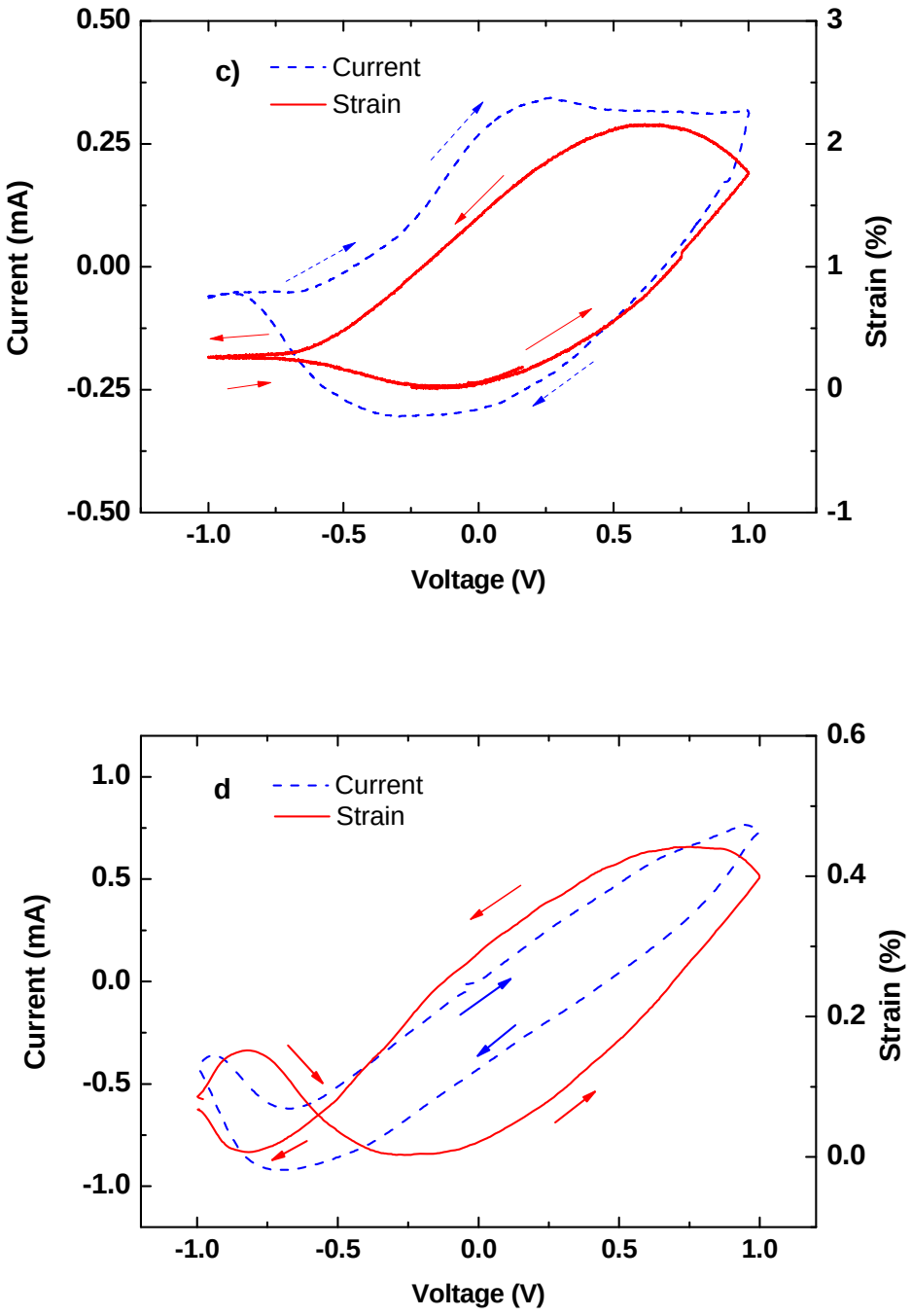

Figure 3. 6 Overlapping cyclic voltammetry and actuation curves for a 15μm thick PPy helix tube at scan rate (a) 5mV/s and (b) 50 mV/s, 44 μm thick PPy helix tube at a scan rate of (c) 5mV/s and (d) 50 mV/s.

The reduction process in PPy helix tubes involves the transport of electrons from the Pt helix to the oxidized layer adjacent to the electrolyte and, secondly, the transport of ions to or from the electrolyte. In Figure 3. 7 a) simplified model is presented as a

PPy film on platinum. The partially reduced PPy is assumed to exist as a layer of fully reduced polymer adjacent to the Pt electrode and a fully oxidized layer adjacent to the electrolyte. Further reduction of the polymer occurs by transport of electrons through the reduced layer and expulsion of a counter-anion to the external electrolyte as shown in Figure 3. 7a). Through this mechanism the oxidized layer becomes progressively thinner and the rate of reduction is determined by the anion diffusion process as described in Section 3.3.

A second mechanism is possible, however, if anion transport is slow. For example, fast voltage scan rates would drive faster reduction and it may not be possible for anion diffusion to keep pace. As shown in Figure 3. 7 b), in this case electrons may be transported to oxidized chains near the surface. Here, anions could be more quickly expelled, or cations from the surrounding electrolyte may penetrate the surface layer to neutralize the counter-anion. Over time, this process leads to a buried layer of oxidized polymer with reduced polymer both at the surface and near the electrode. The buried charge becomes kinetically trapped as the diffusion distance from the electrolyte surface to the buried oxidized layer increases. The expansion of the polymer during the final stages of the cathodic scan at fast scan rates provides evidence for the inclusion of cations into the polymer. The increased free volume may then allow for an increased ion diffusion rate so that the trapped charge can be reduced through the now faster anion diffusion. While speculative, these processes would account for the second reduction peak that occurs at the early stage of the anodic scan at fast scan rates.

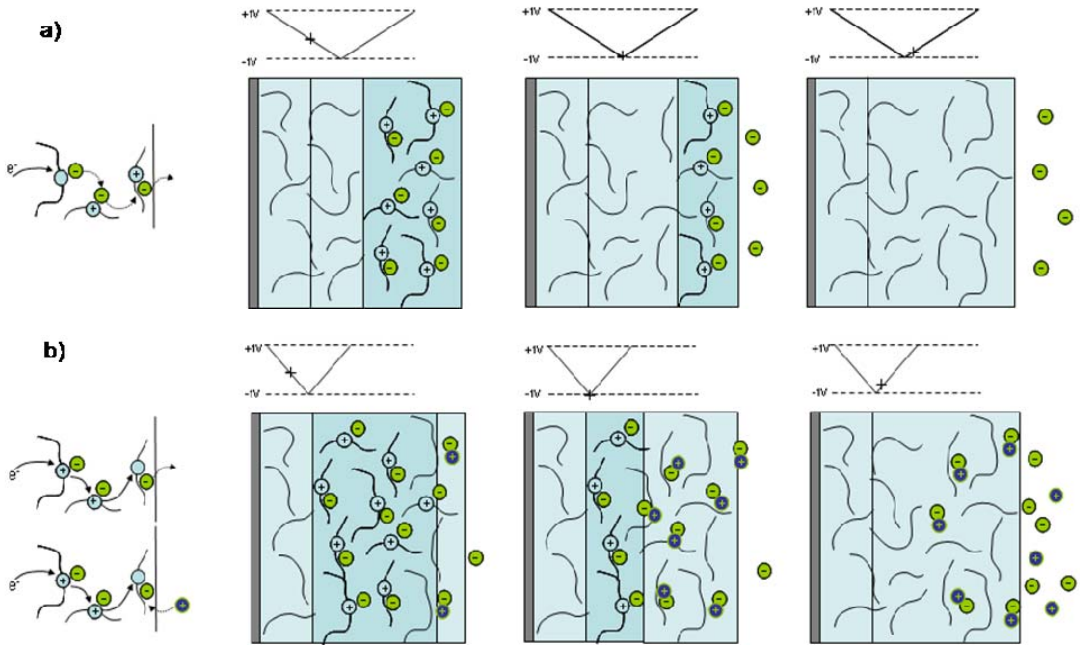

Figure 3. 7 Schematic illustration of reduction processes at a) slow and b) fast scan rates. At left are suggestion electron / ion transport processes. The three panels show cross-sectional views of the PPy on platinum with the approximate electrode potential illustrated by the cross at top. At slow scan rates, anions are readily expelled as electrons are transported from the Pt electrode (far left) to the oxidized surface layer (far right). At faster scan rates, however, electrons may be transported to the surface chains allowing for fast anion expulsion or inclusion of electrolyte cations (as suggested by the expansion observed during reduction at fast scan rates).

3.3.5 Effect of External Load on Actuation

The ability for actuators to operate against an external load is important in their practical application. The actuation strain per redox cycle has been determined for helix tubes of different thicknesses and tested at varying scan rates and isotonic stresses. The contractile strain during the cathodic scan is summarized in Figure 3. 8 for all experimental conditions. It is seen that the actuation strain decreased monotonically for increasing cyclic voltammetric scan rates for helix tubes of all thicknesses tested. The strain also tended to decrease monotonically with an increasing isotonic stress. It should be noted that the range of stresses studied for the different tube thicknesses were different as a result of the limitations of the Aurora lever arm used to apply force. At a

scan rate of 0.2 mV/s there was a large decrease in actuation strain for increasing applied stress for the full range of thicknesses studied. The decrease in actuation strain at increasing applied stress is likely due to a substantial decrease in the modulus of the reduced PPy as predicted by Spinks *et al.* [21]. In contrast, for the thick PPy at scan rates of 10 to 50 mV/s, the actuation strain was essentially independent of stress for the range of stresses studied, but decreased monotonically for increasing scan rates. These results may be related to limited redox reaction occurring in the thicker tubes and at higher scan rates. It has been noted previously that the PPy needs to be extensively reduced to observe a decrease in modulus resulting in a significant reduction in strain of relatively large stresses [21-23].

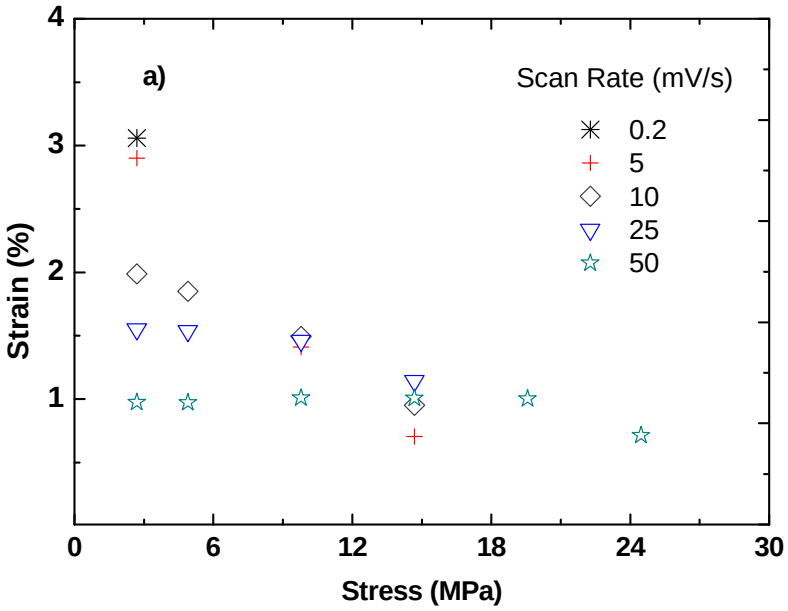

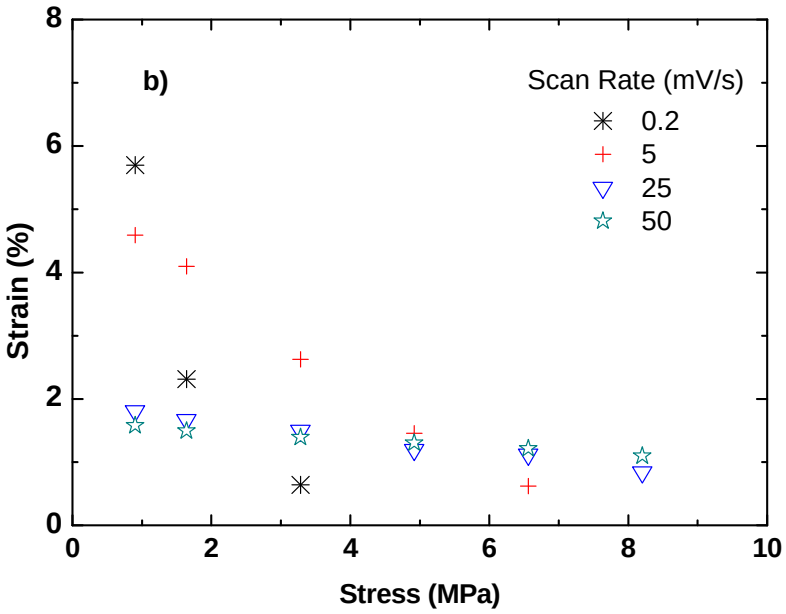
b)
Scan Rate (mV/s)
0.2
5
25
50
Strain (%)
Stress (MPa)
0
2
4
6
8
10

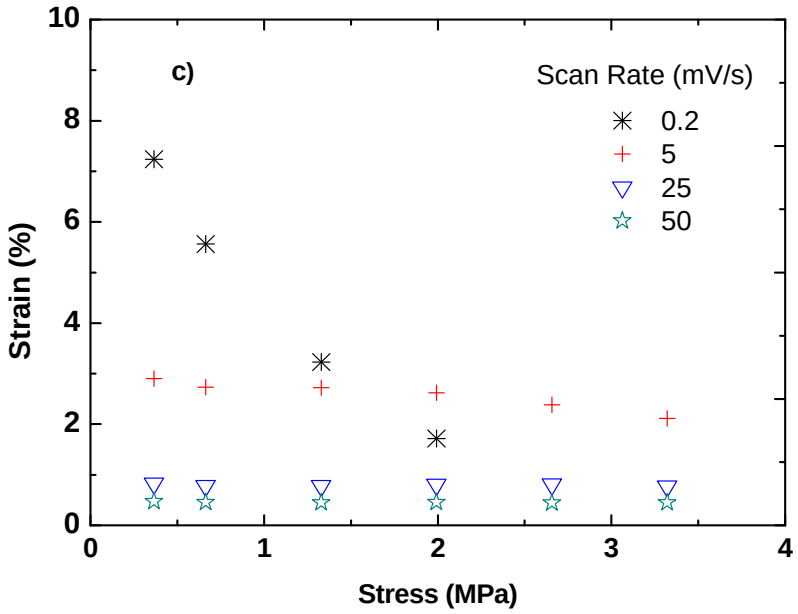
c)
Scan Rate (mV/s)
0.2
5
25
50
Strain (%)
Stress (MPa)
0
1
2
3
4
6
8
10

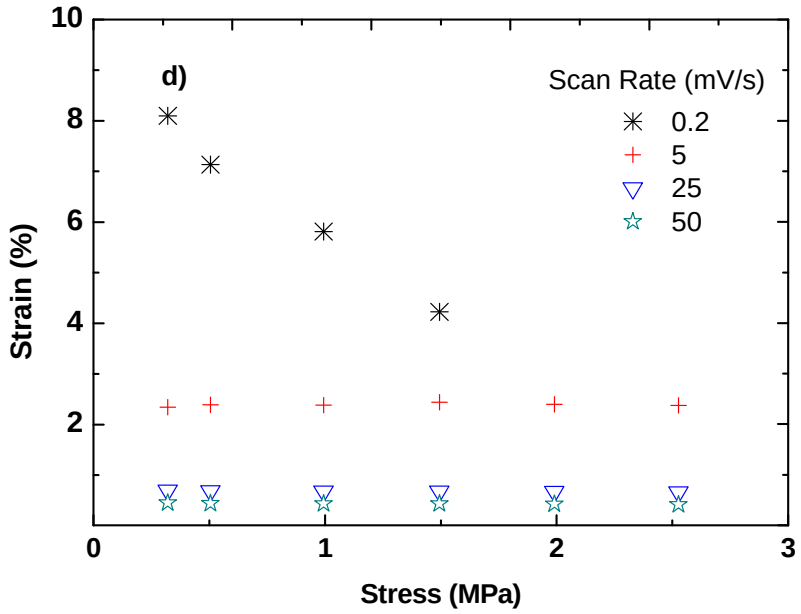

Figure 3. 8 Contractile actuation strain in PPy helix tubes prepared at different wall thicknesses and tested at different strain rates: a) 5 μm thick wall thickness; b) 15 μm thick wall thickness; c) 34 μm thick wall thickness and d) 44 μm wall thickness.

At equivalent applied stresses, it was noted that the maximum actuation occurred in the 15 μm thick helix tube. Both thinner (5 μm) and thicker (34 μm and 44 μm) helix tubes gave smaller actuation strains. The effect of tube thickness on actuation strain under load was most notable at the higher scan rates. For scan rates from 25 to 50 mV/s the thick tubes exhibited substantially less actuation than the thin tubes at equivalent applied stress (Figure 3. 9). As described in Section 3.3.3, the redox reactions were incomplete during the voltage scan at higher scan rates and with thicker tubes. The smaller strains at high scan rates are likely due to the reduced redox activity, the quantitative relationship between strain and charge transferred is considered in Section 3.3.5.

The reason for the anomalously low actuation strain generated by the thinnest helix tube may be due to the restricting effect of the Pt helix wire incorporated into the tube

wall. The actual strain produced in these helix tubes must be affected by the Pt helical wire that is incorporated into the tube wall for the purpose of improving the electrical conductivity along the tube length. The helical wire acts as a spring (with a spring constant measured at 0.05 N/mm) that will limit the free actuation of the PPy. As reported previously, the actuation strain when operating against an external spring decreases as the ratio of the helix tube spring stiffness and the PPy stiffness increases [24]. The latter is determined by the PPy modulus, tube length and tube wall thickness. As the tube wall thickness decreases, so too does the PPy stiffness and so the net actuation will be smaller. This effect may account, at least in part, for the lower than expected strains generated by the thinner helix tubes.

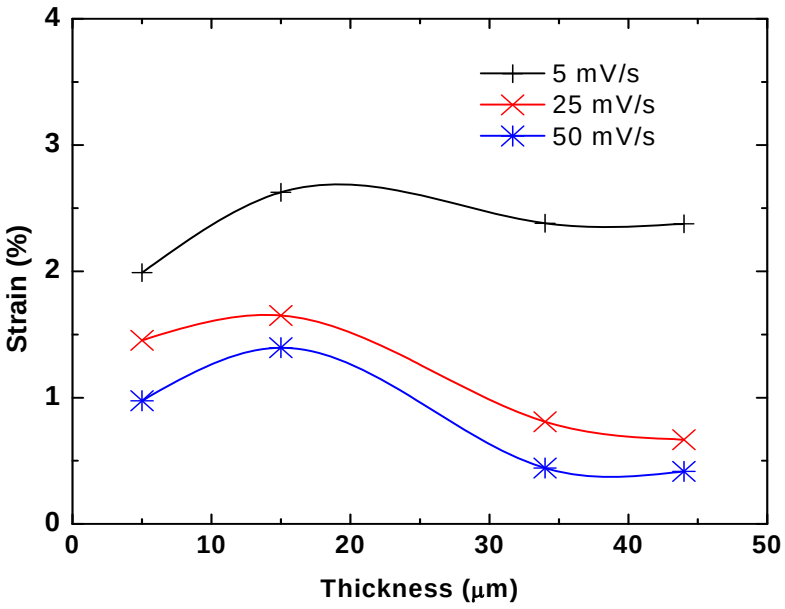

Figure 3. 9 The actuation strain of PPy helix tubes having different wall thicknesses and tested at two different scan rates: 5 and 50 mV/s 2.6 MPa.

Previous work on the effect of layer thickness on the actuation of PPy has considered only bending-type systems. Radharkrishnan and Kar, for example, measured the bending angles of PPy/SO_4^- bi-layers [25]. They found that the bending angle

reaches a maximum at a certain PPy thickness (~8μm) for a given backing material. Below that value, the decreased amount of PPy resulted in a reduced bending angle. For thicker PPy layers, the bending angle also decreased due to the stiffness increasing of the whole bi-layer. These studies were conducted at the equilibrium state of PPy to, hence redox processes were complete and so it is expected that the full thickness of PPy was in the same redox state, unlike in the current study.

3.3.6 Actuation Strain-Charge Relationship

It has previously been reported that the extent of actuation in PPy is directly related to the charge passed [15, 26]. The measured isotonic strains for the 4 different wall thicknesses at three different scan rates are plotted against the charge passed in Figure 3. 10 a). No discernable trend can be seen between strain and charge in these data. The free strain (at zero external stress) to volumetric charge ratio is given in Figure 3. 10 c) and now an approximately linear relationship is seen. The strain to charge ratio for the thinnest wall thickness (5 μm) is significant lower than thicker ones. As mentioned above, the actuation strain in the thin tubes is likely restricted by the mechanical resistance imposed by the Pt helix. The charge consumed was also found to be larger than the theoretical charge for the thin tube tested at the slowest scan rate. Charge may be consumed in other ways (parasitic) rather than directly contributing to strain generation in those thin samples. The volumetric strain to charge ratio (γ) calculated for thick (34, 44μm) samples is $2.3*10^{-10}$ m^3/C (dash line), which is close to the value reported previously [15]. The strain to charge ratio for the 15 μm wall thickness was $1.7*10^{-10}$ m^3/C, slightly lower than the thicker tubes and may be suppressed due to the limiting effect of the Pt helix.

The strain to charge ratio was found to be dependent upon the applied external stress. Data in Figure 3. 10 b) show strains measured at different isotonic stresses for one tube thickness (34μm). For each isotonic stress, an approximately linear relationship is seen between the strain and charge passed. The slope of these lines clearly decreases with an increase in the applied stress.

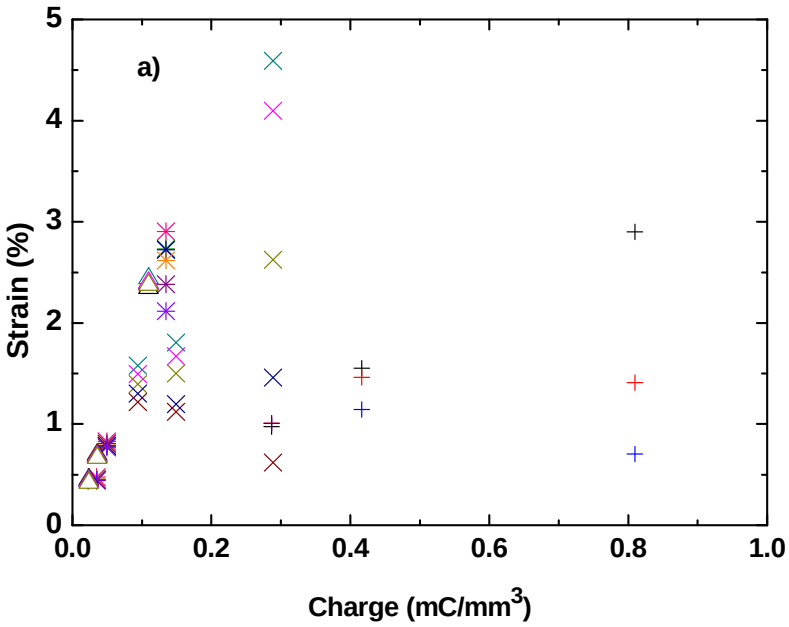

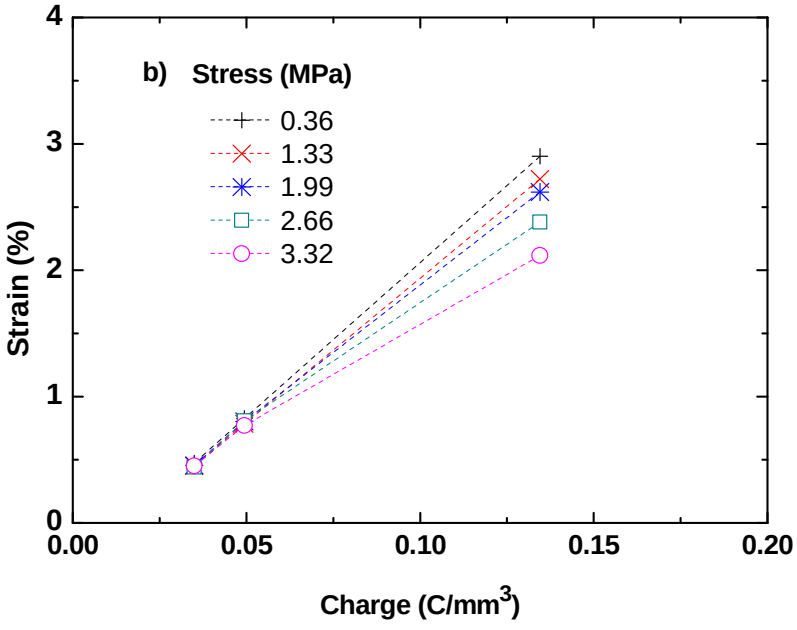

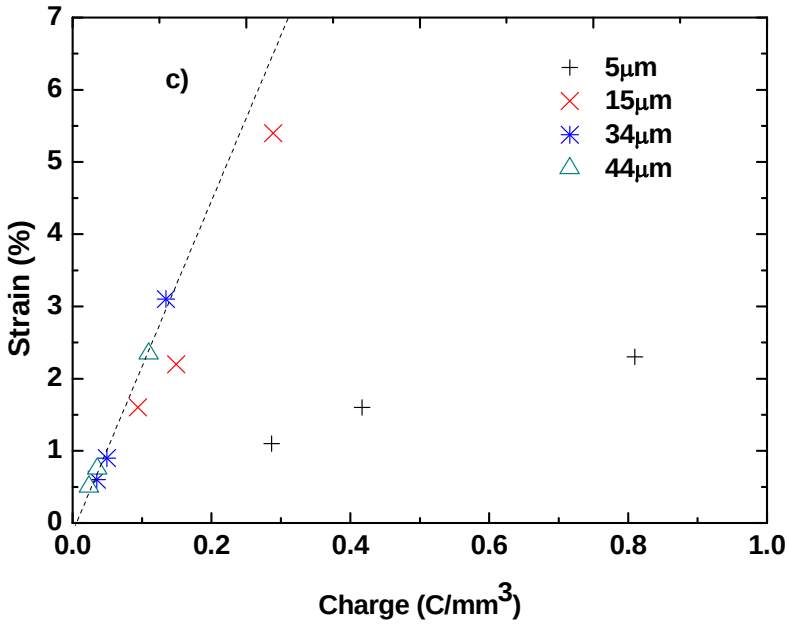

Figure 3. 10 a) strains measured at different isotonic stresses for 34μm tube thickness against charge passed; b) Isotonic actuation strain measured at low stresses (<30 kPa) and at different strain rates for various helix tube thicknesses: 5 μm, 15 μm, 34 μm, 44 μm. Linear fits of strain to charge ratio by using 34 μm and 44 μm thick tubes is presented with dot line.

3.3.7 Effect of Modulus Shift on Actuation Strain

It has been shown previously that an increase in modulus of oxidized PPy compared to the reduced PPy causes a reduction in isotonic strain in direct proportion to the applied isotonic stress [24]. The effect of isotonic stress on the actuation strain has been analyzed using the following equation:

$$\varepsilon = \varepsilon_0 + \sigma\left(\frac{1}{Y'} - \frac{1}{Y}\right) \tag{3.6}$$

in which ε_0 is the charge induced free strain under zero load; Y and Y' are the elastic moduli before and after the potential applied; σ is the stress applied to the actuator.

The results presented in this thesis show that the effect of isotonic stress on the actuation strain during polymer reduction is strongly dependent upon the voltage scan rate. The effect of scan rate is now interpreted based on its effect on both the charge

passed and the composite modulus of the partly-reduced polymer. Thus, the free strain during reduction of the polymer is taken as directly proportional to the charge passed so that $\varepsilon_0 = \gamma Q_v$ where γ is the free strain to charge ratio and Q_v the volumetric charged passed during the cathodic scan.

Reduction of the fully oxidized PPy is assumed to occur by the reverse of the diffusion-controlled oxidation model described in Section 3.3. Thus, a layered structure is assumed to form with a fully reduced layer adjacent to the electrolyte and a fully oxidized layer adjacent to the metal. The thickness of the reduced layer is assumed to increase in direct proportion to the charge passed. The elastic modulus Y_c of the partially reduced polymer can be estimated by the composites "rule of mixtures":

$$Y_c = (1 - \alpha) \cdot Y_{ox} + \alpha \cdot Y_{red} \tag{3.7}$$

where α is the volumetric fraction of charged PPy:

$$\alpha = \frac{Q_v}{Q_{vmax}} \tag{3.8}$$

and $Y_{red}$is the elastic modulus when PPy is fully reduced, and Y_{ox} is the elastic modulus of fully oxidized PPy. The isotonic strain expected for partly reduced PPy is now:

$$\varepsilon = \gamma Q_v + \sigma\left(\frac{1}{Y_c} - \frac{1}{Y_{ox}}\right) = \alpha\gamma Q_{vmax} + \sigma\beta\left(\frac{1}{Y_{red}} - \frac{1}{Y_{ox}}\right) \tag{3.9}$$

where β is the modulus shift factor, given by:

$$\beta = \frac{\frac{1}{Y_c} - \frac{1}{Y_{ox}}}{\frac{1}{Y_{red}} - \frac{1}{Y_{ox}}} = \frac{\alpha}{(1-\alpha)\frac{Y_{red}}{Y_{ox}} + \alpha} \tag{3.10}$$

From previous work the moduli can be estimated as Y_{red} ~70 MPa, and Y_{ox} ~ 140 MPa [27]. Q_{vmax} is calculated as 0.7439 C/mm^3 (using a density of 1.5g/cm^3). As mentioned above, free strain to charge ratio (γ) is fitted as 2.3*10^{-10} m^3/C.

The actuation strain at different scan rate for the 15, 34 and 44 μm wall thickness tubes were calculated and are presented in Figure 3. 11 d), e) & f). The calculation for

5μm wall thickness sample was not carried out as the Pt helix spring greatly reduces the actuation strain (Figure 3. 10 a), and also high creep at high stress made measurement of the contractile strain difficult. The calculated strain matches experiment result quite well for 34 and 44μm thick helix tubes. There is some error between predicted and experiment value for 15μm sample with the predicted values higher than the measured values, particularly at higher stresses. The composite rule of mixtures approach used to determine the modulus of the partially reduced PPy seems to underestimate the extent of modulus shift for the thinner helix tubes, perhaps due to the effect of the Pt spring. Despite this error with the thinner helix tube, the method for predicting the isotonic strain for partially reduced PPy helix tubes is able to show the general effects of applied stress, tube thickness and scan rate.

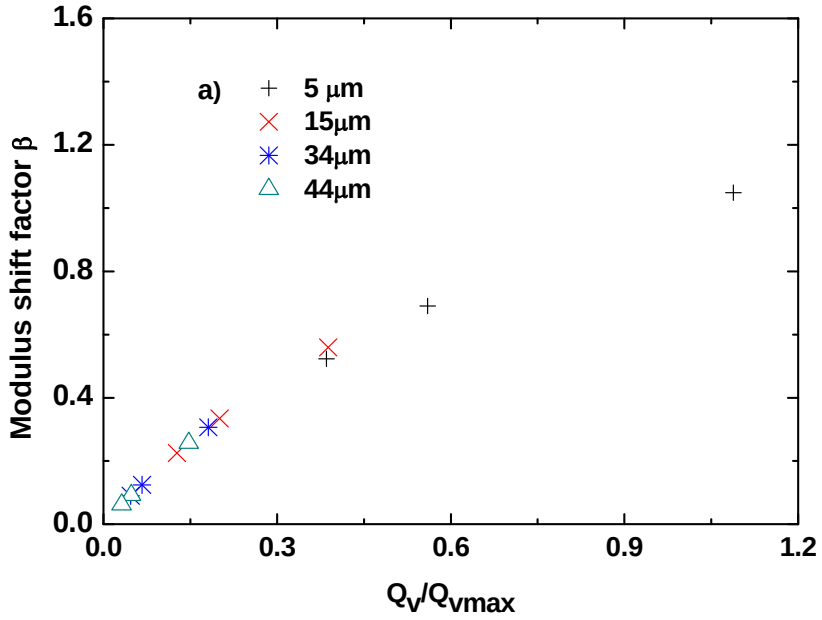

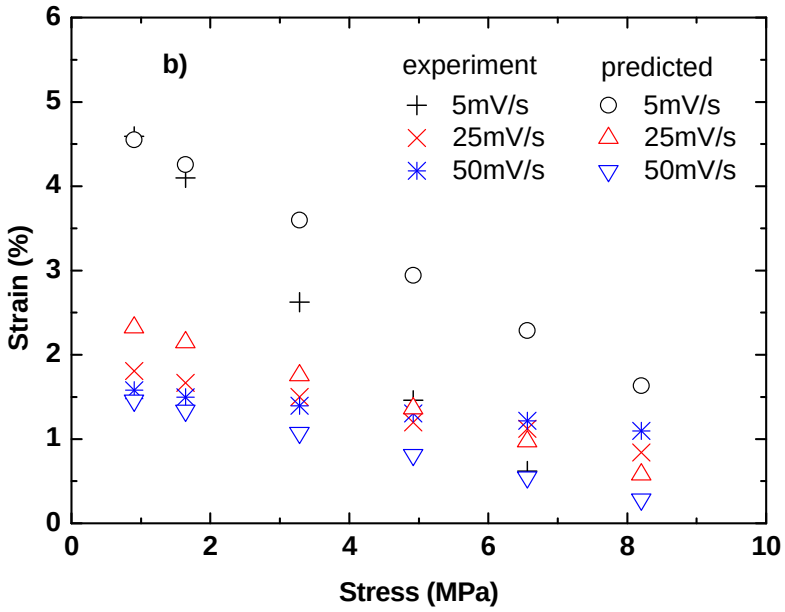
b)
experiment
5mV/s
25mV/s
50mV/s
predicted
5mV/s
25mV/s
50mV/s
Strain (%)
Stress (MPa)
0
1
2
3
4
5
6
0
2
4
6
8
10

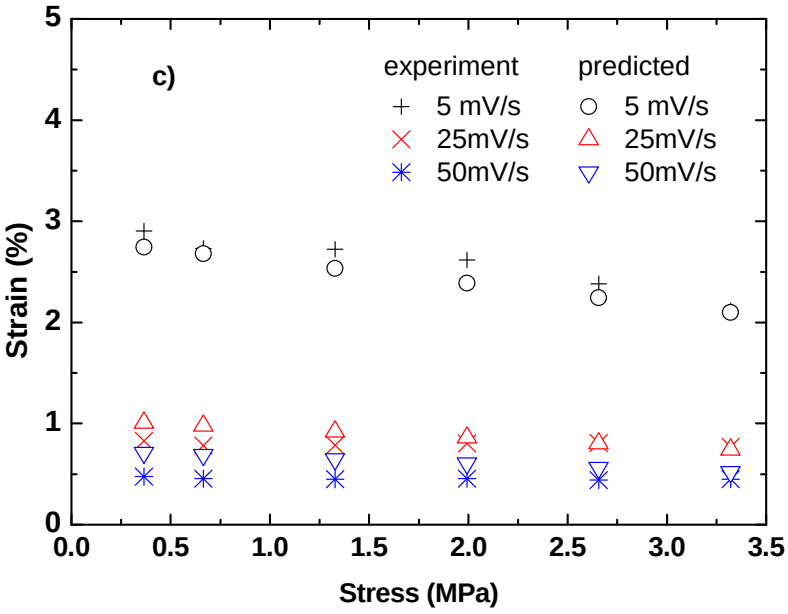
c)
experiment
5 mV/s
25mV/s
50mV/s
predicted
5 mV/s
25mV/s
50mV/s
Strain (%)
Stress (MPa)
0
1
2
3
4
5
0.0
0.5
1.0
1.5
2.0
2.5
3.0
3.5

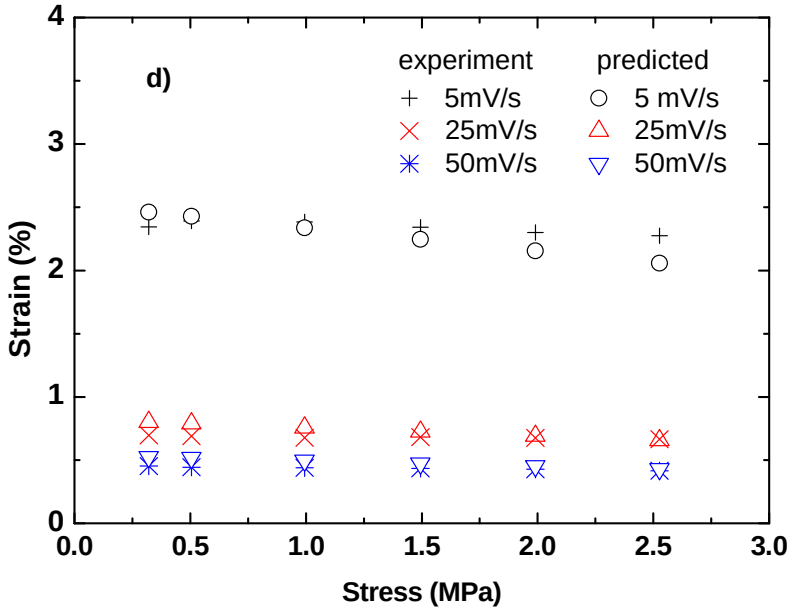

Figure 3. 11 a) Modulus shift factor determined as a function of fractional charging. Calculated isotonic strains at the indicated scan rates for 15 μm (b) 34 μm (c) and 44 μm (d) helix tubes.

Figure 3.12 shows the calculated free strain, modulus shift factor and the overall isotonic strain for 34 & 44 μm wall thickness helix tubes and at different stresses plotted against the extent of charging (α) and using $\gamma = 2.3*10^{-10}$ m^3/C. The strain predicted at 2.6 MPa is 0.48%, 0.73% and 2.5% corresponding to 50, 25 and 5 mV/s respectively, matching result in Figure 3. 9. Free strains ($\sigma = 0$) increase linearly with volumetric fraction of charged PPy (squares) and a strain of ~15% is expected from the fully reduced polymer. (Based on the charging model, this would take 7225 seconds or a scan rate of 0.276mV/s for 34 μm thick helix tubes). Increasing stress reduces the strain achieved at each α value. At low α value, the modulus shift factor is small and hence the strain under stress doesn't change very much compared to the free strain. While at high α value, modulus shift factor become closer to 1. Under this situation, a noticeable decrease in strain can be seen due to an increasing stress. It is must be pointed out that the modulus shift factor is also a function of $\frac{Y_{red}}{Y_{ox}}$. However, $\frac{Y_{red}}{Y_{ox}}$ is unique and constant

for given material.

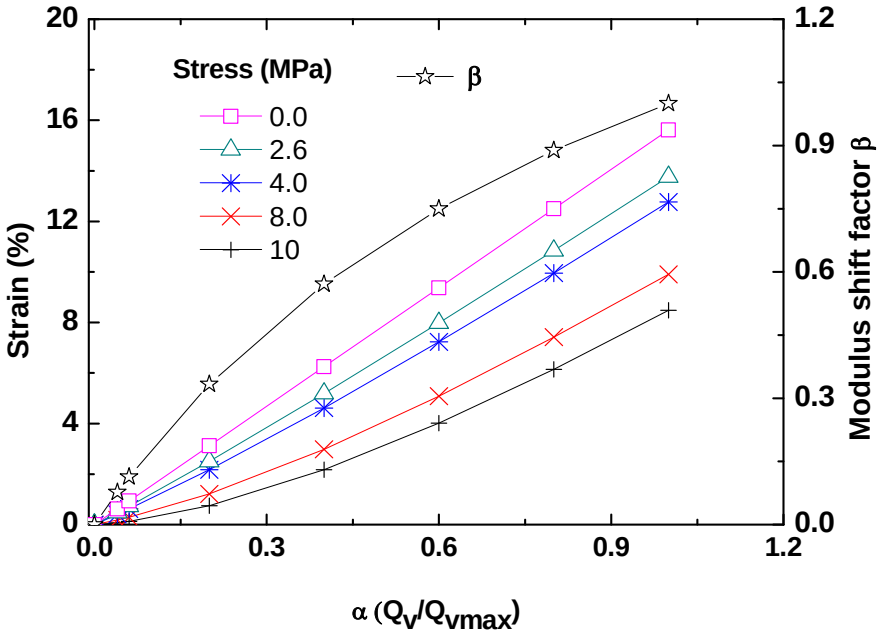

Figure 3.12 Calculated free strain, modulus shift factor and the overall expected isotonic strain for 34μm & 44μm thick helix tubes.

3.3.8 Work and Power out put

Volumetric work per cycle W_v (J/m^3) is another important parameter to evaluate PPy actuators, which is given by:

$$W_v = W / V = \frac{f * |\Delta l_f|}{A * l} = \sigma * |\varepsilon| \tag{3.11}$$

where A and l are the cross-sectional area and the length of the sample; σ presents the isotonic stress applied; ε is the strain generated by the actuators. The volumetric work density produced by the PPy helix tubes is given in Figure 3. 13 for the different tube thicknesses, scan rates and applied isotonic stress. Generally, the work density was found to increase with increasing isotonic stress and with decreasing voltage scan rate. Slower scan rates allow for higher strains, thereby increasing the work density. The

thinner 15 μm helix tubes tended to give higher work density (at equivalent stress and scan rate) than the thicker 34 μm and 44 μm thick tubes. Again, the thinner tubes produced higher strains as a result of the more complete redox reactions occurring.

While the work density generally increased with an increasing isotonic stress, the work density is expected to pass through a maximum with an increase in stress [24]. A maximum in work output was observed for the 15 μm thick tube at the slowest scan rate. In other cases, it is likely that the breaking strength of the helix tube was less than the stress at which maximum work occurs, so that the peak in work output could not be experimentally achieved.

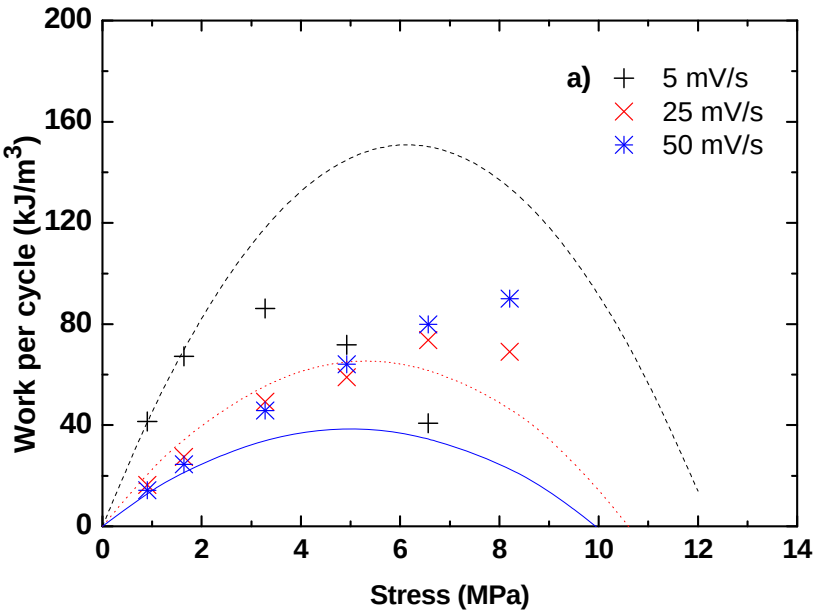

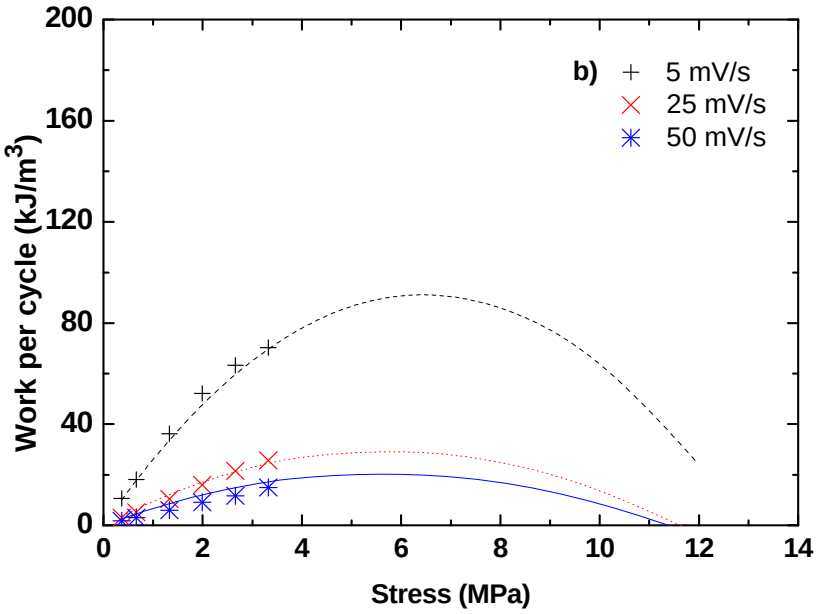
b)
5 mV/s
25 mV/s
50 mV/s
Work per cycle (kJ/m3)
Stress (MPa)
0
40
80
120
160
200
0
2
4
6
8
10
12
14

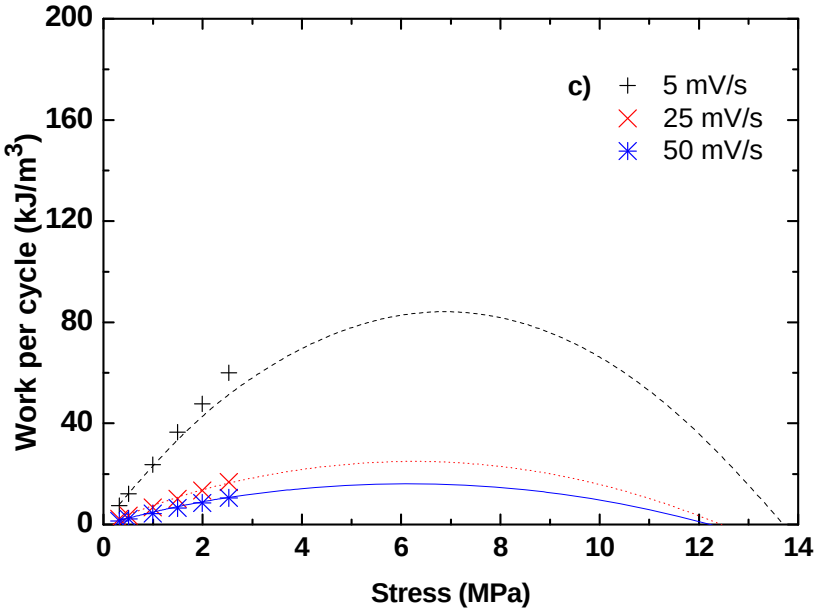
c)
5 mV/s
25 mV/s
50 mV/s
Work per cycle (kJ/m3)
Stress (MPa)
0
40
80
120
160
200
0
2
4
6
8
10
12
14

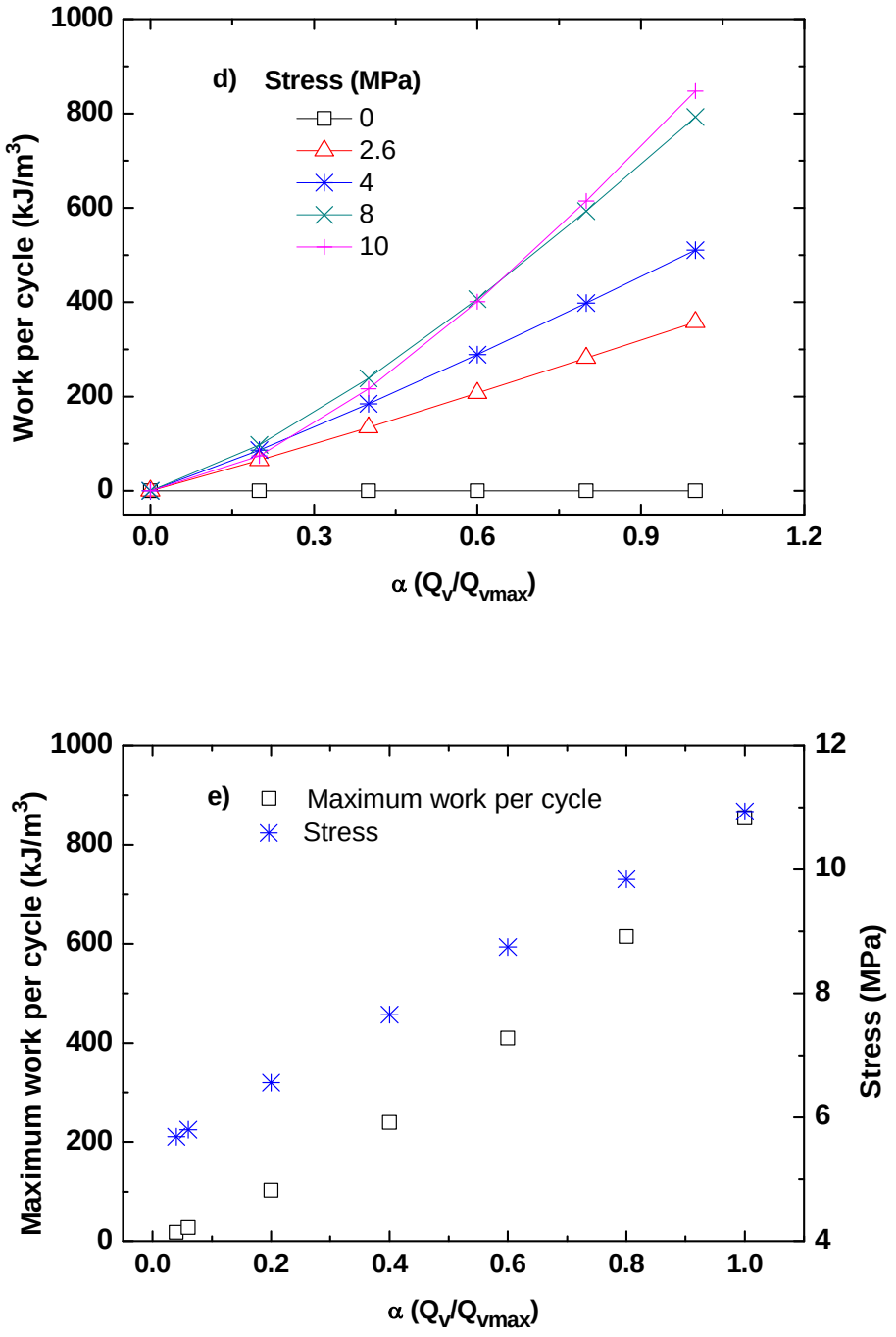

Figure 3. 13 Work for cycle for PPy/PF_6 helix tubes with different thickness under various stress levels. a) 15 µm; b) 34 µm; c) 44 µm. Dash, dot and solid lines represent the prediction value of each scan rate. d) Theoretical prediction of work density as a function of charge ratio; e) theoretical maximum work density prediction and the correspondence stress.

The work output of the helix tubes could be calculated using the approach described in Section 3.6. For partially reduced PPy helix tubes, the volumetric work density can be estimated from:

$$\beta = \frac{\frac{1}{Y_c} - \frac{1}{Y_{ox}}}{\frac{1}{Y_{red}} - \frac{1}{Y_{ox}}} = \frac{\alpha}{(1-\alpha)\frac{Y_{red}}{Y_{ox}} + \alpha}$$

$$W_v = \sigma\varepsilon = \sigma\gamma\alpha Q_{v,\max} + \sigma^2 \left(\frac{\alpha}{(1-\alpha)\frac{Y_{red}}{Y_{ox}} + \alpha} \right) \left(\frac{1}{Y_{red}} - \frac{1}{Y_{ox}} \right) \quad (3.12)$$

The calculated work density values are shown as dashed lines in Figure 3. 13 and agree with the measured values quite well for the thicker helix tubes (34, 44μm). The work density is overestimated for 15 μm thick samples, for the same reasons as given above for the overestimation of strain. The expected work output as a function of the extent of charging is given in Figure 3. 13 d). The work output increases non-linearly with increasing extent of charging due to the higher strains. The effect of applied stress is more complex with a peak in work output expected with increasing applied isotonic stresses. For the stresses used in the calculations given in Figure 3. 13 d), the work output generally increases with increasing stress, for a given charging ratio.

The maximum work density can be predicted as below:

$$\frac{dw_v}{d\sigma} = 0 \quad (3.13)$$

$$\text{hence} \quad w_{vmax} = \frac{1}{4}(\alpha\gamma Q_{vmax})^2 \frac{1}{\beta(\frac{1}{y_{ox}} - \frac{1}{y_{red}})}$$

$$\text{when} \quad \sigma = \frac{\alpha\gamma Q_{vmax}}{2\beta(\frac{1}{y_{ox}} - \frac{1}{y_{red}})}$$

Increasing stress would initially increase the work output. However, continued increase in stress will lead to a drop in work output because of reducing strain. Figure 3. 13 e) shows the expected maximum work per cycle. As shown in the figure, this maximum work output increases for more complete charging of the PPy. The fully reduced PPy is expected to give a maximum work output of ~800 kJ/m^3, which is substantially larger

than experimentally measured in this and other studies [14, 28]. The stress at which this maximum work output occurs is calculated to be ~11 MPa, which is beyond the breaking stresses of helix tubes tested in this study. Improving the strength of the helix tubes would allow substantial improvements in the actuation performance in terms of work output.

While the work density values are useful in determining the effect of applied stress and scan rate on the actuator performance, the actual work output needs to be considered when determining the true effect of the helix tube thickness. Figure 3. 14 shows calculated work outputs for different thickness helix tubes at different applied stresses and assuming the PPy is fully reduced in each case (i.e. α=1). At each applied stress, the work output increases with increasing tube thickness, as expected.

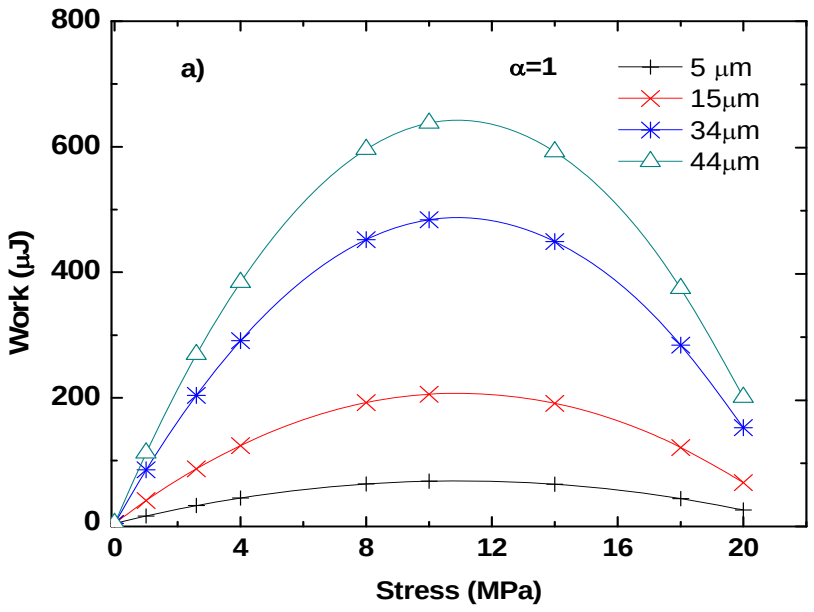

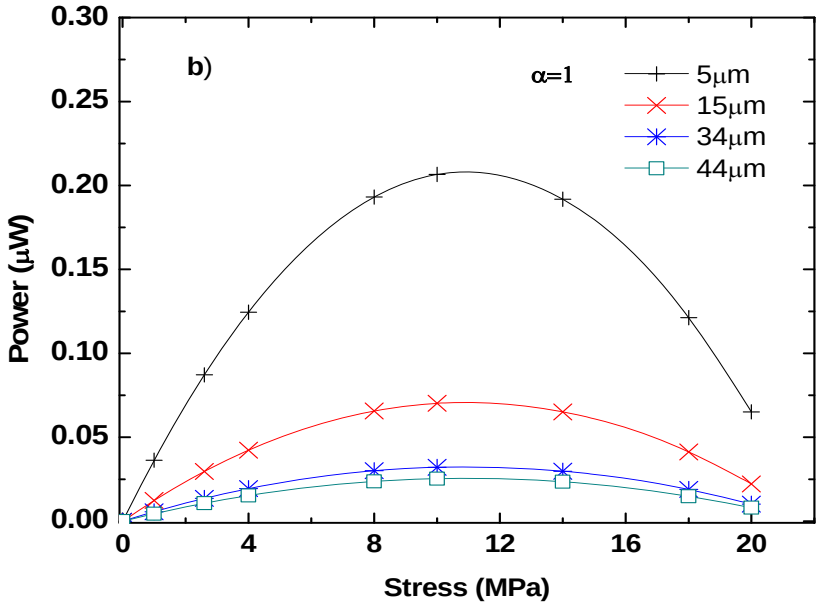

Figure 3. 14. Calculated Work (a) and Power (b) outputs per reduction cycle for PPy/PF_6 helix tubes with different thickness under various stress levels.

It is useful to also consider the power output of the helix tubes. Figure 3. 15 b) shows the calculated power output averaged over the cathodic scan where the scan time is adjusted to allow full reduction of the PPy. Thus, the scan time is determined from

$$t = \frac{\alpha^2 d^2}{2D} = \frac{d^2}{2D} \quad (\alpha = 1)$$

For thicker helix tubes a longer scan time is required to allow full reduction of the polymer. The effect of the longer charging time is that the power output of the thicker helix tubes is now lower than that of the thinner tubes. The shorter time needed to fully reduce the thinner helix tube more than compensates for the smaller work output, giving a higher power output.

The effect of scan rate (and incomplete reduction) of the helix tubes on the measured power output is shown in Figure 3. 15 as power per unit volume. Higher power densities are produced at the higher scan rates. The decreased strain output due to incomplete reduction occurring at higher scan rates is more than compensated by the

shorter time when determining the power output. Calculated power densities are also given in Figure 3. 15 with the power density of the helix tubes calculated using the approach described in Section 3.6 and charging time estimated as in Section 3.3. Again to simplify, the helix tube is treated as a plate.

$$\frac{Q_v}{Q_{vmax}} = 2\sqrt{D}\frac{\sqrt{\Delta V}}{d\sqrt{r}}$$

$$t = \frac{1}{4}\alpha^2 d^2/D$$

As the total time of cathodic scan is 2t, average power density could be estimated from:

$$p = \frac{W_v}{2t} = \frac{\sigma\varepsilon}{2t} = \frac{2D\sigma\gamma Q_{v,\max}}{\alpha d^2} + \sigma^2\left(\frac{\alpha}{(1-\alpha)\frac{Y_{red}}{Y_{ox}}+\alpha}\right)\left(\frac{1}{Y_{red}}-\frac{1}{Y_{ox}}\right)\left(\frac{2D}{\alpha^2 d^2}\right) \quad (3.14)$$

The calculated power outputs agree well with the measured values for the thicker helix tubes. Again the power output is expected to reach a maximum at a stress well beyond the breaking strength of these thicker helix tubes. The highest power density was achieved with the 15 μm helix tube tested at the fastest scan rate.

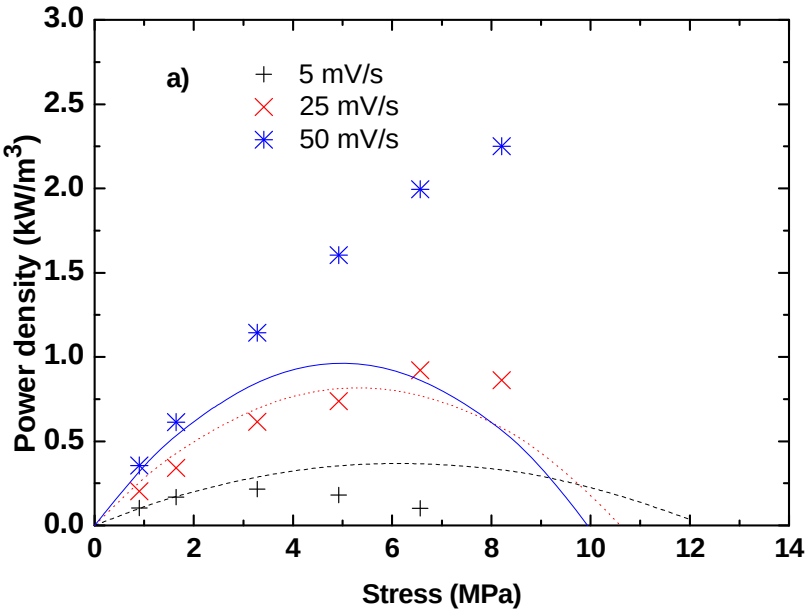

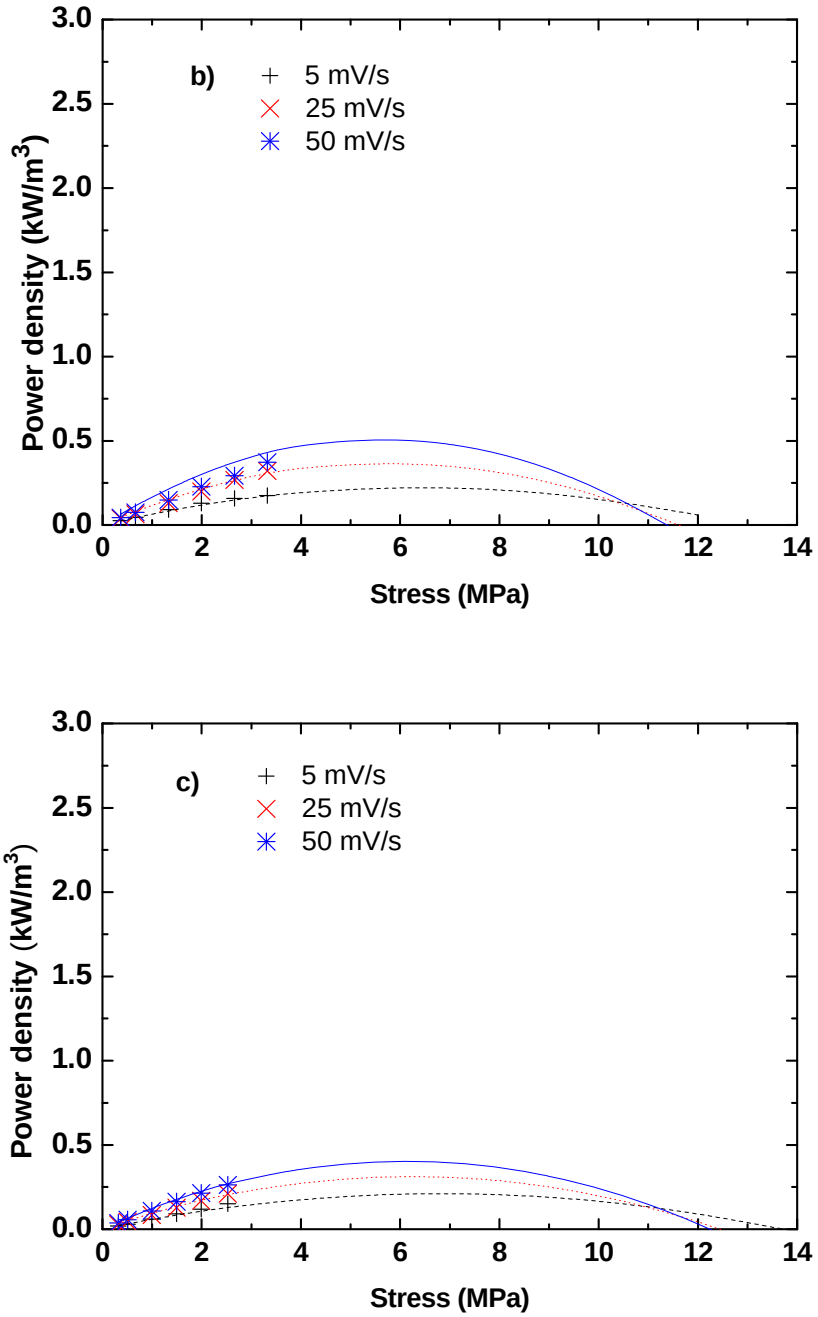

Figure 3. 15 Volumetric power density for PPy/PF_6 helix tubes with different thickness under various stress levels. a) 15 µm; b) 34 µm; c) 44 µm. Dash, dot and solid lines represent the prediction value of each scan rate.

3.4 Conclusions

The aim of this chapter was to investigate the effect of wall thickness on the

actuation behavior of PPy/PF_6 helix tubes. Important actuation parameters considered were strain, work and power output. Most practical applications for actuators require a defined strain to be produced against a known external force in a specified time period. A thinner PPy actuator is likely to respond faster but may produce a lower strain, since the stress is higher. Thus, it is important to quantify the effect of PPy layer thickness on the actuation performance.

From prior studies it was known that the strain produced by PPy actuators is proportional to the charge transferred. It was also known that charging occurred by both electron and ion transport within the polymer so that the rate of charging would depend upon electron and ion conductivities and diffusion distances. One objective of the present chapter was to quantify the effect of PPy layer thickness on the extent of charging and, hence, actuation strain. Using cyclic voltammetry at different scan rates and for different helix tube thicknesses, it was found that the rate of charge transfer could be accurately determined using a simple Fickian diffusion process. Ion diffusion was the rate controlling process with oxidation of the reduced polymer proceeding as a layer of oxidized polymer at the electrolyte side penetrating deeper into the polymer over time. A diffusion coefficient of $4*10^{-11}$ m^2/s was determined from these studies, which was a similar magnitude found for diffusion of other anions in oxidized PPy. With such slow ion diffusion, the time required for full oxidation of the helix tubes increased from 2.25 to 7744 seconds for tubes of wall thickness in the range 5 μm to 44 μm.

A form of "charge trapping" was also observed for the thicker helix tubes at faster scan rates. Here it was postulated that the faster scan rates led to the formation of a buried oxidized layer during the reduction of the PPy. This buried layer formed as a result of cation ingress to the surface of the PPy leading to mixed ion actuation. The

trapped charge could be subsequently reduced during the first part of the anodic scan resulting in a reduction minimum.

It has also been previously recognized that the strain produced by PPy actuators depends upon the external stress and is due to a change in modulus that accompanies a change in oxidation state of the polymer. A second objective of this chapter was to quantify the effect of applied isotonic stress on the actuation strain of PPy helix tubes and to investigate the effect of modulus shift as a function of tube wall thickness. Experimental results showed that the strain decreased with increasing isotonic stress (particularly for the thinner helix tubes) and for higher scan rates. For a given stress, the maximum strain was observed in the 15 μm thick tubes. The thinnest tubes were probably restricted significantly by the mechanical constraint imposed by the helix spring.

The effect of stress on the actuation strain was modeled for the 3 thicker helix tubes by experimentally determining the strain to charge ratio and by estimating the modulus of the partially reduced PPy using the composites "rule of mixtures" approach. The strain to charge ratio was found to depend upon the applied stress. The strain to charge ratio at zero applied stress was similar to previously reported values. The effect of stress on the strain was successfully predicted for the thicker helix tubes. The model demonstrated that the expected strain for fully reduced PPy helix tubes should be ~ 15%.

The strain model also enabled the prediction of the work density of the actuators, with the calculated values in close agreement with the experimental values for the thicker helix tubes. The model results illustrate that a maximum work density would be achieved at a stress level above the breaking stress of the helix tubes. Thus, means to improve the strength of the helix tubes would lead to significant increases in work density.

Finally, the power generated by the PPy helix tubes was investigated. The power was considered as the work done per scan time. The work density of the helix tubes was not dependent on the tube wall thickness (for a given charging level), however, the absolute work done increased with tube thickness (and PPy volume), as expected. The power output, however, decreased with increasing tube thickness despite the higher work output. The much increased charging time required for thicker tubes resulted in a reduced power output.

In conclusion, it was determined that the charging process of PPy helix tubes of typical wall thicknesses was a comparatively slow process dominated by ion diffusion kinetics. Consequently, redox reactions at typical actuation times (100 seconds or less) were incomplete and strains were lower than the maximum possible. Thinner helix tubes would be expected to give higher strains, work and power densities within reasonable actuation times. However, at small tube wall thicknesses the effect of the Pt wire spring became important and strains were consequently limited. The optimal performance occurred around 15 μm wall thickness.

3.5 References

1. Gandhi, M.R., Murray, P., Spinks, G.M. and Wallace, G.G., *Mechanism of Electromechanical Actuation in Polypyrrole.* Synthetic Metals, 1995. **73**(3): p. 247-256.
2. Otero, T.F., *Soft, Wet, and Reactive Polymers. Sensing Artificial Muscles and Conformational Energy.* Journal of Materials Chemistry, 2009. **19**(6): p. 681-689.
3. Genies, E.M. and Pernaut, J.M., *Spectroelectrochemical Studies of the Redox and Kinetic-Behavior of Polypyrrole Film.* synthetic metals, 1984. **10**(2): p. 117-129.
4. Herberg, B. and Pohl, J.P., *Electrochemical Investigations on the Diffusion of Perchlorate Ions in Thin Polypyrrole Layers.* Berichte Der Bunsen-Gesellschaft-Physical Chemistry Chemical Physics, 1988. **92**(11): p. 1275-1279.
5. Tezuka, Y. and Aoki, K., *Direct Demonstration of the Propagation Theory of a Conductive Zone in a Polypyrrole Film by Observing Temporal and Spatial Variations of Potentials at Addressable Microband Array Electrodes.* Journal of Electroanalytical Chemistry, 1989. **273**(1-2): p. 161-168.
6. Aoki, K., Cao, J.A. and Hoshino, Y., *Coulombic Irreversibility at Polyaniline-Coated Electrodes by Electrochemical Switching.* Electrochimica Acta, 1993. **38**(13): p. 1711-1716.
7. Kalaji, M., Nyholm, L. and Peter, L.M., *A Microelectrode Study of the Influence of Ph and Solution Composition on the Electrochemical-Behavior of Polyaniline Films.* Journal of Electroanalytical Chemistry, 1991. **313**(1-2): p. 271-289.
8. Spinks, G.M., Wallace, G.G., Liu, L. and Zhou, D., *Conducting Polymers and Carbon Nanotubes as Electromechanical Actuators and Strain Sensors.* Materials Research Society Symposium Proceedings, 2002. **698**(Electroactive Polymers and Rapid Prototyping): p. 5-16.
9. DellaSanta, A., DeRossi, D. and Mazzoldi, A., *Performance and Work Capacity of a Polypyrrole Conducting Polymer Linear Actuator.* synthetic metals, 1997. **90**(2): p. 93-100.
10. Spinks, G.M., Campbell, T.E. and Wallace, G.G., *Force Generation from Polypyrrole Actuators.* Smart Materials & Structures, 2005. **14**(2): p. 406-412.
11. John, R., Ongarato, D.M. and Wallace, G.G., *Development of a Conducting Polymer-Based Microelectrode Array Detection System.* Electroanalysis, 1996. **8**(7): p. 623-629.
12. Ding, J., et al., *High Performance Conducting Polymer Actuators Utilising a Tubular Geometry and Helical Wire Interconnects.* Synthetic Metals, 2003. **138**(3): p. 391-398.
13. Pailleret, A., Hien, N., Thanh, D. and Deslouis, C., *Surface Reactivity of Polypyrrole/Iron-Oxide Nanoparticles: Electrochemical and Cs-Afm Investigations.* Journal of Solid State Electrochemistry, 2007. **11**(8): p. 1013-1021.
14. Ding, J., et al., *High Performance Conducting Polymer Actuators Utilising a Tubular Geometry and Helical Wire Interconnects.* Synthetic Metals, 2003. **138**: p. 391-398.
15. Madden, P.G., Madden, J.D., Anquetil, P.A., Vandesteeg, N.A., Hunter, I.W., *The Relationship of Conducting Polymer Actuator Material Properties to Performance.* IEEE J. of Oceanic Engineering, 2004. **29**: p. 696-705.
16. West, K., Careem, M.A. and Skaarup, S., *An Impedance Study of the Doping of*

Polypyrrole in Liclo4/Pc. Solid State Ionics, 1993. **60**(1-3): p. 153-159.
17. Mostany, J. and Scharifker, B.R., *Impedance Spectroscopy of Undoped, Doped and Overoxidized Polypyrrole Films.* synthetic metals, 1997. **87**(3): p. 179-185.
18. Tso, C.H., Madden, J.D. and Michal, C.A., *An Nmr Study of Pf6- Ions in Polypyrrole.* synthetic metals, 2007. **157**(10-12): p. 460-466.
19. Smela, E., *Conjugated Polymer Actuators for Biomedical Applications.* Advanced Materials (Weinheim, Germany), 2003. **15**(6): p. 481-494.
20. Skaarup, S., West, K., Gunaratne, L.M.W.K., Vidanapathirana, K.P. and Careem, M.A., *Determination of Ionic Carriers in Polypyrrole.* Solid State Ionics, 2000. **136-137**: p. 577-582.
21. Spinks, G.M., Liu, L., Wallace, G.G. and Zhou, D., *Strain Response from Polypyrrole Actuators under Load.* Advanced Functional Materials, 2002. **12**(6-7): p. 437-440.
22. Pytel, R.Z., Thomas, E.L. and Hunter, I.W., *In Situ Observation of Dynamic Elastic Modulus in Polypyrrol Actuators.* Polymer, 2008. **49**: p. 2008-2013.
23. Samani, M.B., Whitten, P.G., Cook, C.D. and Spinks, G.M., *Modelling of Polypyrrole Actuators.* Materials Research Symposium Proceedings, 2006. **889**: p. 3.1-3.9.
24. Spinks, G.M. and Truong, V.-T., *Work-Per-Cycle Analysis for Electromechanical Actuators.* Sensors and Actuators A: Physical, 2005. **119**(2): p. 455-461.
25. Radhakrishnan, S. and Kar, S.B., *Response Characteristics of Conducting Polypyrrole Bi-Layer Actuators: Role of Backing Layer Polymer.* Sensors and Actuators B-Chemical, 2006. **119**(1): p. 94-98.
26. Otero, T.F., Cascales, J.J.L. and Arenas, G.V., *Mechanical Characterization of Free-Standing Polypyrrole Film.* Materials Science & Engineering C-Biomimetic and Supramolecular Systems, 2007. **27**(1): p. 18-22.
27. Spinks, G.M., Liu, L., Zhou, D. and Wallace, G.G., *Strain Response from Polypyrrole Actuators under Load.* Advanced Functional Materials, 2002. **12**(6-7): p. 437-440.
28. Kaneto, K., Fujisue, H., Kunifusa, M. and Takashima, W., *Conducting Polymer Soft Actuators Based on Polypyrrole Films - Energy Conversion Efficiency.* Smart Materials & Structures, 2007. **16**(2): p. S250-S255.

CHAPTER 4 HIGH STRAIN POLYPYRROLE ACTUATORS

4.1 Introduction

Conducting polymer (CP) actuators usually operate at relatively low voltages and producing competitive advantage over other actuator technologies [1]. The typical strain and stress of PPy actuators are free stroke 1~5% and a blocking stress of 5 MPa [2], resulting in low work density. For PPy/PF_6 helix tubes discussed at the end of chapter 3, those values are quite low and mainly limited by the slow diffusion kinetics and low breaking strength.

Improving the strain generated under stress is an effective way to achieve higher work density. Through adjustments to the polymerization conditions, electrolyte and actuation conditions, the observed strain and stress can be greatly increased. In fact, high strain polypyrrole actuators that exhibit strains larger than 20 % were recently reported [3-5]. These actuation strains are substantially larger than that previously reported for any conducting polymer system and, warrant further investigation.

The high strains reported recently were obtained using unusually slow potential sweeps by Hara et al. [3, 4]. Only a limited number of potential cycles were reported, and strain appeared to diminish over the first few cycles shown. Whether such high strains can be realised over many cycles or at faster strain rates is not known. Understanding and enhancing the conditions required to achieve stable large strain of polypyrrole actuators will help in their commercial realisation.

The degradation of conducting polymer actuators is a complex process and has been reported in a limited number of previous studies. The degradation of actuation with respect to time could be due to chemical degradation of one of the components [6] or irreversible conformational relaxation of the polymer [7]. Many of the studies on chemical degradation have focussed on the electrolyte. For example, ionic liquid [8, 9]

was introduced to replace propylene carbonate as the electrolyte and was shown to greatly enhance the stability of the actuators. Operating over 6000 cycles with just a 20% decrease in strain in ionic liquid compared to 3000 cycles in propylene carbonate with a 75% decrease demonstrated the advantages using ionic liquid. However, when using ionic liquids for high strain polypyrrole films, the stability is still limited to less than 10 cycles [10], suggesting that electrolyte degradation is not the primary cause of reduced actuation in such high-strain systems. Another study [11] measured the total charge for charging and discharge of a polypyrrole actuator in operation and found that the total charge associated with charging was significantly larger than that for discharging. When a stimulation consisting of a constant current pulse was applied to overcome the asymmetric redox behaviour, enhance stability was observed for at least the first hundred cycles.

It also has been deduced that CPs become more rigid when subjected to many charge-discharge cycles [12]. Elastic modulus is one parameter that can be measured in situ during actuation and may give insights into changes taking place within the CP. The solvent, oxidation state and ionic interactions have been proven to affect the elastic modulus [13-15]. Changes to the elastic modulus during the oxidation and reduction have already been shown to affect the observed actuation when the CP is subjected to load [16]. However there is still a lack of information on how elastic modulus changes during many redox cycles.

In this chapter the results of an independent investigation of the high strain systems reported previously is provided. The aim is to provide some insight into the mechanisms that may be the cause of the large actuation. Furthermore, the cycle life of the high strain polypyrrole actuators is explored. To replicate the work of Hara et al, the polypyrrole has been prepared as films (rather than helix tubes) and bis trifluoromethane

sulfonimide (TFSI) used as dopant. Further, films were prepared using methyl benzoate as the electropolymerization solvent, following the method of Hara et al. Films prepared using these conditions have been compared with films prepared from propylene carbonate and using either TFSI or hexafluorophosphate, PF_6 as dopant. In all cases, the strain at low scan rates and the cycle life stability have been investigated.

4.2. Experimental

4.2.1 Reagents and materials

Bis-trifluoromethanesulfonimide lithium (Li.TFSI) salt and tetrabutylammonium bis-trifluoromethanesulfonimidate (TBA.TFSI) were purchased from Fluka. Propylene carbonate (PC) and methyl benzoate (MB) were obtained from Sigma. Pyrrole was obtained from Fluka and was distilled before use. A platinum plate supporting substrates for the electrochemical polymerization of pyrrole with dimensions $25 \times 25 \times 0.1$ *mm* were obtained from Goodfellow®.

4.2.2 Instrumentation

A EG&G Princeton Applied Research Model 363 potentiostat/galvanostat or a BAS CV-27 was used to regulate and measure the current and/or voltage during constant current electropolymerization of pyrrole and for all of the electrochemical studies reported. A MacLab/4e AD analogue to digital converter was used to record electrochemical results.

4.2.3 The preparation of PPy films.

The preparation of PPy films was described previously [17]. The polymerization solution consisted of 0.1 M pyrrole monomer, 0.1 M electrolyte and 1 %(w/w) H_2O in PC or MB. Dissolved $O_{2(g)}$ was removed by bubbling with $N_{2\ (g)}$ for 300 s. Electropolymerization of pyrrole was conducted at a constant current density of 0.1 mA/cm^2 for 12 hours at -31°C.

Following the polymerization of pyrrole, the PPy film was manually peeled off the substrate and then washed with neat solvent to remove residual monomer. The PPy films were then stored in 0.1 M Li.TFSI/$TBAPF_6$ PC solution until further testing. Prior to testing the wet thickness of the PPy films was found to be ~34 μm.

4.2.4 Electrochemical studies

Cyclic voltammograms (CV) were conducted in a 0.1M Li.TFSI/ $TBAPF_6$ PC solution with an organic reference electrode ($Ag\,|\,Ag^+$ in acetonitrile) and a platinum mesh counter electrode. A scan range of -0.9 to +0.7 V with the start point -0.9 V at scan rates ranging from 2 to 400 mV/s was used.

4.2.5 Actuation tests

Actuations tests were performed in 0.1 M Li.TFSI/PC electrolyte using a conventional three electrodes setup, as shown schematically in Chapter 2. The PPy films used for actuation tests were ~10mm in length and 3 mm wide. To achieve electrical and mechanical contact, one clip connected with working electrode was

placed and fixed to the bottom of the cell. The top end was glued to platinum wire using epoxy glue. The gauge length was the length measured between the glue and the clip. When potential was applied, the change in length was measured by a Model 305B Lever Arm Dual Mode System (Aurora Scientific). The counter electrode was platinum mesh and the reference electrode was $Ag \mid Ag^+$ in acetonitrile. The reported actuation strain refers to the change in length due to contraction which is always smaller than or equal to the change in length due to expansion. The contraction occurs when the PPy is reduced. While testing, a small load (~ 30 kPa) was applied to keep the film straight without causing mechanical creep and to avoid the effects of changing modulus on the measured actuation strain.

A small amplitude rectangular force signal was used to measure the dynamic modulus [18]. In this case, the Young's modulus is estimated by $\varepsilon = \frac{\Delta F}{A_0 \Delta L / L_0}$, in which ΔF and ΔL are the change in force and the observed change in length, respectively of the square wave imposed on the applied force. A_0 and L_0 are the original cross sectional area and the original length of the free-standing film.

4.2.6 Physical characterization

The conductivity measurements were performed using standard 4 point method through JANDEL (model RM3). The elastic modulus was carried out by Shimazu tensile test machine. SEM imaging was performed using Leica Stereo Scan 440 microscope.

4.3 Results and discussion

4.3.1 Physical properties of PPy films.

The thickness, conductivity and elastic modulus in the dry state of PPy films were determined in Table 4. 1. A significantly higher conductivity was produced in films prepared using PC as the solvent base for the electrolyte, compared with those films made from MB. Slightly higher conductivity was found in films when TBA.TFSI was used as the electrolyte salt compared with LiTFSI (for the same solvent). Both solvent and dopant affect the Young's modulus (wet and dry), but not in accord with the change in conductivity.

Table 4. 1 Summary of PPy film thickness and properties.

	PPy/LiTFSI/MB	PPy/LiTFSI/PC	PPy/TBATFSI/MB	PPy/TBATFSI/PC*
Thickness (µm)	37	34	36	35
Conductivity ($S.cm^{-1}$)	48.6	125.2	64.7	169
Y's modulus (MPa) (dry)	166	352	240	150
Y's modulus (MPa) (wet)	24.5	37.7	37.5	18

***PPy/LiTFSI/MB= PPy prepared from LiTFSI/Methyl Benzoate; same to others. Elastic modulus at wet state was performed in 0.1M LiTFSI/PC. Films for measuring elastic modulus at dried state were washed with acetone and dried in vacuum under 35˚C for over night. Films for measuring elastic modulus at wet state were soaked in electrolyte for 0.5hr and tested in it.**

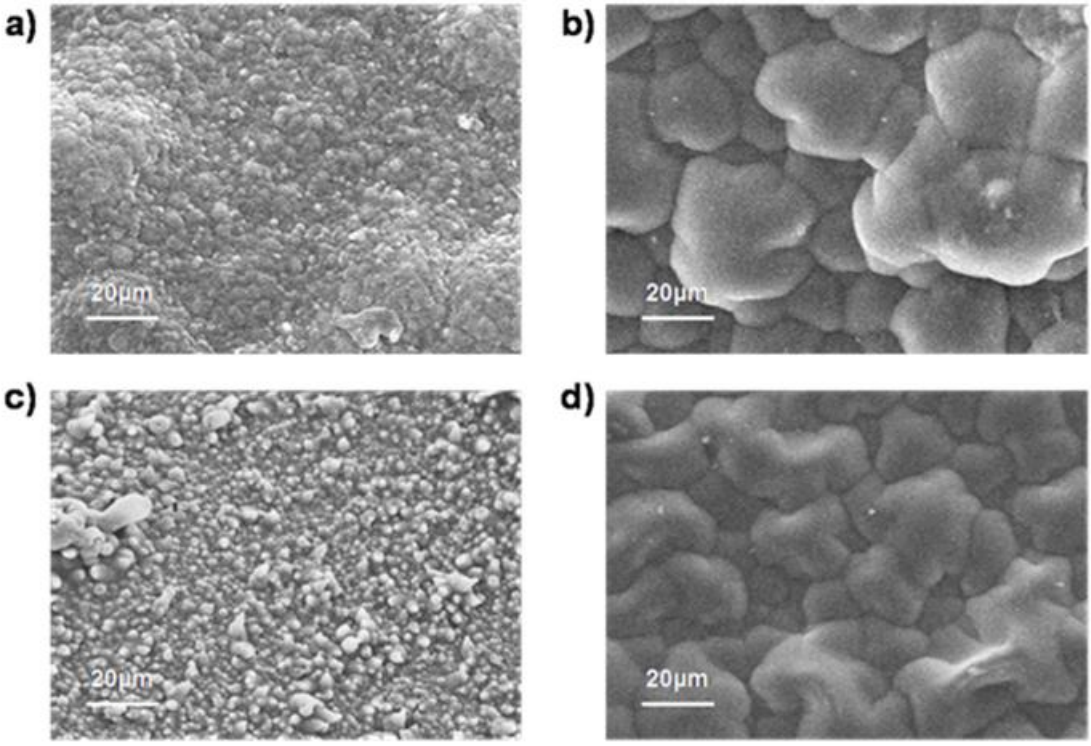

Figure 4.1 The morphology of PPy films; a) PPy/LiTFSI/MB; b) PPy/LiTFSI/PC; c) PPy/TBATFSI/MB d) the electrode side of PPy/TBATFSI/PC.

Figure 4.1 illustrates the morphology of the electrolyte side of PPy films prepared from 4 different polymerization conditions. All 4 SEM pictures show a cauliflower structure, indicating the high surface area of PPy. PPy films prepared from MB have much smaller surface bumps than those found on films produced from PC. Little difference is noted in the surface structure of samples prepared from the different electrolyte salts and from the same solvent.

The morphology of PPy/LiTFSI/MB is as reported by Kaneto [19]. As claimed by Kaneto et al, those materials have loosely packed polymer chains hence allow extremely large strain.

4.3.2 Slow Scan-Rate Actuation

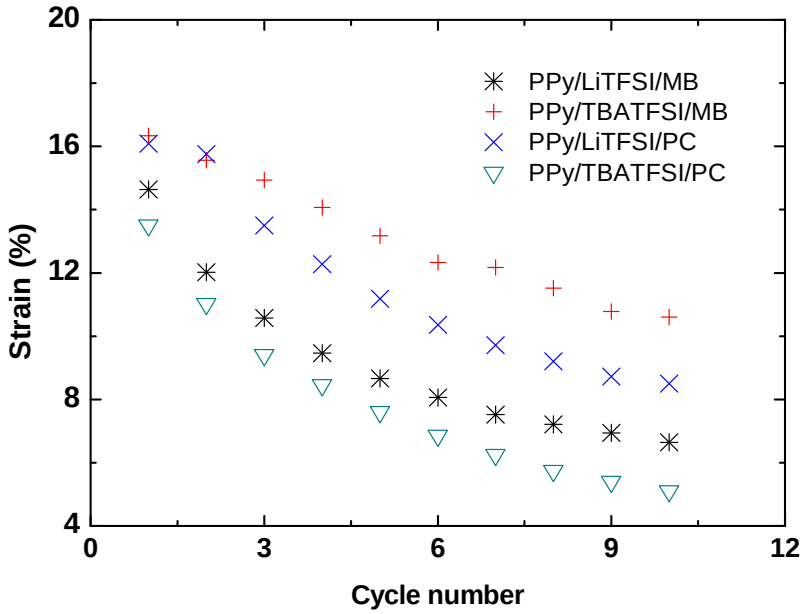

Figure 4. 2 The actuation of PPy films. Scan from -0.9~0.7V (VS Ag/Ag$^+$) at 2mV/s. All samples were tested in 0.1M LiTFSI/PC solution.

Upon oxidization-reduction, the PPy films investigated gave very high electrochemical strain (Figure 4. 2) that decreased rapidly over the first 10 cycles. The highest strain of 16% were obtained in the first cycle for PPy grown from TBATFSI/MB (as reported by Kaneto [20]) and 15% strain of PPy growth from LiTFSI/PC. Hara et al. [3] reported 19.8 % strain for the first cycle of PPy doped with TFSI in the same actuation electrolyte when synthesized from MB, which is slightly higher than the strain reported in Figure 4 for the equivalent system. Small differences in the stress applied to the samples may be the reason for the difference. High strains were observed in all PPy/TFSI samples in their first cycle regardless of their polymerization solvent. Without exception, the strain decreased markedly and after 10 cycles, strains were only 25 – 75% of the original value. For PPy grown from TBATFSI/MB, stability was improved losing only 25% of the initial value after 10 cycles.

4.3.3 Effect of electrolyte concentration on actuation behaviour.

It is still not clear why PPy/TFSI systems could produce significantly higher strains than PPy doped with other dopants, such as PF_6. It has been reported that solvent ingress / egress by osmotic pressure can contribute to actuation in conducting polymers. Bay et al [21] have previously shown that PPy is sufficiently soft for its volume to expand through osmotic pressure. They also noted that the osmotic pressure in inversely related to the ionic concentration and higher actuation strains were achieved when low ionic concentrations were used.

To test if the high strain Li.TFSI system is dependent on the osmotic pressure, actuation was investigated by using three different concentrations of Li.TFSI used during actuation testing (Figure 4.3). The actuation of the PPy was largest in 0.1 M Li.TFSI when compared to 0.01 M Li.TFSI and 1 M Li.TFSI. The actuation observed using 0.1 M electrolyte is initially 2 times that observed using 1 M and after 10 cycles was more than 10 times larger. The increased strain may be a result of the higher osmotic pressure occurring at the lower electrolyte concentration.

As seen in Figure 4.3 c, however, the actuation in the 0.01 M Li.TFSI is smaller than in the 0.1M electrolyte. It would be expected that the osmotic pressure should be greater in solutions of lower electrolyte concentration, leading to larger actuation strains. However, the ionic conductivity of the electrolyte is less efficiency using the 0.01 M concentration leading to a compromise in electrochemistry. Evidence supporting a high resistance cell is provided by the observation that the cyclic voltammogram of the 0.01M solution does not show clear oxidation or reduction peaks, in contrast to the CVs

of the 1st cycle of 0.1M and 1M solutions. The higher solution resistance occurring in the 0.01M solution may therefore restrict the actuation achieved.

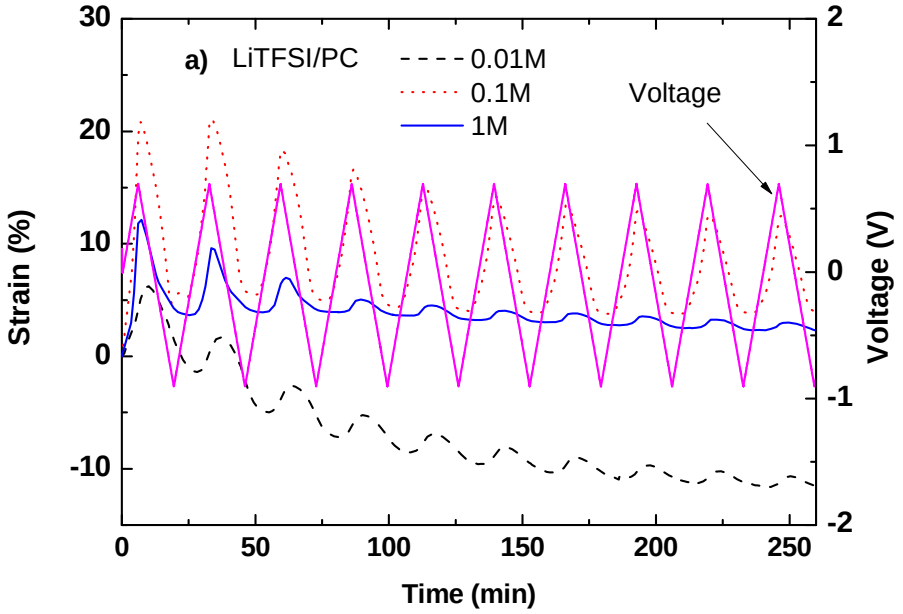

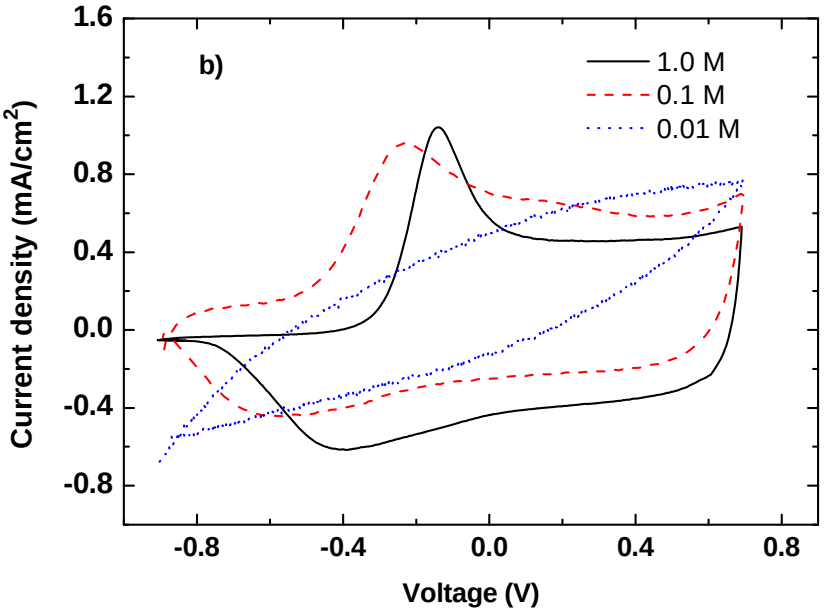

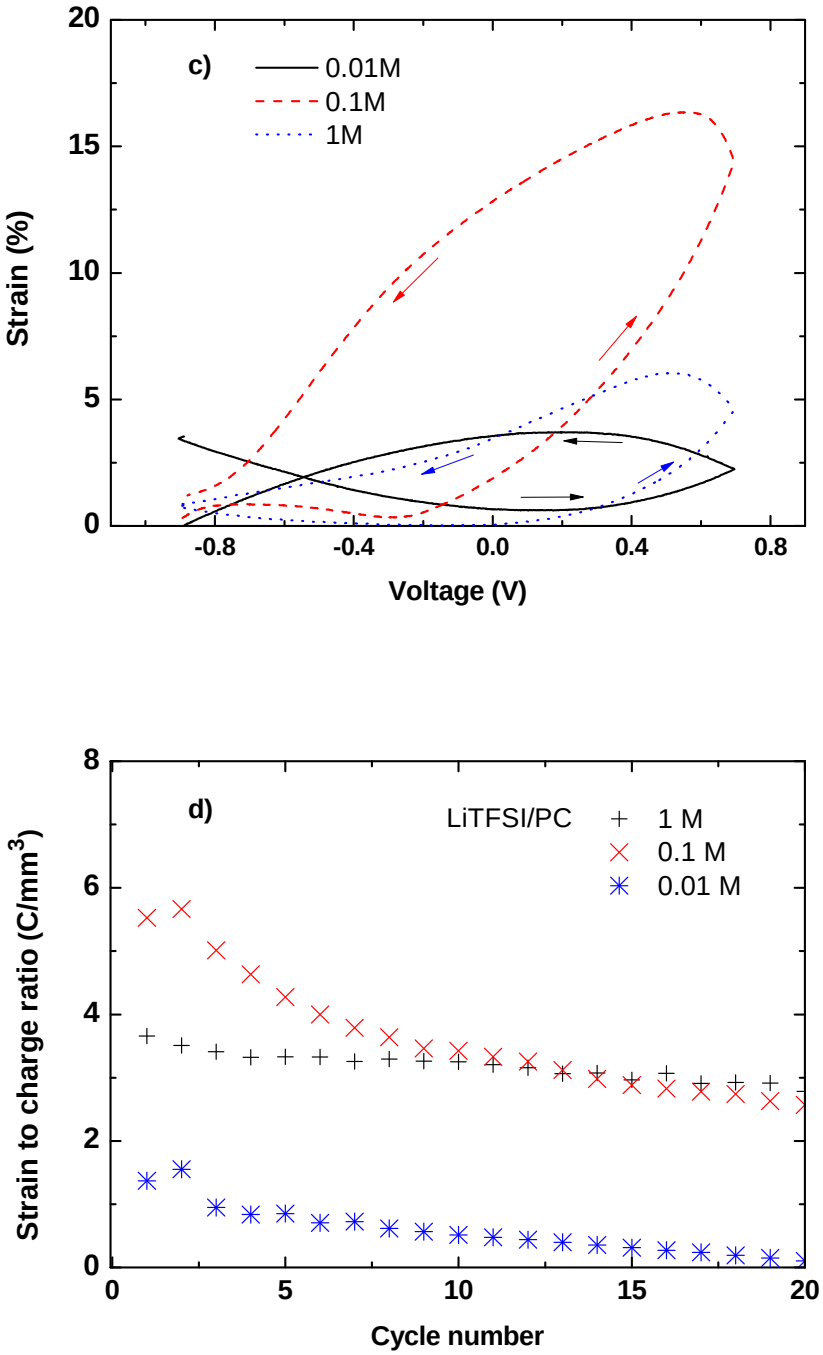

Figure 4.3 a) Actuation of PPy in different concentrations of Li.TFSI in PC over a potential window of -0.9 V to +0.7V; b) Their CV voltammograms. Scanning from -0.9V to 0.7V versus Ag/Ag$^+$ with 2 mV/s scanning speed; c) actuation of first cycle versus voltage; d) strain to charge ratio over cycling.

4.3.4 Stability of PPy/TFSI/PC films.

The high strains produced by PPy/TFSI films are not of practical use in many applications because of the poor cycle life stability of these materials. Further investigation of the cycle life stability was restricted to the PPy films prepared from LiTFSI/PC films. The actuation strain maximum decreased monotonically with each redox cycle from 16% in the first cycle to 6 % in the 20th cycle (Figure 4.4 a). Cyclic voltammograms were recorded *in situ*. Defined oxidation and reduction peaks were observed for the first redox cycle, with oxidation occurring at -0.25 V and reduction at -0.55 V. Comparing the first cycle to the 20th cycle, the oxidation peaks showed a shift toward more positive potentials. Furthermore, the maximum current density of both the oxidation and reduction peaks decreased. The rapid decrease in the charge passed per cycle confirms the deterioration of polypyrrole electroactivity (Figure 4.4 d).

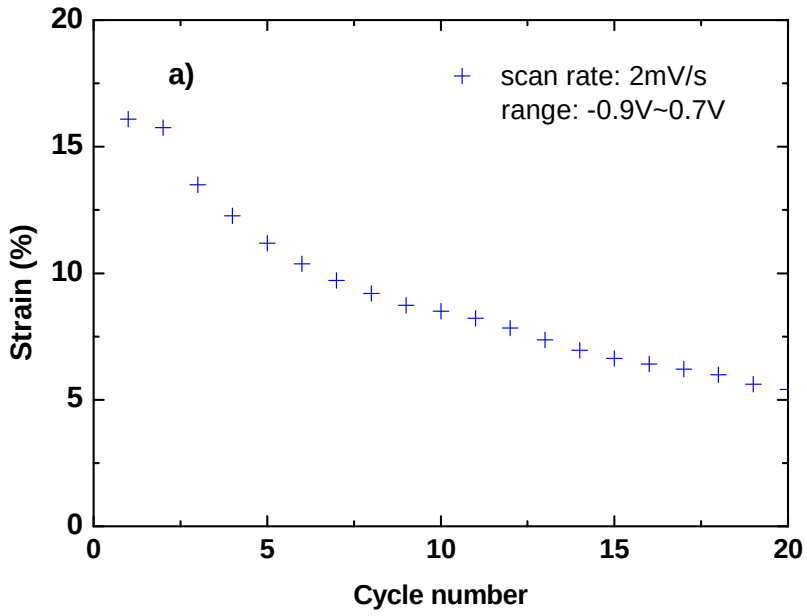

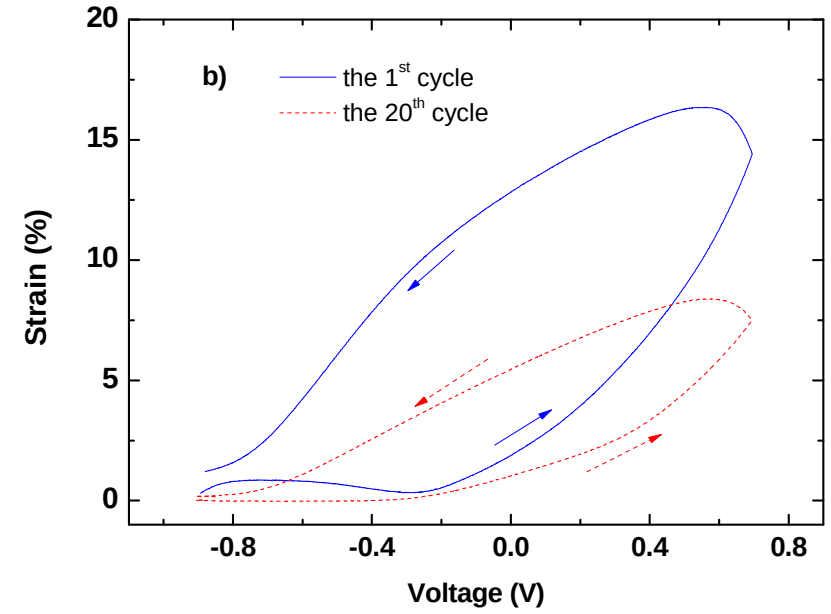
b)
the 1st cycle
the 20th cycle
Strain (%)
Voltage (V)
20
15
10
5
0
-0.8
-0.4
0.0
0.4
0.8

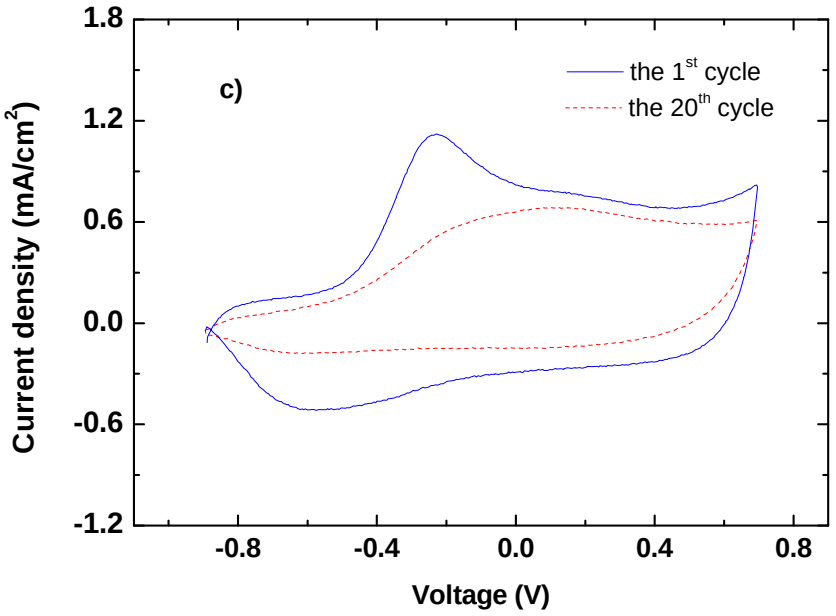
c)
the 1st cycle
the 20th cycle
Current density (mA/cm2)
Voltage (V)
1.8
1.2
0.6
0.0
-0.6
-1.2
-0.8
-0.4
0.0
0.4
0.8

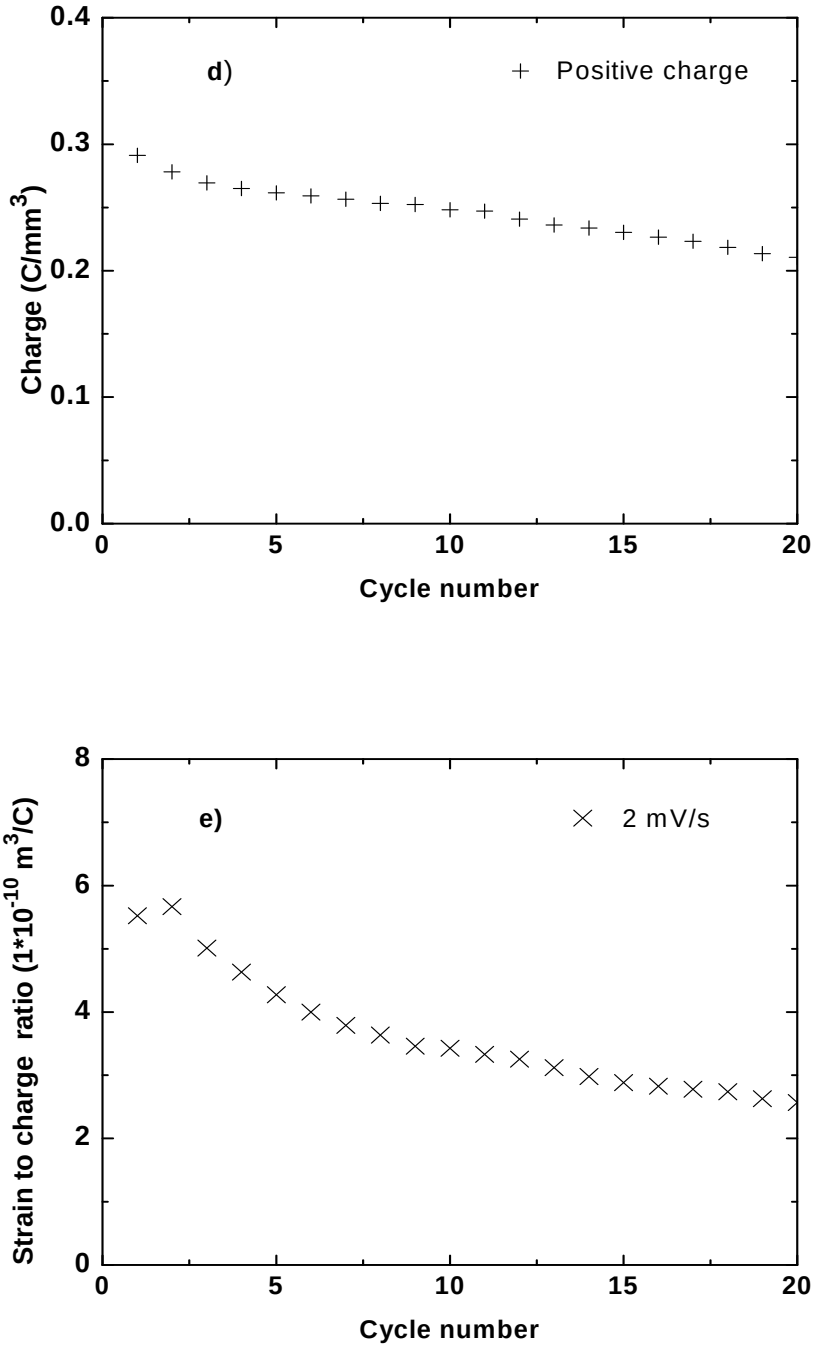

Figure 4.4 Free standing PPy/TFSI film in a 0.1 M Li.TFSI propylene carbonate electrolyte. Scan rate: 2 mV/s. a & b) the observed actuation; c) the cyclic voltammogram of the 1st and 20th cycle; d) Consumed positive volumetric charge; e) strain to volumetric charge ratio.

Analysis of the charge passed per anodic cycle shows a small decrease over the first 20 cycles (Figure 4.4 d). The decrease in charge passed per cycle is smaller than the decrease in strain. The comparison is clearly shown in Figure 4.4 e) where the strain to

charge ratio is determined and plotted as a function of cycle number. The strain to charge ratio decreases by approximately 50% between cycles 1 and 20. Thus, while the electroactivity of the PPy/TFSI clearly decreases over the first 20 cycles, this decrease in charge capacity cannot fully account for the decrease in actuation strain. Processes other than the deterioration in the electroactivity must also be contributing to the strain degradation.

4.3.5 Effect of scan rate on actuation stability.

As noted in Chapter 3, the rate of actuation is strongly affected by the rate of voltage scanning. Increasing the scan rate of the cyclic voltammogram results in a significant reduction in the observed actuation for the PPy films grown from LiTFSI/PC films (Figure 4.5). The results are, therefore, similar to those noted in Chapter 3 and indicate that the PPy/TFSI films are not able to undergo full oxidation / reduction during the voltage scan at the scan rates investigated. Of particular note is that the actuation still degraded substantially over the first 60 cycles at faster scan rates of 5 and 25 mV/s. At even higher scan rates (100-400 mV/s) the decrease in strain is less obvious over the first 120 cycles, although the magnitude of the strain is also considerably smaller than noted at slower scan speeds. As a percentage of the first cycle strain, the strain recorded in the 12^{th} cycle was 82%, 80%, 42%, 26% and 10% for scan rates of 400, 200, 100, 25 and 5 mV/s, respectively. As discussed in chapter 3, the actuation process is believed to be a diffusion controlled process. Increasing scan rate will diminish the charge passed and hence limit the actuation strain.

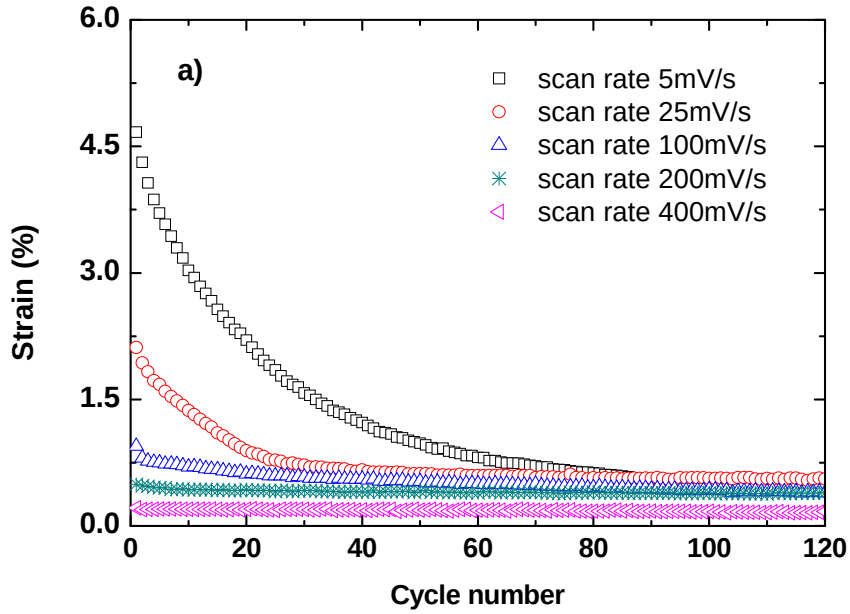
a)
scan rate 5mV/s
scan rate 25mV/s
scan rate 100mV/s
scan rate 200mV/s
scan rate 400mV/s
Strain (%)
Cycle number
6.0
4.5
3.0
1.5
0.0
0
20
40
60
80
100
120

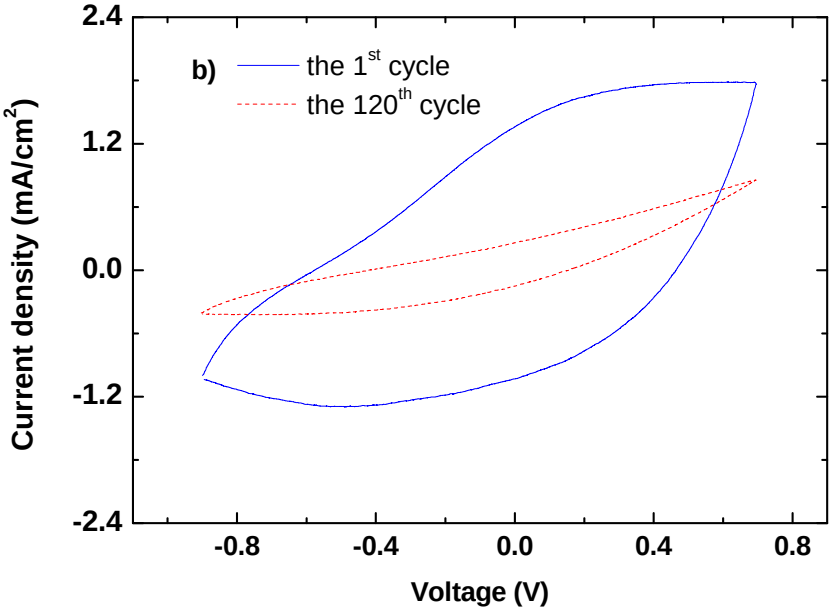
b)
the 1st cycle
the 120th cycle
Current density (mA/cm2)
Voltage (V)
2.4
1.2
0.0
-1.2
-2.4
-0.8
-0.4
0.0
0.4
0.8

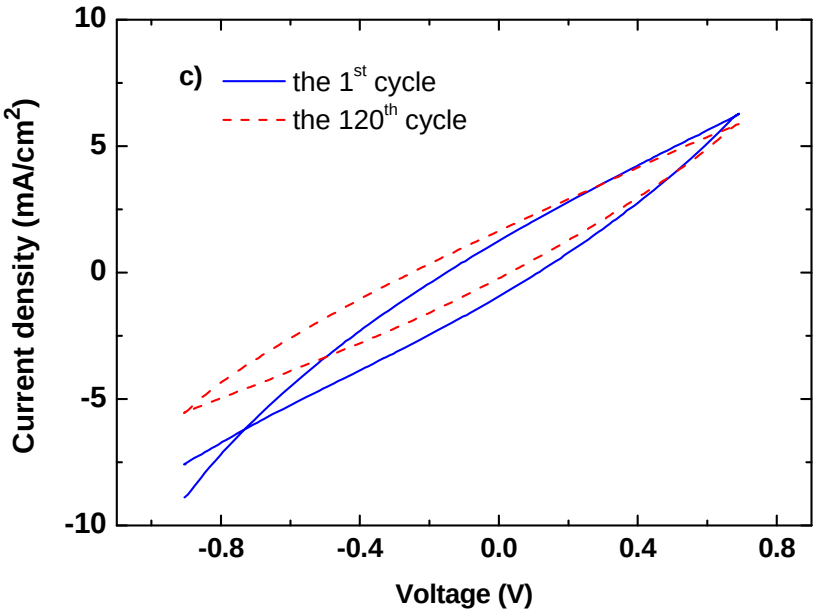
c)
the 1st cycle
the 120th cycle
Current density (mA/cm2)
Voltage (V)
10
5
0
-5
-10
-0.8
-0.4
0.0
0.4
0.8

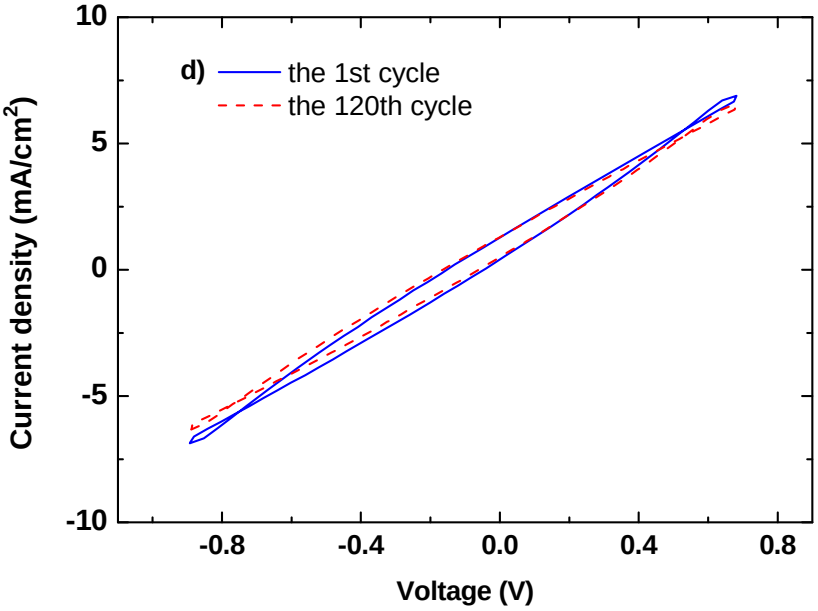
d)
the 1st cycle
the 120th cycle
Current density (mA/cm2)
Voltage (V)
10
5
0
-5
-10
-0.8
-0.4
0.0
0.4
0.8

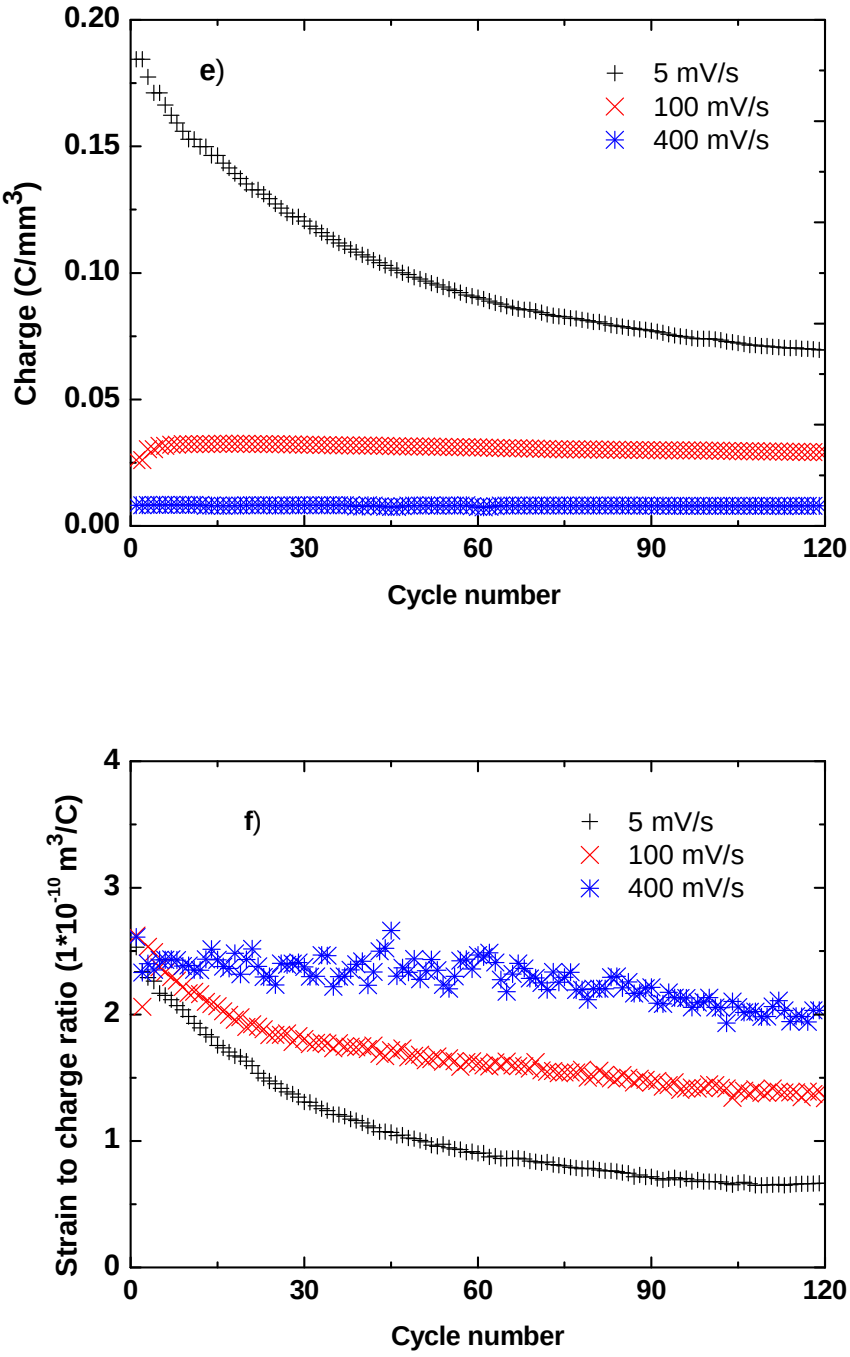

Figure 4.5 The observed actuation of PPy films at different scan rates (a) and their cyclic voltammograms: b) scan rate at 5mV/s; c) scan rate at 100 mV/s; d) scan rate 400mV/s; e) consumed charge (positive only); f) strain to charge ratio over cycles.

The charges passed and strain to charge ratio at selected scan rates of 5 mV/s, 100 mV/s and 400 mV/s were determined (Figure 4.5 e) and f). The decay in charge passed is similar to the decay in strain. Again, the strain decreases more rapidly with cycling

than the charge passed. As can be seen in Figure 4.5 f), the strain to charge ratio decreased in all cases, but decreased more significantly at the slower scan speeds.

4.3.6 Actuation over a limited potential range.

A possible reason of the strain instability is chemical degradation associated with over oxidation leading to a change in the actuation behaviour. Bard et al [22] already realized that such irreversible reactions could start to occur at low potential. In their experiment, the PPy films were found to be unstable at oxidization potentials larger than 0.6 V versus SCE in 0.1M $TBABF_4$ acetonitrile electrolyte [22]. Lewis et al have shown that in aqueous solution the overoxidation of PPy begins at 0.65 V versus Ag/AgCl in pH 6 solution [23]. Further studies using FTIR found that overoxidation of PPy is accompanied with irreversible changes in the molecular structure. The conjugated length can be diminished as nucleophilic attack generates sp^3 carbons on polymer chain [24, 25].

PPy reduction can also lead to a loss in cycling stability. PPy films could become highly compacted with a dense structure when submitted to cathodic potentials. Re-oxidising and re-opening the closed structure requires a higher anodic potential [26]. Otero has noticed that such conformational changes are irreversible [27]. The ‘close potential’ is defined as the potential beyond which no reducing current is observed [28]. The close potential of PPy/ClO_4 in $LiClO_4$ acetonitrile starts at -0.8 V versus SCE [28]. As can be seen in Figure 4.4 c), the close potential of PPy/TFSI is below -0.9 versus Ag/Ag^+.

To avoid actuation instability as a result of overoxidation or a conformational change, the actuation of PPy films has been studied over a limited potential range.

Hence, the minimum voltage was increased to -0.5 V, and the maximum potential limited to +0.2, +0.35 or +0.5V. As evident in Figure 4.7 b), c) & d), over a limited potential range, the shape of the CV resembles that of a capacitor as analysed previously by Madden as a "transmission line" type electrochemical model [29, 30]. The transmission line model described the actuation and electrochemical mechanism while doping level of PPy is low [29]. In the model, as electronic resistance is small compared to the ionic resistance, the system consists of ionic resistance and volumetric capacitances (Figure 4. 6). Those capacitors are gradually charging while external potential is applied, generating rectangular shape of C-V voltammograms.

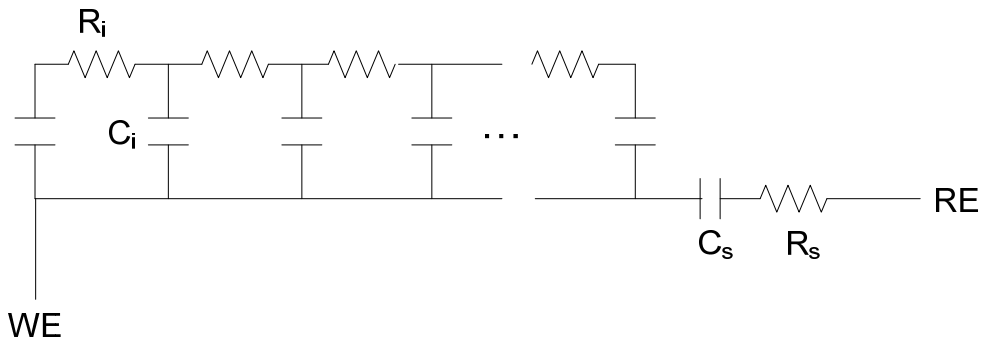

Figure 4. 6 Transmission line model for charging of a conducting film; with R_i representing ionic resistance per volume and C_i represents the capacitance per volume. R_s is the solution resistance and C_s is the unit surface capacitance.

Considerable actuation of the PPy film occurs even though the polymer is not undergoing fully oxidation and reduction. Indeed, for a scan range of -0.5 to -0.5 V the actuation strain for the first cycle was larger than 6% and was still exhibiting more than 2% after 60 cycles (Figure 4.7 e). When the maximum potential was further limited, the strain was reduced. Significantly, a major reduction in strain over the first 60 cycles is evident for all potential ranges investigated. Charge passed also decreased for all potential ranges over the initial cycles (Figure 4.7 g). The charge passed decreased less

significantly than the strain, so the strain to charge ratio also decreased with cycling (Figure 4.7 h)

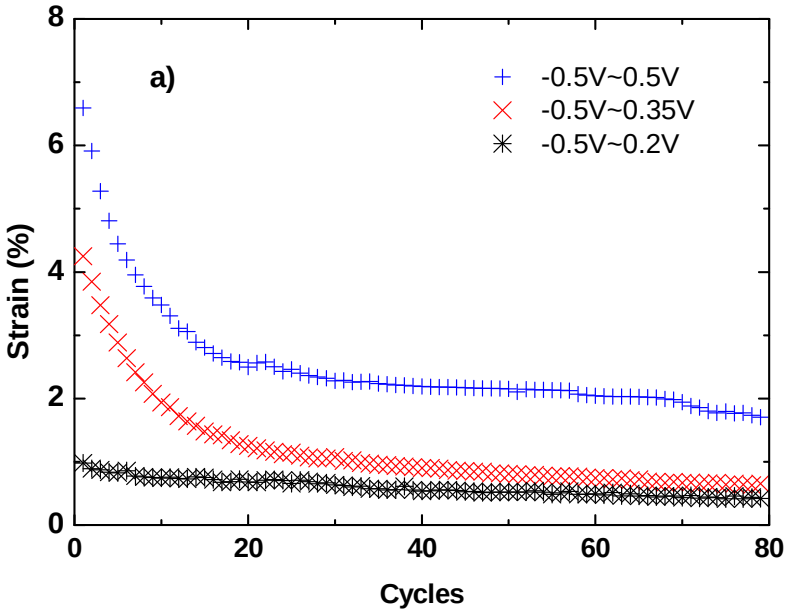

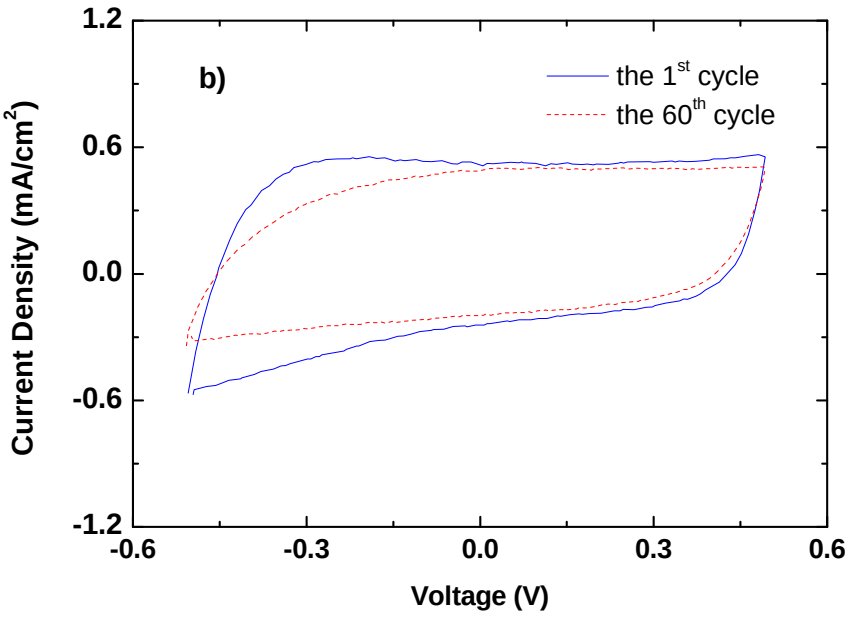

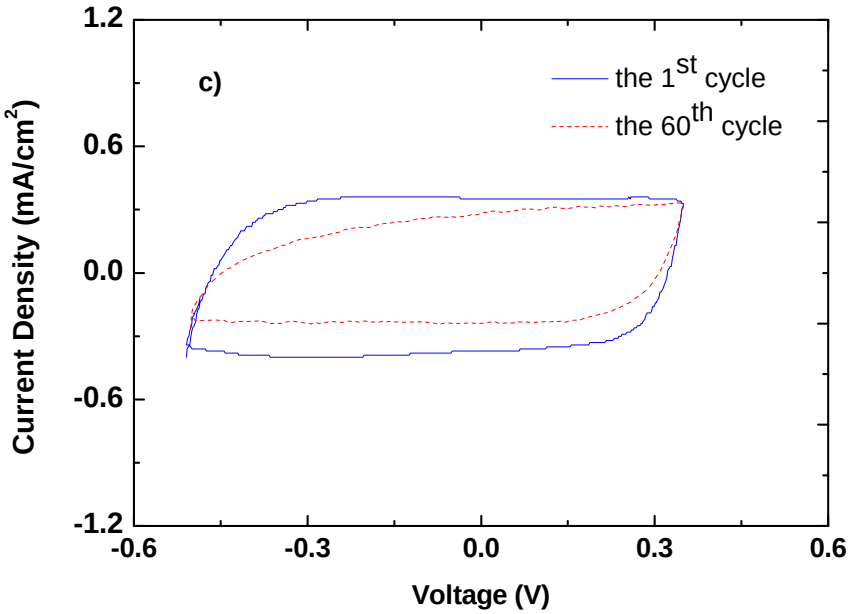
c)
the 1st cycle
the 60th cycle
Current Density (mA/cm2)
Voltage (V)
1.2
0.6
0.0
-0.6
-1.2
-0.6
-0.3
0.0
0.3
0.6

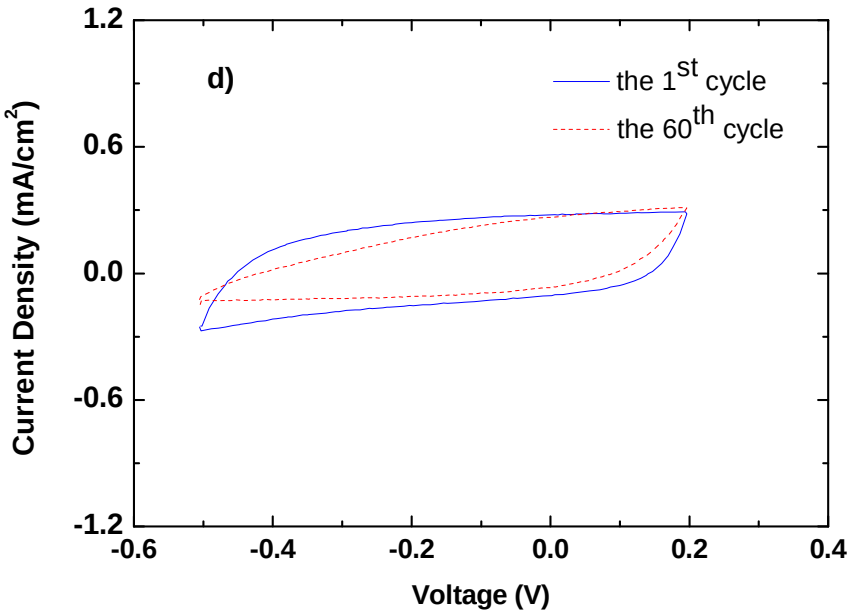
d)
the 1st cycle
the 60th cycle
Current Density (mA/cm2)
Voltage (V)
1.2
0.6
0.0
-0.6
-1.2
-0.6
-0.4
-0.2
0.0
0.2
0.4

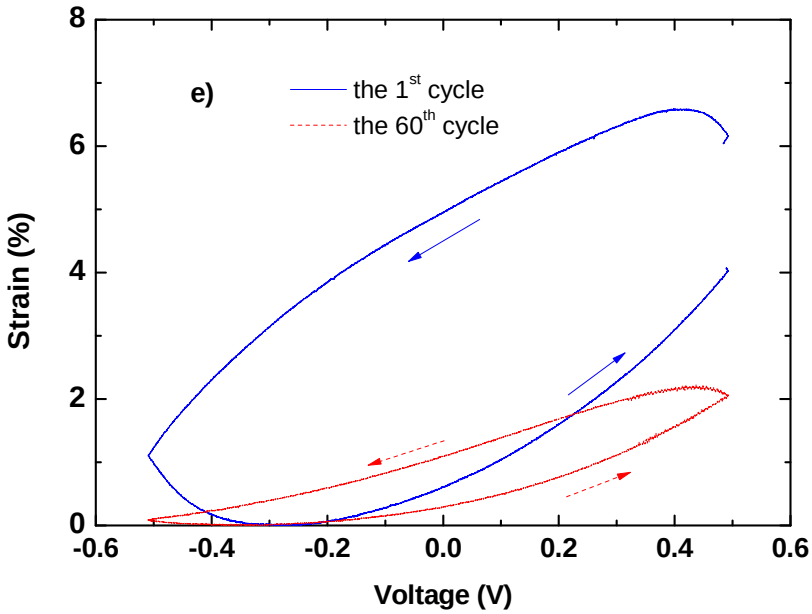
e)
the 1st cycle
the 60th cycle
Strain (%)
Voltage (V)
8
6
4
2
0
-0.6
-0.4
-0.2
0.0
0.2
0.4
0.6

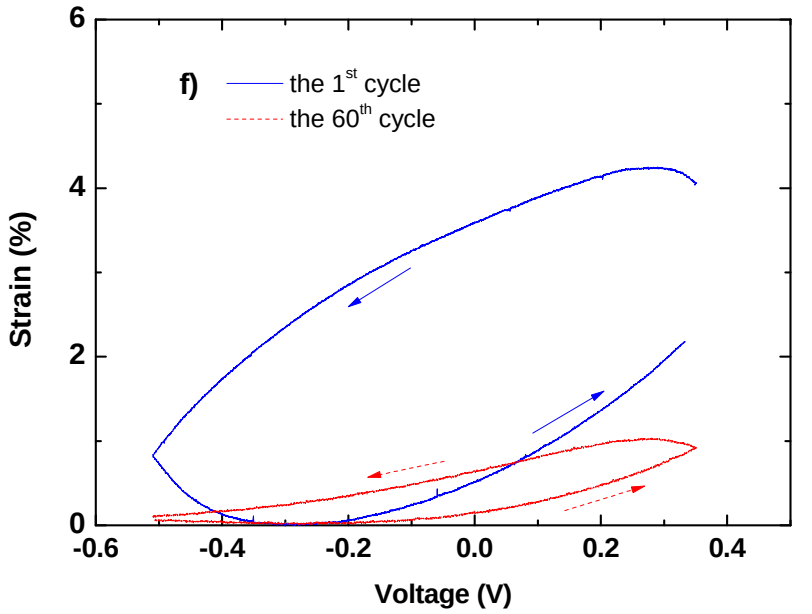
f)
the 1st cycle
the 60th cycle
Strain (%)
Voltage (V)
6
4
2
0
-0.6
-0.4
-0.2
0.0
0.2
0.4

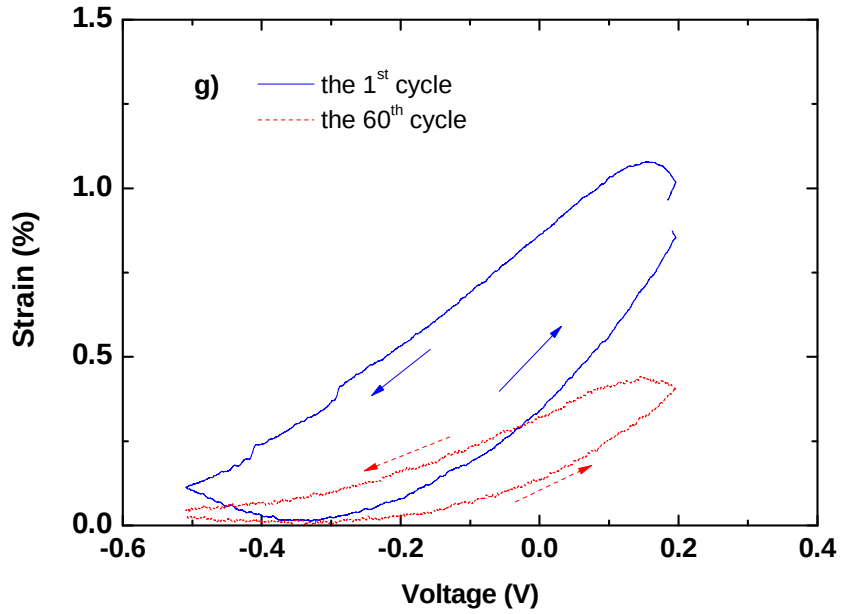
g)
the 1st cycle
the 60th cycle
Strain (%)
Voltage (V)
1.5
1.0
0.5
0.0
-0.6
-0.4
-0.2
0.0
0.2
0.4

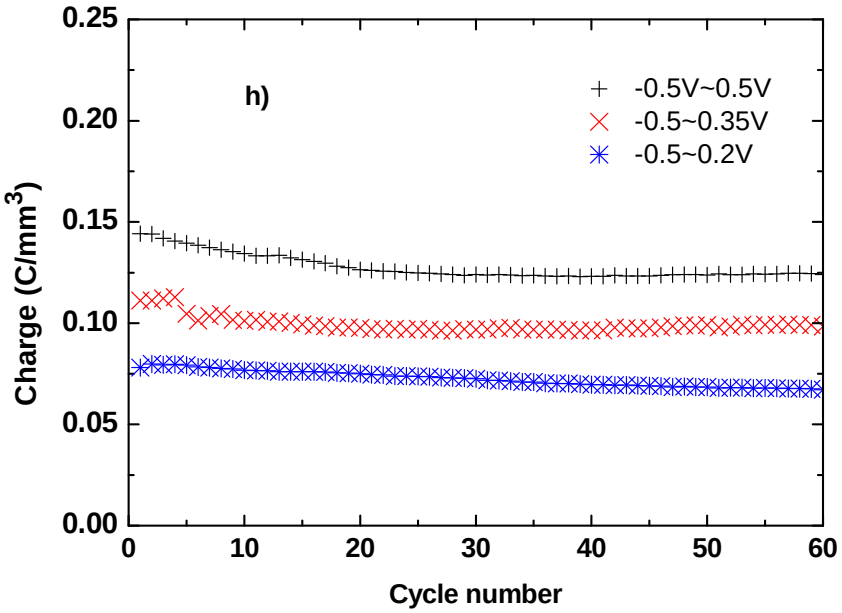
h)
-0.5V~0.5V
-0.5~0.35V
-0.5~0.2V
Charge (C/mm3)
Cycle number
0.25
0.20
0.15
0.10
0.05
0.00
0
10
20
30
40
50
60

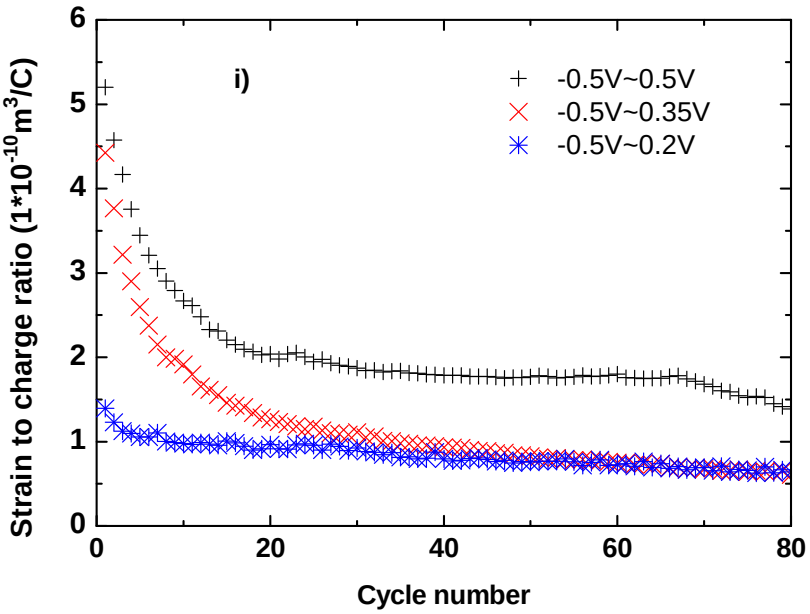

Figure 4.7 Electrochemical capacitance actuation of free standing PPy films (a); their C-V deformation while cycling: b) scan range -0.5~0.5V; c): scan range -0.5~0.35V d): scan range -0.5~0.2 V; the actuation behaviour for the scan range e) -0.5~0.5V; f) -0.5~0.35V; g) -0.5~0.2V;h) Charge consumed (Positive only); i) Strain to charge ratio over cycles; All scan rates were 2 mV/s.

The charge consumed decreased by less than 20% in all cases (Figure 4.7 h), which was a much smaller decrease than noted above for the wider potential range. It is likely that the limited potential range successfully avoided major conformation changes and overoxidation. However, reducing the potential scan range does not help to enhance the stability. As found in Figure 4.7 e~g), strain losses of more than 60% were obtained for all cases. Even when the potential was limited to the range of -0.5 V to 0.2 V, the strain was still reduced from 1.2% to 0.4% over 60 cycles.

4.3.7 Effect of cycling on elastic modulus

The elastic modulus was measured in-situ during actuation to gain an insight into structural changes that might be occurring within the PPy. For these tests, a small amplitude square wave stress pulse between 0.16 MPa and 0.22 MPa was applied

(Figure 4.8). The maximum applied load of 0.22 MPa is sufficiently small to avoid mechanical creep of the PPy films over the period of the test. The resultant strain was of the order of 0.05% and was considerably smaller than the actuation strain. Two groups of in-situ elastic modulus were recorded corresponding to the test condition listed in section 4.3.5: -0.9V~0.7V versus Ag/Ag^{+} using various scan rates and over a narrow scan range using 2 mV/s scan rate, as shown in Figure 4.9 & Figure 4.10.

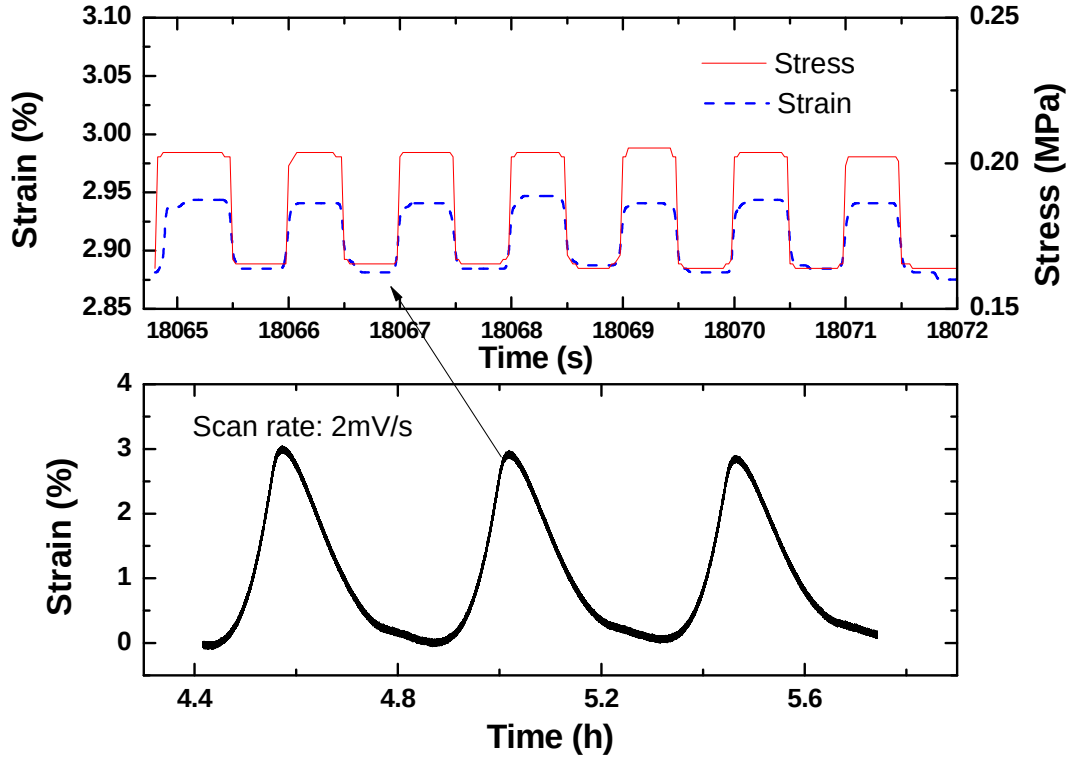

Figure 4.8 In situ modulus test during actuation. Voltage scan range is from -0.9V to 0.7 V with scan rate of 2 mV/s. As shown in the upper panel, a small amplitude stress pulse was also applied giving a resultant strain that could be converted to an elastic modulus value.

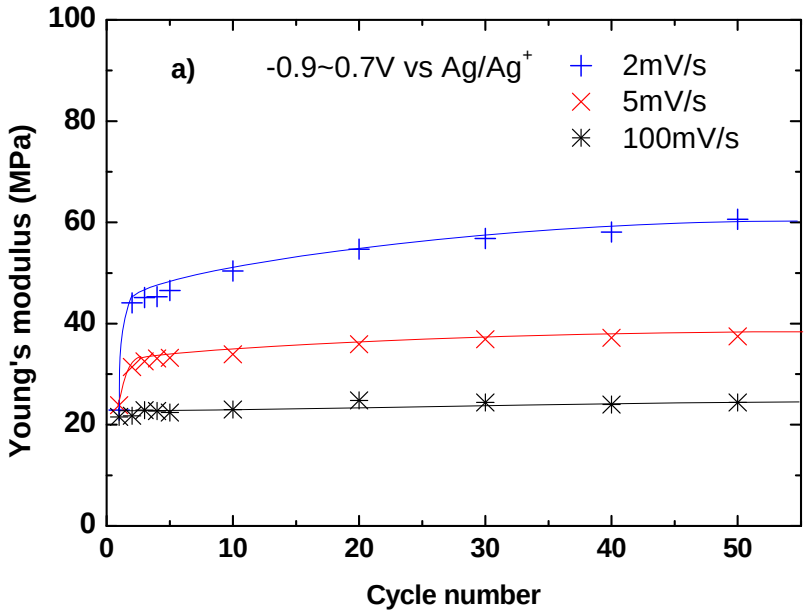
a)
-0.9~0.7V vs Ag/Ag+
2mV/s
5mV/s
100mV/s
Young's modulus (MPa)
Cycle number
0
20
40
60
80
100
0
10
20
30
40
50

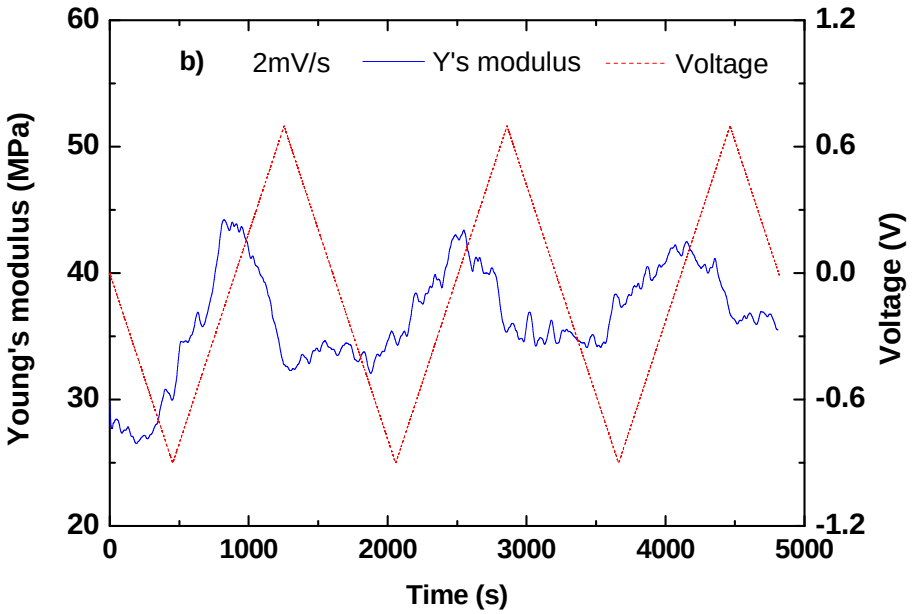
b)
2mV/s
Y's modulus
Voltage
Young's modulus (MPa)
Voltage (V)
Time (s)
20
30
40
50
60
-1.2
-0.6
0.0
0.6
1.2
0
1000
2000
3000
4000
5000

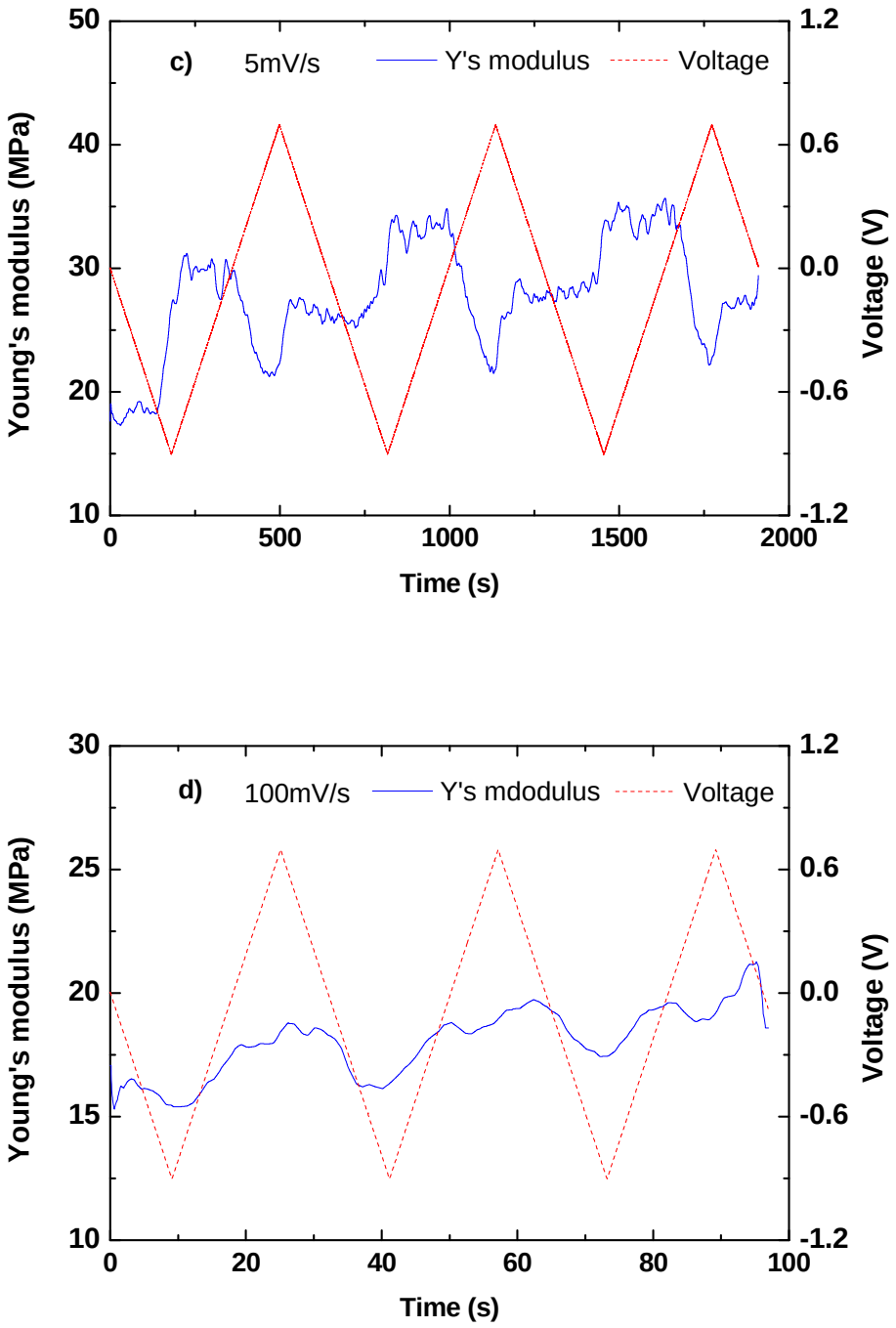

Figure 4.9 a) The elastic modulus of PPy films during voltage scanning. A potential window of -0.9 to +0.7 V was applied. First three cycles of using 2 mV/s, 5mV/s and 100 mV/s are shown in b)~d) respectively.

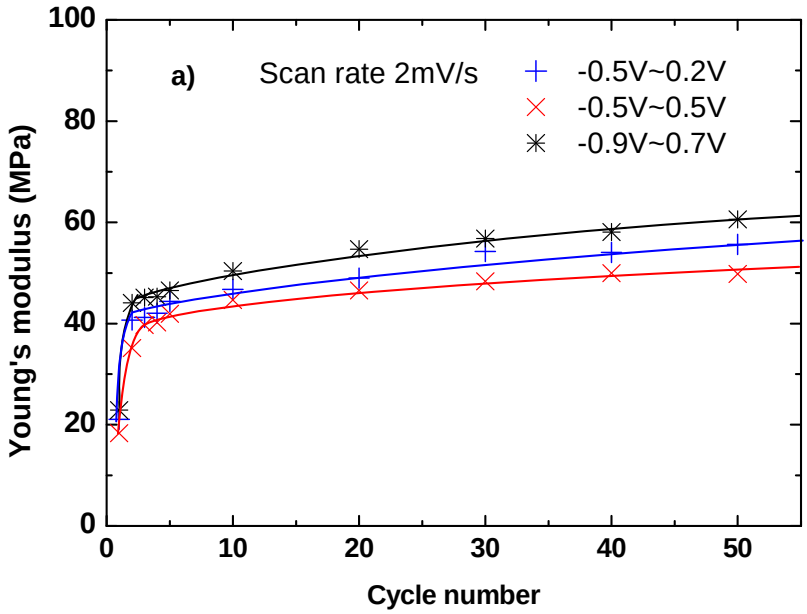
a)
Scan rate 2mV/s
-0.5V~0.2V
-0.5V~0.5V
-0.9V~0.7V
Young's modulus (MPa)
Cycle number
0
20
40
60
80
100
0
10
20
30
40
50

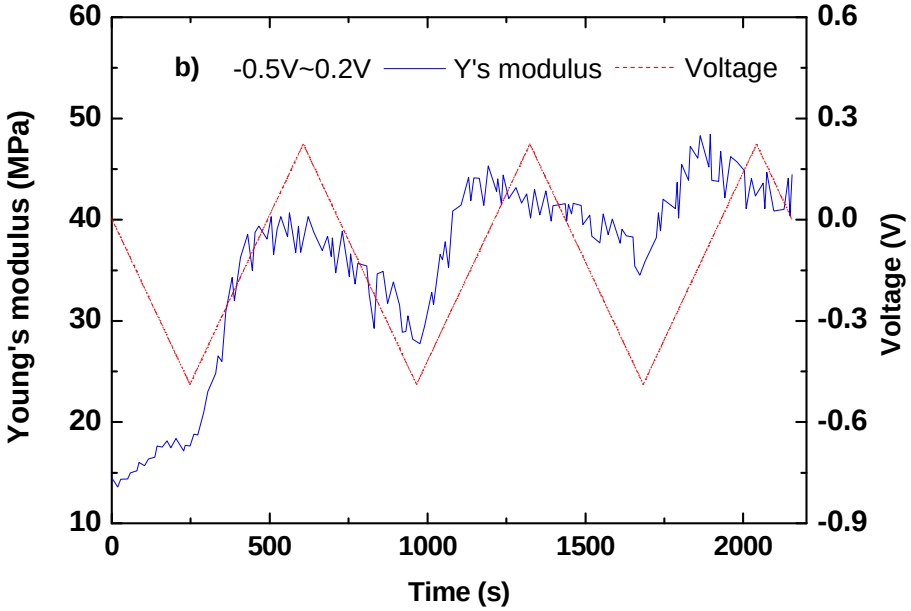
b)
-0.5V~0.2V
Y's modulus
Voltage
Young's modulus (MPa)
Voltage (V)
Time (s)
10
20
30
40
50
60
0
500
1000
1500
2000
-0.9
-0.6
-0.3
0.0
0.3
0.6

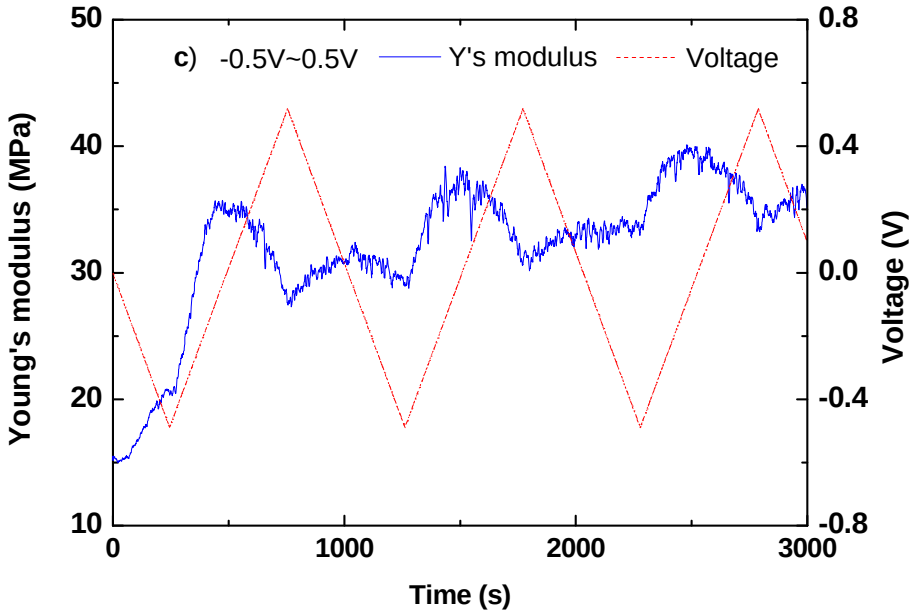

Figure 4.10 a) The elastic modulus of PPy films during voltage scanning for a potential various potential windows. First three cycles of -0.5V~0.2V and -0.5 V ~0.5 V were shown in b) & c).

In all cases, there was observed a gradual increase in modulus with each cycle. At a scan rate of 2 mV/s in three scan ranges, the dynamic modulus started at around 20 MPa, before climbing to about 60 MPa after 40 cycles (Figure 4.10). Similarly, at a scan rate of 5 mV/s, the modulus started at 20 MPa and climbed each cycle to 35 MPa after 40 cycles. In contrast, at a scan rate of 100 mV/s, the modulus increased only slightly from 16 MPa to 19 MPa over the first 100 cycles. The increase in Young's modulus corresponds to the degradation of actuation strain and is probably a consequence of the same process.

The Young's modulus change per voltage cycle showed a complicated behaviour. During a typical cathodic scan, the modulus first increased and then decreased with increasing potential (Figure 4.9). The change in modulus in all cases was quite small and the change in modulus tended to decrease with increasing scan rate (Figure 4.9). By

increasing scan rate and reducing scan range, the modulus tended to increase monotonically with potential.

It should be noted that the change in modulus does not account for the decrease in actuation strain, as the latter was measured at near zero applied stress so that the effect of a changing modulus on strain is negligible. As pointed out previously, the evolution of PPy can be reflected on shifting of elastic modulus.

The modulus of polypyrrole films is comparable to that of a rigid elastomer, being larger than that for swollen elastomers, but less than that for dry polymers. At small and moderate strains the modulus is governed by intra-molecular interactions. A modulus in the order of 10 MPa implies either a very highly swollen system such that a reduction in entropy is contributing, or strong intra molecular interactions that are not readily screened by the solvent.

4.3.8 Current control versus voltage control.

Spinks et al [11] have shown that careful selection of the current control parameters allows for a dramatic increase in cycle life stability compared to voltage scanning with a linear ramp. In their study they found that during linear ramp voltage scanning, even using equilibrium voltage, PPy is still progressing to a more oxidized state cycle by cycle. Evidence is the positive charge is slightly larger than negative charge in one cycle. The result is a reduced capacity to oxidize the polymer in later cycles, resulting in a smaller actuation strain. Using current control will effectively avoid such phenomena since the amount of charge injected during the oxidation and reduction cycle can be matched. A merit of using current control is the prevention of over oxidation [24] of the PPy which was proposed as the reason for the increase in cycle life [11].

In this experiment, actuation strains were measured by employing a square wave current stimulation with a current density similar to that observed during the cyclic voltammograms. Through optimizing the current density and pulse time, the strain stability was significantly enhanced over the first 100 cycles. Two examples are shown in Figure 4.11: 8 mA/cm^2 for 30 s (240 mC/cm^2) and 12 mA/cm^2 for 15s (180 mC/cm^2). In the former case a strain in the first cycle of ~8% dropped to 4.5% over 40 cycles and then remained constant. In the latter case a smaller charge was injected per cycle over a shorter period of time and resulted in an initially smaller strain of ~4%. Significantly, the strain remained approximately constant for 100 cycles. The voltage needed to produce each current pulse cycle was recorded and shown in Figure 4.10 b). A stable voltage was noted for the shorter pulses / smaller charge, whereas some drift in voltage was noted for the longer pulses / higher charge. It was also noted that the voltage range was much wider than applied during voltage scans, particularly in the cathodic region.

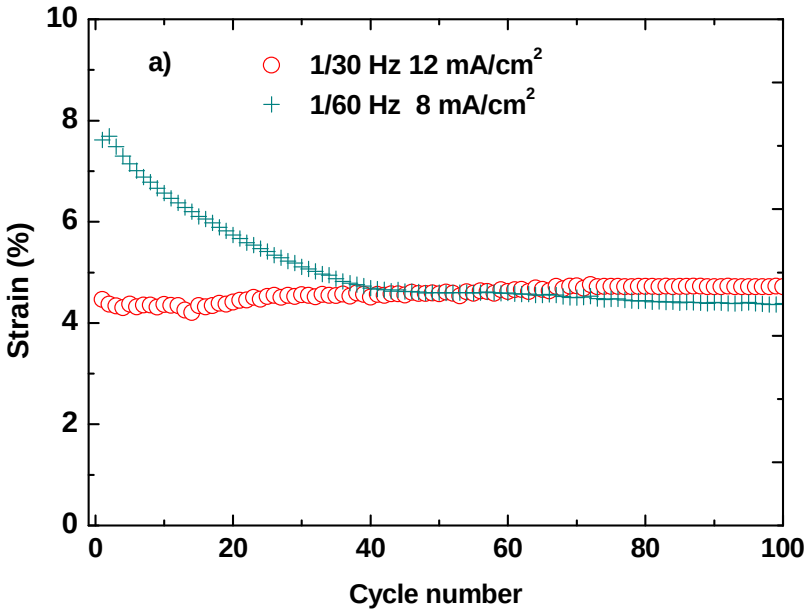

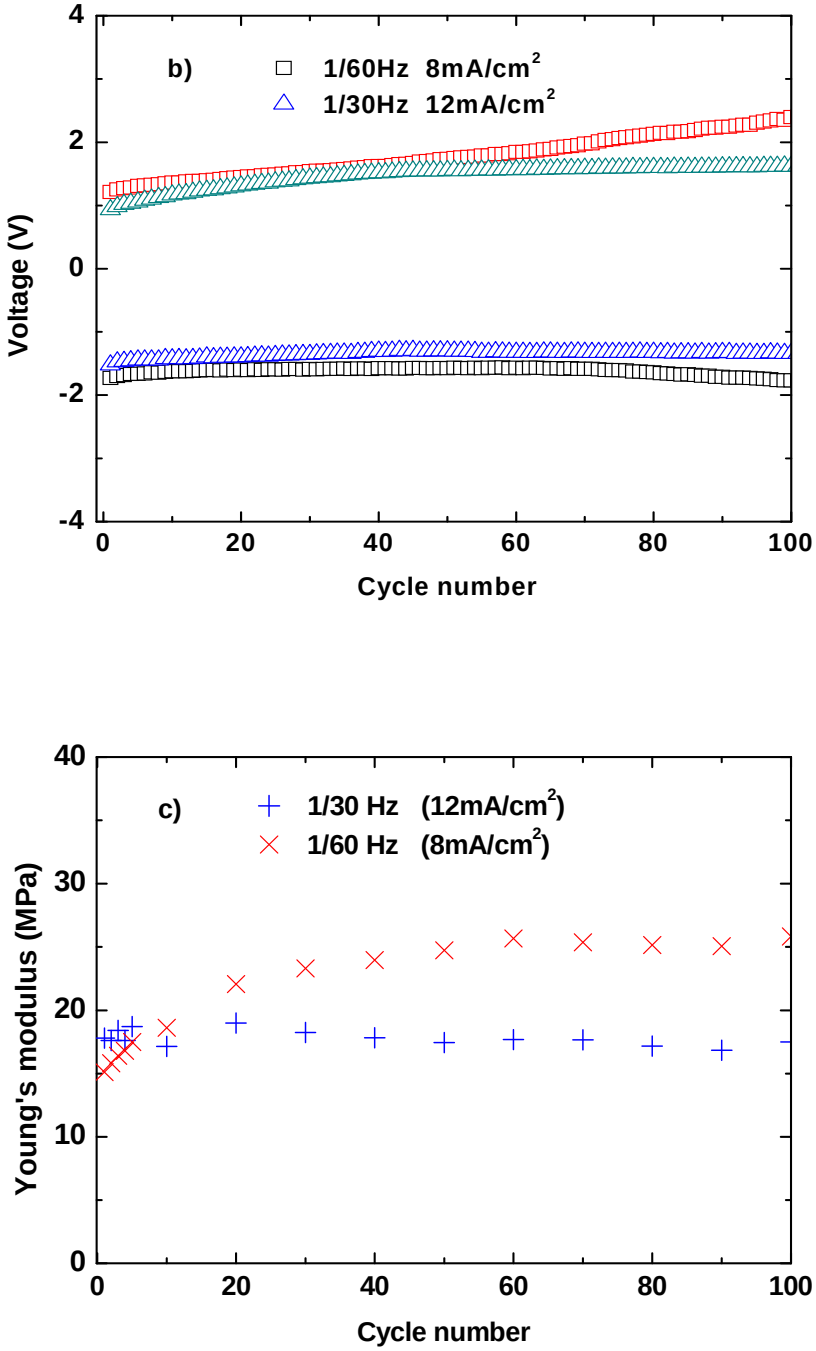

Figure 4.11 The strain (a), maximum/minimum potential of each pulse cycle (versus $Ag|Ag^+$) (b) & elastic modulus (c) changing of PPy films by current scanning. First 100 cycles were presented.

The in situ elastic modulus measured during current cycling also proves that current control can avoid structure change within the PPy films. As seen in Figure 4.11, the in situ elastic modulus measured during the longer pulse / higher charge increased

approximately two times of its original value during the first 60 cycles, which is similar to the change in modulus noted above for voltage cycling. When shorter /smaller charge pulses were used, however, very little change was noted in the in situ modulus over 100 cycles. These same conditions gave very stable actuation results, confirming that the structural changes leading to an increase in modulus are linked to the decline in actuation capacity.

4.4 Relationship between modulus change and actuation stability

The results presented in this chapter demonstrate a clear link between changes to the actuation strain and changes to the Young's modulus of the PPy films that occur upon repeated redox cycling. In each case, it is likely that the two changes are linked. Figure 4. 12 plots the measured actuation strain against the measured Young's modulus for repeated cycling at different electrochemical conditions. In all cases, there is a monotonic decrease in strain caused by a steady increase in modulus that occurs upon repeated cycling. The rate of strain decay and modulus increase is greatest when wider potential limits were used and when slower scan rates were used.

It is well established that the equilibrium swelling of polymers by solvents is determined by a thermodynamic balance between the affinity of the polymer for the solvent and the mechanical elasticity of the polymer network [31]. In crosslinked rubbers and hydrogels, the extent of swelling is reduced when the crosslink density is increased. Similarly, there is a direct connection between the extent of crosslinking (or other intermolecular interactions) and the polymer's modulus. Since actuation in PPy is caused by the swelling due to ingress of ions and solvent, the extent of actuation will be sensitive to the degree to which the polymer chains are bonded together. Any process

that increases the molecular interactions will reduce the amount of actuation strain. Such processes will also result in an increase in modulus.

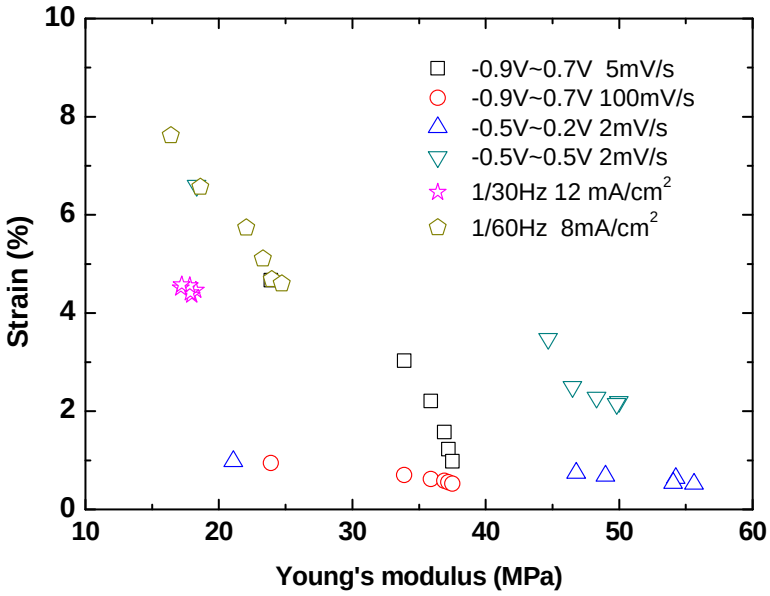

Figure 4. 12 Relationship between actuation strain and Young's modulus for various experimental conditions and over multiple redox cycles.

Heinze et al have previously described a mechanism whereby oxidation of conducting polymers can lead to increased intermolecular bonding [32], and it is possible that such processes may be the cause of decreased actuation in PPy/TFSI described in this chapter. Heinze et al also have proposed a reaction mechanism whereby the close proximity of two radical cations (polarons) formed during the oxidation of conducting polymers can form a "dimerized" state. Thus, a covalent bond forms between the two adjacent sites. The reaction can be reversed, although the higher stability of the dimerized state means that a lower potential is needed to achieve the original unbound state. The series of reactions and intermediary steps were successfully modelled by Vorotyntsev and Heinze to generate cyclic voltammograms with close similarity to experimentally measured curves [33]. Clearly, if chemical bonds form during the oxidation of PPy/TFSI and if these bonds are not completely reversed during the reduction cycle then the swelling in

the subsequent oxidation would be expected to be smaller. Similarly, it would be expected that such reactions would lead to an increase in modulus.

4.5 Conclusions

High strain actuators based on PPy doped with TFSI were investigated. The high strains, slow response and poor cycle-life stability as reported in recent literature were all confirmed. First cycle strains as high as 16% were recorded at low scan rates, but diminished rapidly at higher scan rates. The possible contribution of solvent ingress/egress to the actuation due to osmotic pressure was investigated by altering the electrolyte concentration. The results were inconclusive. While previous work had suggested that lower electrolyte concentrations would favour a larger osmotic pressure contribution to actuation, the results presented in this thesis show a more complicated behaviour. Upon reducing the electrolyte concentration from 1M to 0.1M to 0.01M, the actuation strain first increased and then decreased. The possible contribution to the reduced actuation at the lowest electrolyte concentration from a low electrolyte conductivity was a suggested as a possible cause of this unexpected behaviour.

Cycle life stability was found to be poor whenever large strains were achieved. Strains decreasing by as much as 75% over the first 50 cycles or so. The most stable response was obtained by using current control for actuation, where a stable 4% strain was produced for 100 cycles. Quite stable responses were also obtained when fast voltage scan rates were used, however, the strains were small due to incomplete redox reactions occurring.

The effect of voltage scan range was investigated to determine whether over-oxidation or conformational changes that may occur at potential extremes may be responsible for the poor cycle stability of actuation. Significant changes in the shape of the CVs was noted upon repeated cycling over a wide potential range. The charge passed per cycle also decreased and this reduction in electroactivity of the PPy was thought to be at least partially responsible for the diminished actuation. However, it was observed that the strain:charge ratio decreased upon repeated cycling, demonstrating that the actuation decay was caused by processes other than the degradation in electroactivity. Cycle life studies conducted over a narrow potential range also showed a decrease in charge passed per cycle. The strain and strain:charge ratio also decreased per cycle showing that the degradation was not due solely to the higher anodic or cathodic potentials.

A clear relationship was observed between the actuation stability of the PPy films and their elastic modulus. The degradation of actuation strain in PPy was accompanied by increasing modulus in all cases. Prior work had suggested that oxidation of conducting polymers may introduce covalent bonds between chains that are not easily reversed during cathodic potential scans. The increase in bonding between PPy chains would account for both the decrease in actuation strain and the increase in modulus.

Finally, it was observed that current pulses effectively increased the stability of actuation strain. In these circumstances, the modulus was also stable over repeated cycles. For reasons that are not yet known, the current pulses appear to produce reversible changes in the structure of the PPy, thus allowing for a stable actuation response. Perhaps the lower cathodic potentials that result from current pulsing enable the full reversal of any intermolecular bonding that is produced from the oxidation of the polymer. Further structural investigations are needed to confirm these suggestions.

4.6 References

1. Smela, E., *Conjugated Polymer Actuators for Biomedical Applications.* Advanced Materials, 2003. **15**(6): p. 481-494.
2. Baughman, R.H., *Conducting Polymer Artificial Muscles.* Synthetic Metals, 1996. **78**(3): p. 339-353.
3. Hara, S., et al., *Free-Standing Gel-Like Polypyrrole Actuators Doped with Bis(Perfluoroalkylsulfonyl)Imide Exhibiting Extremely Large Strain.* Smart Materials & Structures, 2005. **14**: p. 1501-1510.
4. Hara, S., et al., *Gel-Like Polypyrrole Based Artificial Muscles with Extremely Large Strain.* Polymer Journal, 2004. **26**(11): p. 933-936.
5. Yamato, K., et al., *Stability of Electrochemomechanical Strains in Polypyrrole Films Using Ionic Liquids.* Synthetic Metals, 2009. **159**: p. 839-842.
6. Debiemme-Chouvy, C. and T.T.M. Tran, *An Insight into the Overoxidation of Polypyrrole Materials.* Electrochemistry Communications, 2008. **10**(6): p. 947-950.
7. West, B.J., et al., *Chronoamperometric Study of Conformational Relaxation in Ppy(Dbs).* Journal of Physical Chemistry B, 2009. **113**: p. 1277-1293.
8. Lu, W., et al., *Use of Ionic Liquids For .Pi.-Conjugated Polymer Electrochemical Devices.* Science, 2002. **297**(5583): p. 983-987.
9. Ding, J., et al., *Use of Ionic Liquids as Electrolytes in Electromechanical Actuator Systems Based on Inherently Conducting Polymers.* Chemistry of Materials, 2003. **15**(12): p. 2392-2398.
10. Yamato, K., et al., *Stability of Electrochemomechanical Strains in Polypyrrole Films Using Ionic Liquids.* synthetic metals, 2009. **159**(9-10): p. 839-842.
11. Spinks, G.M., et al., *Enhanced Stability and Control of Polypyrrole Electromechancial Actuators.* Synthetic Metals, 2004. **140**: p. 273-280.
12. Otero, T.F., M. Marquez, and I.J. Suarez, *Polypyrrole: Diffusion Coefficients and Degradation by Overoxidation.* Journal Of Physical Chemistry B, 2004. **108**(39): p. 15429-15433.
13. Murray, P., et al., *In-Situ Mechanical Properties of Tosylate Doped (Pts) Polypyrrole.* Synth. Met., 1997. **84**(1-3): p. 847-848.
14. Murray, P., et al., *Electrochemical Induced Ductile-Brittle Transition in Tosylate-Doped (Pts) Polypyrrole.* synthetic metals, 1998. **97**(2): p. 117-121.
15. Otero, T.F., J.J.L. Cascales, and G.V. Arenas, *Mechanical Characterization of Free-Standing Polypyrrole Film.* Materials Science & Engineering C-Biomimetic and Supramolecular Systems, 2007. **27**(1): p. 18-22.
16. Spinks, G.M., et al., *Strain Response from Polypyrrole Actuators under Load.* Advanced Functional Materials, 2002. **12**(6-7): p. 437-440.
17. McGovern, S.T., et al. *Fast Bender Actuators for Fish-Like Aquatic Robots - Art. No. 69271l*. in *Conference on Electroactive Polymer Actuators and Devices (EAPAD 2008)*. 2008. San Diego, CA: Spie-Int Soc Optical Engineering.
18. Samani, M.B., et al. *Modelling of Polypyrrole Actuators*. in *Symposium on Electroresponsive Polymers an Their Applications held at the 2005 MRS Fall Meeting*. 2005. Boston, MA: Materials Research Society.
19. Hara, S., et al., *Free-Standing Gel-Like Polypyrrole Actuators Doped with Bis(Perfluoroalkylsulfonyl)Imide Exhibiting Extremely Large Strain.* Smart Materials & Structures, 2005. **14**(6): p. 1501-1510.

20. Susumu Hara, et al., *Free-Standing Gel-Like Polypyrrole Actuators Doped with Bis(Perfluroroalkylsulfonyl)Imide Exhibiting Extremely Large Strain* smart materials and structures, 2005. **15**: p. 1501-1510.
21. Bay, L., et al., *Mechanism of Actuation in Conducting Polymers: Osmotic Expansion.* Journal of Physical Chemistry B, 2001. **105**: p. 8492-8497.
22. Bull, R.A., F.R.F. Fan, and A.J. Bard, *Polymer-Films on Electrodes .7. Electrochemical-Behavior at Polypyrrole-Coated Platinum and Tantalum Electrodes.* Journal of the Electrochemical Society, 1982. **129**(5): p. 1009-1015.
23. Lewis, T.W., et al., *Studies of the Overoxidation of Polypyrrole.* synthetic metals, 1997. **84**(1-3): p. 403-404.
24. Li, Y.F. and R.Y. Qian, *Electrochemical Overoxidation of Conducting Polypyrrole Nitrate Film in Aqueous Solutions.* Electrochimica Acta, 2000. **45**(11): p. 1727-1731.
25. Rodriguez, I., B.R. Scharifker, and J. Mostany, *In Situ Ftir Study of Redox and Overoxidation Processes in Polypyrrole Films.* Journal of Electroanalytical Chemistry, 2000. **491**(1-2): p. 117-125.
26. Otero, T.F., H. Grande, and J. Rodriguez, *Conformational Relaxation During Polypyrrole Oxidation: From Experiment to Theory.* Electrochimica Acta, 1996. **41**(11-12): p. 1863-1869.
27. Otero, T.F., MAnuel Mrquez, and I.J. Surez, *Polypyrrole: Diffusion Coefficients and Degradation by Overoxidation.* The Journal of Physical Chemistry B, 2004. **108**(39): p. 5.
28. Otero, T.F. and I. Boyano, *Comparative Study of Conducting Polymers by the Escr Model.* Journal of Physical Chemistry B, 2003. **107**(28): p. 6730-6738.
29. Tso, C.H., J.D. Madden, and C.A. Michal, *An Nmr Study of Pf6- Ions in Polypyrrole.* synthetic metals, 2007. **157**(10-12): p. 460-466.
30. Warren, M.R. and J.D. Madden, *A Structural, Electronic and Electrochemical Study of Polypyrrole as a Function of Oxidation State.* synthetic metals, 2006. **156**(9-10): p. 724-730.
31. Treloar, L.R.G., *The Physics of Rubber Elasticity*. 1975, Oxford: Oxford University Press.
32. Vorotyntsev, M.A. and J. Heinze, *Charging Process in Electron Conducting Polymers: Dimerization Model.* Electrochimica Acta, 2001. **46**(20-21): p. 3309-3324.
33. Vorotyntsev, M.A., E. Vieil, and J. Heinze, *Charging Process in Polypyrrole Films: Effect of Ion Association.* Journal of Electroanalytical Chemistry, 1998. **450**(1): p. 121-141.

CHAPTER 5 CREEP BEHAVIOUR OF PPY-EMPIRICAL MODELLING

5.1 Introduction:

Practical applications for actuators require that those materials operate against an external load. The actuation behaviour against isotonic load has been well analysed by Spinks and Truong[1], showing that a change in elastic modulus affects the actuation strain and work output. More studies indicate that the load plays an important role during the actuation: in most cases, the strain amplitude will decrease as the load increases [2]; the energy conversion efficiency will have a maximum value [3]; the electrical response changes because of the configuration of the polymer chain under load [4].

An important issue related to the effect of external load is the problem of creep. Polymers usually creep under stress with slow and permanent strain occurring at constant stress. Thus, if accurate position control is required, creep must be eliminated or controlled. The creep behaviour of poorly solvated materials like conducting polymers is not understood. Thermoplastics below their glass transition have been studied for many years, with creep at low stresses being very slow due to the slow relative motion of polymer chains. In contrast, the molecular reorganisation of synthetic rubbers and chemically crosslinked hydrogels is so fast that relative motion is only hindered by crosslinks, and hence, creep does not occur without chemical reaction or rearrangement of localised physical bonds. Conducting polymers immersed in an electrolyte fall between these two boundaries, the polymer is above its glass transition temperature, but, has strong intramolecular bonding, as such is not highly swollen. The intermolecular bonds are usually prone to creep under low loads.

Previous studies have noted creep in PPy can produce a large deformation when stressed and recovery after release the stress [5]. The creep was also apparent at both the

oxidized and reduced state [3, 6]. Madden et al have concluded that the stress which will cause obvious creeping is significantly lower than the tensile strength of PPy films. The materials they were using have tensile strength of 120MPa (in dry state) while the creep can be found under stress of 20MPa [7]. While PPy soaked in electrolyte (PC for instance), the mechanical stiffness and strength decreased considerably [7] and as PPy become softer, the creeping is easier to observe, even under low stress.

The creep behaviour of CPs could be more complex than conventional polymers as the mechanical properties of CPs varies depending on their oxidized/reduced state. It is well established that the elastic modulus of CPs changes significantly with oxidation state. However, the effect of oxidation state on the creep behaviour has not previously been fully investigated.

In this chapter, the actuation of PPy under various constant voltages and external loads has been examined and analysed through a simple model in an attempt to analyse the creep behaviour. The actuation strain is considered to be the sum of the charge-induced strain and load-induced strain. The latter is influenced by the viscoelastic properties of the PPy. Thus, the viscoelasticity of polypyrrole doped with trifluoromethanesulfonimide (PPy/TFSI) has been investigated as a function of the applied electrochemical potential. A mathematical description based on the classical 4 element spring / dashpot model was adapted to fit the time-dependent strain behaviour of PPy/TFSI. Another empirical model describes the charge-induced strain. An attempt is made to predict the experimental results resulting from a change in applied voltage at a constant applied load by combining the charge-induced strain with the spring/dashpot viscoelastic model.

5.2 Experimental

5.2.1 Polypyrrole film preparation:

PPy films were produced using a similar method as described in chapter 4. Bis-trifluo-romethanesulfonimide lithium (LiTFSI) and propylene carbonate (PC) were obtained from Sigma. Pyrrole was obtained from Fluka and distilled before using. The PPy/TFSI film was deposited on the glassy carbon electrode, by adapting the constant current of 0.1mA/cm^2. The polymerization solution consisted of 0.1 M pyrrole, 0.1M LiTFSI and 0.1% (w/w) deionised water. Oxygen was removed by bubbling dried nitrogen for 10 minutes. Before reaction, the solution was stored in a freezer at -30ºC for 8 hours. After 12 hours polymerization, the polypyrrole film was peeled off from the substrate. The film was then washed with acetone and soaked in Li.TFSI/PC solution before further testing. Generally, the films were cut to around 3mm wide and 12mm long and the thickness of the film was approximately 34 μm.

5.2.2 The actuation test

Actuation tests were performed in 0.1 M Li.TFSI/PC electrolyte using a conventional three electrode setup. The PPy films used for actuation tests were cut to ~10 *mm* in length and 3 mm wide. To achieve electrical and mechanical contact, one end connected to the working electrode was fixed to the bottom of the electrochemical cell. The other end was glued to platinum wire using epoxy glue. The gauge length was the length measured between the glue and the clip. The actuation testing equipment is shown schematically in Chapter 2.

When potential was applied, the change in length was measured by a Model 305B Lever Arm Dual Mode System (Aurora Scientific). The counter electrode was platinum mesh and the reference electrode was $Ag|Ag^{+}$ in acetonitrile. The reported actuation strain refers to the change in length due to contraction which is always smaller than or equal to the change in length due to expansion. The contraction occurs when the PPy is being reduced. While testing, a small load (~ 30 kPa) was applied to keep the film straight without causing mechanical creep.

5.2.3 The creep test

The creep test in this chapter is different to the approaches used by Kaneto et al [3, 5, 6] where a voltage pulse was applied to a PPy film held at constant stress. In the present study, the creep behaviour was investigated when PPy was first stabilized under different redox state.

The set up for the creep test was exactly the same as the actuation test. The creep of PPy was determined in three different redox states: oxidized state by applying a positive potential, state as freshly grown and reduced state by applying negative potential. At each state, a step force was applied and lasted for at least 600s. Creep test under oxidized and reduced state was determined as follow: apply voltage; wait until the PPy reaches its equilibrium state (i=0); apply step force for another 20 minutes holding voltage constant; finally removing the stress to allow for strain recovery. All those tests were conducted at room temperature.

Note that new Samples were always used when starting another round of tests to avoid the history dependant effect and the instability of PPy/TFSI system as described in Chapter 4.

5.2.4 Fitting methods

The fitting parameter family was determined by using Origin 8.0 non-linear fitting tool box. This curve fitting tool allows all parameters to be determined that yield an analytical strain which best fits the experimental strain. The equations were written by Origin C. The initial guess data were chosen using approximate fits generated using Microsoft Office Excel.

5.3 Results and Discussion

In order to avoid the cycle-to-cycle variation in actuation in PPy/TFSI films (as described and discussed in Chapter 4), each test was performed using fresh samples. All the samples were tested under relatively low stress and strain for short periods of time in an attempt to remain in the linear creep region. The samples were saturated with 0.1 M LiTFSI/PC solutions before testing.

5.3.1 Stress-Free Actuation.

Initially the actuation at near-zero load was considered to investigate the time dependency of strain resulting from electrochemical charge injection. Note that the effects of changes in mechanical properties on the overall strain are negligible at near zero stress. The effects of higher stress on the actuation behaviour are considered in subsequent sections.

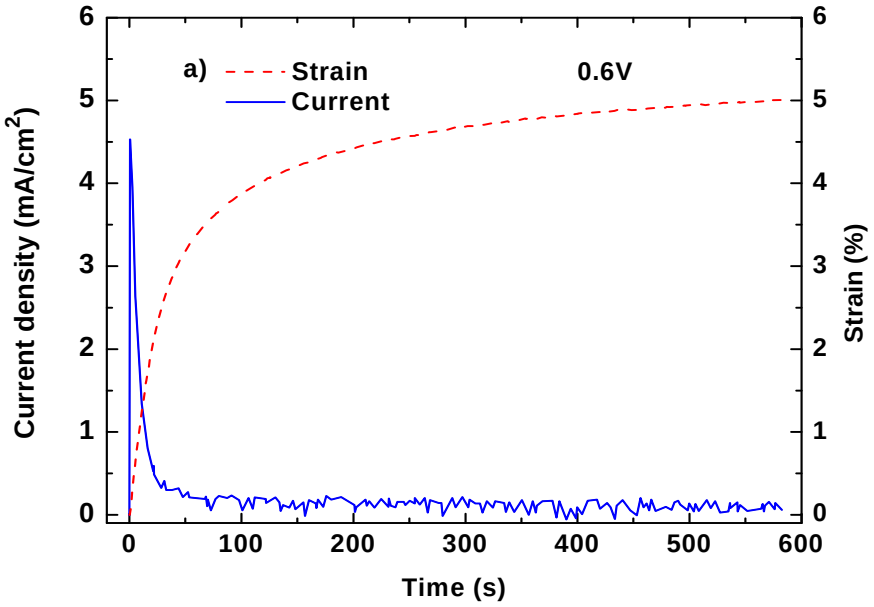
a)
Strain
Current
0.6V
Current density (mA/cm^2)
Strain (%)
Time (s)
0
1
2
3
4
5
6
0
100
200
300
400
500
600

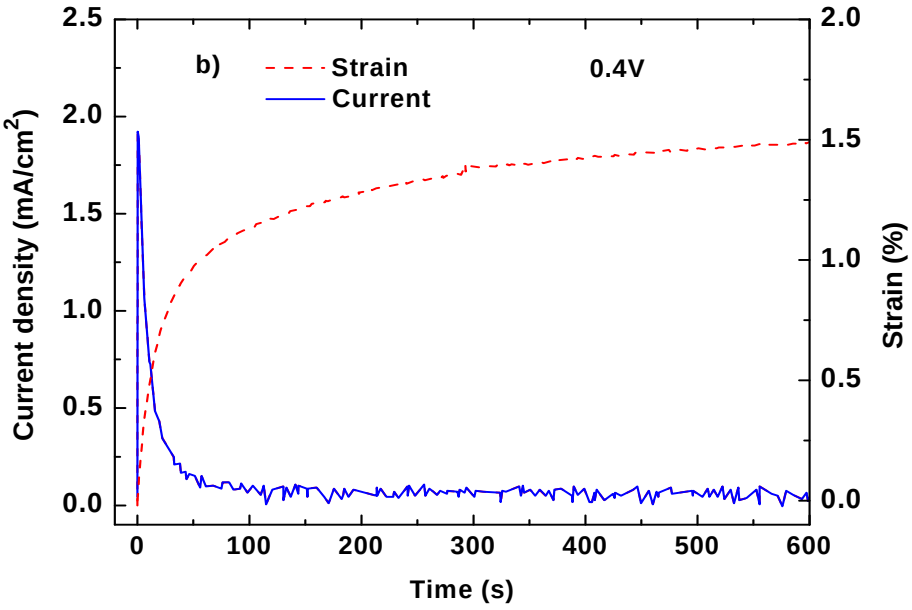
b)
Strain
Current
0.4V
Current density (mA/cm^2)
Strain (%)
Time (s)
0.0
0.5
1.0
1.5
2.0
2.5
0
100
200
300
400
500
600

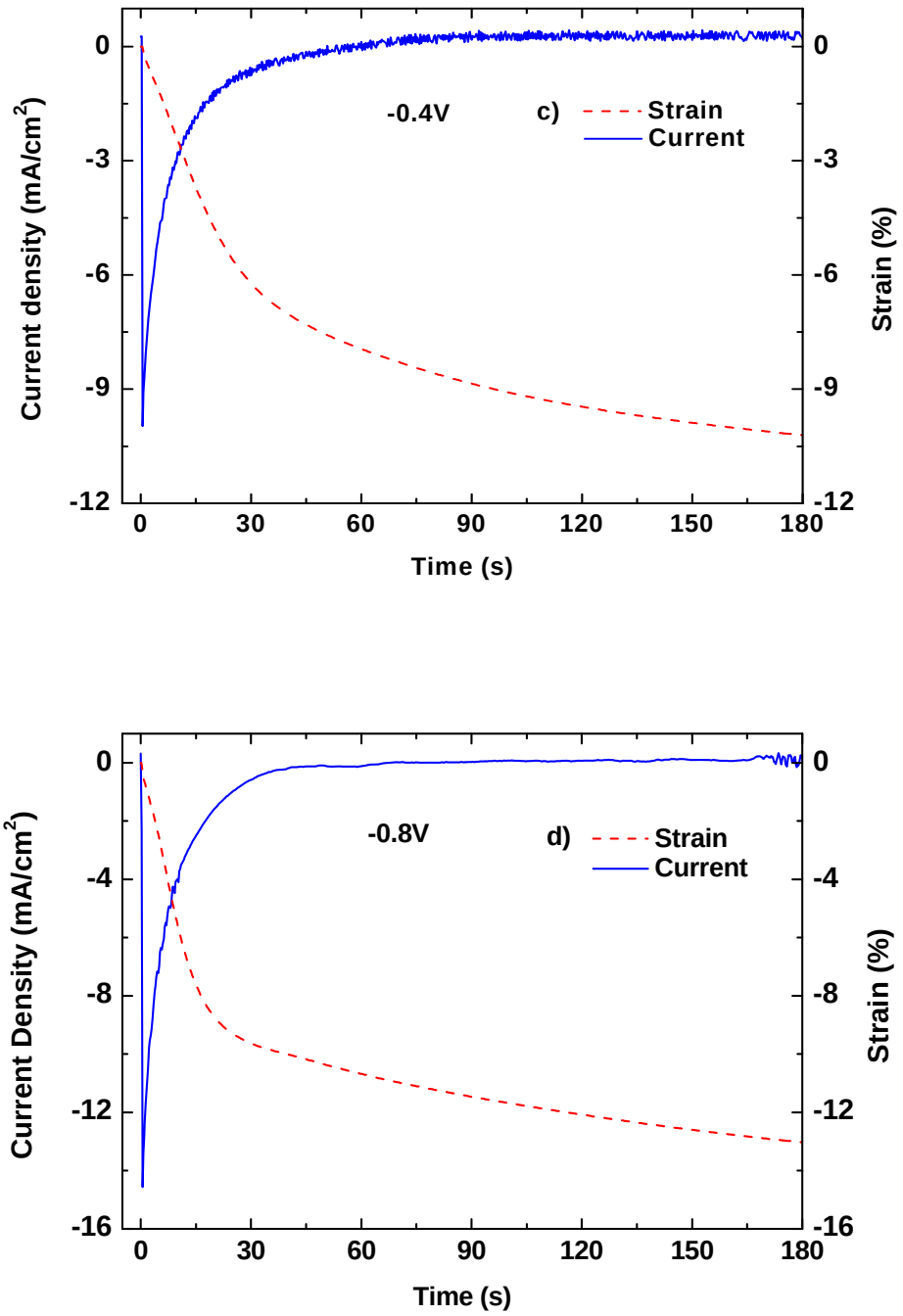

Figure 5. 1 The current flow and actuation of the free standing PPy/TFSI film under 0 stress; a)~d) +0.6V,+0.4V,-0.4V & -0.8V (versus Ag|Ag$^+$).

Figure 5. 1 illustrates the experimental data showing the current passed and strain resulting from an applied constant potential of 0.6V (a), 0.4V (b), -0.4V (c) and -0.8 V(d). While the current rapidly decays to nearly zero within the first 30-60 seconds, the

strain continues to increase for a much longer time. As described in previous work, there may be two contributions to the charge-induced strain in PPy. Skaarup at co-workers have shown, for example, that strain in PPy involves two processes. A fast response where cations with tightly bound water enters the polymer and a slower process involving the ingress of loosely bound water as a result of osmotic pressure [8].

As has been analysed in chapter 3, the strain generated in PPy helix tubes during a voltage ramp could be analysed based on a normal Fickian diffusion model. The charged layer thickness (d_c) could be estimated from:

$$d_c = 2\sqrt{Dt} \tag{5.1}$$

in which D is the diffusion co-efficient and t is time.

For the simple plate model consisting of a layer of fully oxidized polymer penetrating into the reduced polymer over time, then:

$$\frac{d_c}{d} = \frac{Q_v}{Q_{vmax}} \tag{5.2}$$

in which d is the total thickness of PPy film, Q_v is the total charge passed and Q_{vmax} is the theoretical charge as defined in chapter 3 .

$$Q_v = 2Q_{vmax}\frac{\sqrt{Dt}}{d} \tag{5.3}$$

Through using a strain to charge ratio (γ), the actual strain can be estimated as:

$$\varepsilon = \gamma Q_v = 2\gamma Q_{vmax}\frac{\sqrt{Dt}}{d} \tag{5.4}$$

Hence the strain is proportional to square root of time. To simplify, let

$$\kappa = 2\gamma Q_{vmax}\frac{\sqrt{D}}{d} \tag{5.5}$$

Then we get

$$\varepsilon = \kappa\sqrt{t} \text{ or } \varepsilon \propto \sqrt{t} \tag{5.6}$$

A similar relationship is found in electrochemistry where the Cottrell equation shows that the charge accumulated is also proportional to $\sqrt{t}$.

Figure 5. 2 shows the strain measured when a voltage of +0.4V was applied for 10 minutes. The strain increases rapidly at first and then more slowly. The dashed line in the figure is the best fit of a diffusion model to the data. Clearly, the agreement between experimental and calculated values is poor. In an attempt to improve the fitting, two diffusion based elements were included (Figure 5. 2 b) to simulate fast and slow actuation processes. A better fit to the experimental data was achieved with two diffusion components to the actuation strain. It should be noted that a single diffusion term was found to be sufficient to describe the actuation under voltage ramp described in Chapter 3. One possible difference relates to the time duration. In chapter 3 for instance, the typical time spent on 5mV/s anodic ramp scanning to +1 V for each cycle is 200s, much less than the time involved in the creep studies. Longer test time allows the slow actuation part to be more significant. It is also possible that the PPy.TFSI films show a larger "osmotic pressure" component to actuation strain than occurs in $PPy.PF_6$. Since the osmotically driven solvent ingress appears to be a slow process, the accurate modelling of strain over longer time periods in PPy.TFSI requires the two separate contributions.

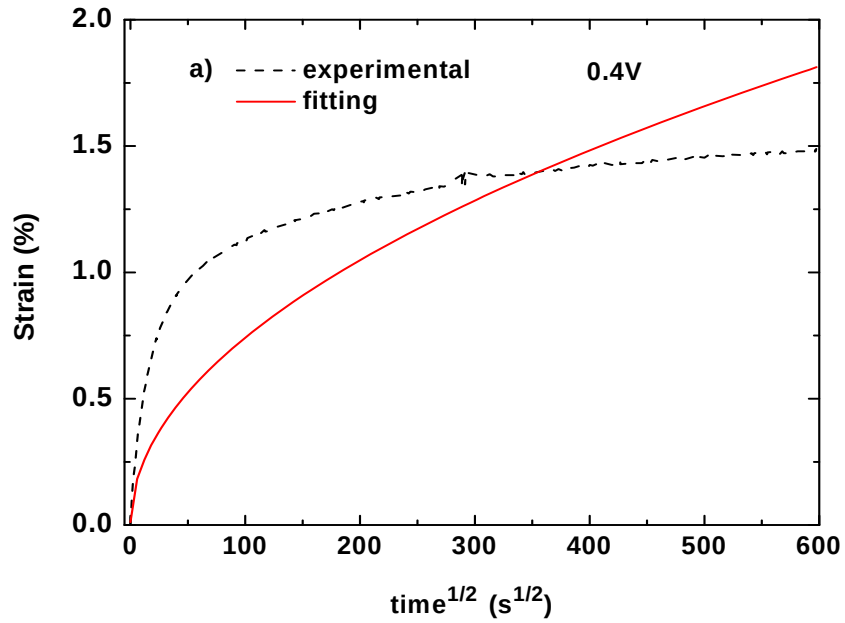
a)
experimental
fitting
0.4V
Strain (%)
time^1/2 (s^1/2)
0.0
0.5
1.0
1.5
2.0
0
100
200
300
400
500
600

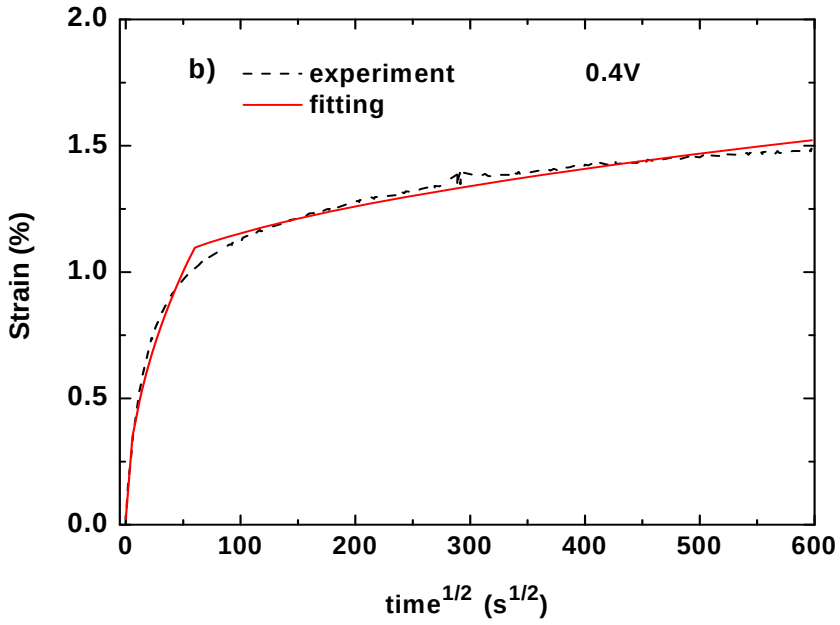
b)
experiment
fitting
0.4V
Strain (%)
time^1/2 (s^1/2)
0.0
0.5
1.0
1.5
2.0
0
100
200
300
400
500
600

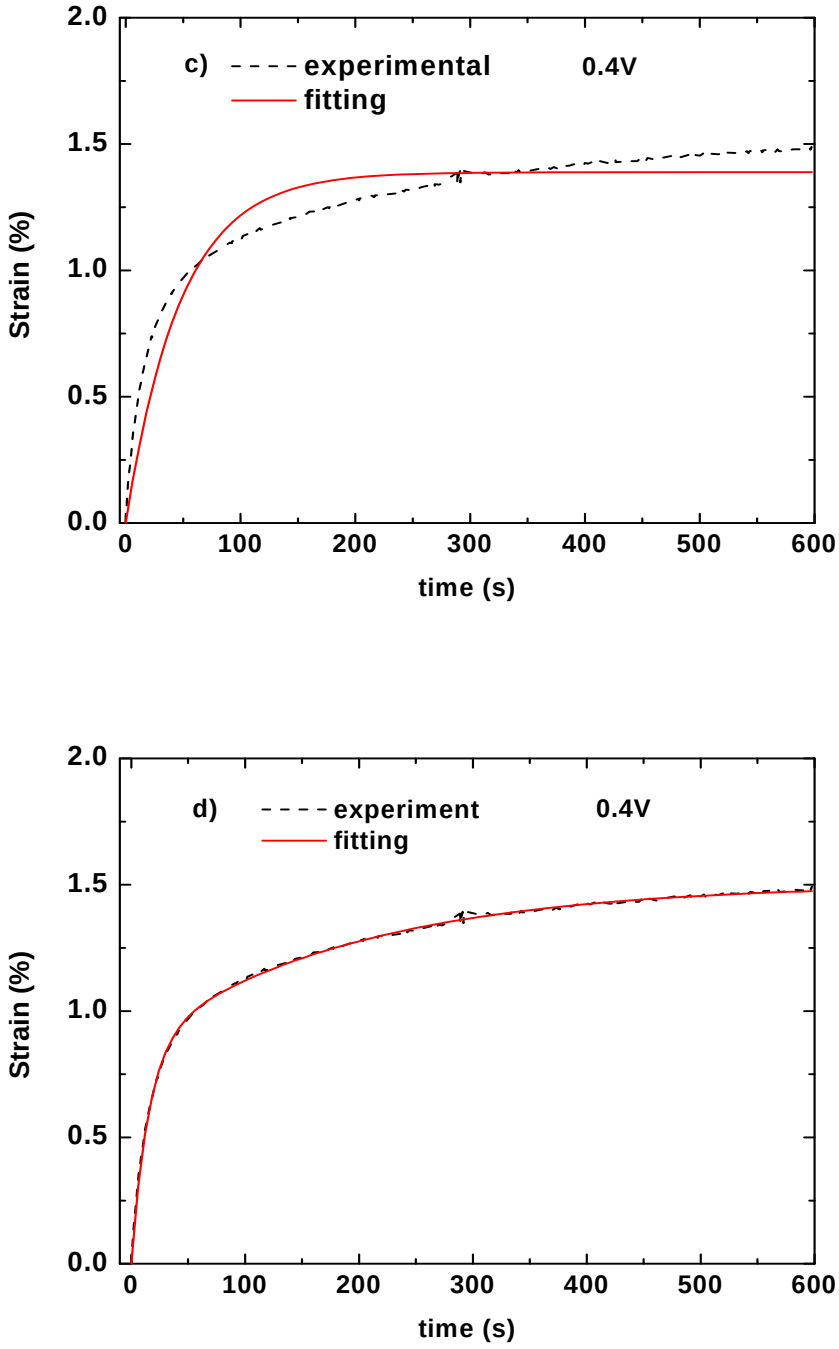

Figure 5. 2 Attempts of fitting free strain experiment at 0.4V versus Ag|Ag$^+$. a) fitting using single diffusion parameter; b) fitting using two diffusion parameter; c) fitting using one exponential function; d) fitting using two exponential functions.

An alternative to the simple diffusion model for PPy charging has been given by Otero [10] where an exponential relationship was introduced:

$$\mathrm{In}\left(1-\frac{Q_v}{Q_{vmax}}\right)=-bt \qquad (5.7)$$

where

$$D = \frac{bd^2}{2} \tag{5.8}$$

in which d is thickness of polymer film, D is diffusion coefficient and b is a linear variation which is function of anodic potential [9].

Hence, the injected charge is calculated as:

$$Q_v = Q_{vmax}\left(1 - \exp\left(-\frac{2Dt}{d^2}\right)\right) \tag{5.9}$$

and again by using strain to charge ratio:

$$\varepsilon = \gamma Q_v = \gamma Q_{vmax}\left(1 - \exp\left(-\frac{2Dt}{d^2}\right)\right) \tag{5.10}$$

Let $\tau_Q = \frac{d^2}{2D}$,if t_0 refers to time when charge induced, then:

$$Q_v = Q_{vmax}\left(1 - \exp\left(\frac{t_0 - t}{\tau_Q}\right)\right) \tag{5.11}$$

$$\varepsilon = \varepsilon_{Q\max}(1 - \exp(\frac{t_0 - t}{\tau_Q})) \tag{5.12}$$

The strain produced at +0.4V is modelled using one and two exponential functions, as shown in Figure 5. 2 c) and d). Excellent agreement between the calculated and experimental values is obtained with two exponential strain terms. Thus, two strain generators are used in series to represent fast and slow strains resulting from the application of an electrochemical potential (Figure 5. 3).

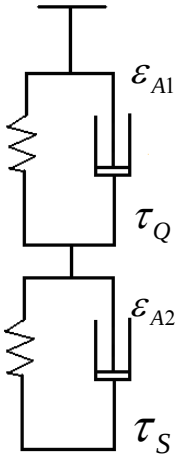

Figure 5. 3 The strain generators, including a fast and a slow charging part.

The strain response is empirically fitted to two separate charge-induced processes. It has been assumed that the faster actuation process (ε_{A1}) is based on a component that is directly related to the charge transfer and is modelled as an exponential element with a relaxation time for charge injection (τ_Q) and a maximum strain ($\varepsilon_{Q\max}$) expected from charge injection:

$$\varepsilon_{A1} = \varepsilon_{Q\max}(1-\exp(\frac{t_0 - t_1}{\tau_Q})) \tag{5.13}$$

The second actuation strain element is the strain resulting from other processes such as solvent ingress/egress resulting from osmotic pressure differences between the PPy film and the exterior electrolyte. This second process is also modelled as an exponential with time too:

$$\varepsilon_{A2} = \varepsilon_{s\max}(1-\exp(\frac{t_0 - t_1}{\tau_s})) \tag{5.14}$$

Here ε_s is the maximum strain expected from solvent diffusion and other processes and τ_s is the relaxation time for these processes.

Charge relaxation time τ_Q can also be evaluated. Since we know that:

$$Q_v = Q_{vmax}(1 - \exp\left(-\frac{t_0 - t}{\tau_Q}\right)) \quad (5.15)$$

when $t = \tau_Q$, $\mathrm{Q_v} \approx 0.633\mathrm{Q_{vmax}}$. Relaxation times for charge injection at different potentials has been determined from the integrated current data given in Figure 5.1 and are given in Table 5.1. Using these values and the estimated parameters listed in Table 5.1, the strain / time data at each potential were fitted with two exponentials. A comparison of calculated and experimental results is given in Figure 5.4 and the final fitted parameters are given in Table 5.2.

Table 5. 1 The first guessing fitting parameters.

	Charge per volume (mC/mm^3)	Charge induced strain (%)(calculated)	Charge relaxation time (s)
0.6V	30	3.0	25
0.4V	12	1.0	15
-0.4V	-50	-8.5	30
-0.8V	-67	-10.5	16

Table 5. 2 . The empirically fitting parameters of voltage induced strain.

	$\varepsilon_{Q\max}$	τ_Q	$\varepsilon_{s\max}$	τ_s
0.6V	3.08%	23.2	1.98%	179
0.4V	0.86%	15.2	0.64%	192
-0.4V	-8.85%	30.3	-5.86%	680
-0.8V	-10.40%	15.0	-6.54%	392

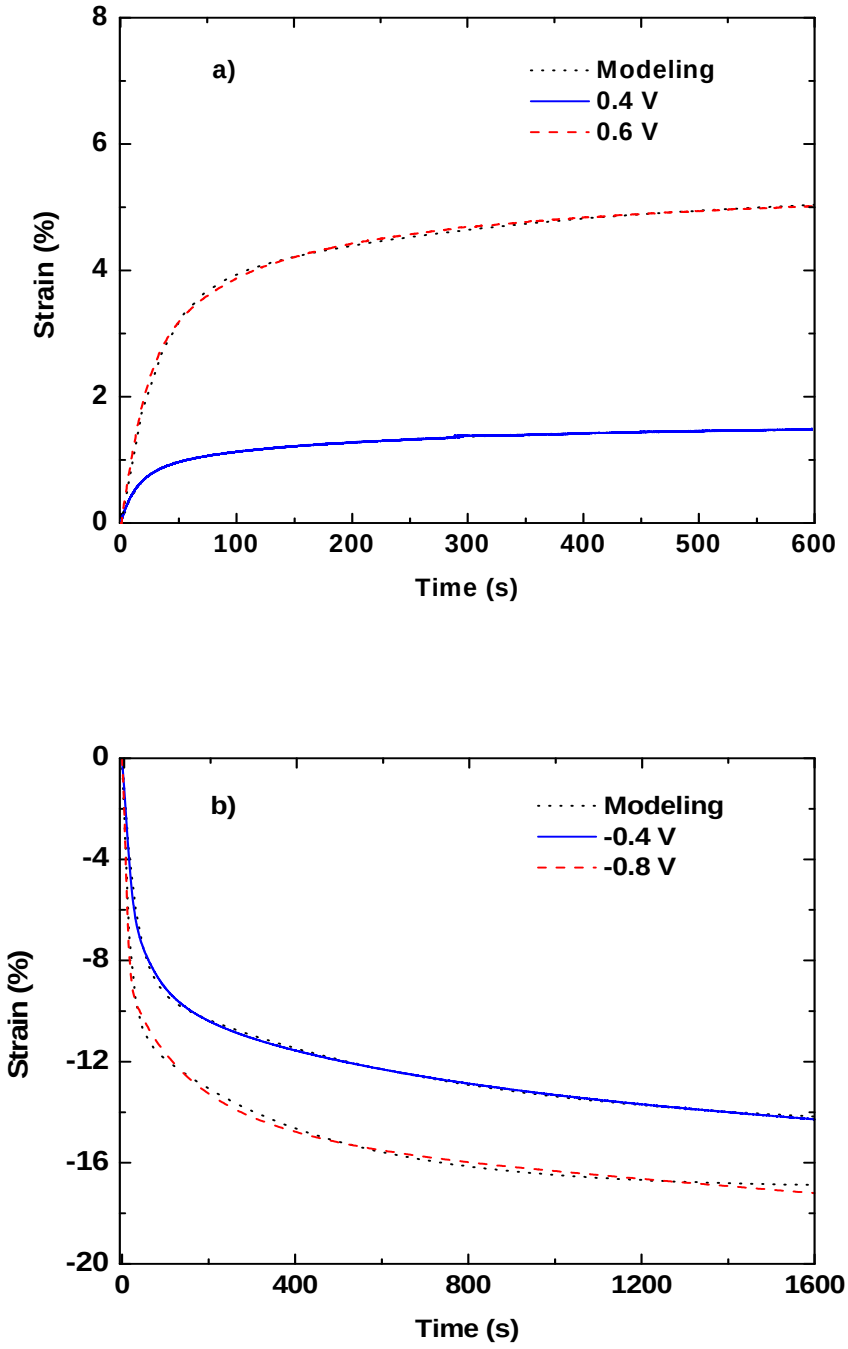

Figure 5. 4 The actuation behaviour of PPy/TFSI films under continuous voltage stimulation (VS Ag|Ag$^+$). A low stress of 30 kPa was applied to keep the free standing film straight.

At all potentials it is seen that there is excellent agreement between the experimental and calculated strain response. Since the calculated results are based on a semi-empirical approach, the interpretation of the fitting parameters is limited. However,

there appears to be an increase in the direct charge induced strain when more extreme (anodic or cathodic) potentials were applied. A higher applied voltage will lead to more charge transfer and consequently increased injection/ejection of ions. Higher potentials also increase the amount of strain resulting from slower, osmotic-type processes. This semi-empirical approach will be used below to estimate the strain resulting from a voltage pulse for PPy films under constant load.

5.3.2 Viscoelastic Behaviour PPy/TFSI films:

The strain response of PPy films resulting from an applied stress were determined at different redox states. Tensile creep tests at constant stress were performed on PPy at open circuit conditions for a 5 minute loading (Figure 5. 5), and under various applied potentials for 20 minutes loading (Figure 5. 6). As shown in Figure 5. 5, the PPy film shows a typical viscoelastic response with a fast increase in strain occurring upon the application of an external stress followed by a slower strain that continues to increase over the constant stress period. The stress was removed after 5 minutes and the PPy film showed a fast following by a slow recovery that was not fully completed after the 5 minute recovery time. Creep tests were performed at open circuit conditions at three different stresses. The strains increased approximately linearly with stress.

Figure 5. 6 shows the results of similar creep tests performed on PPy/TFSI films at various electrochemical potentials. In each case the film was conditioned at near zero load by applying the potential until the actuation strain (i.e. voltage-induced strain) achieved a steady state. A conditioning time of 20 minutes was required for positive potentials and 2 hours for negative potentials. After this conditioning period a stress in the range of ~0.5 MPa was applied and held constant for roughly 20 minutes followed

by a recovery at near zero load for a further 20 minutes. The loading and recovery phases of the test are shown in Figure 5. 6. The most significant feature observed from Figure 5. 6 is that the creep strain is larger and recovery less complete when oxidation potentials were applied (+0.4 and +0.6V) compared to the behaviour at both open circuit and negative potentials.

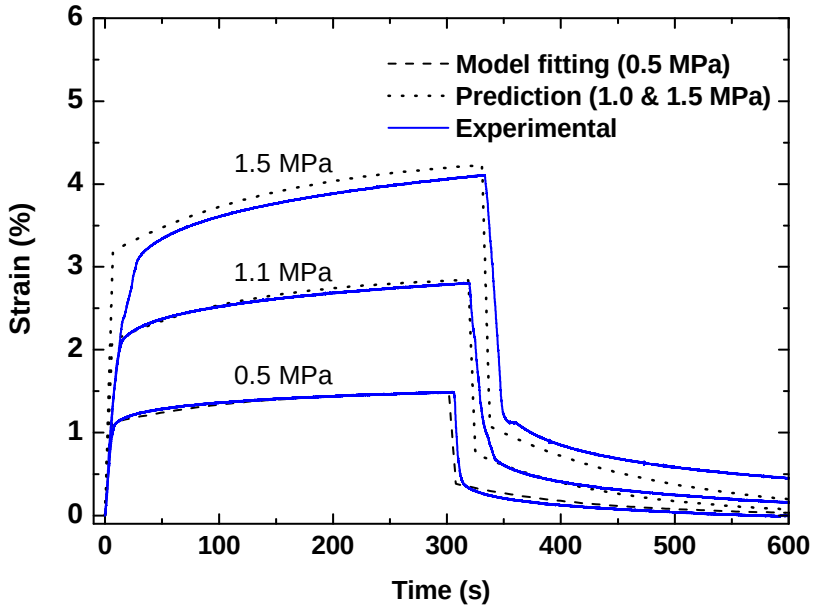

Figure 5. 5 The creep and recovery behaviour of Polypyrrole films under open circuit conditions. An initial load of 30 kPa is applied to keep the samples straight. Stresses between 0.5 and 1.5 MPa were applied for 300 s, and returned to 30 kPa for another 300 s.

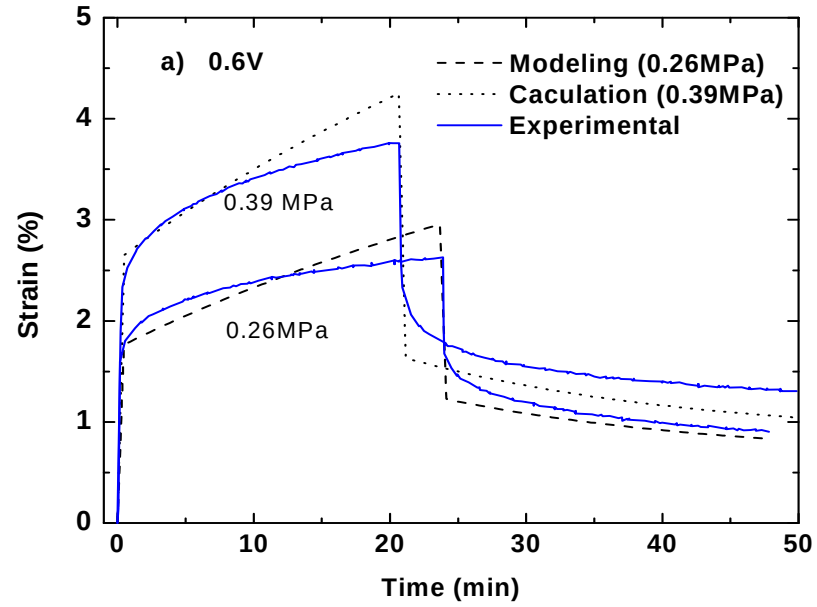
a) 0.6V
Modeling (0.26MPa)
Caculation (0.39MPa)
Experimental
0.39 MPa
0.26MPa
Strain (%)
Time (min)
0
1
2
3
4
5
0
10
20
30
40
50

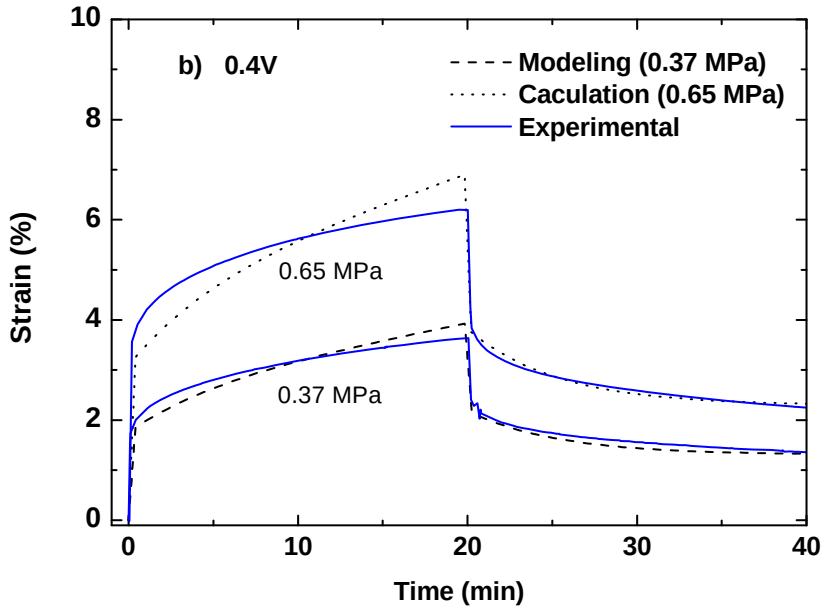
b) 0.4V
Modeling (0.37 MPa)
Caculation (0.65 MPa)
Experimental
0.65 MPa
0.37 MPa
Strain (%)
Time (min)
0
2
4
6
8
10
0
10
20
30
40

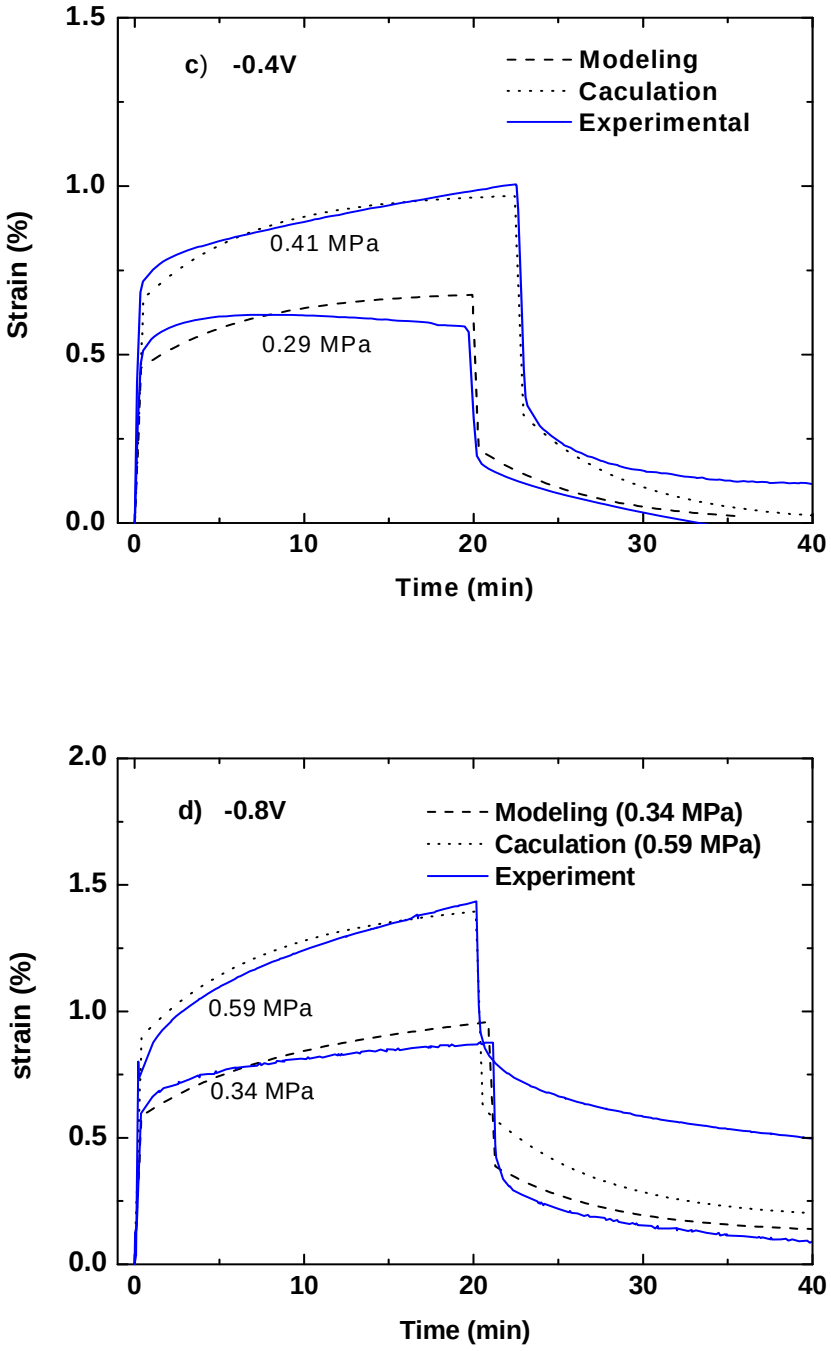

Figure 5. 6 The creep and recovery of polypyrrole films. An initial load of 30 kPa is applied to keep the samples straight. a) A voltage of 0.6V vs Ag|Ag$^+$ was applied. The stress was added in after 20mins and kept for 20 minutes. Then it reduced to 30 kPa for another 20 minutes. b) same test as a) using 0.4V vs Ag|Ag$^+$ c) A voltage of -0.4V vs Ag|Ag$^+$ was applied. After 2 hours, stress was introduced to the system and kept constant for 20 minutes. Then it returned to 30 kPa for another 20 minutes. d) same test as c) using -0.8V versus Ag|Ag$^+$. All tests were conducted under room temperature.

5.3.3 Viscoelastic Modelling of PPy/TFSI films:

A simple linear 4 element spring-dashpot viscoelastic model was used to describe the viscoelastic response of the polymers (Figure 5. 7). The spring element at the top gives the instantaneous elasticity, which is described by the 'instantaneous modulus' (E_1). The dashpot in series with the top spring gives the non-recoverable creep strain and is characterized by the viscosity term η_1. The spring and dashpot in parallel offer the delayed elastic strain (delayed modulus) and a relaxation time, which are characterized as E_2 and τ. When a stress σ is applied each contribution to strain at time (t) between t_0 and t_1 can be determined as follows:

Instantaneous elastic strain:

$$\varepsilon_i(t_0 \sim t_1) = \frac{\sigma}{E_1} \tag{5.16}$$

Delayed elastic strain:

$$\varepsilon_d(t_0 \sim t_1) = \frac{\sigma}{E_2}[1 - \exp(\frac{-(t - t_0)}{\tau})] \tag{5.17}$$

Viscous strain:

$$\varepsilon_v(t_0 \sim t_1) = \frac{\sigma}{\eta_1}(t - t_0) \tag{5.18}$$

If the stress, σ, is released at time = t_1, the strain elements at time (t) between t_1 and t_2 are given by the superposition principle, which leads to:

Instantaneous elastic strain:

$$\varepsilon_i(t_1 \sim t_2) = 0 \tag{5.19}$$

Delayed elastic strain:

$$\varepsilon_d(t_1 \sim t_2) = \varepsilon_d' \exp(\frac{-(t - t_1)}{\tau}) \tag{5.20}$$

Viscous strain:

$$\varepsilon_v(t_1 \sim t_2) = \varepsilon_v' \tag{5.21}$$

Where the ε_d' ε_v' are the delayed elastic strain and viscous strain at t_1, respectively.

The total strain (ε) is given as below:

$$\varepsilon = \varepsilon_i + \varepsilon_d + \varepsilon_v \tag{5.22}$$

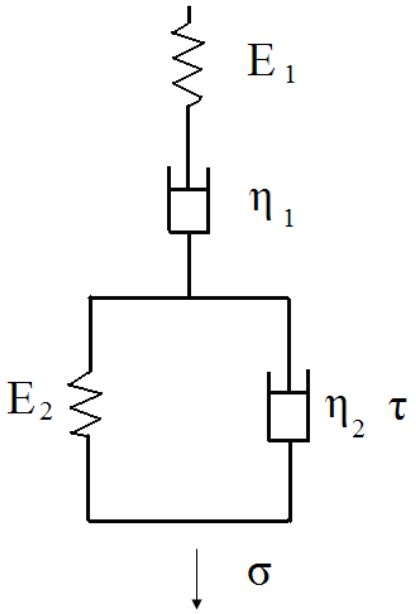

Figure 5. 7 Standard 4-element linear viscoelastic model.

Table 5. 3 Summary of the fitted viscoelastic parameters.

	$E_1(MPa)$	$E_2(MPa)$	$\eta_1(Pa \cdot s)$	$\tau(s)$
Open cycle state	45.4	119.25	$4.9*10^{33}$	120
Oxidized state (0.6V)	15.0	30.7	$5.7*10^{11}$	1240
Oxidized state (0.4V)	21.0	41.5	$3.4*10^{12}$	315
Reduced state (-0.4V)	64.7	120	$3.4*10^{12}$	386
Reduced state (-0.8V)	60.3	120.1	$3.5*10^{12}$	400

The fitting parameters and the goodness of fit to the experimental results are summarized in Table 5. 3, Figure 5. 5 & Figure 5. 6. For each experimental condition, the fitting values were calculated from the lower stress test and then applied to the other stress conditions. Reasonable agreement between the calculated strains and the experimental results were achieved at open circuit conditions (Figure 5. 5). The strains predicted from the fit to the viscoelastic behaviour at 0.5 MPa and applied to the 1.0 MPa and 1.5 MPa results give reasonable agreement. The main discrepancy in results was evident in the final strain, where the predicted strains tended to zero, while some residual strain was experimentally measured at the end of the relaxation time.

Similar analyses were applied to the PPy/TFSI films conditioned at various potentials before application of the stress pulse Figure 5. 6. In all cases, the 4 element model was capable of representing the general shape of the creep and recovery curves, with reasonable accuracy. In most cases it appeared that the instantaneous recovery upon removal of the stress was smaller than the instantaneous strain initially measured when the stress was first applied. Such behaviour suggests that the elastic modulus of the film increased during the hold period. An increase in the instantaneous modulus (E_1) implies that the intermolecular bonding within the PPy increased whilst the sample was under load. An increase in elastic modulus during loading is not unusual in materials; in particular, rubber goes through an increase in E under applied load due to stress induced crystallisation. The mechanism for the increase in PPy modulus whilst under load is not understood. It should be pointed out that the four – element model assumes that the viscoelastic parameters remain constant and so the calculated values from this model will not match exactly the real behaviour of the PPy films.

Despite the differences in the experimental and measured strain data, it is possible to compare the viscoelastic parameters for PPy/TFSI as a function of oxidation state.

One significant effect is the dramatic decrease in viscosity that occurs when the sample is both oxidized and reduced. At open circuit potential, very little permanent viscous response occurs, while when the film is either oxidized or reduced there is considerable non-recovered creep. Secondly, the elastic strain response is also sensitive to the applied potential, with an increase in both the instantaneous modulus and the delayed modulus as the PPy becomes more reduced. These moduli values increase in the order of oxidized, open circuit, reduced.

5.3.4 The elastic modulus shift under constant potential.

Various previous studies have considered how the modulus of PPy depends on different oxidation/reduction or contraction/expansion state [6, 10-12]. Pytel *et al.* show how the modulus shifts while switching the potential [13]. They concluded that the elastic modulus was increasing while ions are expelled from the film and decreasing while ions are brought in. They attributed the decreasing of the modulus to the plasticization of the polypyrrole, which has also been observed before through static experiments [11].

Dynamic changes to the elastic modulus at constant potentials were further considered in light of the four-element viscoelastic model. The aim was to determine how the instantaneous elastic modulus changes during the equilibration process at both oxidising and reducing potentials. A small square wave stress (0.05MPa) with frequency 10Hz was applied to the system. The dynamic modulus was estimated from $\varepsilon = \frac{\Delta F}{A_0 \Delta L / L_0}$, in which the ΔF and ΔL are the force range and length change, respectively, A_0 and L_0 are the cross-sectional area and the original length of the free-standing film.

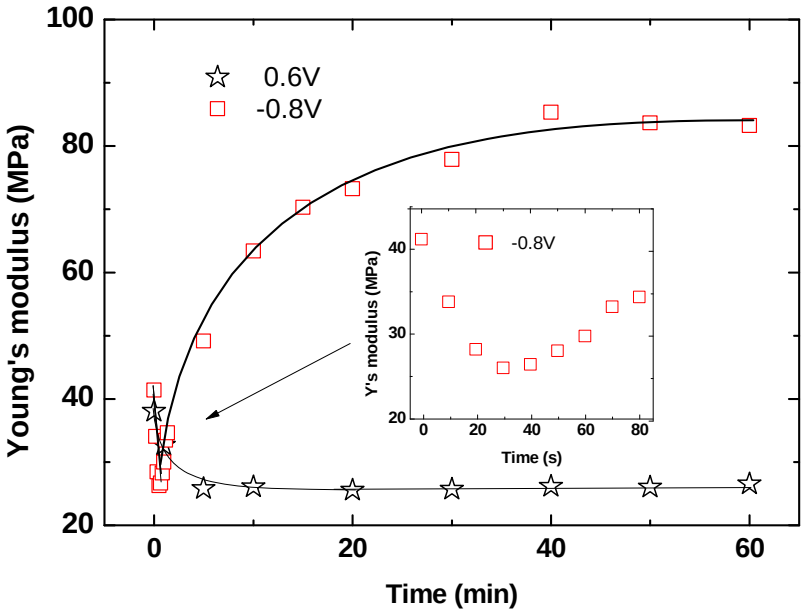

Figure 5. 8 Instantaneous modulus of free standing PPy/TFSI films measured over time at constant voltage stimulation (VS Ag|Ag$^+$).

The dynamic elastic modulus changes occurring during oxidation and reduction of PPy/TFSI are illustrated in Figure 5. 8. The oxidation response is quite rapid with the modulus decreasing from the open circuit value to a constant value within 5 minutes. The change in modulus during reduction is both slower and more complicated. The modulus initially drops quickly during the first 30 seconds of reduction to half (22 MPa) its original value (44 MPa). Then the modulus increases more slowly reaching its highest value and remaining stable after about 60 mins at double the original open circuit value (89 MPa). The changes in modulus will be sensitive to the extent of intermolecular bonding which, in turn, depends upon interactions between charged chains and dopant ions, and will also depend upon any plasticising effects. It is possible that the initial reduction causes a reduction in ionic crosslinking, covalent bonding or dipolar interactions causing a decrease in modulus. The gradual compaction of the polymer structure over time, may then lead to the slow increase in modulus. It is

possible that the reduction in modulus during oxidation is due to the plasticising effect due to the ingress of solvent.

The modulus measurement taken from tensile testing (Figure 5. 9) is in accordance with the dynamic results (Figure 5. 9). After 1 hour of potential conditioning, the modulus under 0.6 V is lowest, following by open cycle state and then reduced state (-0.8V).

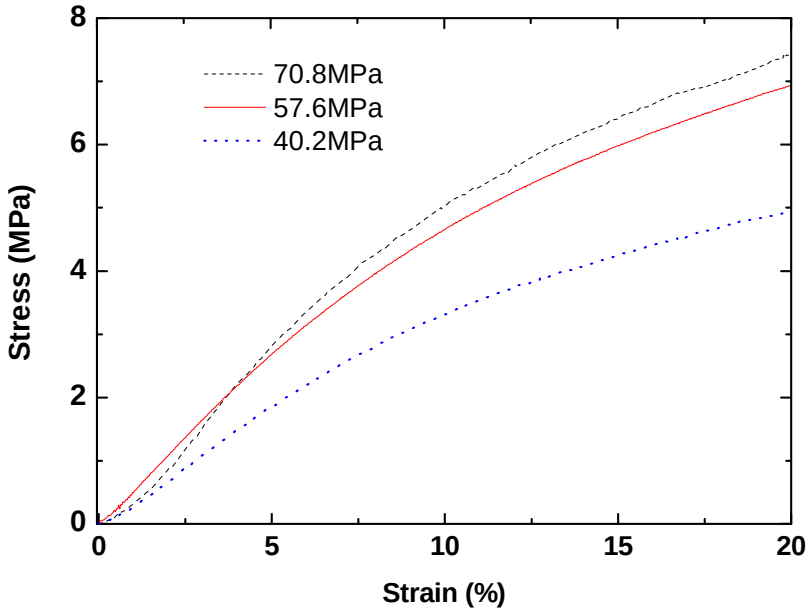

Figure 5. 9 The Young's modulus of PPy/TFSI film at different redox state: -0.8V (dash line), open cycle (solid line) and +0.6V (dot line). All sample tested in Li.TFSI/PC solution (0.1M). Reference used is Ag|Ag$^+$. Before testing, the samples were kept under constant volts for 1 hour.

5.4 PPy actuation under combined stress and voltage stimulus

Normally the actuator works against an external stress. Hence, it is necessary to combine the viscoelastic strain and the voltage induced strain. To simplify the process, a step stress was first applied and then an electrochemical stimulation was introduced. As shown in Figure 5. 10, the initial stress was applied at open circuit potential and the

viscoelastic strain response allowed to reach equilibrium over 20 minutes. At this time a voltage pulse of +0.4V, -0.4V or -0.8V was applied and the resultant strain measured.

At the positive potential of +0.4V the voltage-induced strain was positive (expansion) with greater expansion observed when higher stresses were applied. The expected strain response was calculated from the previously-developed viscoelastic and charging models and are shown as dashed lines in Figure 5. 10 a). The strain from 0 – 20 minutes was successfully modelled using the viscoelastic model and using parameters obtained from PPy/TFSI at open circuit potential. The strain from 20 – 40 minutes was calculated as the sum of the charge induced strain and the strain resulting from a change in the viscoelastic parameters. In this case the viscoelastic parameters were assumed to change instantaneously when the potential was applied at t=20 min:

$0 < t < 20$ mins:

$$\varepsilon = \varepsilon_i + \varepsilon_d + \varepsilon_v = \frac{\sigma}{E_1} + \frac{\sigma}{E_2}[1 - \exp(\frac{-t}{\tau})] + \frac{\sigma}{\eta_1} t \tag{5.23}$$

$20 < t < 40$ mins:

$$\varepsilon = \varepsilon_i' + \varepsilon_d' + \varepsilon_v' + \varepsilon_{A1} + \varepsilon_{A2} = \frac{\sigma}{E_1'} + \varepsilon_d(t_1) + \frac{\sigma}{E_2'}[1 - \exp(\frac{-(t-t_1)}{\tau'})] + \varepsilon_v(t_1) + \frac{\sigma}{\eta_1'}(t - t_1)$$

$$+ \varepsilon_Q(1 - \exp(\frac{t_0 - t_1}{\tau_Q})) + \varepsilon_s(1 - \exp(\frac{t_0 - t_1}{\tau_s})) \tag{5.24}$$

The parameters used in the calculations are given in Table 5. 2 & Table 5. 3. The expected strains resulting from the +0.4V potential pulse applied at t=20 mins gives a reasonable representation of the measured strains (Figure 5. 10). An expansion occurs when the potential is applied and the expansion is larger when higher stresses were used, reflecting the reduction in E_1 and E_2 terms that accompany PPy/TFSI oxidation.

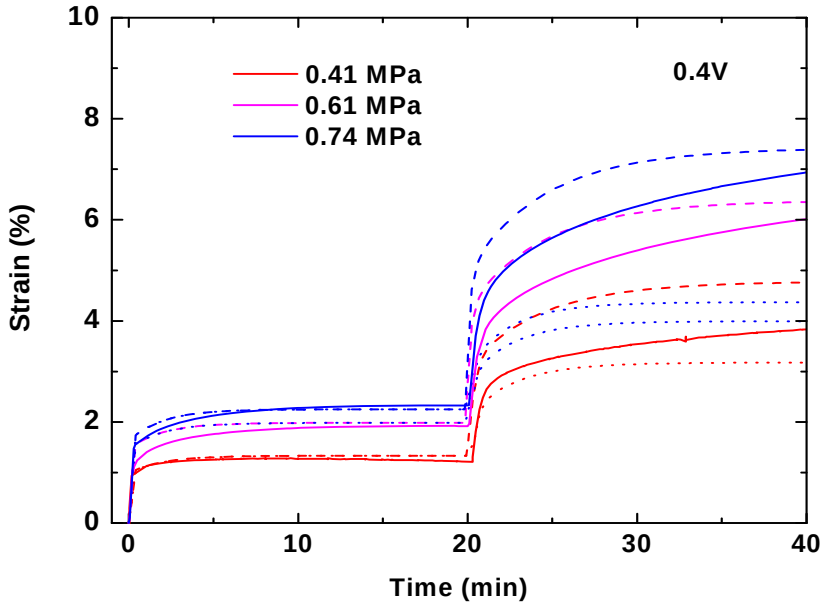

Figure 5. 10 The modelling and experimental strain of PPy/TFSI films under different constant stress at +0.4V. Modelling results (dashed lines) are based on an instantaneous change in viscoelastic properties at t=20 min; The dotted line is the calculated strain response assuming no change in viscoelastic properties.

The magnitude of the calculated strains are, however, over-estimated compared with the measured strains. While the calculation assumes that the mechanical properties change immediately the potential pulse was applied, it is likely that these properties change slowly as the polymer becomes increasingly oxidized through its entire thickness. A similar process was described in Chapter 3 for the change in elastic modulus of PPy/PF_6 helix tubes. Dotted lines in Figure 5. 11b) represent calculated strains where it is assumed that no change in mechanical properties occurs upon the application of the potential pulse. The dotted line represents the charge induced strain only. It is seen that the experimental strain follows the predicted charge induced strain closely in the initial phase but later deviates towards the strain predicted as resulting from both charging and mechanical properties change.

Figure 5.11 shows experimental and calculated results for the strain produced at -0.4V and -0.8V, respectively. In these cases the strain decreases when the potential was applied due to reduction and contraction of the film. Interestingly, the extent of contraction was smaller when a larger stress was applied. The calculated strain values over-estimate the contractile strain and to a greater degree for the higher stress. The strain calculation was based on both changing and unchanging viscoelastic parameters, with only a small effect on the calculated strains. The instantaneous modulus was shown above to increase slightly upon the application of -0.4V. This small increase in modulus would be expected to cause contraction of the PPy film to an increasing extent with increasing applied stress. It should be noted that at the small stresses used in the present study, the effect of changing modulus on the actuation strain would be of the order of just 0.2%, which is much smaller than the overall measured strains. The reason why there is such a significant difference in strains at the different stress levels at -0.4V is unclear. The previously measured mechanical property changes suggest that the effect of the applied stress should be small and in the opposite direction to that shown in the experimental results.

The discrepancy between calculated and measured actuation strains is even more striking for the samples tested at -0.8V. As shown in Figure 5.11, the strain caused by the application of this potential first causes a sharp contraction followed by a fast expansion and then by a slower contraction. The second phase (fast expansion) is affected by the applied stress and is larger for higher stresses. The modelling results completely miss the initial fast contraction and fast expansion. The calculated results resemble the final slow contraction only.

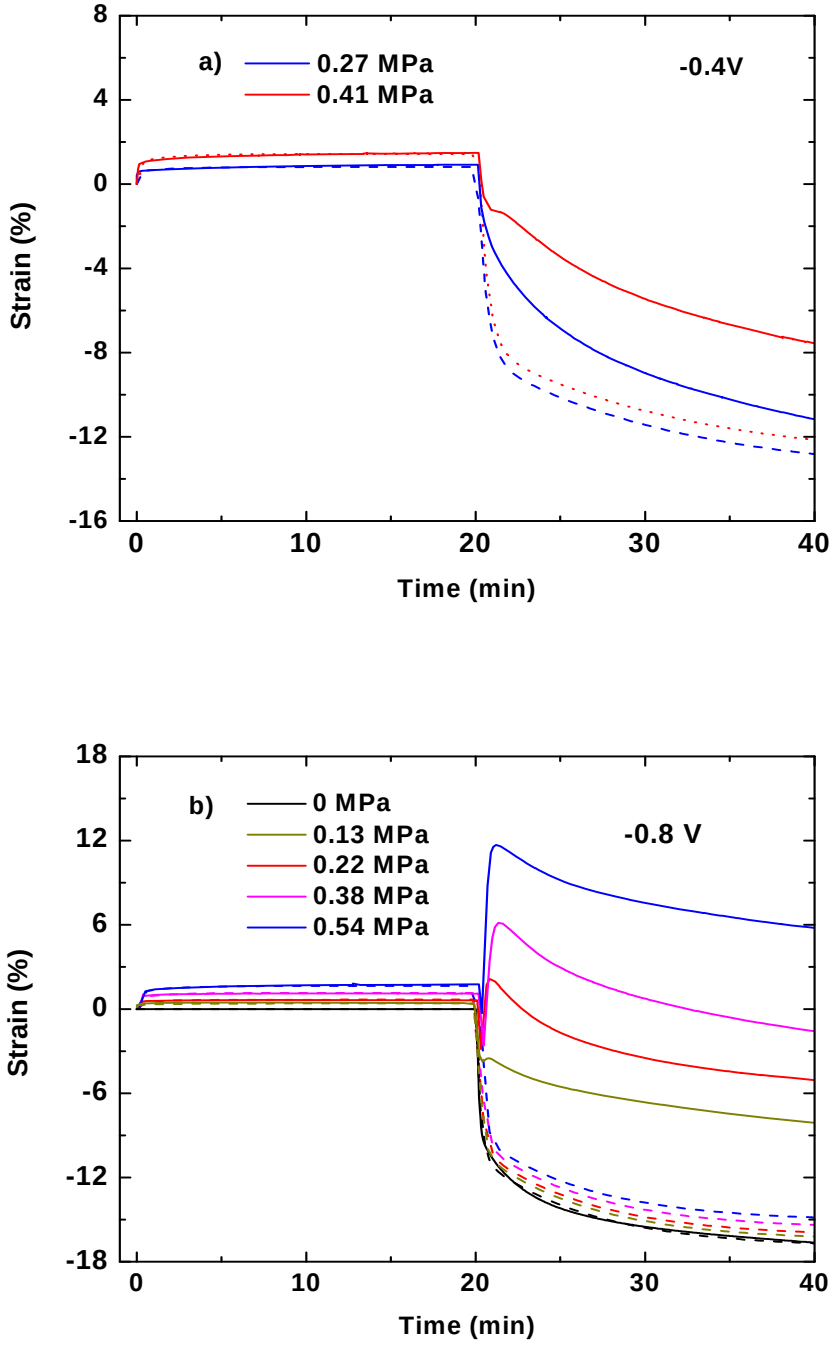

Figure 5. 11 The modelling and experimental strain of PPy/TFSI films under different constant stress at a) -0.4V and b) -0.8V (VS Ag/Ag$^+$). The dashed lines represent the modelling prediction.

A possible cause of the initial fast contraction and expansion may be related to the dynamic changes noted above in the elastic modulus. At -0.8V the modulus was found to decrease rapidly initially before increasing over a longer time period. It is possible

that the initial decrease in modulus may produce an increase in actuation strain. However, the magnitude of the change in strain from the measured changes in modulus is expected to be 0.5%, which is much smaller than the expansion that is seen to occur soon after -0.8V was applied to the PPy/TFSI films. The complicated strain response to a cathodic potential step is, therefore, unexplained at present.

5.5 Summary and Conclusions:

In this chapter, viscoelastic creep behaviour of PPy/TFSI films was investigated and an empirical model was developed. Creep has been recognised as a problem affecting the accurate position control of conducting polymer actuators, but little information is available in the literature concerning the mechanisms of creep in these materials. It is known from previous work that the elastic modulus of conducting polymers depends upon the polymer's oxidation state. The viscoelastic behaviour of these materials is also likely affected by the extent of oxidation and the main aim of the present chapter was to determine how the creep and recovery of PPy/TFSI was affected by an applied electrochemical potential. Since the application of such potentials also causes actuation, an attempt has been made to separate the actuation strain and the viscoelastic strain.

Initially the viscoelastic behaviour of PPy/TFSI was investigated using the 4 element viscoelastic model. Fresh PPy/TFSI films were conditioned at different electrochemical potentials before a tensile stress applied and then released. The stress-induced creep strain and recovery were fitted to the 4-element model. The fitting parameters were then used to estimate the creep and recovery at different stress levels and reasonable agreement between the calculated and measured strains were obtained.

The viscous contribution at all stresses and potentials investigated was quite small, indicating that the "creep" in these films is mainly a delayed elastic response that can be mostly fully recovered upon the removal of the stress.

An evaluation of the fitting parameters revealed a consistent trend with a decrease in the elastic moduli (instantaneous and delayed) with an increased degree of oxidation. In addition, the viscosity parameter was also smallest in the most oxidized state. These changes suggest that molecular movement becomes easier in the oxidized state for PPy/TFSI allowing greater chain uncoiling (elastic deformation) and slip (viscous deformation) under stress. Plasticisation of the films by solvent could be the cause of the decreased bonding and increased free volume that allow increased molecular movement. The plasticisation effects must outweigh the increased intermolecular bonding that can also occur in oxidized PPy due to ionic interactions and dimerisation. It should be noted that the latter effect was thought to be responsible for the increased modulus upon repeated voltage cycling of PPy/TFSI, as reported in Chapter 4. Only fresh films were used in the studies reported in the present Chapter and the changes in mechanical properties occur during the first oxidation (or first reduction). It is known that the actuation is largest in the first cycle, due mostly to a large influx of solvent. It is likely that this increased swelling accounts for the decrease in modulus and viscosity.

To evaluate the effect of the PPy/TFSI viscoelasticity on the actuation behaviour, it was necessary to first investigate the actuation at near zero stress. The actuation strain was found to be dependent on two time separate processes based on the time response to a voltage pulse. The strain was modelled semi-empirically based on a fast response with the same time constant as charge injection and a slower response. The former was similar to that used in Chapter 3 to model the strain of PPy.PF_6 helix tubes. In the case of PPy.TFSI films, it was found that an exponential strain responsed fitted the

experimental data better than the Fickian diffusion model used in Chapter 3. The slower response may be due to solvent ingress resulting from osmotic pressure or other processes such as conformational changes. Excellent fits between experimental and calculated strains were obtained when both strain responses were modelled as exponential functions.

Finally, the actuation of PPy.TFSI films under constant tensile load was investigated. The load was applied at open circuit potential and allowed to achieve an approximately steady state before a voltage pulse was applied. The stress response at all stresses used was accurately predicted by the viscoelastic model at open circuit conditions. The voltage-induced actuation was modelled by superimposing the zero-strain actuation (two processes) and the strain due to the change in viscoelastic parameters.

Reasonable predictions of the actuation response under load was achieved at positive potentials. Interestingly, the actuation strain was increased when higher applied stresses were used. This observation is the opposite to that found in most other studies of PPy actuation, however, the effect of load was suitably predicted by the decrease in elastic moduli that accompany an increase in oxidation state of PPy.TFSI. The modelling approach used assumed that the mechanical properties of the PPy.TFSI changed immediately upon the application of the pulse potential. However, it is likely that these properties change gradually as the polymer swells and as described in Chapter 3. Indeed, it appeared that the predicted strains matched better the measured strains after some time had elapsed following the potential pulse.

Quite unexpected and complicated strain responses were observed for PPy.TFSI pulsed to negative potentials. At the more extreme potential used (-0.8V), the strain first decreased, then increased sharply and then decreased more slowly. The second sharp

increase was found to be dependent upon the applied load. Only the final gradual decrease in strain was predicted by the zero-strain actuation and viscoelastic model. The transient behaviours observed were not at all predicted by the prior observations or empirical models.

The reasons for the transient behaviour of PPy.TFSI during its first reduction are unknown. The effects were only observed when the films were first subjected to an applied stress at open circuit potential. Although the strains introduced by the stress were small, it appears that the stress caused some form of molecular change within the PPy.TFSI that affected the manner in which in responded to a reducing voltage. The transient strain effects were of a large magnitude and probably too large to be caused by changes in the mechanical properties of the films, since the applied stresses were quite small. Film shrinkage and expansion must then be due to ingress or egress of ions and / or solvent. A decrease in length upon reduction is usually associated with the ejection of anions, while an increase in length can be caused by the incorporation of cations from the surrounding electrolyte. It may be possible that the sustained small stress applied to the PPy.TFSI films causes a structural reorganisation that favours cation incorporation, perhaps as a result of stronger binding of anions. Detailed structural analysis of the PPy films would be needed to further elucidate these mechanisms. Such studies are beyond the scope of the current thesis.

Until now, there has not been a theoretical study to explain the creep behaviour of PPy. The widely used viscoelastic model for polymers is purely empirical, although the parameters used can be related to chain movement within the solid polymer. The present study has shown that creep and relaxation in PPy.TFSI is qualitatively similar to other polymers and is reasonably modelled by the 4-element model. Coupling the PPy viscoelastic response to the actuation remains a challenge. It is obvious from the results

of the present study that there is an interaction between the applied stress and the actuation mechanisms – at least for the first reduction of PPy.TFSI. The nature of the interaction is not clear. The result is that it is not possible to simply add together the actuation expected at zero stress with the stress-induced viscoelasticity to predict the time-dependent strain. Consequently, further work is needed to develop a model to describe/predict the total strain of CPs including the creep part. Such a model is quite useful and necessary for CPs actuators, especially when the effect of creep cannot be neglected such as when position control is required, or, when the creep strain contributes a significant part of the whole strain (working under high loads).

5.6 References

1. Spinks, G.M. and Truong, V.-T., *Work-Per-Cycle Analysis for Electromechanical Actuators.* Sensors and Actuators A: Physical, 2005. **119**(2): p. 455-461.
2. Spinks, G.M., Liu, L., Zhou, D. and Wallace, G.G., *Strain Response from Polypyrrole Actuators under Load.* Advanced Functional Materials, 2002. **12**(6-7): p. 437-440.
3. Kaneto, K., Fujisue, H., Yamato, K. and Takashima, W., *Load Dependence of Soft Actuators Based on Polypyrrole Tubes.* Thin Solid Films, 2008. **516**(9): p. 2808-2812.
4. Madden, J.D., Madden, P.G., Anquetil, P.A. and Hunter, I.W., *Load and Time Dependence of Displacement in a Conducting Polymer Actuator*, in *Electroactive Polymers and Rapid Prototyping*, Y. BarCohen, et al., Editors. 2002, Materials Research Society: Warrendale. p. 137-144.
5. Kaneto, K., Suematsu, H. and Yamato, K., *Training Effect and Fatigue in Polypyrrole-Based Artificial Muscles.* Bioinspiration & Biomimetics, 2008. **3**(3): p. 6.
6. Kaneto, K., Fujisue, H., Kunifusa, M. and Takashima, W., *Conducting Polymer Soft Actuators Based on Polypyrrole Films - Energy Conversion Efficiency.* Smart Materials & Structures, 2007. **16**(2): p. S250-S255.
7. Madden J.D, Rinderknecht D., Anquetil P.A and I.W, H., *Creep and Cycle Life in Polypyrrole Actuators.* Sensors and Actuators A: Physical, 2007. **133**: p. 210-217.
8. Jafeen, M.J.M., Careem, M.A. and Skaarup, S., *Speed and Strain of Polypyrrole Actuators: Dependence on Cation Hydration Number.* Ionics, 2010. **16**(1): p. 1-6.
9. Otero, T.F. and Boyano, I., *Comparative Study of Conducting Polymers by the Escr Model.* Journal of Physical Chemistry B, 2003. **107**(28): p. 6730-6738.
10. Murray, P., Spinks, G.M., Wallace, G.G. and Burford, R.P., *In-Situ Mechanical Properties of Tosylate Doped (Pts) Polypyrrole.* Synth. Met., 1997. **84**(1-3): p. 847-848.
11. Murray, P., Spinks, G.M., Wallace, G.G. and Burford, R.P., *Electrochemical Induced Ductile-Brittle Transition in Tosylate-Doped (Pts) Polypyrrole.* synthetic metals, 1998. **97**(2): p. 117-121.
12. Otero, T.F., Cascales, J.J.L. and Arenas, G.V., *Mechanical Characterization of Free-Standing Polypyrrole Film.* Materials Science & Engineering C-Biomimetic and Supramolecular Systems, 2007. **27**(1): p. 18-22.
13. Pytel, R.Z., Thomas, E.L. and Hunter, I.W., *In Situ Observation of Dynamic Elastic Modulus in Polypyrrole Actuators.* Polymer, 2008. **49**(8): p. 2008-2013.

CHAPTER 6 GENERAL CONCLUSIONS AND FUTURE WORK

6.1 General conclusions

As mentioned in chapter 1, predicting the actuation strain is very important for engineering applications. When a voltage stimulus is applied to the actuator, it is required that a defined strain or stress (or combination) is generated at a defined time. This thesis has concentrated on improving the understanding of the processes that affect the time-dependent strain occurring in polypyrrole actuators. It has been assumed that the total strain produced by these materials is the superposition of three time-dependent parts:

$$\varepsilon = \varepsilon_{\text{actuation}} + \varepsilon_{\text{elastic}} + \varepsilon_{\text{creep}} \quad (6.1)$$

where the first term represents the strain generated directly from charge injection and occurs due to ion and solvent ingress/egress and conformational changes. The second and third contributions are only evident when an external stress is applied to the actuator (as is expected in all applications). These two contributions reflect changes in the basic mechanical properties of the polymer that may accompany charge injection. While there have been previous work on each of the three contributions separately, there has been no work done to combine the whole strain together either theoretically or empirically. The ambition of this thesis was an attempt to evaluate the main effects which influence actuation strain and, perhaps, build a universal model containing all those main effects. As described in chapter 3, 4 & 5, strains could be affected by charge induced, stress applied, degradation and creeping. The main findings from each Chapter are now summarised and compared.

6.1.1 Time dependant charging process

The first requirement in achieving an actuation response from CP materials is to inject electrochemical charge into the polymer. The kinetics of charge injection were investigated in two systems: PPy/PF_6 helix tubes (Chapter 3) and PPy/TFSI fresh films (Chapter 5). PPy/PF_6 helix tube actuators were used as these materials have been shown to increase the actuation speed compared with films as a result of improved conductivity arising from the incorporated Pt helix wire [1]. PPy/TFSI was of interest because of its reported very high strains achieved at slow voltage scan rates [2]. The reasons for the large, slow strain response in such materials are not fully understood.

The charging process was found to be slow in both systems. The rate of charging in the PPy/PF_6 helix tubes was modelled as a diffusion controlled process. Averaged over a full voltage scan, the amount of charge injected varied with the ½ power of the scan time, as occurs in Fickian diffusion. The oxidation process could be viewed as involving the diffusion of ions from the electrolyte through the tube wall with the thickness of the oxidized layer increasing over time. The average diffusion coefficient obtained from this semi-empirical approach agreed well with values reported in the literature. Another phenomenon to be noticed was a kind of charge trapping effect. It occurred in thick samples at high scan rates and gives another reduction peak during the first part of the anodic voltage scan. A possible explanation was proposed that involved the competing movement of anions and cations within the polymer. From a practical viewpoint, the study highlighted the very long times needed to fully oxidize / reduce PPy helix tubes of thicknesses in the tens of microns range. To achieve full redox within a few seconds (as may be required in some applications) then tube wall thickness cannot exceed 10 μm. Such materials can be fragile and the influence of the Pt helix on strain generation cannot be ignored.

PPy/TFSI films showed a different time-dependence upon charging compared with the PPy/PF_6 helix tubes. Charge transferred followed an exponential rather than $t^{1/2}$ function in the PPy/TFSI studies. The difference in voltage input likely affected the rate of charge transfer. While linear voltage scans were used to oxidize / reduce the PPy/PF_6 helix tubes, a voltage step was used for the PPy/TFSI films. Current is known to decay exponentially after a voltage step in electrochemical systems [3]. A further difference between the two systems relates to their efficiency of electron conduction. The oxidation of the polymer requires electron migration from the oxidation site to the metal connector as well as diffusion of an anion from the electrolyte to the oxidation site. The electron conduction depends on the electronic resistance of the polymer which is increased with increasing distance between the oxidation site and the metal connector. The advantage of the helix tube design is to keep this distance small. In PPy films, however, the long distances from the metal connector (at the film ends) to the site of oxidation can further impede the rate of redox reaction.

Attempts to model the charge transfer processes in the systems studied have followed a semi-empirical approach. More rigorous methods for analysing charge transport in conducting polymers are available in the literature, but their complexity has limited their applicability. The semi-empirical approaches adopted here attempt to capture the main features and highlight the important role of electronic conductivity within the polymer and the transport of ions into and out of the polymer as the key processes in determining the rate of charging and discharging. Thus, any practical means to increase conductivity and reduce diffusion times will potentially speed up the actuator response. The conversion of charging into an actuation strain is summarised in the next three sections where firstly the strain at zero external load is considered and then the effects of an external load are included.

6.1.2 Zero-stress actuation response

The study of the actuation at zero external stress (the "free strain") provides information on the fundamental molecular mechanisms responsible for strain generation. The free strain of PPy/PF_6 helix tubes and PPy/TFSI free standing films have been reported in this thesis. The strain:charge ratio is a sensible means for comparing these systems, as differences in electroactivity are minimised. Thus, the strain:charge ratio reflects the amount of strain generated (at zero stress) for an increment of charge injected into the polymer. Differences in strain;charge ratio would reflect fundamental differences in reaction to charging, such as larger or smaller ions entering / leaving the polymer; different solvent contents within the polymer; or different degrees of conformational changes.

From the investigations conducted in this thesis, it was found that all systems studied showed similar strain:charge ratios, although the ratio was strongly dependent upon the time scale over which the actuation occurred. The strain:charge ratio of PPy/PF_6 was found to be ~$2.3*10^{-10}$ m^3/C for the thicker-walled helix tubes (the ratio was lower in thinner walled tubes due to the constraint imposed by the helix wire) when tested at fast scan rates (5-50 mV/s, Chapter 3). However, when tested at slower scan speeds (2 mV/s) much higher strains were obtained with consequently higher strain:charge ratios (Chapter 4). Similarly, the strain:charge ratio of PPy/TFSI free standing films (in the first few cycles) increased significantly at slow scan rates. At fast scan rates the strain:charge ratio was similar to that for PPy/PF_6 helix tubes (~$2.3*10^{-10}$ m^3/C) and increased to ~$6*10^{-10}$ m^3/C when using slow scan rate (2mV/s, can been seen in Figure 4.4 and Figure 4.5, chapter 4).

Further study over longer actuation times of PPy/TFSI films indicated that the free actuation strain seemed to be contributed by two processes, which has been proposed previously [5, 6]. A better fit to the actuation strain over a long time scale was achieved using two components rather than one component. One of these contributions was taken as directly related to charge, with the same time-dependency. It was found that the strain increased significantly after the charge injected had reached its limit, suggesting a second, slower contribution to strain. Adding the two contributions was found to give excellent fits to the strain-time data. As a consequence, during long time test, a higher strain:charge ratio was calculated. As proposed previously [5,6], the second contribution to the actuation strain was thought to be due to slow solvent ingress driven by osmotic pressure. Attempts to verify this mechanism by altering the concentration of the electrolyte (and thereby adjust the osmotic pressure) were not completely successful, probably due to the negative effects of a decreasing ionic conductivity at low electrolyte concentration.

Regardless of the exact mechanisms of actuation occurring, the fact that PPy actuators show a slow response to charge injection has significant practical outcomes. Firstly, it is clear that predicting the strain requires detailed knowledge of the kinetics of the slow process. It is not possible to calculate a strain based solely on the charge injected, as it has been shown in this thesis that strain continues to change after the polymer is fully charged. Accurate control of PPy actuators would, therefore, require proper modelling of the slow strain process. Secondly, the slow process contributes significantly to the overall strain generated by PPy actuators. As many applications require high strain, there is a possibility that high strains can be generated in shorter times by optimising the geometry of the PPy to favour a faster “slow” process. Since diffusion of solvent is likely involved in the “slow” process, any means to increase the

diffusion rate will increase its contribution to strain at higher speeds. Kaneto has suggested that high strains in PPy/TFSI are favoured by the porous nature of the films [4]. Using thin films or modifying the PPy composition may further increase diffusion speeds.

6.1.3 Effect of redox state on PPy mechanical properties

The mechanical properties (e.g. elastic modulus) of CPs depend on their redox state. Previous studies have shown that the elastic modulus of PPy/PF_6 in the oxidized state is higher than that when the polymer is reduced. Since the polymer expands when oxidized, the increasing modulus upon oxidation leads to a contraction. At higher applied stresses the overall actuation strain decreases [7]. Experimental results given in chapter 3 were identical to those findings. Further, the effect of partial oxidation of the polymer (as occurs at higher scan rates) was modelled as a two layer structure where the overall modulus was given by a rule-of-mixtures approach. This model gave reasonable agreement with the measured strain response at different applied stresses.

In contrast to the PPy/PF_6 helix tubes, the elastic modulus of PPy/TFSI free standing films showed a higher modulus in the reduced state compared to the oxidized state. The reduction of the PPy/TFSI films lead to complex changes in modulus, with first a sharp decrease followed by a slower increase in modulus. The fast and slow changes in modulus perhaps reflect the fast and slow actuation responses described above. However, the oxidation process involved only a slow decrease in modulus. As described in the literature, there are lots of factors that contribute to changing in modulus. Plasticization due to solvent ingress likely decreases modulus. Stiffening of PPy chains (due to oxidation and formation of charged groups) and ionic crosslinking

between charged PPy chains are likely to increase modulus [8-10]. Since both effects can occur during oxidation / reduction it is not clear which factor dominates for a given polymer. It appears that the oxidation of PPy/PF_6 is dominated by chain stiffening and/or ionic crosslinking leading to an increase in modulus. In PPy/TFSI, however, the plasticising effect due to solvent ingress during oxidation appears to be the dominant effect. Thus, the initial decrease in modulus during the reduction of PPy/TFSI may be due to the loss of charged groups and ionic crosslinking between chains. The slower increase in modulus that follows may be due to the slow release of solvent that reduces the plasticising effect.

Creep testing of PPy/TFSI films was also conducted to investigate the viscoelastic behaviour of these materials in different redox states. Through fitting creep and recovery strain of PPy/TFSI using the classic 4 element spring and dash-pot model, changes in the various of other viscoelastic parameters at different redox states was quantified. The four element model was quite successful in predicting the creep strain and recovery and the films were shown to behave linearly with stress. As seen in chapter 5, all viscoelastic parameters (instantaneous modulus, delayed elastic modulus and viscosity) all changed with the polymer's redox state. The moduli values and viscosity all decreased when oxidizing PPy/TFSI and decreased when reducing the polymer. The results are corresponding to static and dynamic elastic modulus tests.

6.1.4 Actuation under external load.

Practical applications for actuators require them to operate against an external load. As such, the effect of the applied load on the actuator material's dimensions will contribute to its "actuation". A simple scenario is depicted in Figure 6.1a) showing

isotonic actuation (constant stress) that causes a net contraction in the actuator. If the elastic modulus of the actuator material decreases when the voltage is applied, then there will be an increase in length. If the elastic modulus increases when voltage is applied, a decrease in length will be observed. The overall length change is the sum of the actuation strain that would occur at zero stress (ε_0) and the change in length caused by a change in modulus. The latter depends upon the applied stress and for linear-elastic materials the overall actuation strain is given by:

$$\varepsilon = \varepsilon_0 + \sigma\left(\frac{1}{Y'} - \frac{1}{Y}\right) \tag{6.2}$$

in which σ is the stress applied to the actuator. Y' and Y are the elastic moduli in the final and initial states. The slope of strain-stress curve is $\frac{1}{Y'} - \frac{1}{Y}$. As shown in Figure 6.1c and d) the work output and power output (per unit volume of actuator material) pass through maxima with increasing applied stress. Data presented in Chapter 3 generally supported these expected relationships when PPy/PF_6 helix tubes were actuated at moderate voltage scan speeds. Under these conditions, the time-dependent osmotic strains and viscoelastic effects on strain were quite small and a linear-elastic simplification was suitable. The study showed that the while the work output increased when thicker PPy tubes were used, the power output decreased significantly due to the much increased time required for full actuation in these systems. Thick CPs allows larger loads to be applied, however it will take a longer time to reach its fully charged state. Thin ones have fast response but only low load could be applied.

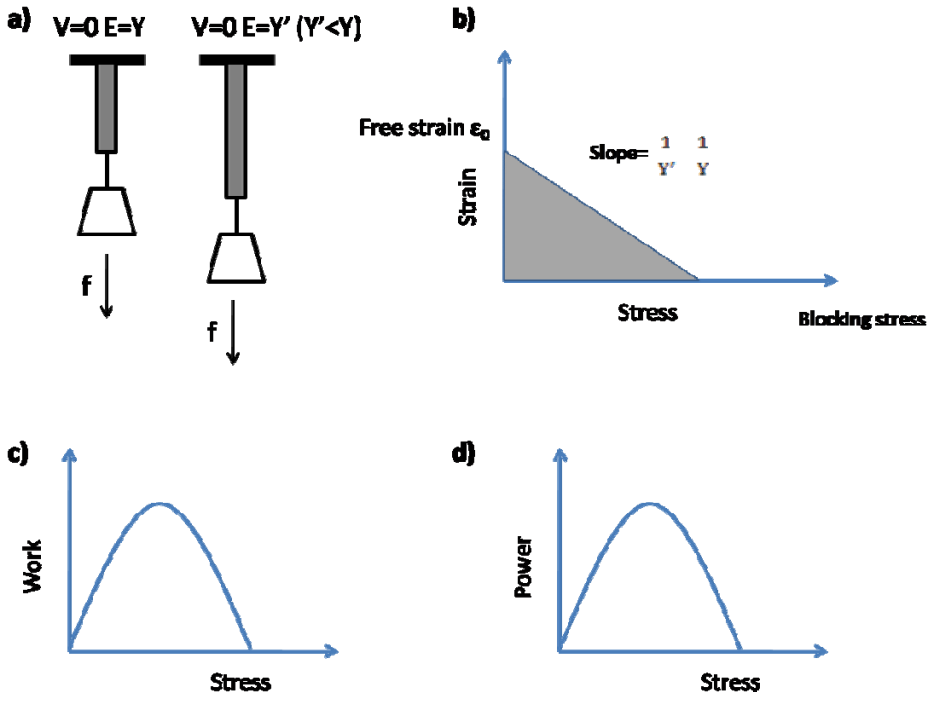

Figure 6. 1 Actuation process under external load

The effect of changing mechanical properties during actuation of PPy materials was extended in Chapter 5 to include viscoelasticity effects. An attempt was made to predict total actuation combining free actuation elastic strain and creep strain. The predicted strains were reasonably accurate for the oxidation of PPy/TFSI films. Importantly, the model was able to predict a larger strain when a higher isotonic stress was applied, as was experimentally observed. Unfortunately, the same model was unsuccessful in predicting the time-dependent strain resulting from the reduction of the polymer. Quite unexpected results were measured that seem to result from a change in behaviour occurring during the pre-load period. The reasons for such behaviour remain unknown.

6.1.5 Instability of PPy/TFSI system

A final time-dependent effect was also evident from cycle life studies of PPy/TFSI films where the actuation strain amplitude diminished sharply upon repeated cycling. Similar instability was also recorded for PPy/PF_6 films when scanned at slow scan rates. Several approaches aimed at understanding the degradation and enhance the stability of PPy/TFSI films were made. The effects of voltage scan range, scan rate and current versus potential cycling were considered. In all cases where high strains were achieved, it was also observed that the strain decreased upon continued cycling. The most stable strains were produced using current pulsing to ensure that equal amounts of oxidation and reduction occurred in each cycle. Using these measures a 4% strain was achieved for 100 cycles without noticeable degradation.

Perhaps the instability in high strain PPy actuators could be related to irreversible chemical reactions and/or structural changes within the PPy itself. Dynamic in situ elastic modulus was collected while scanning the samples using different range and rate. It is also found that elastic modulus is always changing in close accord with the actuation strain stability of the PPy actuators. The changes in modulus suggest structural changes within the polymer, such as crosslinking, that may also affect the ability of the polymer to swell when electrochemically charged. The exact nature of the structural / chemical changes occurring is unknown at present.

6.2 Future work

The following suggestions for future work are aimed at increasing the practical usefulness of PPy actuators by suggesting means for increasing strain, strain rate and

work and power output. Improving stability and understanding (or reducing) creep also have significant practical consequences.

Strain rates are clearly limited by the slow diffusion of ions and solvent into and out of the polymer. To achieve higher strain rate, the diffusion times need to be reduced. Besides reducing the polymer thickness, another possible way is to make the PPy porous. The porous material will have a greater contact between the polymer and electrolyte so that diffusion times are reduced.

As found in chapter 3, it is always found that the PPy helix tubes were broken before reaching the stress corresponding to its maximum work density. Hence improving the strength of PPy could extend its working stress and produce a greater work output. Incorporating another material to build a stronger composite may achieve this aim. For instance, introducing carbon nanotubes (CNTs) can improve conductivity and strength [11]. It is necessary, however, that such additives do not decrease the free strain by restricting polymer matrix expansion.

In chapter 4 it was shown that current control was superior to voltage control in terms of actuator stability. However, a full study on current control in terms of the effect of external stress, viscoelastic behaviour and strain rate has not been completed. The real application of current control for CP actuators requires further work.

Quite unexpected and unusual creep behaviour of was noted in Chapter 5 for PPy/TFSI films during reduction after a pre-load hold period. As pointed out, shifting of mechanical properties is a dynamic process during oxidation / reduction of PPy. The assumption used in this thesis that the actuation strain is simply the sum of the free strain and the stress-induced strain is clearly not valid during the reduction of PPy/TFSI films. Thus, further work is required to understand the interactions between stress and actuation performance.

6.3 References

1. Ding, J., et al., *High Performance Conducting Polymer Actuators Utilising a Tubular Geometry and Helical Wire Interconnects.* Synthetic Metals, 2003. **138**: p. 391-398.
2. Hara, S., Zama, T., Takashima, W. and Kaneto, K., *Gel-Like Polypyrrole Based Artificial Muscles with Extremely Large Strain.* Polymer Journal, 2004. **36**(11): p. 933-936.
3. Suarez, I.J., Otero, T.F. and Marquez, M., *Diffusion Coefficients in Swelling Polypyrrole: Escr and Cottrell Models.* Journal Of Physical Chemistry B, 2005. **109**(5): p. 1723-1729.
4. Hara, S., Zama, T., Takashima, W. and Kaneto, K., *Tris(Trifluoromethylsulfonyl)Methide-Doped Polypyrrole as a Conducting Polymer Actuator with Large Electrochemical Strain.* Synthetic Metals, 2006. **156**(2-4): p. 351-355.
5. Bay, L., Jacobsen, T., Skaarup, S. and West, K., *Mechanism of Actuation in Conducting Polymers: Osmotic Expansion.* J. Phys. Chem. B, 2001. **105**: p. 8492-8497.
6. Jafeen, M.J.M., Careem, M.A. and Skaarup, S., *Speed and Strain of Polypyrrole Actuators: Dependence on Cation Hydration Number.* Ionics. **16**(1): p. 1-6.
7. Spinks, G.M., Liu, L., Zhou, D. and Wallace, G.G., *Strain Response from Polypyrrole Actuators under Load.* Advanced Functional Materials, 2002. **12**(6-7): p. 437-440.
8. Murray, P., Spinks, G.M., Wallace, G.G. and Burford, R.P., *Electrochemical Induced Ductile-Brittle Transition in Tosylate-Doped (Pts) Polypyrrole.* synthetic metals, 1998. **97**(2): p. 117-121.
9. Bahrami-Samani, M., Cook, C.D., Madden, J.D., Spinks, G.M. and Whitten, P.G., *Quartz Crystal Microbalance Study of Volume Changes and Modulus Shift in Electrochemically Switched Polypyrrole.* Thin Solid Films, 2008. **516**(9): p. 2800-2807.
10. Koehler, S., Bund, A. and Efimov, I., *Shear Moduli of Anion and Cation Exchanging Polypyrrole Films.* Journal of Electroanalytical Chemistry, 2006. **589**(1): p. 82-86.
11. Baughman, R.H., Zakhidov, A.A. and de Heer, W.A., *Carbon Nanotubes - the Route toward Applications.* Science, 2002. **297**(5582): p. 787-792.